

AD-A139 236

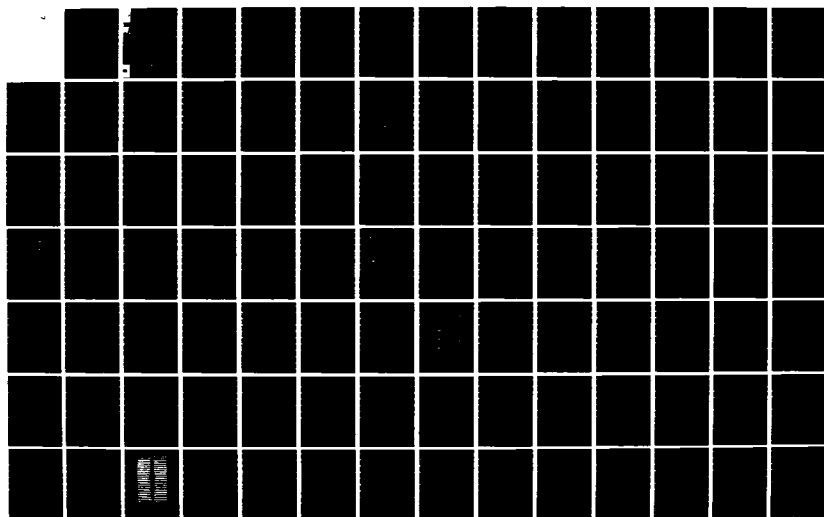
LOAD-TRANSFER CRITERIA FOR NUMERICAL ANALYSIS OF
AXIALLY LOADED PILES IN (U) ARMY ENGINEER WATERWAYS
EXPERIMENT STATION VICKSBURG MS R L MOSHER JAN 84
WES-TR-K-84-1

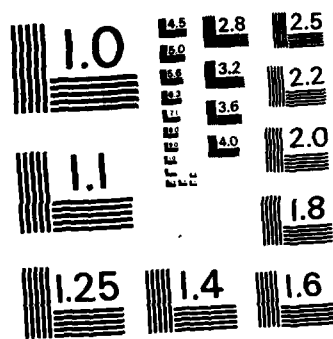
1/5

UNCLASSIFIED

F/G 13/13

NL





MICROCOPY RESOLUTION TEST CHART
NATIONAL BUREAU OF STANDARDS - 1963 - A

12

TECHNICAL REPORT K-84-1

LOAD-TRANSFER CRITERIA FOR NUMERICAL ANALYSIS OF AXIALLY LOADED PILES IN SAND

PART I: LOAD-TRANSFER CRITERIA

by

Reed L. Mosher

Automatic Data Processing Center
U. S. Army Engineer Waterways Experiment Station
P. O. Box 631, Vicksburg, Miss. 39180

AD A139236



January 1984
Final Report

Approved For Public Release; Distribution Unlimited

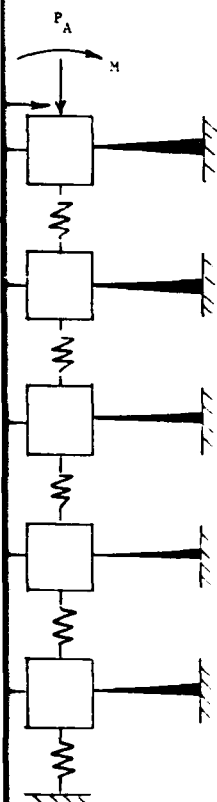


Prepared for U. S. Army Engineer Division,
Lower Mississippi Valley
P. O. Box 80, Vicksburg, Miss. 39180

84 03 19 001

DTIC FILE COPY

my Corps
Engineers



Destroy this report when no longer needed. Do not
return it to the originator.

The findings in this report are not to be construed as an
official Department of the Army position unless so
designated by other authorized documents.

The contents of this report are not to be used for
advertising, publication, or promotional purposes.
Citation of trade names does not constitute an
official endorsement or approval of the use of such
commercial products.

Unclassified

SECURITY CLASSIFICATION OF THIS PAGE (When Data Entered)

REPORT DOCUMENTATION PAGE		READ INSTRUCTIONS BEFORE COMPLETING FORM
1. REPORT NUMBER Technical Report K-84-1	2. GOVT ACCESSION NO.	3. RECIPIENT'S CATALOG NUMBER
4. TITLE (and Subtitle) LOAD-TRANSFER CRITERIA FOR NUMERICAL ANALYSIS OF AXIALLY LOADED PILES IN SAND PART I: LOAD-TRANSFER CRITERIA; PART II: LOAD PILE CAPACITY CURVES FOR STEEL AND CONCRETE PILES		5. TYPE OF REPORT & PERIOD COVERED Final report (in two parts)
7. AUTHOR(s) Reed L. Mosher		6. PERFORMING ORG. REPORT NUMBER
9. PERFORMING ORGANIZATION NAME AND ADDRESS U. S. Army Engineer Waterways Experiment Station Automatic Data Processing Center P. O. Box 631, Vicksburg, Miss. 39180		8. CONTRACT OR GRANT NUMBER(s)
11. CONTROLLING OFFICE NAME AND ADDRESS U. S. Army Engineer Division, Lower Mississippi Valley P. O. Box 80, Vicksburg, Miss. 39180		10. PROGRAM ELEMENT, PROJECT, TASK AREA & WORK UNIT NUMBERS
14. MONITORING AGENCY NAME & ADDRESS (if different from Controlling Office)		12. REPORT DATE January 1984
		13. NUMBER OF PAGES Part I--386, Part II--290
		15. SECURITY CLASS. (of this report) Unclassified
		15a. DECLASSIFICATION/DOWNGRADING SCHEDULE
16. DISTRIBUTION STATEMENT (of this Report) Approved for public release; distribution unlimited.		
17. DISTRIBUTION STATEMENT (of the abstract entered in Block 20, if different from Report)		
18. SUPPLEMENTARY NOTES Available from National Technical Information Service, 5285 Port Royal Road, Springfield, Val. 22161.		
19. KEY WORDS (Continue on reverse side if necessary and identify by block number) Concrete piles (LC) Numerical analysis (LC) Piling (Civil engineering) (LC) Sand (LC) Steel piles (LC)		
20. ABSTRACT (Continue on reverse side if necessary and identify by block number) > Part I describes a study of load-transfer criteria for analysis of axially loaded piles in sand using the discrete springs soil model. Various analysis methods for axially loaded piles are presented, along with a literature review of pile behavior in sands focusing on the changes the soil undergoes during pile installation. Available criteria for spring representation of soil are pre- sented and summarized. The criteria are compared with actual field data from pile load tests and are critically evaluated based on these comparisons. (Continued)		

DD FORM 1 JAN 73 1473 EDITION OF 1 NOV 65 IS OBSOLETE

Unclassified

SECURITY CLASSIFICATION OF THIS PAGE (When Data Entered)

Unclassified

SECURITY CLASSIFICATION OF THIS PAGE(When Data Entered)

20. ABSTRACT (Continued)

Because of the poor performance of the available criteria, new criteria are proposed. The new criteria use maximum side and tip resistance values presented by Castello (1980). Castello's values are modified by the author to reflect the field data from the Lower Mississippi Valley. Displacement functions for side and tip resistance are developed based on correlations with field data for pile load tests. The new criteria are evaluated against pile load test data. Use of the criteria is demonstrated in an outline of an analysis. The new criteria are used to develop a set of design curves for the practicing engineer.

Part II of this report is published under a separate cover, and presents load capacity curves for select steel and concrete pile.

Unclassified

SECURITY CLASSIFICATION OF THIS PAGE(When Data Entered)

PREFACE

This report presents load-transfer criteria for numerical analysis of axially loaded piles in sand. The work in developing the criteria was done as part of the applications support provided by the Automatic Data Processing (ADP) Center, U. S. Army Engineer Waterways Experiment Station (WES), to the U. S. Army Engineer Division, Lower Mississippi Valley (LMVD).

Work on the project was coordinated with LMVD by means of conferences and telephone conversations with Messrs. Frank J. Weaver and James A. Young, Geology, Soils and Materials Branch, Engineering Division, who provided technical guidance on the desired results. Mr. Young also made a detailed review of this report.

The work was done by Mr. Reed L. Mosher, Computer-Aided Design Group, (CADG), ADP Center, WES, under the guidance and supervision of Dr. N. Radhakrishnan, Special Technical Assistant, ADP Center. This report is essentially a thesis submitted to Mississippi State University by Mr. Mosher in partial fulfillment of the requirements for a Master of Science degree. The considerable help provided by Mr. Dennis Williams, CADG, in completing this report and generating pile capacity curves included in Part II of this report is appreciated.

Part II of this report is published under a separate cover, and presents load capacity curves for select steel and concrete pile.

Commanders and Directors of WES during the period of the work were COL Nelson P. Conover, CE, and COL Tilford C. Creel, CE. Technical Director was Mr. F. R. Brown.

Accession For	
NTIS GRA&I	<input checked="checked" type="checkbox"/>
DTIC TAB	<input type="checkbox"/>
Unannounced	<input type="checkbox"/>
Justification	
By	
Distribution/	
Availability Codes	
Dist	Avail and/or Special
A-1	



CONTENTS

	<u>Page</u>
PREFACE.	i
CONVERSION FACTORS, NON-SI TO SI (METRIC) UNITS OF MEASUREMENT	iv
CHAPTER 1: INTRODUCTION	1
CHAPTER 2: OVERVIEW OF PILE FOUNDATIONS	4
History of Piles.	4
Pile Types.	6
Pile Installation	8
Review of Pile Design/Analysis.	10
Static Formula.	10
Tip-Bearing Capacity.	12
Skin Friction	15
Pile-Driving Formulas	18
New Concepts.	22
Elastic Solid Model	26
Discrete Spring Model	32
Mechanics of an Axially Loaded Pile	35
Review of the Interpretation of Pile Load Tests Results	42
Residual Stresses	52
Standard Penetration Test	59
Behavior of Axially Loaded Piles in Sands	62
Summary	86
CHAPTER 3: LOAD-DEFORMATION CRITERIA.	88
Review of Criteria.	88
Coyle-Sulaiman Criteria	88
Vijayvergiya Criteria	96
Parker and Reese Criteria	101
Other Criteria.	113
Summary of Criteria	113
CHAPTER 4: EVALUATION OF PUBLISHED CRITERIA	117
Arkansas River Lock and Dam No. 4 Pile Tests.	117
Ascalmore Creek-Tippo Bayou Control Structure Pile Tests.	121
Red River Lock and Dam No. 1 Pile Tests	124
Comparison of Criteria with Field Test Results.	133
Evaluation of Criteria.	138
Summary	148
CHAPTER 5: PROPOSED CRITERIA.	150
Displacement Function for Side Resistance	151
Displacement Function for Tip Resistance.	164
Comparison of Computed and Actual Butt and Tip Performance.	177
Comments.	189
Outline of Analysis Procedure	190
Design Curves	206
Summary	213
CHAPTER 6: SUMMARY AND CONCLUSIONS.	218

CONTENTS

	<u>Page</u>
REFERENCES.	222
APPENDIX A: LOAD-TRANSFER CURVES FROM IDEALIZED TRIAXIAL CURVES BASED ON PARKER AND REESE CRITERIA	A1
APPENDIX B: RESULTS OF FIELD PILE TESTS.	B1
APPENDIX C: COMPARISON OF AVAILABLE CRITERIA TO FIELD PILE TEST DATA.	C1
APPENDIX D: RESULTS OF HYPERBOLIC CURVE FITTING OF FIELD f - z CURVES	D1
APPENDIX E: PROCEDURES FOR PARTIALLY SUBMERGED PILES	E1
APPENDIX F: LIST OF SYMBOLS.	F1

CONVERSION FACTORS, NON-SI TO SI (METRIC)
UNITS OF MEASUREMENT

Non-SI units of measurement used in this report can be converted to SI (metric) units as follows:

<u>Multiply</u>	<u>By</u>	<u>To Obtain</u>
feet	0.3048	meters
inches	2.54	centimeters
miles (U. S. statute)	1.609347	kilometers
pounds (force) per square foot	47.88026	pascals
pounds (force) per square inch	6.894757	kilopascals
pounds (mass) per cubic foot	16.01846	kilograms per cubic meter
square feet	0.09290304	square meters
tons (force) per square foot	95.76052	kilopascals
tons (2000 lb mass)	907.18474	kilograms
square inches	6.4516	square centimeters
pounds (mass)	0.45359237	kilograms

LOAD-TRANSFER CRITERIA FOR NUMERICAL ANALYSIS
OF AXIALLY LOADED PILES IN SAND

PART I: LOAD-TRANSFER CRITERIA

CHAPTER 1: INTRODUCTION

The Corps of Engineers installs hundreds of piles in the construction of navigation and flood control facilities in the Lower Mississippi Valley. Pile foundations are utilized to overcome poor subsoil conditions that are encountered in the construction of these facilities. The subsoil conditions that must be overcome generally involve soils at or near the surface that are unable to provide adequate support without unacceptable deformation. Typical examples of these subsoil conditions in the Lower Mississippi Valley are clay and silt layers ranging from 5 to 70 ft* in thickness over medium to dense sand. Piles transfer the loads from structures into the underlying sand-soil stratum. This transfer of loads is extremely complex, highly indeterminate, and difficult to analytically quantify.

In practice, pile foundations have typically been designed based on either the pile-driving formulas or the static formula. The static formula has been considered the more reliable of the two. With the static formula, the pile capacity is based on the static soil resistance determined by the limit equilibrium theory for the tip of the pile and friction between two surfaces for side resistance. The soil parameters used in the static formula are derived from field and/or laboratory tests. For representative soil conditions in the Lower Mississippi Valley, charts have been developed, employing the static formula, that yield the pile capacity for a given depth of penetration in the sand-soil stratum.

* A table of factors for converting non-SI units of measurement to SI (metric) units is presented on page iv.

The practicing foundation engineer must make a number of simplifying assumptions in the design procedure for axially loaded piles. These assumptions have been necessary to quantify the behavior of the pile-soil system. One of the most grossly oversimplifying assumptions in the static formula is that the ultimate bearing capacity of the soil at the tip of the pile and the ultimate skin friction along the pile shaft are mobilized simultaneously with no regard to displacement compatibility of these separate components. Another oversimplifying assumption is that the soil conditions extant prior to installation are still present after placement of the pile.

In recent years, a number of investigators have been researching new analytical and numerical procedures which lessen the number of simplifying assumptions in modeling the behavior of the pile-soil system. These investigators have taken two different approaches: one based on modeling soil as a continuum, the other on modeling the soil as a set of discrete springs. The discrete springs model was chosen for the basic analysis procedure for axially loaded piles in sand because of its simplicity. In this model, the soil is represented by springs that relate the shear developed along the pile shaft and resistance at the tip to the displacement at these points.

The objective of this report is to establish criteria for shear developed (shear transfer) along the pile shaft due to a given movement and for tip resistance due to a given tip movement based on correlations with field data. Chapter 2 presents a brief history of pile foundations, a review of the design/analysis methods (both old

and new concepts), a review of the interpretation of pile load tests, and a literature review of axially loaded piles in sands that considers the changes the soil undergoes during installations. In Chapter 3, the available criteria for spring representation of soil are presented and summarized. Chapter 4 contains a comparison of these criteria with actual field data from pile load tests with a critical evaluation based on these comparisons. New criteria are presented and evaluated in Chapter 5. The new criteria are used to develop a set of design curves for the practicing engineer. These curves are presented in Chapter 5 along with a detailed procedure for utilizing this analysis technique.

CHAPTER 2: OVERVIEW OF PILE FOUNDATIONS

History of Piles

A pile is a vertical or slightly slanted structural foundation member with a relatively small cross-sectional dimension compared to its length. The end of the pile which connects to the superstructure at ground surface is termed the pile "head" or "butt"; the end placed in the soil is termed the pile "tip"; and the portion of the pile between the head and the tip is the "shaft" (Figure 1).

Piles are one of man's oldest remedies to problems involved in founding structures on soft soil. Prehistoric man built his dwelling on piles to raise it above water or to protect himself from wild animals or hostile neighbors. Anthropologists have found ancient dwellings on piles in Lake Lucerne in Switzerland. The Romans built a number of bridges across the Rhine founded on pile foundations. In 58 A.D., Vitruvius described the use of tree trunks as piles in construction work. Venetians built their city on a number of small marshy islands in the inlet of the Lagoon of Venice to protect themselves from the bloodthirsty Huns. Again they used piles, some of which are still present in building foundations.

Early man used piles that were installed by hand mallets, hand-operated machine mallets, rams, treadmills, and waterwheel drivers. The invention of the first steam pile driver by Nasmyth in 1850 revolutionized their use. They could be driven to greater depths enabling them to carry greater loads, and the driving time required

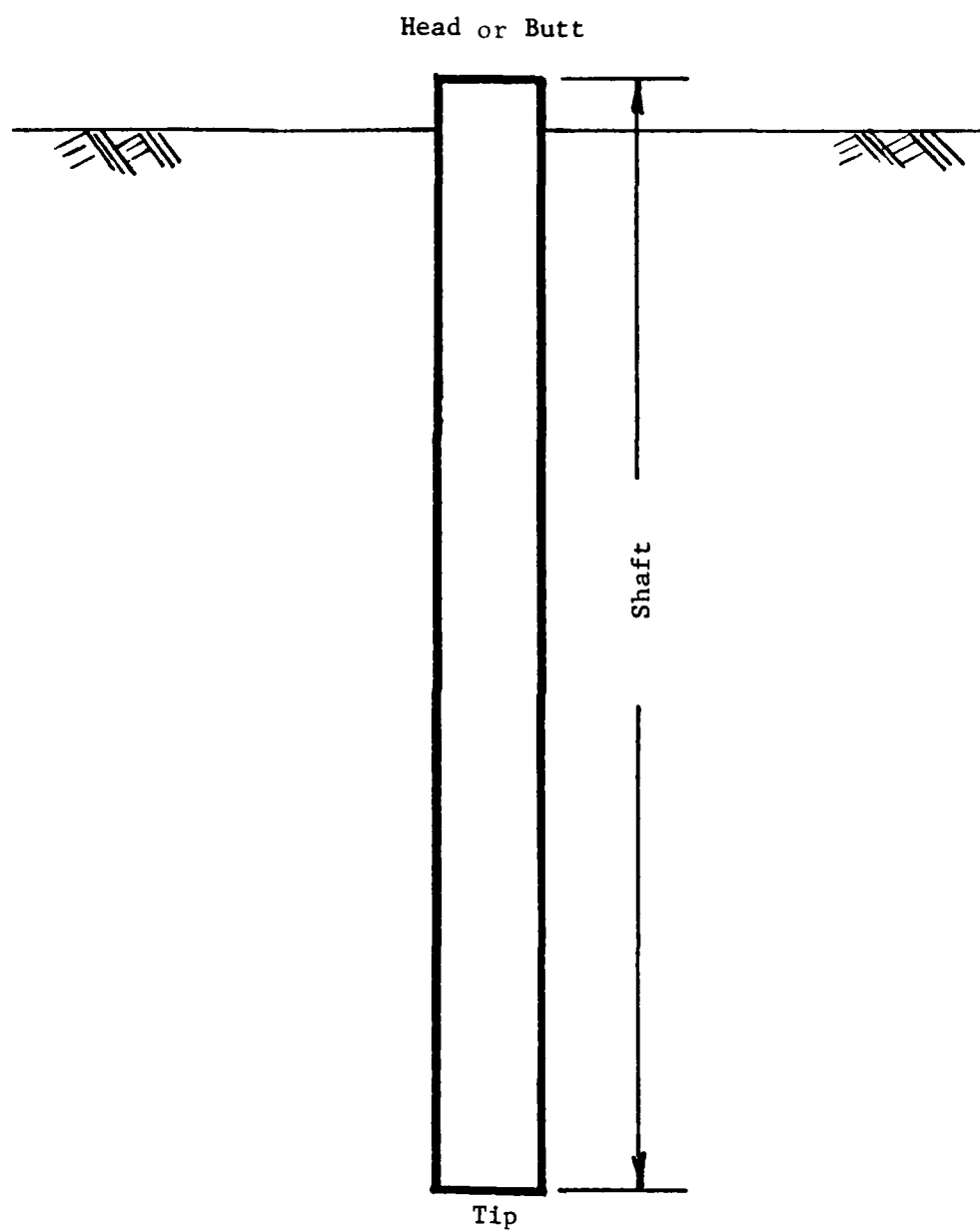


Figure 1. Vertical Pile

decreased which increased their economic advantage.

Piles are applied to difficult foundation conditions such as offshore construction, construction on soils with high groundwater tables, construction on soft soils, to provide stability when scour occurs, and to resist unusually high lateral forces from horizontal loads. Piles are generally used for two purposes: (1) to increase the load carrying capacity of the foundation and (2) to reduce the settlement of the foundation. These are accomplished by transferring loads through soft stratum to stiffer stratum at a greater depth or by distributing loads through the stratum by friction along the pile shaft, or by some combination of the two.

Pile Types

Large, mature trees were the first material to be used for piling. Their use was well established in foundation construction by Roman times, details of which were presented by Vitruvius in 58 A.D. They are still the most common type of piling employed in the world today. In many situations, they provide a reliable and economical foundation. They generally range in length from 10 to 80 ft with diameters of 1 to 2 ft. Timber pilings have two main limitations: first, they usually do not come in lengths over 80 ft and it is very difficult to splice them; secondly, they can be damaged when driven in highly resistant soil. If damaged, they lose their ability to carry loads.

In the early 1900's, several types of concrete piles were available to the construction industry. Today, the engineer has a wide variety of them to choose from for particular projects. This wide variety may be divided into two groups: cast-in-place and precast. Cast-in-place piles are installed by driving a casing (shell, pipe) into the ground, clearing it out, and filling it with concrete. As concrete is placed, the casing may be raised out of the ground, or it may be left in place. Precast concrete piles are manufactured at a concrete casting plant. They are generally used in carrying fairly heavy loads through a soft stratum to a firmer or stiffer stratum. They are usually reinforced for bending so that they can be handled and driven without cracking and may be prestressed so as to prevent cracking or spalling during driving. They are manufactured in given lengths with joints that may be used to splice them together. If the length is misjudged before construction, they may be spliced together to obtain the given length during construction.

Steel piles are used often in modern construction. They come in basically two shapes: steel pipe and steel H shapes. The pipe shapes are usually in two forms, either open-ended or closed-ended. These steel piles are often used when penetration resistance is high and great depths are needed. They are easily sectioned together or spliced together to provide more length during driving. Steel H piles penetrate the ground most readily of all piles due to their relatively small displacement of material. Steel H piles are suitable for penetrating to rock and through hard material with the least amount of

effort and in the shortest time because of this small displacement. For many applications they may be the only pile that can be used without using jetting or coring. Steel piles can carry heavy loads which may reduce the number of piles needed for a foundation. They are also often used when large lateral loads occur because of their high bending strength.

Pile Installation

Current construction practice for installation of piles may be divided into three basic categories: driving, boring, and jetting. Jetting and boring will not be considered in this report because they are seldom used in sands. The oldest and most common method of installation is impact driving of piles. This was the method used by the first steam pile driver. Impact hammers or drop hammers originated with the Romans who, in the early days, used stone blocks hoisted by rope over a pulley guide and then dropped. The block was guided to its destination by vertical poles that are similar to today's pile leads. Piles are currently driven by means of a ram/hammer or by a vibratory forced generator. A hammer operates between a pair of vertical guides called leads suspended from the boom of a crane. The leads are connected to the base of the crane by a horizontal member called a spotter. The spotter guides the leads to proper alignment for the pile. The leads have rails which guide the hammer during its descent.

Impact driving can be performed with five types of hammer: a drop hammer, single-action hammer, double-action hammer, differential acting hammer, and diesel hammer. The drop hammer works by raising a

ram with a cable run over the top of a framework back to a drum or a gear shaft. A tripping mechanism releases the ram once it reaches the top of the framework. It free falls along the guide rails and is allowed to strike the head of the pile, thus driving it into the ground. For a single-action hammer, steam or air is forced into a cylinder that raises a piston connected to the ram. The ram is dropped by releasing the pressure. Hammers of this type are always used in leads. A double-action hammer uses steam or air to raise the ram and to add additional energy on the downstroke. Differential acting hammers also employ steam or air to raise the ram and to add energy on the downstroke. The diesel hammer originated in Europe. It uses a closed system in which diesel fuel is ignited to raise the ram. The hammer forms a self-contained unit including fuel tank and injectors. A diesel hammer is lighter and more portable than a steam hammer. Most impact hammers used today are either steam or diesel.

Vibratory drivers consist of force generators attached to the pile head by clamps with a static weight. The driving force is from a pair of counterrotating eccentric weights arranged so that the horizontal components of their centrifugal force cancel whereas the vertical components are added. The pulsating force facilitates the penetration of the pile under the influence of the constantly acting downward weight. Vibratory drivers differ from one another according to the frequency of the power source. If the frequency is adjustable, the driver is called a "resonant" driver because by adjusting the frequency the natural frequency of the system can be attained which will assist the penetration by making effective the full downward

weight of the hammer and the pile itself.

Review of Pile Design/Analysis

Into the latter part of the 19th century, the design of piling was based totally on prior experience and rule-of-thumb criteria. The first attempt at theoretical evaluation of pile capacity was published in Engineering News under "Piles and Pile Driving" edited by Wellington in 1893. This approach is still known today as the "Engineering News pile-driving formula." Since then, a number of attempts have been made to predict the capacity of piles, and a large number of reports of field experience have become available. The two basic approaches that have been used or followed in the theoretical attempts to evaluate pile capacity are the pile-driving formulas and the static formula. The pile-driving formulas base pile capacity on the resistance of the pile to driving. The static formula bases pile capacity on the static soil resistance after the pile is driven. This resistance is evaluated in two parts: limit equilibrium theory for the tip resistance, and friction between two surfaces for side resistance.

Static Formula

The static formula has been used for years to determine the ultimate axial capacity of a pile, P_u . The ultimate axial capacity of a pile is separated into two components: the ultimate shear resistance along the shaft of the pile, P_s ; and the ultimate tip bearing capacity, P_t (Figure 2). The two are generally assumed to develop

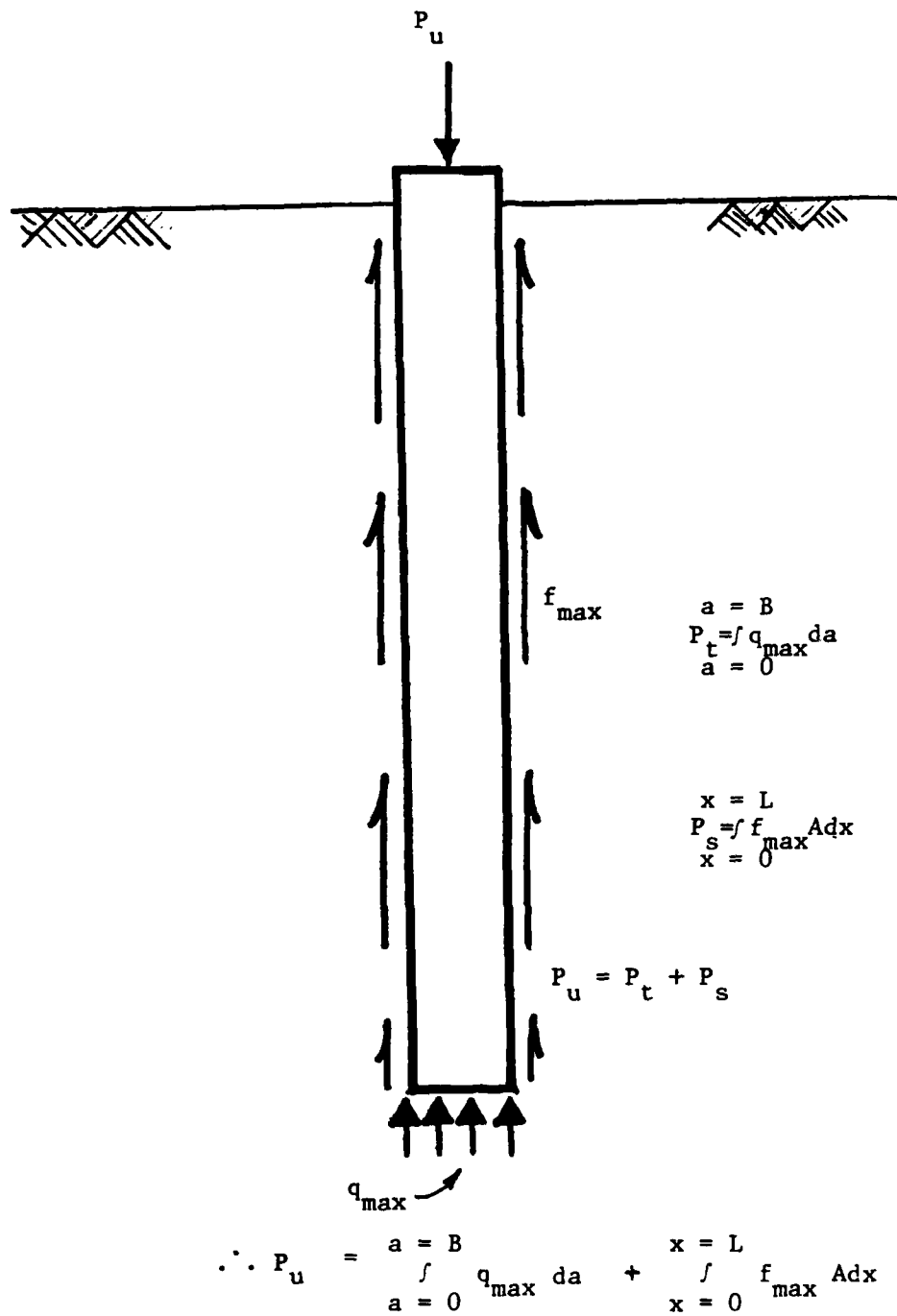


Figure 2. Forces on Pile for the Static Formula

independent of each other. The sum of the two gives the ultimate axial capacity:

$$P_u = P_t + P_s \quad (1)$$

where

P_u = the ultimate axial capacity

P_t = the ultimate tip-bearing capacity

P_s = the ultimate shear resistance, or "skin friction,"
along the shaft

Tip-Bearing Capacity

The ultimate tip-bearing capacity of a pile is derived from the classical bearing capacity theory for a strip load at the surface. The first theoretical formulation for bearing capacity is attributed to Caquot (1934) and Buisman (1930) in the mid-1930's, who extended Prandtl (1920) and Reissner's (1924) work on punch failure. Prandtl's theoretical approach considered the plastic flow in a semi-infinite weightless continuum due to a distributed infinite strip load on a frictional surface. In Caquot and Buisman's approach, the soil was assumed to be modeled by a semi-infinite continuum having the following properties: (1) Mohr-Coulomb failure criteria govern the soil failure; (2) the strength at any point is independent of strain; (3) the elastic deformations are negligible with respect to plastic deformations; and (4) volume change due to stress is negligible. The above assumptions describe the behavior of a rigid perfectly plastic material which would have a stress-strain diagram as shown in Figure 3. This type of problem is solved by limit equilibrium analysis for plasticity theory.

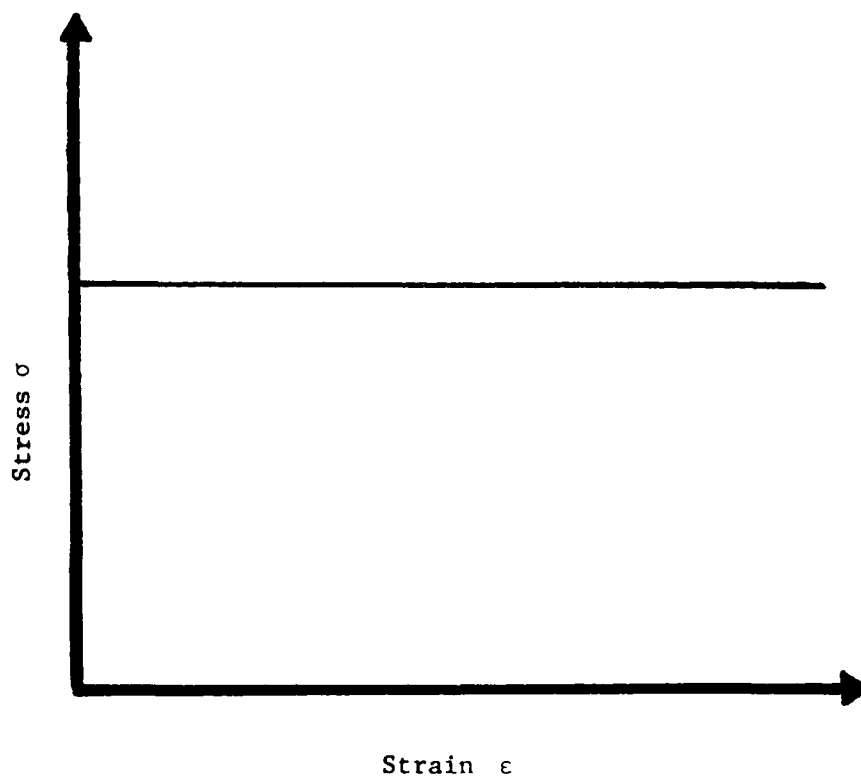


Figure 3. Stress-Strain Behavior for a Perfectly Plastic Material

Limit analysis for plasticity theory requires the establishment of a representative kinematic failure mechanism for the prescribed boundary and discontinuous conditions. The kinematic failure mechanism is referred to as the "failure pattern." The stresses applied must satisfy the equations of equilibrium for the kinematic configuration resulting from the failure conditions. This is called "limit equilibrium." Limit equilibrium results if the stress state is reached in the soil mass so that a change, no matter how small, in the surface forces will cause a loss of equilibrium or collapse.

Since the first attempt, a number of different solutions have followed introducing different assumptions for the surface conditions and the failure pattern or different empirical correlations from experimental data.

One of the first and most famous contributors was Terzaghi (1943). His equation for determining the bearing capacity of footings is still used today:

$$Q_{\max} = 2\bar{B} (\delta_c c N_c + q_1 N_q + \delta_\gamma \gamma \bar{B} N_\gamma) \quad (2)$$

where

$2\bar{B}$ = the width of footing

N_c, N_q, N_γ = the bearing factors

δ_c, δ_γ = the shape factors

q_1 = overburden pressure

γ = unit weight of soil

c = cohesion

The bearing capacity factors and the shape factors are dimensionless factors dependent on the internal angle of friction, ϕ , of the soil. For cohesionless soils ($c = 0$), the equation can be written as

$$Q_{\max} = 2\bar{B}(q_1 N_q + \delta_Y \gamma \bar{B} N_\gamma) \quad (2a)$$

For piles, the γN_γ term becomes negligible compared to the $q_1 N_q$ term and yields the equation

$$P_t = A_t(q_1 N_q) \quad (2b)$$

where

$$q_{\max} = q_1 N_q$$

A_t = the area of the tip of the pile

Other derivations for ultimate tip-bearing capacity using the same general assumptions but different failure patterns have been developed. These solutions are presented in Figure 4 for the different failure patterns that have been used. For sands, some of the various numerical values are plotted in Figure 5 to show the wide range of the bearing capacity factors, N_q . A good review of bearing capacity equations for piles can be found in Sherman, Holloway, and Trahan (1974).

Skin Friction

The skin friction represents the maximum shear resistance developed at the pile-soil interface. The evaluation of the ultimate skin friction is based on the simple laws of physics for the sliding of two rigid bodies surface to surface. The unit resistance of two

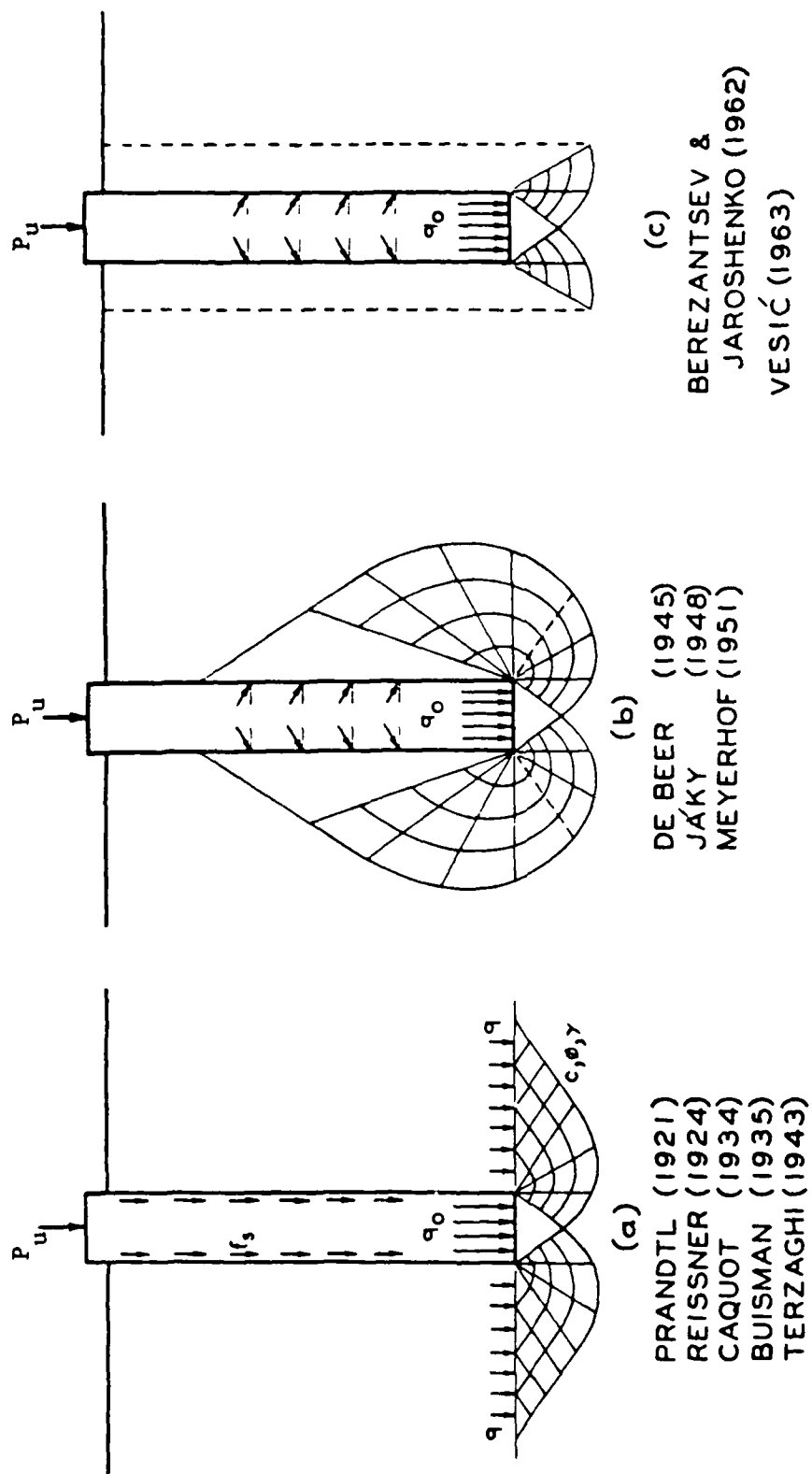


Figure 4. Pile Foundation Failure Patterns (Vesic 1967)

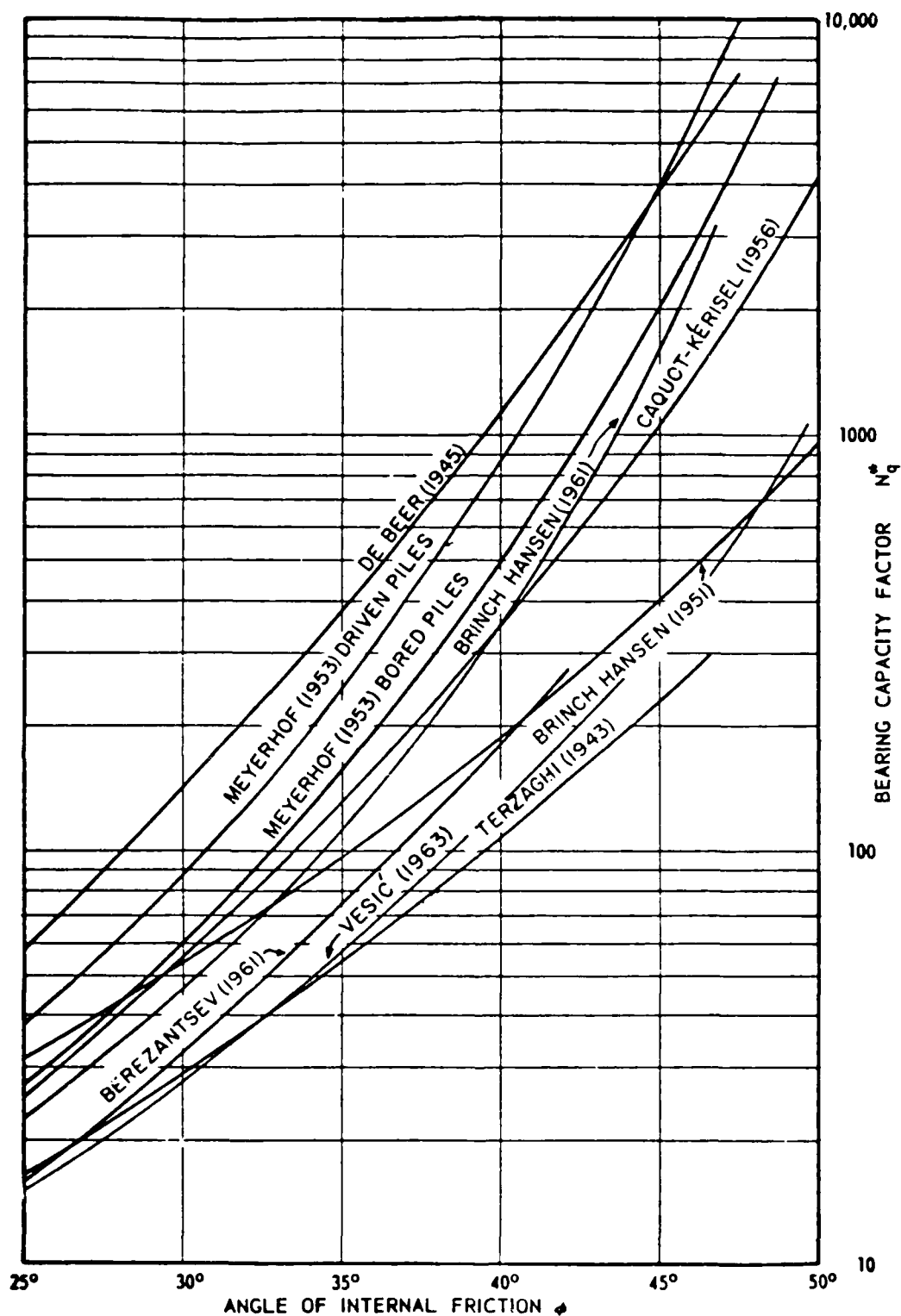


Figure 5. Bearing Capacity for Deep Circular Foundations
(After Vesic 1967)

sliding surfaces is due to the friction and the adhesion of these two surfaces:

$$f = c_a + \sigma_n \tan \delta \quad (3)$$

where

c_a = the adhesion between the shaft and soil

σ_n = the normal stress on the shaft

$\tan \delta$ = the coefficient of friction between the shaft and soil

For sands, the adhesion is equal to zero, and the side resistance is due only to friction. The normal stress is assumed to be equal to the horizontal earth pressure where the horizontal earth pressure is determined by multiplying the vertical stress at a point by the coefficient of lateral earth pressure, K . The vertical stress is taken as the effective overburden pressure. The unit side resistance is

$$f = K \gamma D \tan \delta \quad (3a)$$

and the total side resistance is

$$P_s = \frac{\gamma D^2}{2} \tan \delta A_s \quad (4)$$

where

A_s = the surface area of the pile shaft

γD = effective overburden pressure

Pile-Driving Formulas

The equations which relate the resistance of penetration of the pile under the blow of the hammer to the static resistance of the pile against a vertical static load are known as dynamic pile formulas. For almost a century, foundation engineers have tried to obtain the information needed to design pile foundations by measuring the

penetration of the pile due to a hammer of known weight being dropped on the head of the pile from a known height. The dynamic pile formulas enjoy great popularity among practicing engineers due to their simple procedure for design.

The editors of Engineering News have on file over 450 different pile-driving formulas. The reliability of a number of these formulas for predicting the capacity of piles has been investigated by Sorensen and Hansen (1957), Agerschau (1962), Flaate (1964), Housel (1966), and Olsen and Flaate (1967). These studies are summarized in Poulos and Davis (1980). In the 450 different formulas for predicting the ultimate pile capacity from the hammer blow count, the values of ultimate capacity vary over a very wide range. These formulas, no matter how sophisticated, group various parameters in one lump sum adjustment making it very difficult to determine the factors controlling pile capacity. The poor degree of reliability demonstrated by the pile-driving formulas has reduced their use to that of merely a check for the relative capacity of piles within the same foundation.

In the 1930's, it was recognized that the behavior of a pile being driven was not governed by a simple dynamic formula but rather by a one-dimensional wave equation. An exact mathematical solution to the wave equation was not possible for most practical problems. In 1960, A. E. L. Smith developed numerical procedures based on direct element idealization of the hammer-pile-soil system (Figure 6) which could be used for extremely complex pile-driving problems.

Texas A&M University has conducted extensive research on the application of the wave equation to pile-driving analysis and has developed a computer program to analyze a single pile during driving.

The wave equation models the behavior of the pile due to driving much better than the pile-driving formulas. The model allows for many of the lump variables in pile-driving formulas to be investigated independently.

All pile driving analysis procedures have a deficiency that leads to uncertainty of the static ultimate pile capacity. One assumption which is inherent in this method is that the dynamic resistance (the resistance to rapid penetration) is identical with static resistance under slow penetration. The rapid penetration is resisted not only by skin friction, cohesion, and point resistance, but also by the viscosity of the soil.

The method requires an assumed resistance from the soil and a distribution of that resistance along the pile shaft. This is the focal point for many of the uncertainties in the method. Accuracy in applying the wave equation is highly dependent on the assumed rheological model of soil resistance. The dynamic pile-soil interaction behavior is extremely complex. As a pile penetrates, discontinuous shear deformations develop at the tip and along the shaft. Beneath the tip, the soil is compressed and displaced as the region adjacent to the tip is sheared and deformed. The soil along the shaft is severely sheared. Rapid hammer blows on the head of the pile may severely reduce the skin friction from that of the static condition.

Soil behavior is a function of the stress-strain history, in situ stress, stress path, and strain rate. The driving of a pile induces excess pore water pressures in the surrounding soil which alter the stress-strain behavior of the soil. Determining the representative soil parameters for the pile-driving analysis is at best a crude exercise of engineering judgment.

New Concepts

The approaches in the previous section are based on finding the ultimate capacity of a pile with no regard to the deformation necessary to reach this ultimate capacity. Both methods arrive at the ultimate capacity of a pile by assuming that the maximum bearing capacity of the soil at the tip of the pile and the maximum shear resistance of the soil at the pile-soil interface along the pile shaft are mobilized at the same time with no consideration to the displacement compatibility of the pile-soil system.

Vesic (1977a) states that the static formula contains an implied assumption that both the pile tip and all points of the shaft have moved sufficiently with respect to adjacent soil to develop simultaneously the ultimate tip and side resistance of the pile. The displacement required for maximum side resistance is small in comparison to the displacement required to achieve the ultimate tip capacity (Figure 7). In medium to dense sand, an ultimate tip capacity may never be reached.

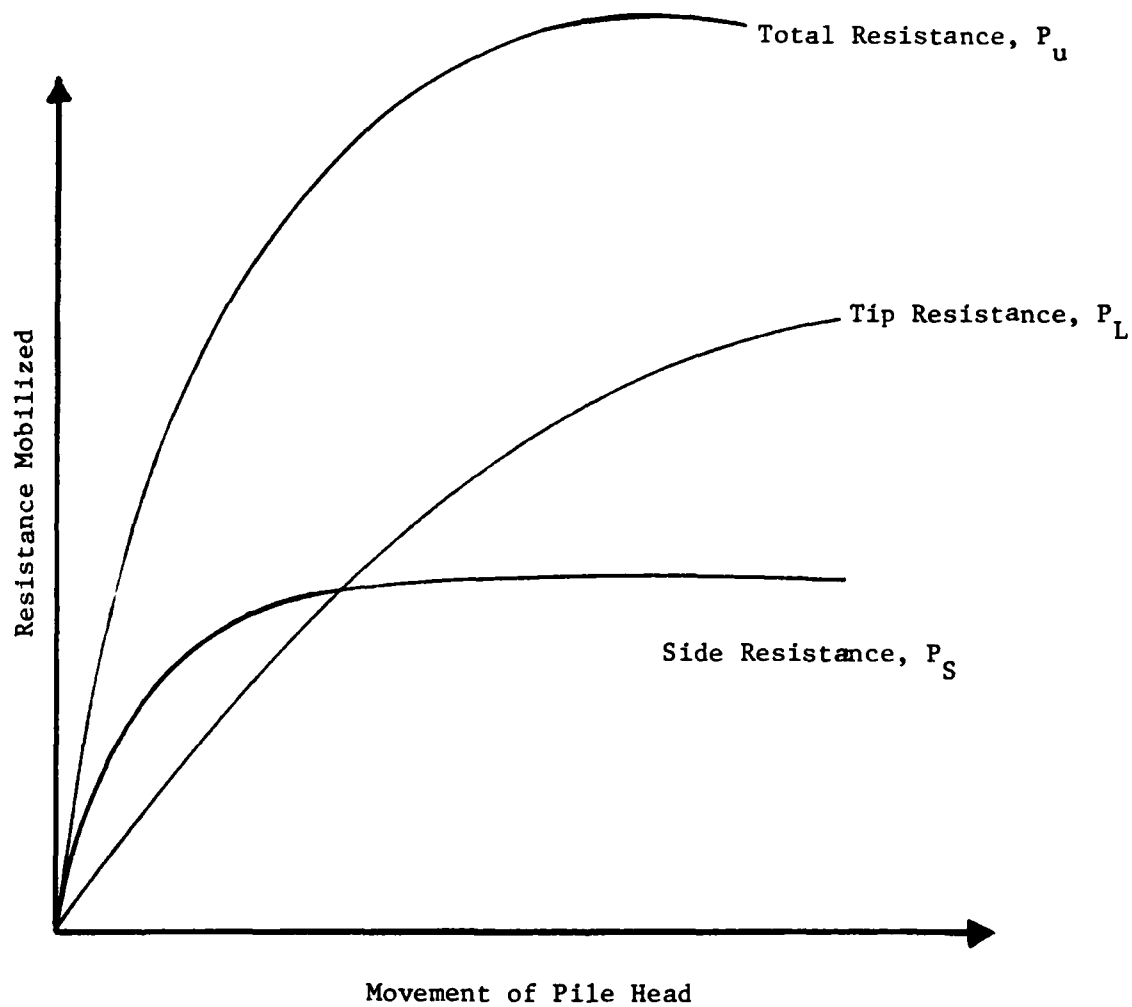


Figure 7. Typical Load-Movement Characteristics of an Axially Loaded Pile in Sand

Without question, the best method for the design of pile foundations has been to base the design on field load tests at the site under actual conditions. A load test will yield the load-displacement behavior of the head and tip of the pile. From this load-displacement curve, the ultimate capacity can be determined by applying a given failure criterion. The failure criteria are based on allowable displacement. Allowable displacement is the displacement that will not cause damage to the superstructure. It would seem logical that any new theoretical or analytical approach would consider displacement of the pile head, although this has not been the case until the present.

Not only is the load-displacement behavior of the pile important in determining the load carrying capacity of pile, but it is also important for predicting the performance of the superstructure. Traditionally, the design of a major facility is divided into two components: the design of the superstructure, and the design of the foundation. The design of the superstructure, is based on assumption of a rigid foundation. The loads are applied and analyzed to yield the shears, moments, and thrusts in the structural members and the loads to be transmitted to the foundation. The foundation is then designed to carry these loads. The design of the foundation is often divided into two parts itself: ultimate load carrying capacity, and ultimate settlement. The displacements that the foundation undergoes are generally not considered in the design of the superstructure,

although in reality these displacements may affect the shear, moment, and thrust within the superstructure and then ultimately affect the design of the total structure.

In recent years, a number of investigators have been exploring theoretical approaches that consider the load-deformation behavior between the structure and the soil. These types of analyses are called Soil-Structure Interaction (SSI) analyses. Two basic approaches have been explored by the investigators: one based on modeling the soil as a continuous medium, and the other based on modeling the soil as a set of discrete springs.

To model soil as a continuous medium, one must rely on the engineering field of continuum mechanics to derive the theoretical approach. For complex conditions which include most soil problems, closed-form solutions have a very limited application. A sophisticated approximation must be employed. Such procedures are finite element, finite difference, and boundary element solutions. The key to arriving at a useful theoretical approach of this type is in choosing the correct stress-strain behavior of the soil and the soil-structure interface. To arrive at a stress-strain model for soil that will be of practical application, there must be some means for predicting the behavior either by in situ testing or laboratory experimentation. Without this, the model is virtually useless as a tool for design or analysis. General stress-strain models available from the field of continuum mechanics are linear elastic, plastic,

nonlinear elastic, viscoelastic, or some combination of these. Of these models, the elastic solid is the simplest to use and the one most often applied to pile foundations.

Elastic Solid Model

D'Appolonia and Romuadi (1963) were among of the first to utilize elastic theory in the analysis of load transfer in end bearing piles. Since then a number of investigators have employed elastic theory in the analysis of pile foundations: Thurman and D'Appolonia (1965), Nair (1967), Poulos and Davis (1968), Poulos and Mattes (1969a, 1969b), Butterfield and Banerjee (1971a, 1971b), Banerjee and Davies (1977), and Randolph and Wroth (1978). In this approach the pile is generally divided into uniformly loaded elements whose displacement must be compatible with the surrounding soil. The displacements in the compressible pile element are due to an imposed axial load at the pile head. The displacement in the soil is due to stresses induced from the pile shaft and tip. These stresses and displacements are computed using Mindlin's (1936) equations for a load within an elastic continuum. The major difference between these procedures is in the shear stress distribution along the pile shaft: whether a point load, uniformly loaded circular area at the center of each element, or uniformly distributed load around the circumference of each element. The latter has been found to be the most satisfactory (Poulos and Davis 1980). A detailed description of the approach is presented in Poulos and Davis (1980).

With use of Mindlin's equations, the effect of the shear stress at one point on the shaft or at the tip can be considered for all other points within the system. The soil surrounding the pile is assumed to be a homogeneous, linear elastic, isotropic solid defined by a modulus of elasticity, E_s , and a Poisson's ratio, γ_s , (Figure 8). The pile is divided into elements (Figure 9). The load transfer for the pile element is

$$\Delta P_i = P_i - P_{i-1} = f(z_i) \quad (5)$$

The load-transfer function, f_z , for the soil is replaced by a set of n equations of the form

$$U_{s,i} = \frac{B}{E_s} \sum_{j=1}^n I_{ij} f_j + I_{ip} q_j \quad (6)$$

and an equation for the tip

$$U_t = \frac{B}{E_s} \sum_{j=1}^n I_{tj} f_j + I_{tt} q_t \quad (7)$$

where U = the displacements vector of the soil

I_{ij} = the influence factor for settlement of element j caused by forces P_j . The influence factors are determined by Mindlin's solution for stresses and displacement in a semi-infinite elastic solid from point loads in the interior of the solid. If no slippage occur, there are n equations of the form

$$U_{p,j+1} - U_{p,j} = \frac{P \Delta L}{E_p A} \quad (8)$$

If slippage occurs they are replaced by

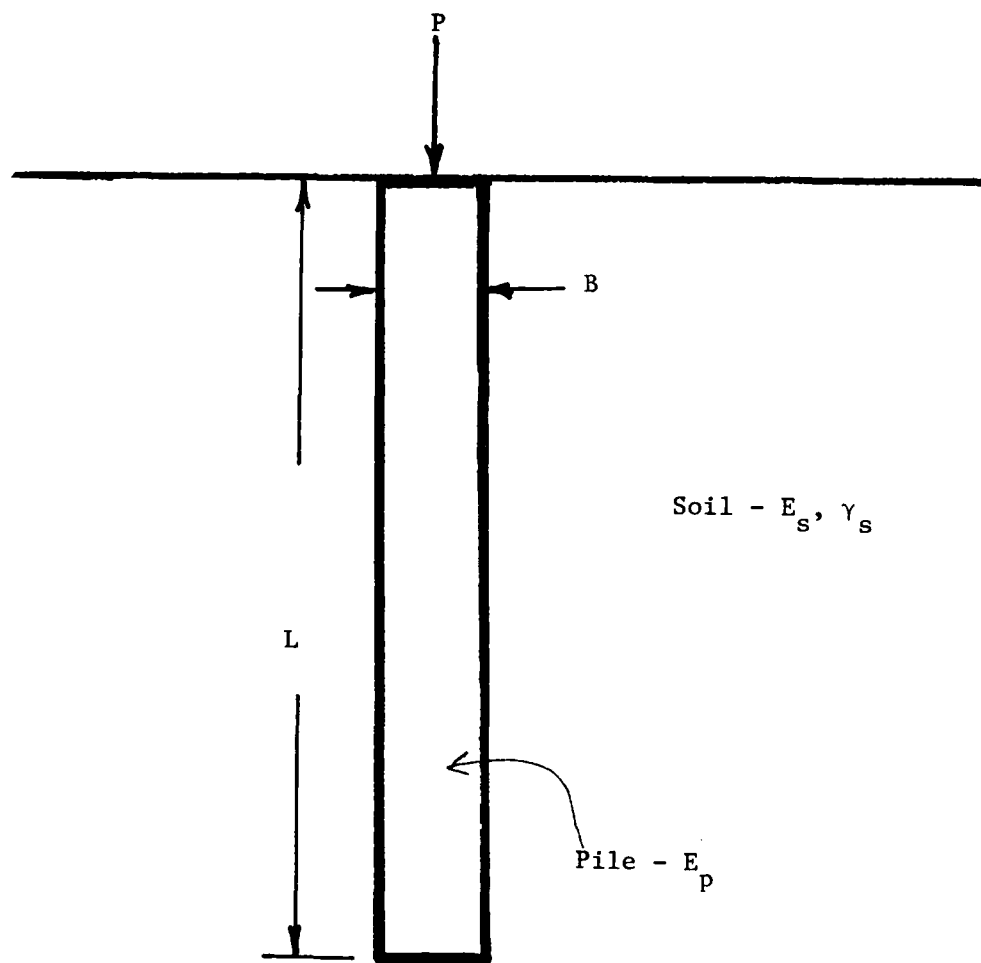


Figure 8. Problem Idealization

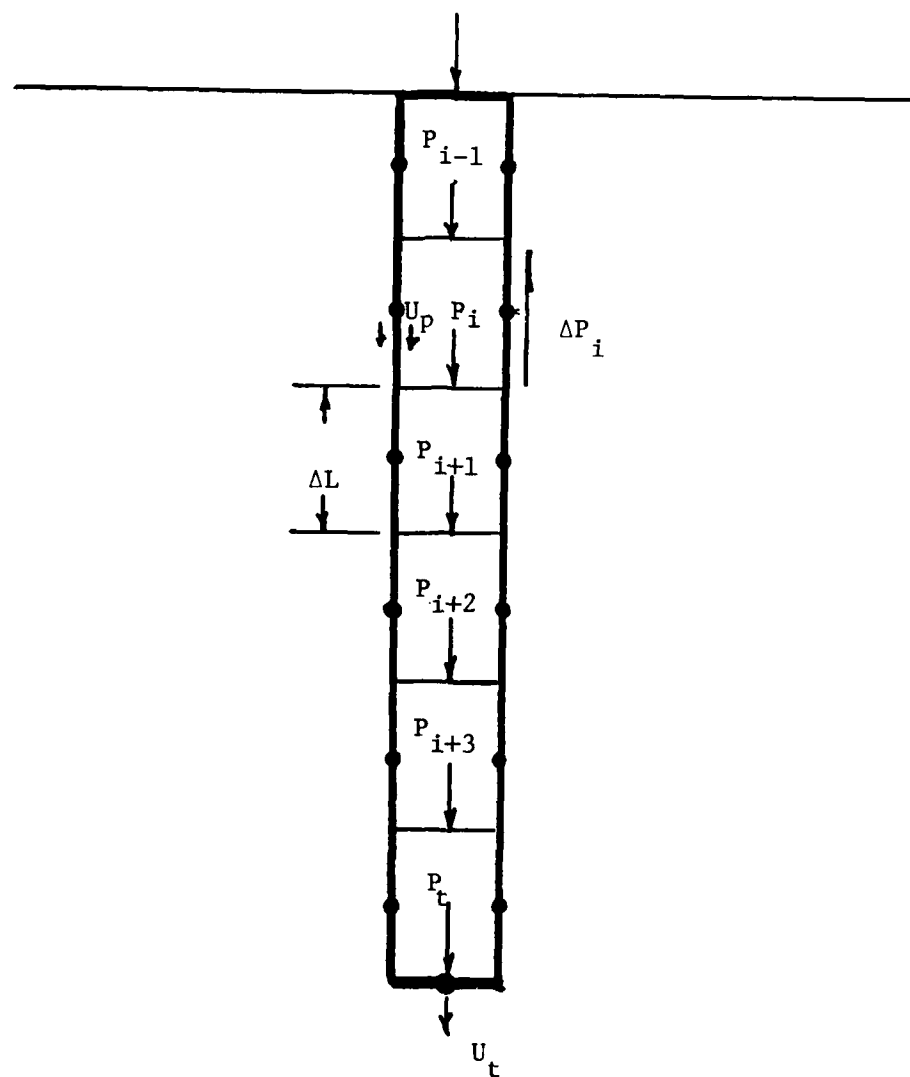


Figure 9. Load-Transfer Analysis by Elastic Solid Approach

$$\Delta P_i = f_s A_s \Delta L$$

(9)

where f_s is the maximum side resistance for the point considered.

This yields $2n+1$ equations for n unknown forces and $n+1$ unknown displacements. These are written in a matrix form and solved on a digital computer.

The assumption of a linear elastic system greatly oversimplifies the pile-soil system. Poulos and Davis (1980) present empirical corrections for pile driving effects, nonlinear stress-strain behavior, etc., all based on observations from the field and model tests. The method allows for tension to occur in the soil which most soils can take very little of, if any. Load transfer by Mindlin's solution may induce significant tensile stress beyond the point of the load application. Tensile stress could cause a considerably different stress distribution surrounding the pile than would actually occur in the soil.

This is shown in Figure 10: the left side of the distribution is due to uniform shear load along the pile shaft; the right side shows the distribution due to a point load. Tensile stresses are developed along the shaft due to the tip load. For the stresses due to skin friction to have an effect along the shaft, they must be significantly larger than the tip load.

This model has some serious limitations as stated by two of its most prominent advocates, Poulos and Davis (1980): "Soil and rock are

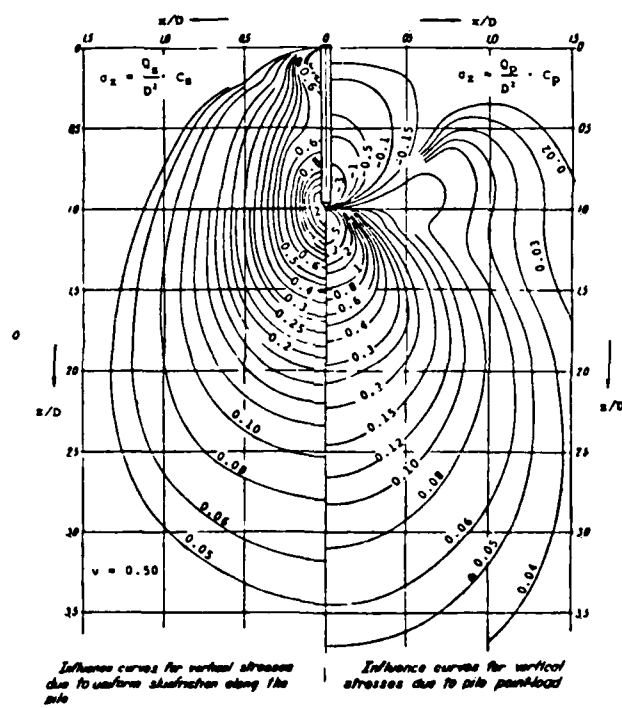


Figure 10. Distribution of Vertical Stresses Around a Pile in an Elastic Continuum (After Vesic 1977)

not ideal elastic materials in that the stress and strain are not linearly related, strains are not fully recoverable on reduction in stress, and strains are not independent of time. The best that can be said is that, the strains in the soil increase as the stress increases." Even with these limitations, the linear elastic model is often utilized. Attempts to use more sophisticated stress-strain behavior models have shown some promise, but they are too difficult to use in practice because of the complex numerical procedures and the difficulty in determining soil parameters from laboratory or in situ tests.

Discrete Spring Model

Modeling the soil as a set of discrete springs was first suggested by Winkler for beams on elastic foundations. The concept was later applied to laterally loaded piles by Matlock and Reese (1960) and to axial loaded piles by Reese and Seed (1957). The discrete set of springs is known as Winkler springs. For beams on elastic foundations, the set of springs is called a Winkler foundation. Axially loaded and laterally loaded pile analyses are classified as beam-column analyses with springs modeling the soil (Figure 11).

These are the general governing differential equations for the beam-column system shown in Figure 12:

$$\frac{d}{dx} \left(EA \frac{du}{dx} \right) - K_x u = q_x \quad (10)$$

$$\frac{d^2}{dx^2} \left(EI \frac{d^2 v}{dx^2} \right) + \frac{d}{dx} \left(P \frac{dv}{dx} \right) + K_y v = q_y \quad (11)$$

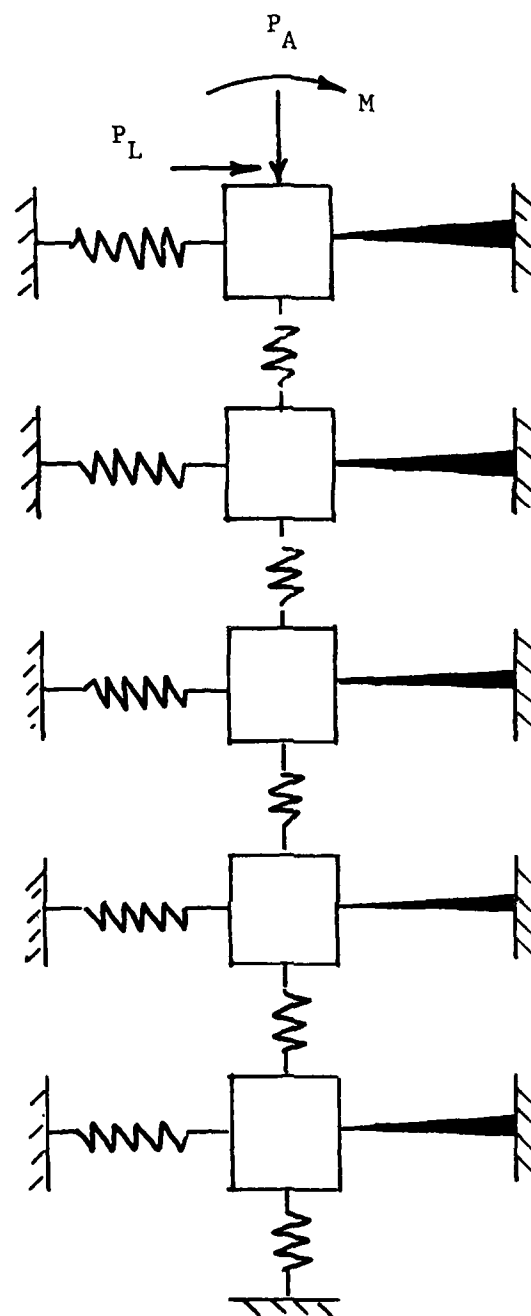


Figure 11. Beam-Column Idealization of a Pile

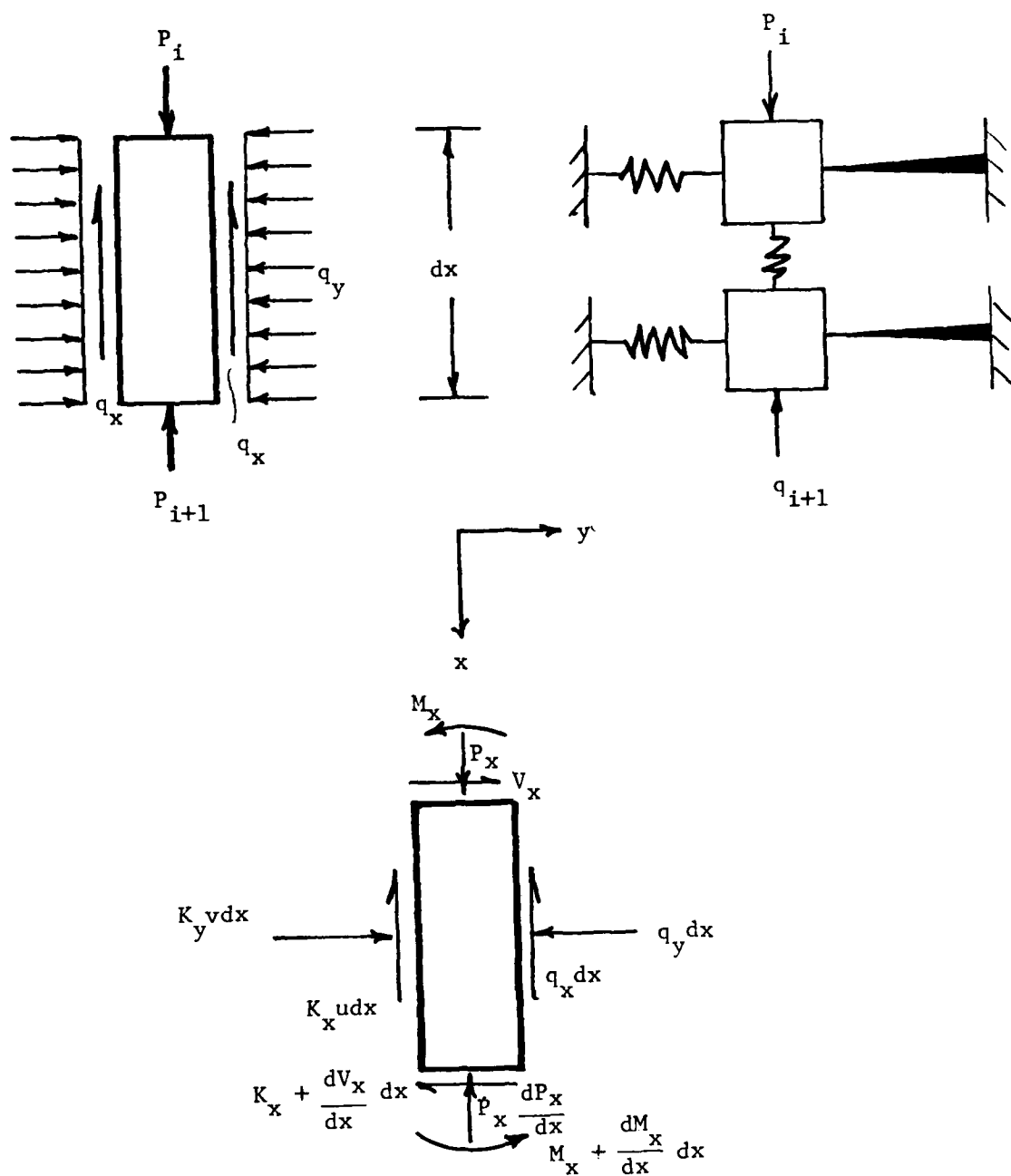


Figure 12. Free Body Diagram for Beam-Column Analysis

where I = moment of inertia

P = axial force

K_y, K_x = spring constants

v, u = displacements in y and x direction, respectively

with the force-deformation relationship as

$$P = -EA \frac{du}{dx} \quad (12)$$

$$M = EI \frac{d^2v}{dx^2} \quad (13)$$

$$V = \frac{d}{dx} \left(EI \frac{d^2v}{dx^2} \right) + P \frac{dv}{dx} \quad (14)$$

Mechanics of an Axially Loaded Pile

A vertical load applied at the head of a vertical pile is resisted by the shearing resistance of soil along the pile shaft and bearing resistance developed at the tip of the pile (Figure 2). Mathematically, this is stated as

$$P_u = \int_{X=0}^{X=L} fAdx + P_t \quad (15)$$

The above is the basis for the static formula (Equation 1). The equation only ensures that the forces along the shaft and at the tip and head of the pile are in equilibrium.

If an increment of the pile is considered, as shown in Figure 13, summing force along the pile (x-direction) using the beam-column equation gives

$$\Sigma F_x = 0 \quad \frac{dP_x}{dx} = K_x(u) \quad (16)$$

with a force-deformation relationship of

$$P = -EA \frac{du}{dx} \quad (17)$$

Substituting the force-deformation relationship into Equation 16 and rearranging yields the governing differential equations:

$$\frac{d}{dx} \left(EA \frac{du}{dx} \right) - K_x(u) = 0 \quad (18)$$

The boundary conditions on the axially loaded pile are

$$\frac{d}{dx} \left(EA \frac{du}{dx} \right) = P_u \quad \text{for } x = 0$$

$$\frac{d}{dx} \left(EA \frac{du}{dx} \right) = P_t \quad \text{for } x = L$$

so the equation can be written as

$$\frac{d}{dx} \left(EA \frac{du}{dx} \right) = K_x(u) \quad (18a)$$

Either a finite difference or a finite element solution can be used to solve these equations.

For the finite element solution, the pile is divided into beam elements with distributed nonlinear springs (Figure 11), and the load-displacement relationship for each element is written to form a system of simultaneous equations:

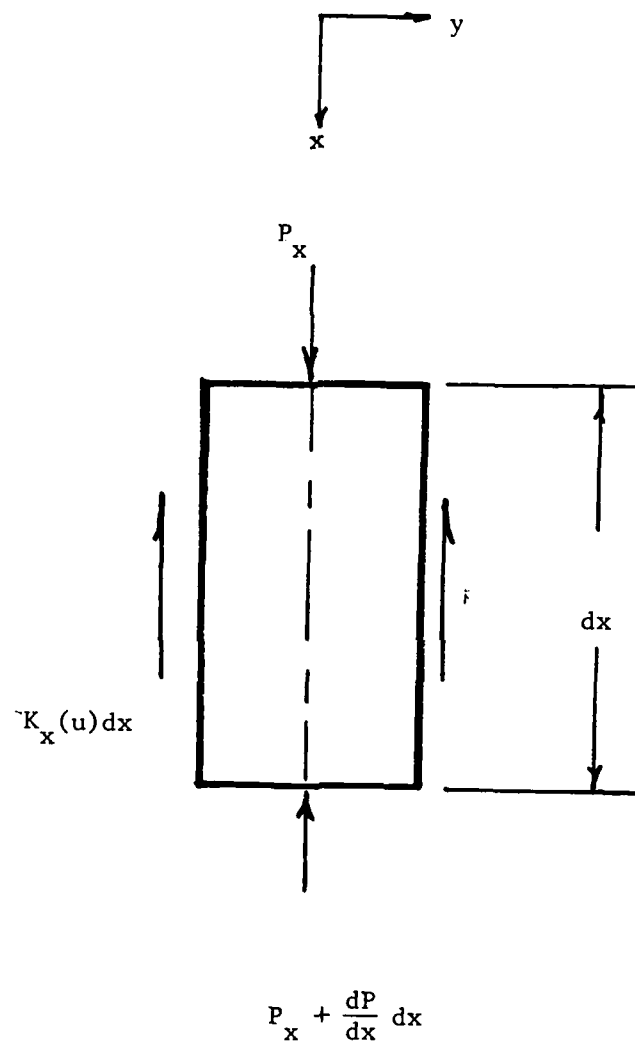


Figure 13. Free Body Diagram for One Increment of An Axially Loaded Pile

$$[F] = [S_b + S_s][U] \quad (19)$$

where

F = forces at end of each element

S_b = axial stiffness of the beam

S_s = stiffness provided by the soil

U = displacement at end of each element

The equation is then solved for the specified boundary conditions, the forces, and the displacements within and along the pile.

For the finite difference solution, the pile is divided into increments as shown in Figure 14, and the force in the pile is described by:

$$P_{i+1} = P_i - \frac{dP_i}{dx} \quad (5)$$

The change in force in the pile is equal to the side resistance:

$$\frac{dP_i}{dx} = K_x(u) \quad (20)$$

Then
$$\frac{dP_i}{dx} = EA \frac{d^2u}{dx^2} \quad (18b)$$

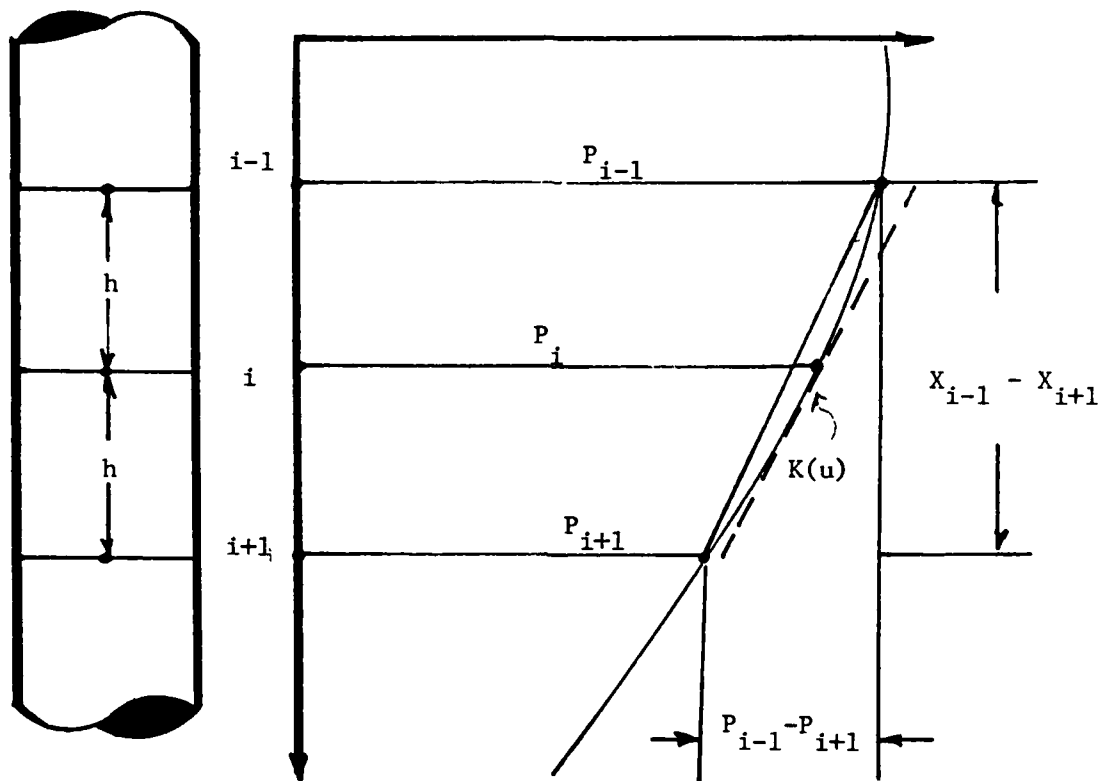
Integrating gives

$$P_i = \frac{du}{dx} (EA) \quad (18c)$$

Writing in finite difference form gives

$$\frac{du}{dx} = \frac{u_{i-1} - u_{i+1}}{2h} \quad (18d)$$

$$\frac{d^2u}{dx^2} = \frac{\frac{du}{dx}_{i-1} - \frac{du}{dx}_{i+1}}{2h} \quad (18c)$$



$$\frac{dP_i}{dx} = \frac{P_{i-1} - P_{i+1}}{X_{i-1} - X_{i+1}}$$

$$2h = X_{i-1} - X_{i+1}$$

$$\frac{dP_i}{dx} = \frac{P_{i-1} - P_{i+1}}{2h} = K(u)$$

Figure 14. Finite Difference Idealization

From Figure 14,

$$K_x(u) = \frac{P_{i-1} - P_{i+1}}{2h} \quad (20a)$$

$$P_{i-1} - P_{i+1} = 2h K_x(u) \quad (20b)$$

The change in force in the pile is assumed to be linear across an increment

$$P_{i-1} - P_i = h K_x(u) \quad (20c)$$

Substituting Equation 18d for du/dx in Equation 18c, P_i , can be written as

$$P_i = EA \frac{u_{i-1} - u_{i+1}}{2h} \quad (20d)$$

Rewritten

$$\frac{2hP_i}{EA} = u_{i-1} - u_{i+1} \quad (20d)$$

If the pile section has a constant E and A, the following is true:

$$\frac{hP_i}{EA} = u_i - u_{i+1} \quad (20e)$$

$$\frac{hP_i}{EA} = u_{i+1} = u_i$$

Thus, starting at the tip, the force is determined and the corresponding displacement, u , is computed. The procedure is continued until the force at the head is obtained.

The load-displacement behavior of piles has been based on field data and empirical correlations with soil parameters. This approach has fallen under criticism by some theoreticians due to the fact that the springs in the system are not connected, making the response of

each spring in the system independent of the others. The interactions between springs along the pile are accounted for in the correlation by developing the spring behavior from field pile data where the interaction of springs is built into the correlation. Criteria for the springs developed from field data have the influence of the continuous nature of the soil implicitly represented.

This brings us to a fundamental question in soil mechanics and foundation engineering. Given that soils are highly discontinuous and are made up of small particles resting on each other, adhering to each other, and chemically bonding to one another, it is difficult to obtain a theoretical model for the soil based on a continuous medium. This has led to two different fundamental approaches to foundation analysis. One approach is derived from the theoretical consideration of the soil as a continuous medium and the geometry configurations of the particular problem. An example of this is the determination of the ultimate bearing capacity of a footing based on Terzaghi's bearing capacity equations derived from limit equilibrium theory. The magnitudes of the bearing capacity factors, N_c , N_q , N_γ , are only dependent on the strength parameters of the soil which are measured by in situ or laboratory tests. Improvements to theoretical approaches are advanced by better analytical and/or numerical procedures and better techniques for estimating the soil properties. The second approach to foundation analysis has been based on empirical correlations. These empirical approaches have been used for decades. An excellent example of this is the correlation between standard penetration tests and liquefaction potential of sands. The

empirical approach can only be as good as the test data that it is based on. Having a large quantity of good quality observations is necessary for finding a good correlation. The empirical approach may be equal to or even better than the theoretical approach, for example, in the determination of liquefaction potential for sands.

The latter approach has been used with great success in the design and analysis of pile foundations, especially laterally loaded piles and axially loaded piles in clay. This extensive usage has been stimulated by a large volume of offshore construction and related research. There has been a lack of information in the literature on axially loaded piles in sands. To develop an empirical approach field data must be available. For piles, the field data are obtained from pile load tests. The next section outlines the procedures that are used to interpret the pile load tests and determine the soil parameters at the test sites.

Review of the Interpretation of Pile Load Test Results

Load tests can be classified under two categories: (1) verification of a design calculation, (2) investigation of the pile-soil system. The load tests employed for verification are generally inexpensive tests yielding the load-displacement behavior of the butt (Figure 15). Only limited information is gained in a test of this type. To investigate the pile-soil interaction, the pile must be instrumented in a fashion that will give the distribution of the load within the pile for a given butt load and displacement (Figure 16). A

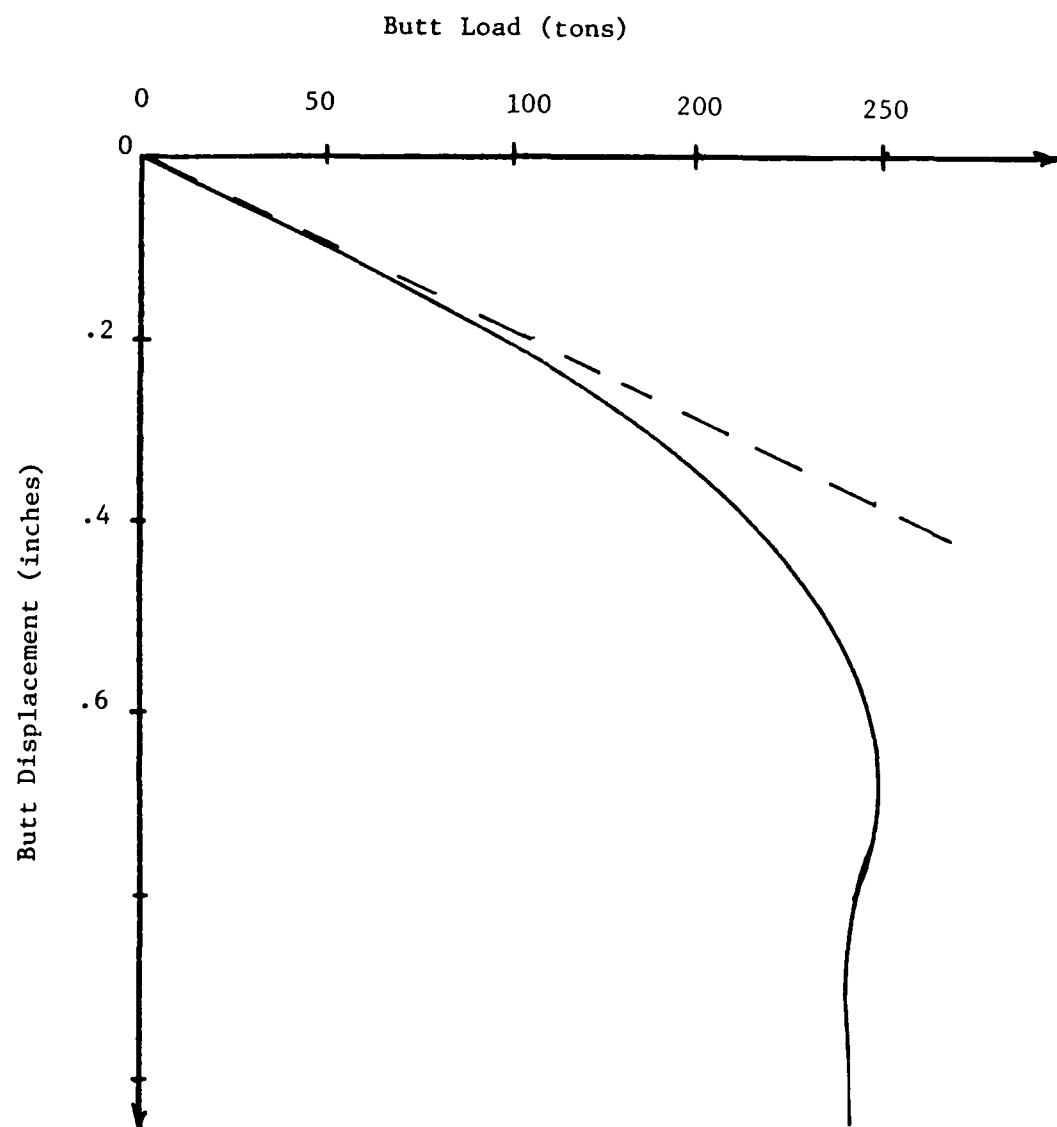


Figure 15. Simple Load Test

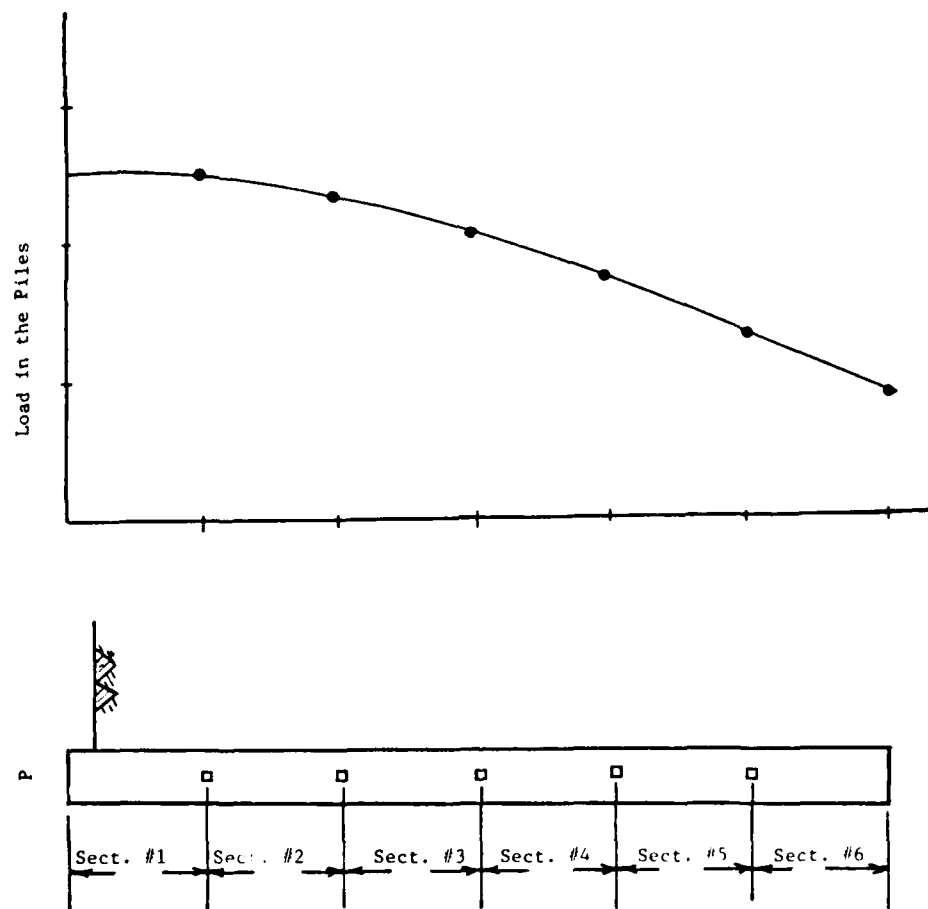


Figure 16. Distribution of Load in a Pile

test of this type requires careful planning and more elaborate instrumentation than the verification test and is more costly. Although more expensive, the test is very cost-effective when weighed against the fundamental insight into the pile-soil interaction that is obtained from the test. Reese (1979) advised that, when possible, the test piles should be loaded to failure, a sizable number should be instrumented, and for nearly all piles the behavior prior to the application of the load should be predicted.

No one single standard procedure exists for the testing of piles subject to axial load. The American Society for Testing and Materials has set forth procedures in "Testing Piles Under Axial Compressive Loading" (D 1143) for the instrumentation and loading of axially loaded piles. Unstrained rods (telltales) and strain gages are the most common instruments used for determining the load distribution in the pile, while load cells are employed to determine the load at the pile head and dial gages to measure the movement.

Piles are instrumented to obtain the axial load at the head versus head settlement, the axial load at the head versus tip settlement, and the load distribution along the pile shaft for each load increment applied. Typical types of plots for this information are shown in Figures 17 and 18. The field data from pile tests do not provide pile-soil interaction information directly. The data must be analyzed and interpreted to yield the necessary information.

Reese (1979) described a method for analyzing data from a test on instrumented deep foundations under axial load. For a given distance along the pile, x_k , and a load distribution curve, the slope

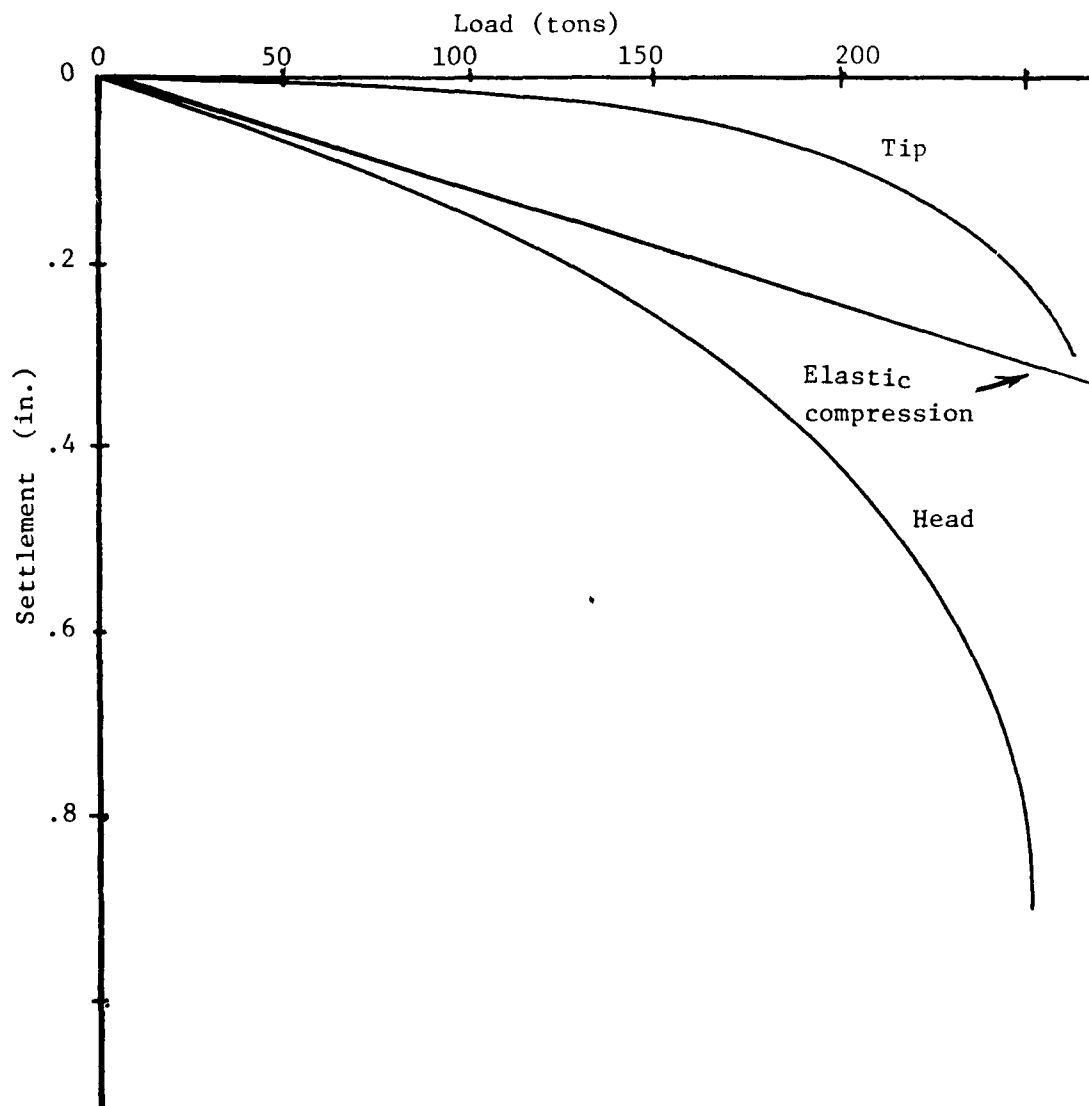


Figure 17. Pile Tip and Head Settlement Versus Butt Load

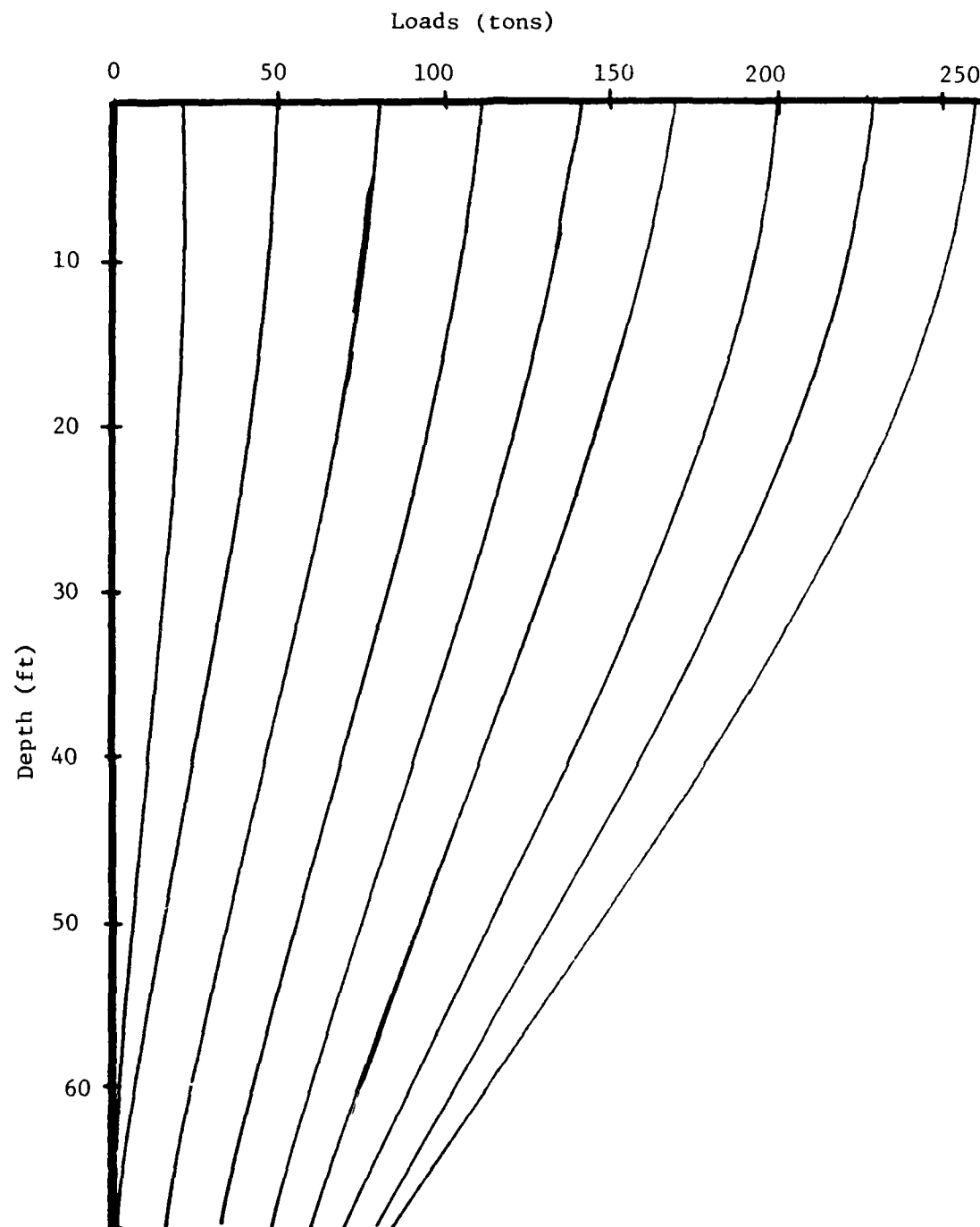


Figure 18. Load Distribution Within Pile Shaft

of that curve, dP/dx , divided by the circumference of the pile at a given length yields the unit load transfer (Figure 19). The integration of the area under the load distribution curve divided by the approximate value of axial stiffness yields the compression of the pile for the lengths selected. That compression subtracted from the movement at the top of the pile for the load being considered yields the vertical movement of the pile, z . Thus, using this procedure, points on the load transfer, f , versus pile movement, z , curves can be plotted at depths x_k (Figure 20).

The detailed steps for analyzing the field data are:

- (1) Starting at the pile head, compute the elastic compression in each pile segment using the average of the measured loads at the ends of the segment (Figure 21).
- (2) Determine the tip settlement for the load increment considered by subtracting from the displacement at the pile head the total elastic compression of the pile.
- (3) Starting at the tip, calculate the total displacement of the midpoint of each segment by considering the settlement of the tip and the elastic compression.
- (4) The load transfer within a section is assumed to vary linearly throughout the section. Starting at the pile head the difference between the measured loads at the top and bottom of each section is assumed to be the load transferred to the surrounding soil. Dividing the difference by the surface area of that section gives the shear transferred to the soil at the midpoint of that section.
- (5) Then, plotting the shear transfer and total movement at the midpoint of each section for each load increment gives the shear transfer versus pile movement along the shaft (Figure 20).

The transfer along a shaft can be estimated for piles with just the information on tip and head movement. The skin friction can be

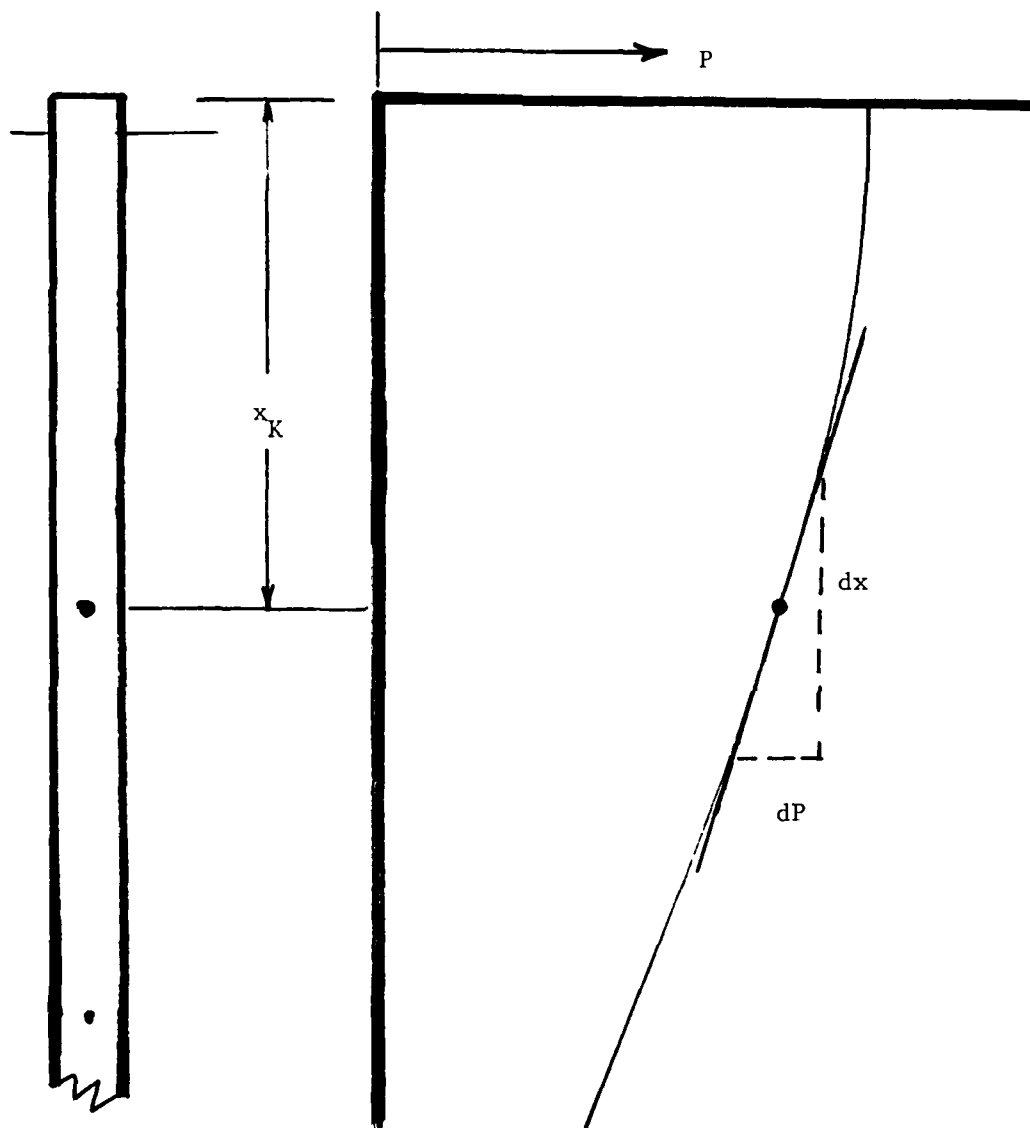


Figure 19. Load Transfer from Load Distribution Data
(After Reese 1978)

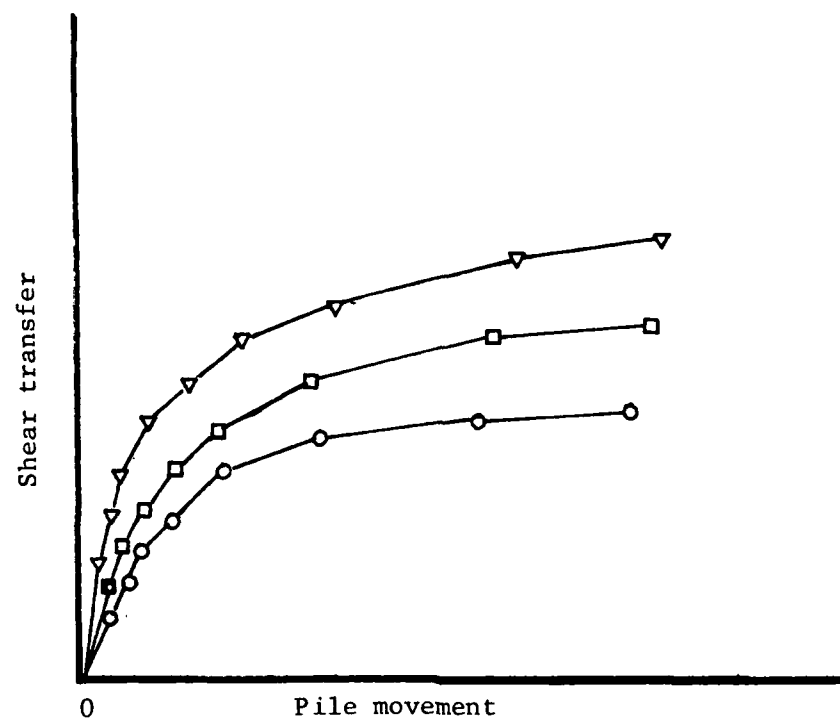
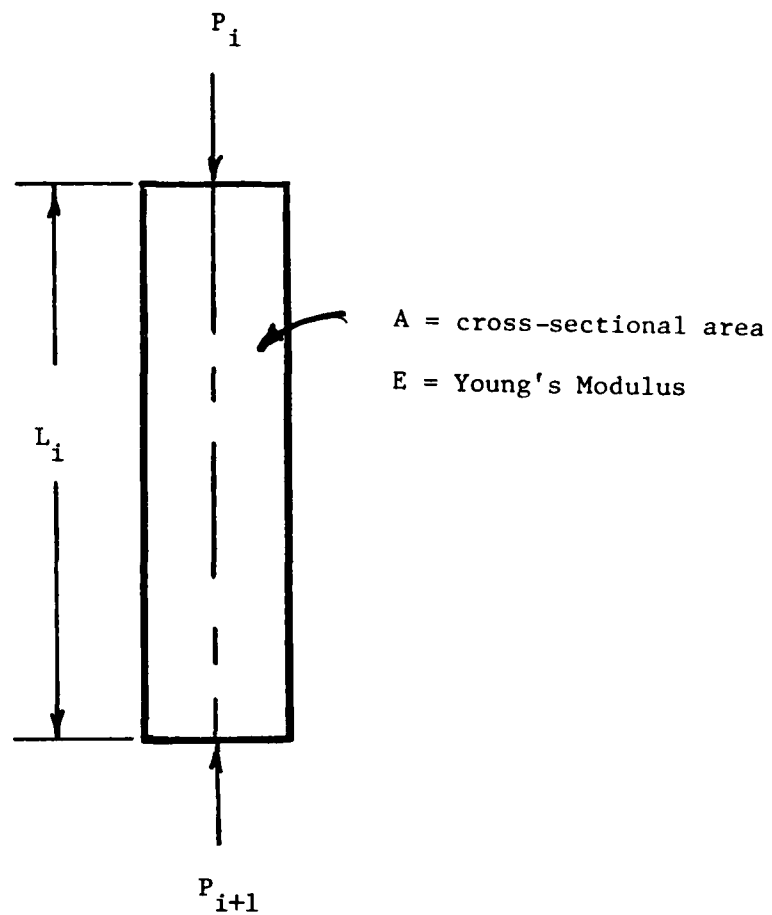


Figure 20. Plot of Shear Transfer Versus Pile Movement (After Reese 1978)



$$\Delta_i = \frac{\frac{P_i + P_{i+1}}{2} L_i}{A E}$$

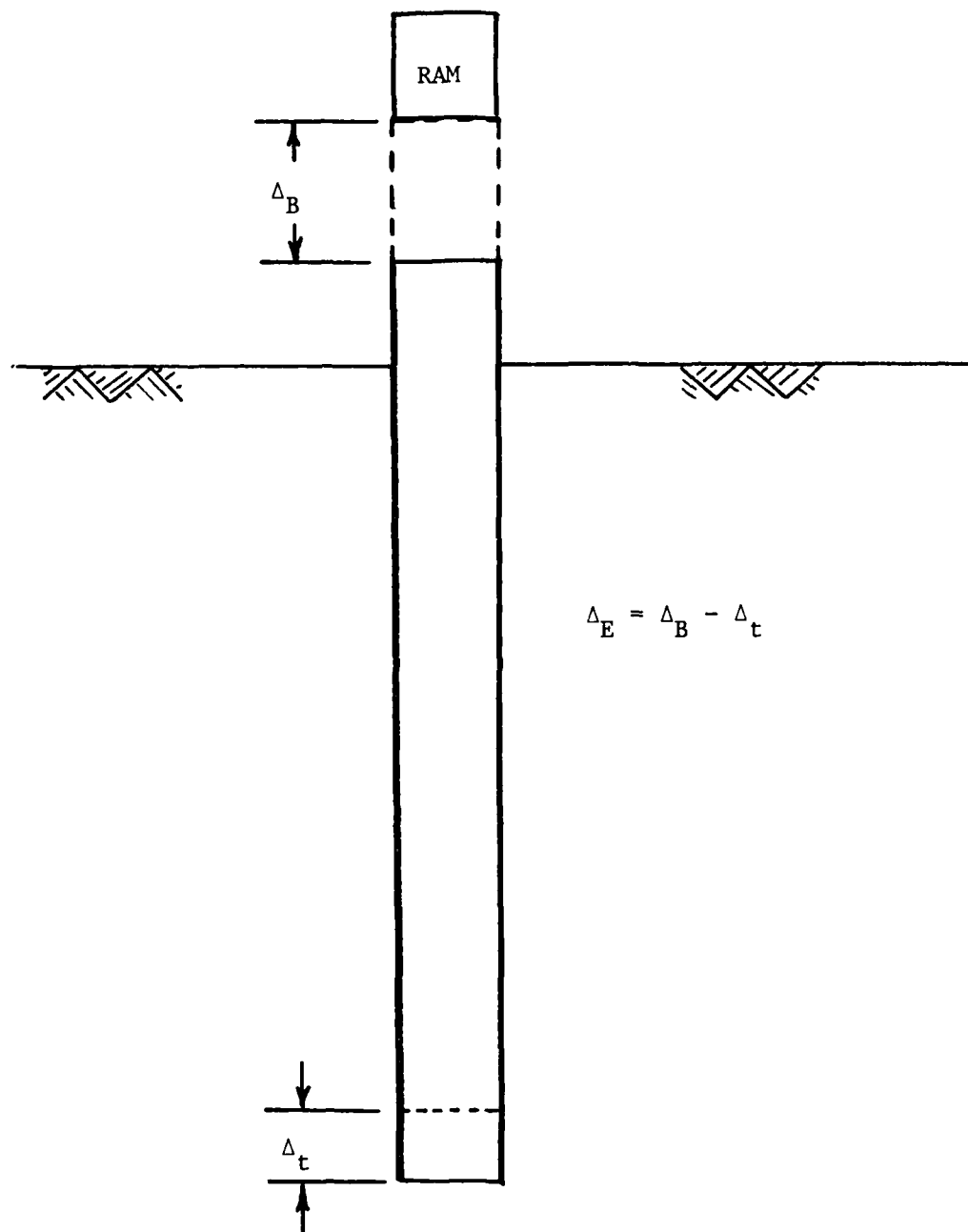
Figure 21. Elastic Compression of Pile Segment

obtained by plotting two curves: a curve showing the elastic compression in the pile as a function of the applied load, and a curve showing the downward movement of the pile tip as a function of applied load. From the first of these two plots, it is possible to find out whether or not the pile is behaving principally as a friction pile or an end bearing pile. From the second curve using assumptions that the amount of skin friction support for the pile is limited to some maximum value, this maximum value of skin friction is substantially mobilized with pile movements considerably less than required to cause a bearing capacity failure. The bearing stratum will deflect linearly until the applied load approaches its ultimate bearing capacity. The curve defining tip behavior can then be constructed.

Residual Stresses

To understand and determine the exact performance of pile tests, the residual stresses in the pile must be accounted for. The process of impact driving induces stresses in the pile-soil system before piles are ever loaded in the testing procedure. If the ram delivers its blow to the pile head the momentum of the ram is transferred to the pile creating an impulse energy that compresses the pile and impels it into the soil (Figure 22). After each blow, the total rebound of the pile is prevented by the side resistance on the shaft causing residual compression stresses to remain in the pile, which can be shown using a mechanical model of the pile-soil system (Figure 23).

The side resistance in the upper section of the pile is due to negative skin friction, while in the lower section the side resistance



Δ_B = movement of the butt from the blow of the ram
 Δ_t = movement of the tip from the blow of the ram
 Δ_E = elastic compression

Figure 22. Physical Representation of Driving

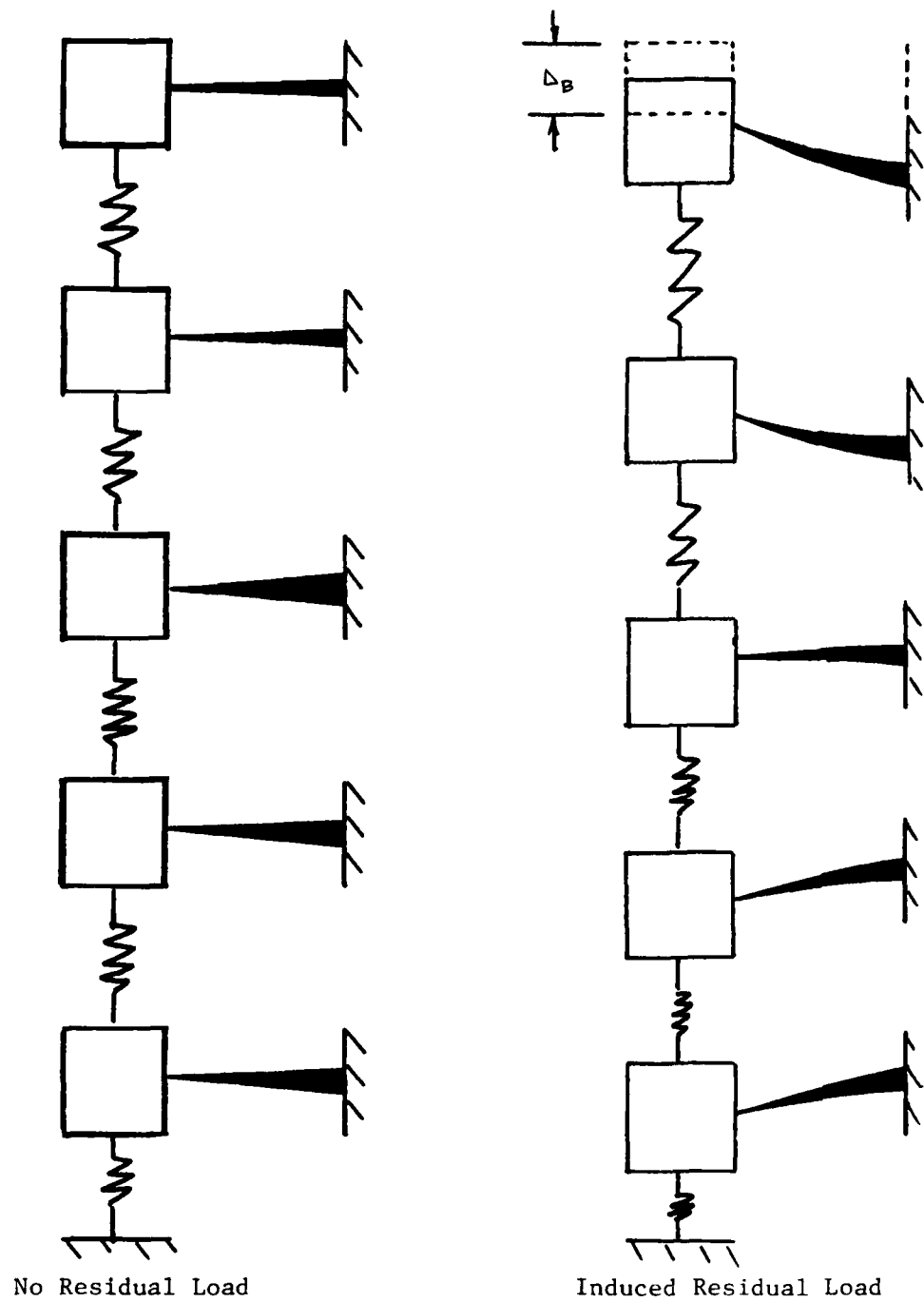
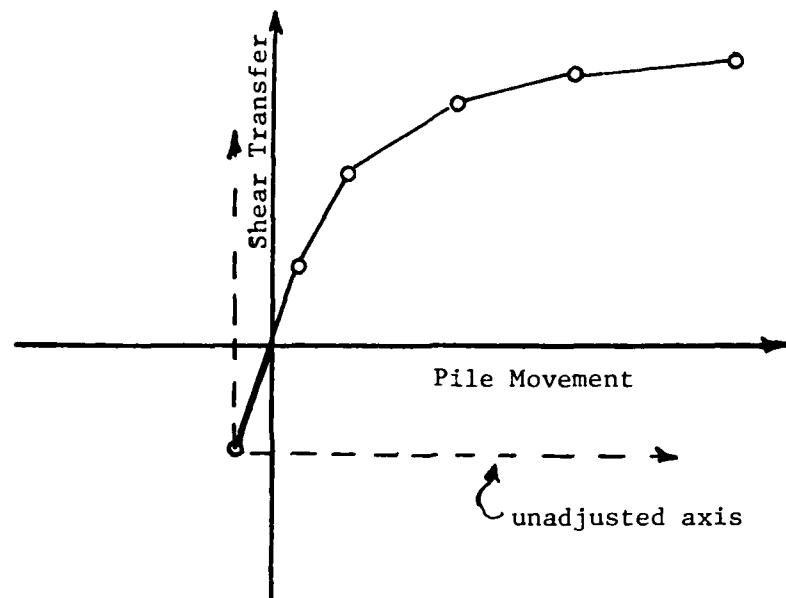


Figure 23. Mechanical Model of a Pile Before and After Driving

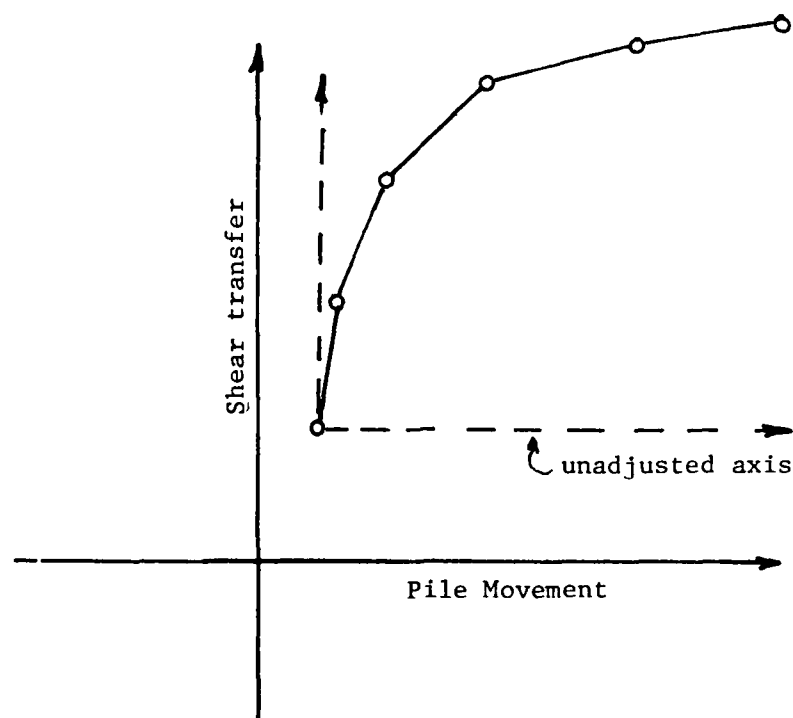
results in preloading the soil before a load is even applied to the pile. Figure 24 show the soil behavior in the upper and lower section of the pile due to residual load in the pile. The effect of not adjusting for the residual load is shown in Figure 24 also. If the plot is not adjusted, the shear transfer can be grossly overestimated in the upper section and underestimated in the lower section.

The importance of the effects of residual stresses on the interpretation of load test data can best be demonstrated by hypothetical pile test results shown in Figure 25. Curve mc and curve mt in Figure 25a show the measured load distribution in the pile. The resulting side resistance from the measured load distribution is shown in Figure 25b. The residual stresses are shown as curves r. Adjusting the measured load distribution for residual loads yields the actual load distribution in the pile as a result of the applied loads, curves c and t. If the measured distribution was used without adjustment for residual stresses, it would lead to an overestimated side resistance and an underestimated tip capacity. Failure to consider the residual stress in the pile could cause serious deficiencies in a design based upon the pile test.

Residual stresses in pile tests were first recognized to be significant in the Old River Low-Sill structure (Mansur and Kaufman 1958). An effort was made to measure the residual stresses by means of strain rods, but this proved to be unsuccessful as a result of temperature changes and manipulation of the strain rods prior to and during driving. In the Arkansas River pile tests, residual stresses were recorded and considered in the analysis of the test data. The



Upper Section



Lower Section

Figure 24. Load-Transfer Behavior Under Residual Loading

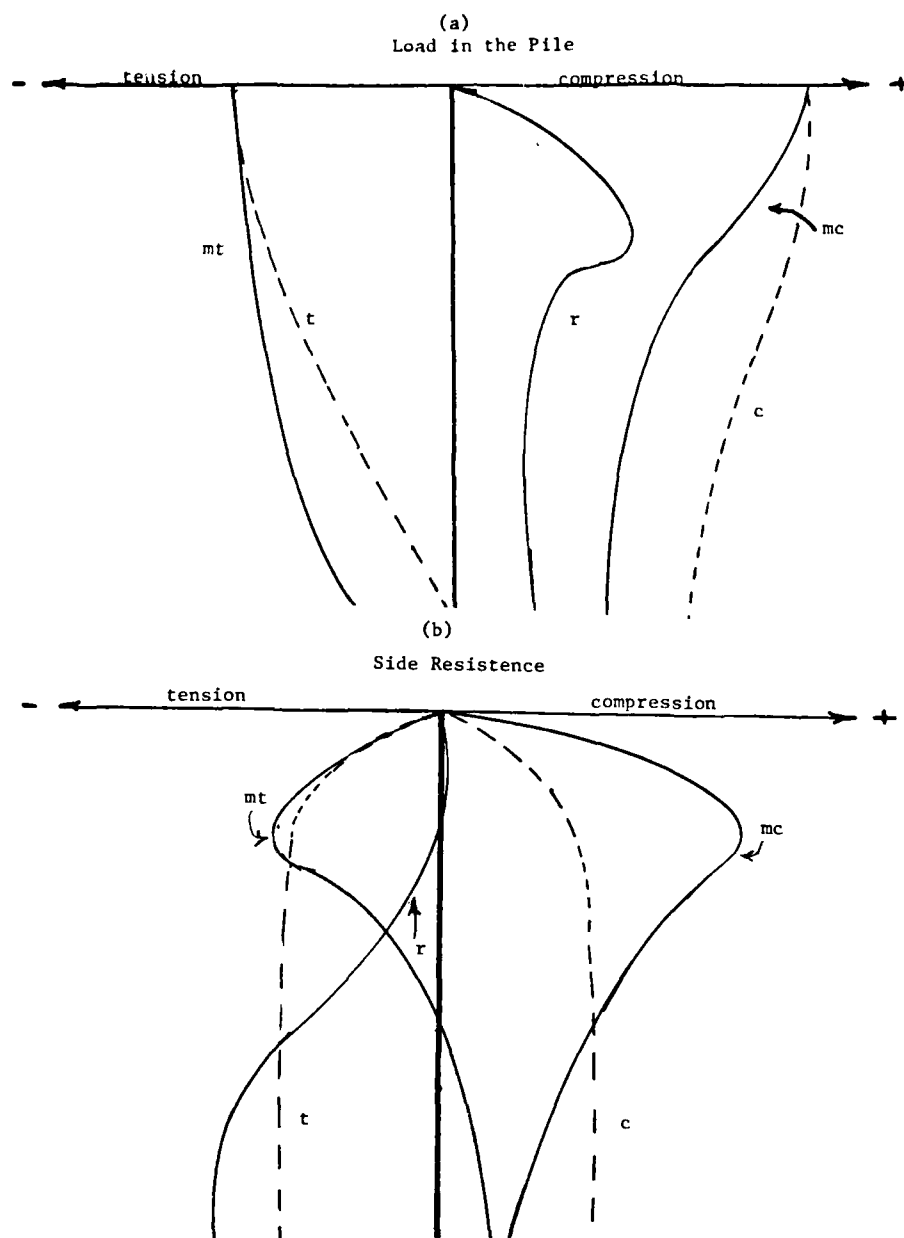


Figure 25. Hypothetical Pile Test to Show Effect of Residual Loads in the Pile

graph procedure used in the Arkansas River tests was presented by Hunter and Davisson (1969). Their methodology calls for the test pile to be instrumented so that the distribution of loads along the shaft can be determined. Readings are made before driving, after driving, and during each load cycle. The load distribution in the pile is plotted in Figure 25. For a compression test, the measured loads at each instrumentation point in the pile at zero butt load are added to the measured load distribution under an incremental butt load. The newly formed distribution from this procedure is curve c (Figure 25a); it is adjusted for residual stresses from driving or from the previous load cycle. For tension tests (Figure 25), residual loads in the pile are shown at the end of the compression test by curve r. Curve mt is the load distribution in the pile after the tension load was applied. Curve mt shows a tension load at the tip; however, this is an impossibility, because the resistance at the tip has to be zero. The compression test locked in residual stresses in the pile causing the reading at the tip to show a tension load. Hunter and Davisson's (1969) adjustment for a tension test was to subtract the measured loads in the pile at the end of the compression test curve, r, from the measured load distribution for the applied tension load at the butt. The newly formed distribution, curve t, is the load transferred to the soil from the shaft.

Holloway, Clough, and Vesic (1978) presented a more sophisticated procedure which would approximate pile-soil interaction behavior throughout the installation and load test. This is based on the one-dimensional wave equations for the driving behavior coupled

with a static equilibrium solution. A finite difference computer program was written for the analysis. The method also can be used to predict residual stresses due to driving before the actual pile driving and can be used to determine stresses in the pile from driving.

Standard Penetration Test

In cohesionless soils, field investigations have been limited due to the fact that undisturbed samples of high quality are hard to obtain. For this reason, standard penetration test (SPT) results are used to estimate the angle of internal friction for the sands involved in the tests in this report. The angle of internal friction and the relative density have significant effects on the unit side resistance and point resistance. This was shown in Castello's (1980) report. Since the standard penetration test is the only feasible means of determining material properties, a closer look should be taken at the relationship between the standard penetration test with results given in blows per foot (N values) of penetration and the angle of internal friction. Correlations have been developed between the two. To obtain accurate results, corrections must be applied to the field blow counts to account for factors that affect the blow count and may lead to erroneous values. Factors affecting blow counts are removal of overburden, overburden pressure, saturated fine or silty sands below the water table, type equipment, and its operation. The three factors that will be considered for correction to N values are removal of

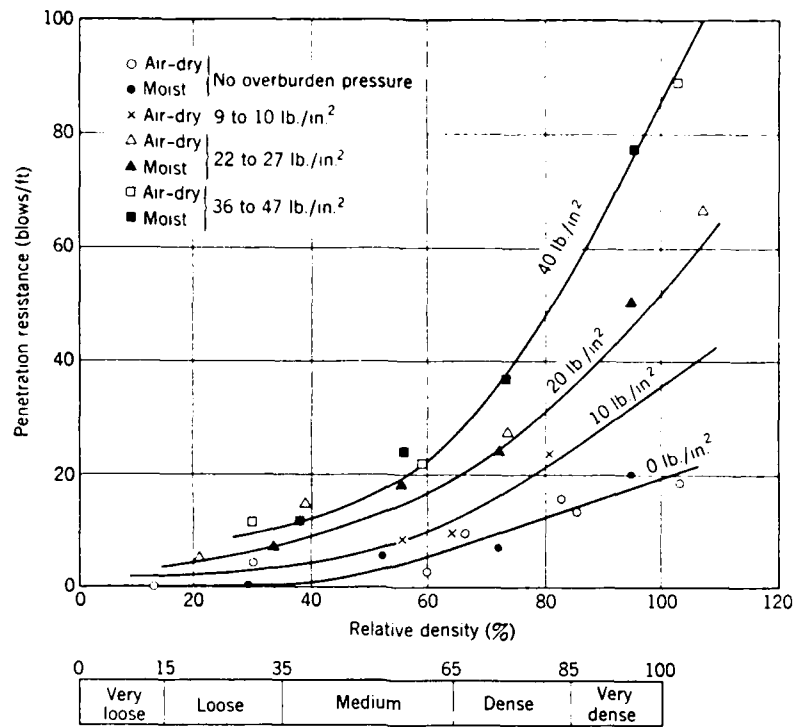
overburden, saturated fine or silty sands for N values below the water table, and the effect of overburden pressure during the performance of the test. All these factors will be considered in analyzing the SPT tests for the results used in this report.

Mansur and Kaufman (1958) found a reduction in N values obtained from standard penetration tests as a result of excavation of material at the Low-Sill Structure. The removal of 50 ft of overburden reduced the N values by as much as 50 percent. At the Arkansas River test, Mansur and Hunter (1964) also discovered a reduction in N values due to removal of the overburden. A reduction of 15 percent was found due to an excavation of 20 ft. Based on these results, a reduction in N values of an average of 1 percent for each foot of material removed was used in correcting the standard penetration test for the test sites in this report. N values were further reduced if the test piles penetrated either saturated fine sand or silty sand by the equation (Bowles (1977)).

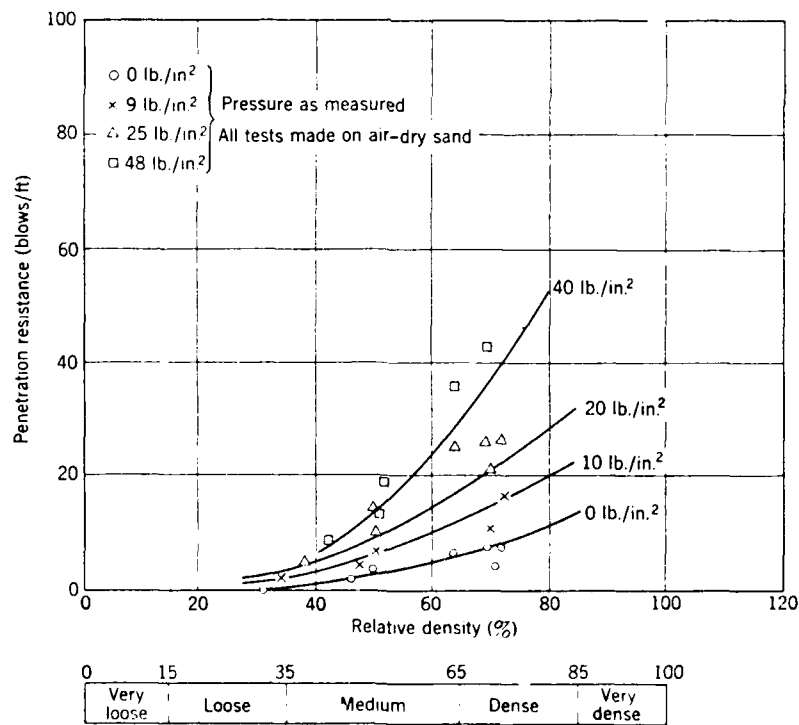
$$N_c = 15 + \frac{1}{2} (N_f - 15) \quad (21)$$

where N_f is the field-measured blow count.

Gibbs and Holtz (1957) found that different overburden pressures give different blows per foot for soil of the same relative density. They developed charts (Figure 26) that relate N values to relative density, D_r , for a given effective pressure. Once the relative density, D_r , is found, the angle of internal friction can be found from Meyerhof's (1956) equations:



(a) Coarse sand



(b) Fine sand

Figure 26. Results of Standard Penetration Tests (Gibbs and Holtz 1957)

$$\text{for } > 5\% \text{ fine } \phi = 25 + 25 D_r \text{ (in degrees)} \quad (22a)$$

$$\text{for } < 5\% \text{ fine } \phi = 30 + 25 D_r \text{ (in degrees)} \quad (22b)$$

Peck, Hanson, and Thornburg (1974) present an equation for a correction factor, C_N , for effective vertical overburden pressure to be applied to field N values:

$$C_N = 0.77 \log_{10} \frac{20}{\sigma_v} \quad (23)$$

where σ_v is the effective vertical overburden pressure in tons/sq ft.

Bazaraa (1967) presented a set of equations to correct the field blow count for the effects of overburden pressure:

$$\sigma_v < 1.5 \text{ ksf} \quad N_c = \frac{4^{\frac{N_f}{4}}}{1 + 2\sigma_v} \quad (24a)$$

$$\sigma_v > 1.5 \text{ ksf} \quad N_c = \frac{4^{\frac{N_f}{4}}}{3.25 + 0.5\sigma_v} \quad (24b)$$

Figure 27 shows a plot of these two methods for the correction of the N value for the effects of overburden pressure. The method presented by Peck, Hanson, and Thornburg (1979) will be used in this study. Once the corrected N value has been determined, the angle of internal friction can be obtained from the empirical correlation by Peck, Hanson, and Thornburg (1974) shown in Figure 28.

Behavior of Axially Loaded Piles in Sands

"A surprising fact for your students in soil mechanics is that, although men have built on deep foundations for many centuries, the

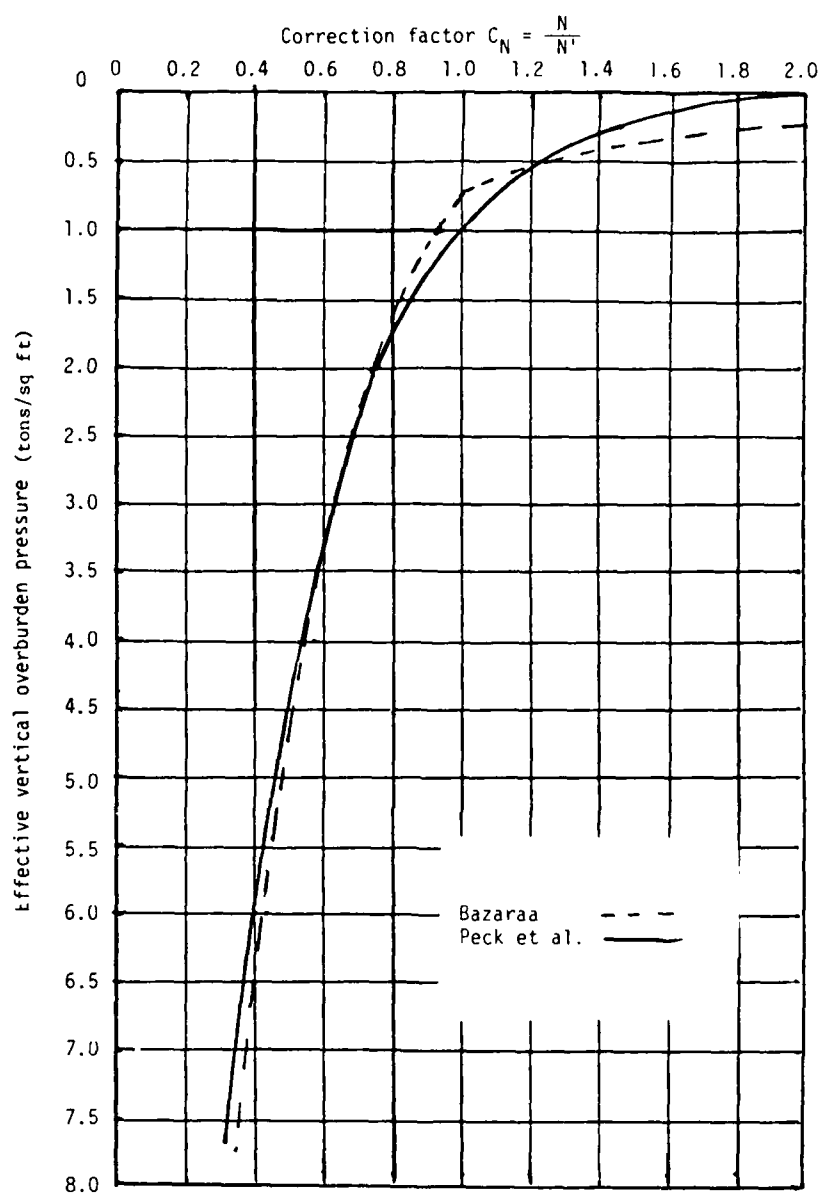


Figure 27. Comparison of Correction Factors for Overburden Pressure

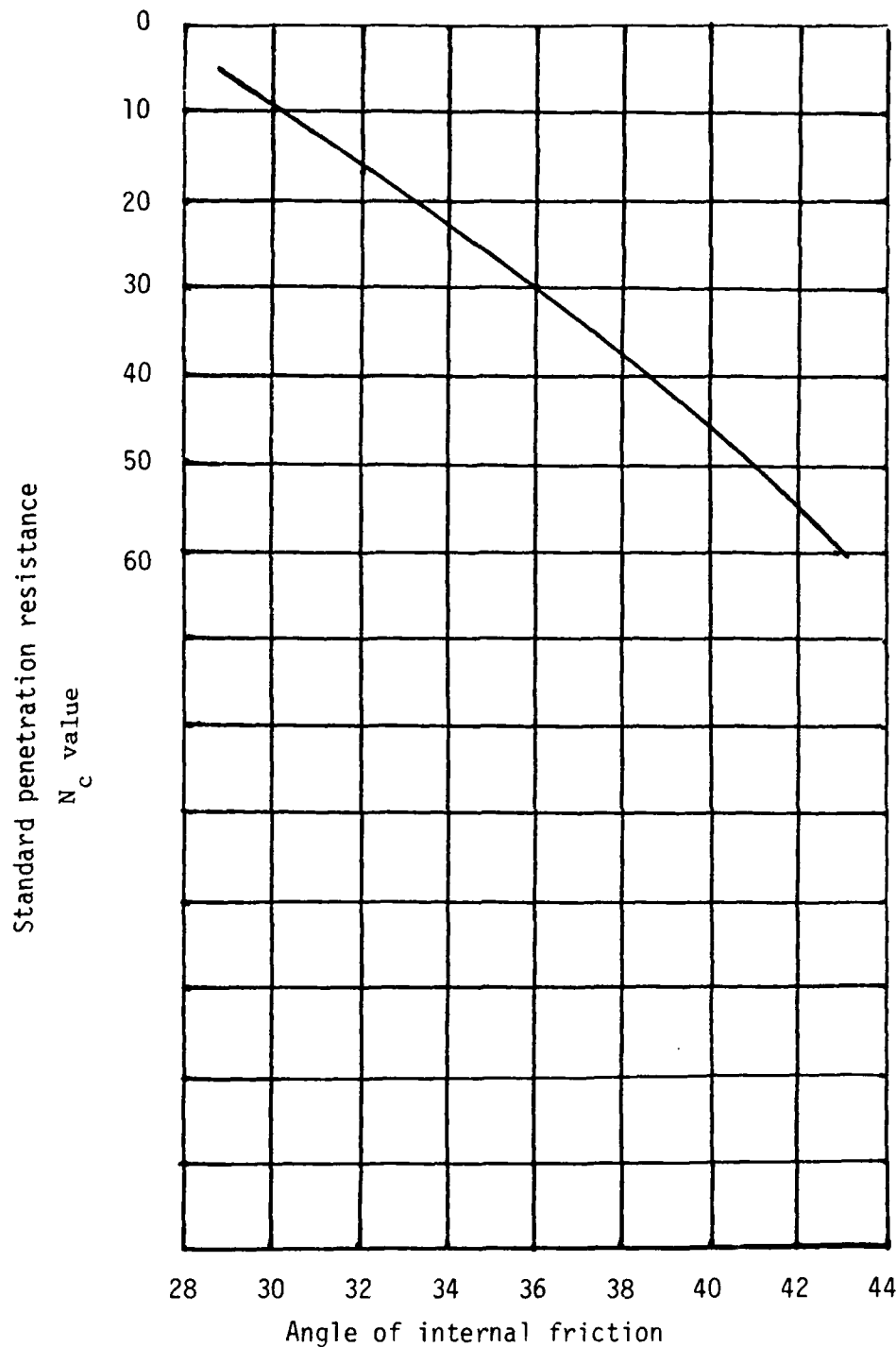


Figure 28. Correlation of N Values with Angle of Internal Friction (After Peck, Hanson, and Thornburg 1974)

basic laws of the bearing capacity of these deep foundations are still unknown." (Kerisel 1964).

This lack of knowledge of pile behavior is not due to lack of interest but rather due to the complexity of the problem. The problem of side and tip resistance of a pile is a complex one with many variables. This complexity has resulted in very limited information in the literature on the subject. The general approach for side resistance has been based on earth pressure theory and friction between two solids. The development of the point bearing and the side resistance is generally treated independently in design/analysis of pile foundations. The load carried by the tip is commonly estimated by extending the classical bearing capacity theory for shallow foundations. The side resistance is usually estimated assuming the development of friction between the pile shaft and the surrounding soil as if they were two solids. The pressure on a surface between the pile and soil is determined by lateral earth pressure theory which is assumed to be related directly to the vertical earth pressure from the overburden soil. The lateral earth pressure is generally assumed to be from one-half to one times the vertical earth pressure, but some feel it may approach values equivalent to the passive pressure which may be between two to three times greater than the vertical pressure. The friction angle is assumed to vary between one-half to the equivalent of the internal angle of friction, ϕ . It is generally established from values determined in laboratory tests. The direct application of conventional earth pressure theory to determine the capacity of piles has perhaps occurred without due consideration to

such facts as the lack of definite shear planes and the presence of arching in the vicinity of the pile.

Instrumented field pile tests and model tests, both large- and small-scale, in homogeneous sands have shown that the side resistance and point resistance do not increase at a constant rate with increasing depth. It was once believed that the side resistance and point resistance for homogeneous sands would increase linearly with increasing depth for a constant angle of internal friction ϕ . The increase was attributed to increasing overburden pressure as the depth increased. Examining the static formula, the only variable that changes in a homogeneous soil is the normal pressure computed as the overburden pressure, which increases linearly with depth.

It has been found that the side resistance and point resistance increase approximately linearly with depth to a critical depth shown in Figure 29, beyond which the rate of change decreases with depth. Vesic (1967) performed a number of field and model tests that showed this phenomenon; examples of this are shown in Figures 30 and 31. Very little is known about the cause of this, and much less is known about a method of predicting its occurrence. To develop some insight into the behavior of a single pile driven in the sand, a review of the literature was conducted.

The key to developing and understanding this phenomenon that occurs in axially loaded piles in sands is to consider the changes that the soil undergoes during installation. The method of installation of a pile has a direct influence on its behavior. The piles that are examined in this report were installed by driving with

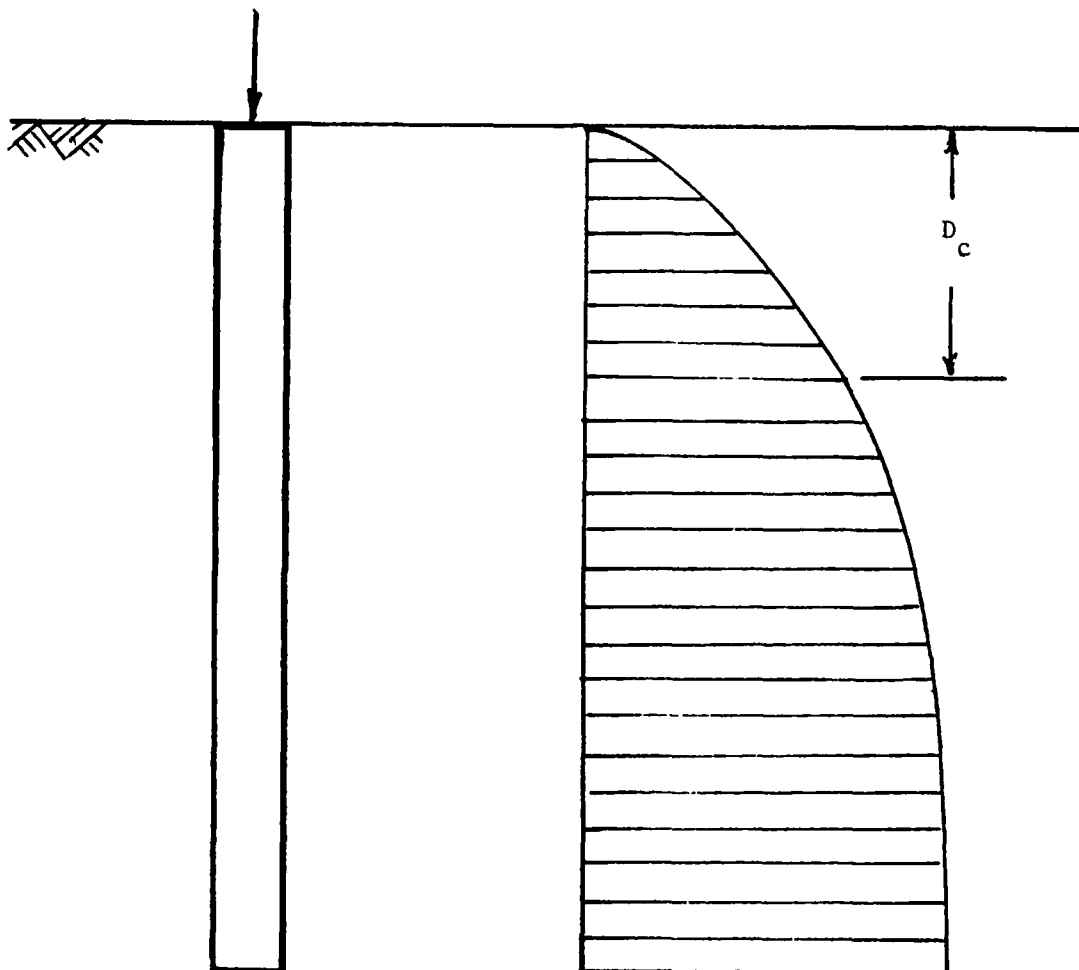


Figure 29. Tip and Side Resistance Change with Depth

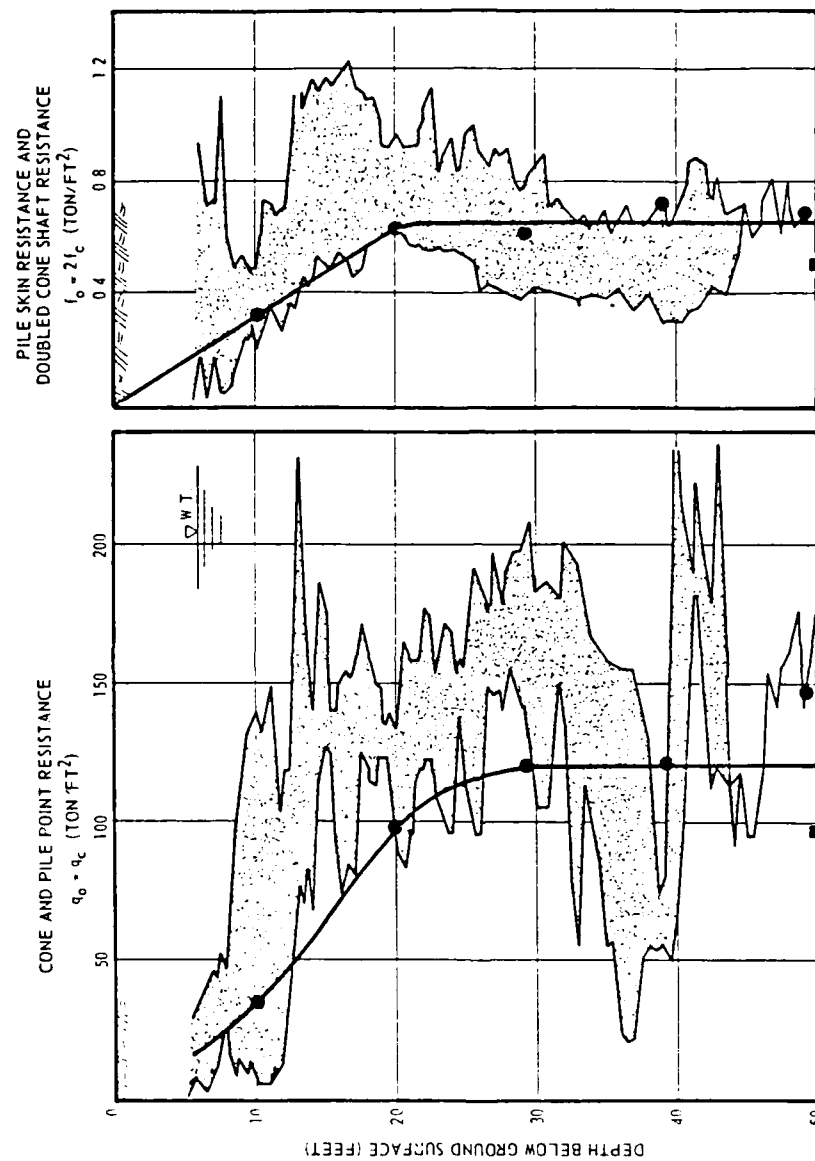


Figure 30. Variation of Point and Skin Resistance with Depth
(Vesic 1967)

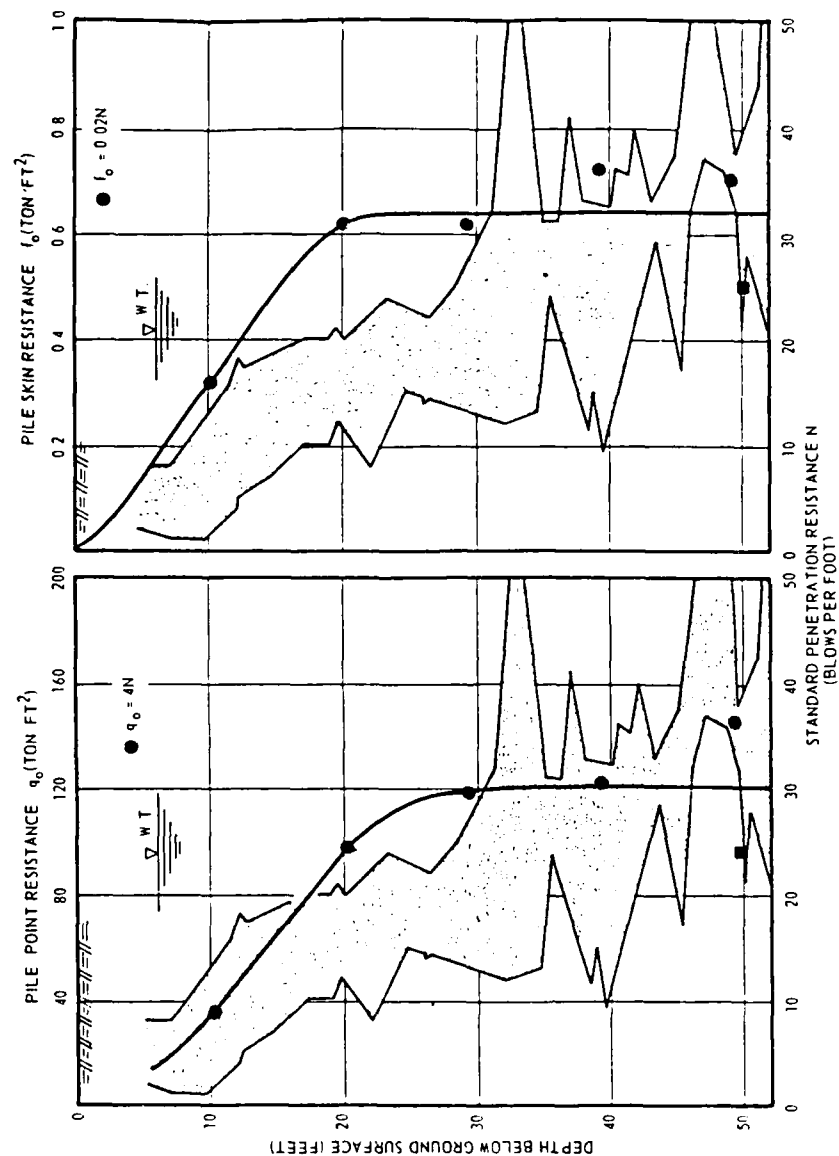


Figure 31. Point and Skin Resistance Compared with Standard Penetration Data (Vesic 1967)

either an impact hammer or a vibratory hammer. These two methods of installation are the most common methods used for piles in sands. Driving generally creates more disturbance than any other method of installation. A number of investigations have been conducted on the effects of driving on the behavior of piles. This section will review these studies and investigate the effect of driving on a design procedure.

The act of driving piles in sand causes an altering of the soil conditions in the vicinity of the pile. The soil conditions that were present prior to driving are permanently changed. If this change is not considered in the design, the design will not reflect the actual soil conditions or the correct behavior of the pile. For many years, this change in soil conditions due to installation was known to occur, but little was understood about its influence on pile behavior.

Meyerhof (1959) investigated the compaction of the sand around the shaft and under the tip of a pile after driving. He studied the increase in relative density from the process of driving the pile and its effect on the ultimate load capacity of the pile. The compaction of the sand around the pile is due to the displacement from the insertion of the pile into the soil and the vibration from the hammer's impact. This causes a permanent rearrangement and a crushing of the soil particles in the vicinity of the pile. The degree of compaction is governed by the intensity and the duration of the pressure introduced in the soil by the impact of the hammer.

Meyerhof (1959) performed a number of laboratory tests to develop a relationship between degree of compaction and induced

pressure from the impact hammer. He correlated this information with field data to determine the degree of compaction around the pile tip and shaft for a field pile. He developed a method to compute the degree of compaction in the vicinity of the pile based on the maximum pressure at the tip from the impact pressure at the pile head determined by a dynamic pile formula. The state of stress in the soil under the tip consisted of a zone where the shear strength is fully mobilized, a plastic zone that extended out some distance from the tip, to a zone that was in the elastic state prior to the driving. To develop a plastic zone, the stress induced must be of the magnitude to produce substantial permanent deformation under the tip of the pile. The permanent deformation causes the compaction and the densification of the sand in the immediate vicinity of the pile. Once the magnitude of the pressure at the tip is determined, the stress in the surrounding soil can be computed by classical plasticity theory and by elasticity theory beyond the failure surface (Figure 32). From these calculated stresses, the relative density (DR) is determined from Meyerhof's correlation developed from laboratory tests for change in relative density due to compaction. The angle of internal friction, ϕ , corresponding to the new relative density determined from the stresses in the soil may be reduced from results of standard or static penetration tests. The zone of the new angles of internal friction, ϕ , decreases with depth from the tip of the pile in the plastic zone until it reaches the elastic zone. Once it has reached the elastic zone, the angle of internal friction, ϕ , essentially remains unchanged. The distance from the tip to the elastic zone was

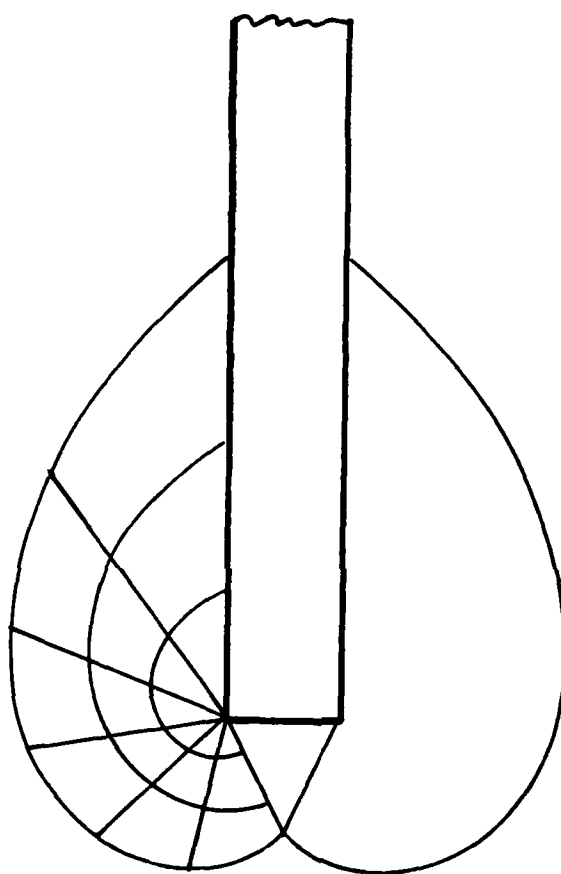


Figure 32. Plastic Zone and Shear Pattern

found to range from about 8 diameters directly below the tip to about 3 diameters on the side, forming a tear drop shaped bubble around the tip. Figure 33 show a comparison by Meyerhof (1959) of observed and estimated results for a driven pile.

Robinsky and Morrison (1964) conducted a study of the effects of shape and volume on the capacity of pile models in sand. They also investigated the displacement and compaction of the sand around these models. As Meyerhof (1959) had stated before, the action of driving the pile into the sand creates a zone of compacted sand in the vicinity of the pile. The extent of this compacted zone and the behavior of the soil in the zone are affected by the volume and shape of the pile and the method of driving. By the means of radiograph techniques, they found that each of their model test piles formed a similarly shaped displacement envelope surrounding the pile. The shape was that of an elongated bubble that extended below the tip in a spherical shape and up to the ground surface, which can be approximated by a vertical cylinder narrowing as it approaches the ground surface as shown in Figure 34. The width of the envelope was found to be dependent on the diameter of the pile, increasing with increasing pile diameter, roughness of the surface, pile taper, and increasing sand density. The pile capacity for each of the sand densities varies directly with the diameter of the envelope, regardless of the pile diameter, shape, or surface roughness. Both displacement and compaction of the sand were evident in the envelope, with most of the compaction being done by the tip as it was driven into the soil. No shear plane failure was observed. A complex

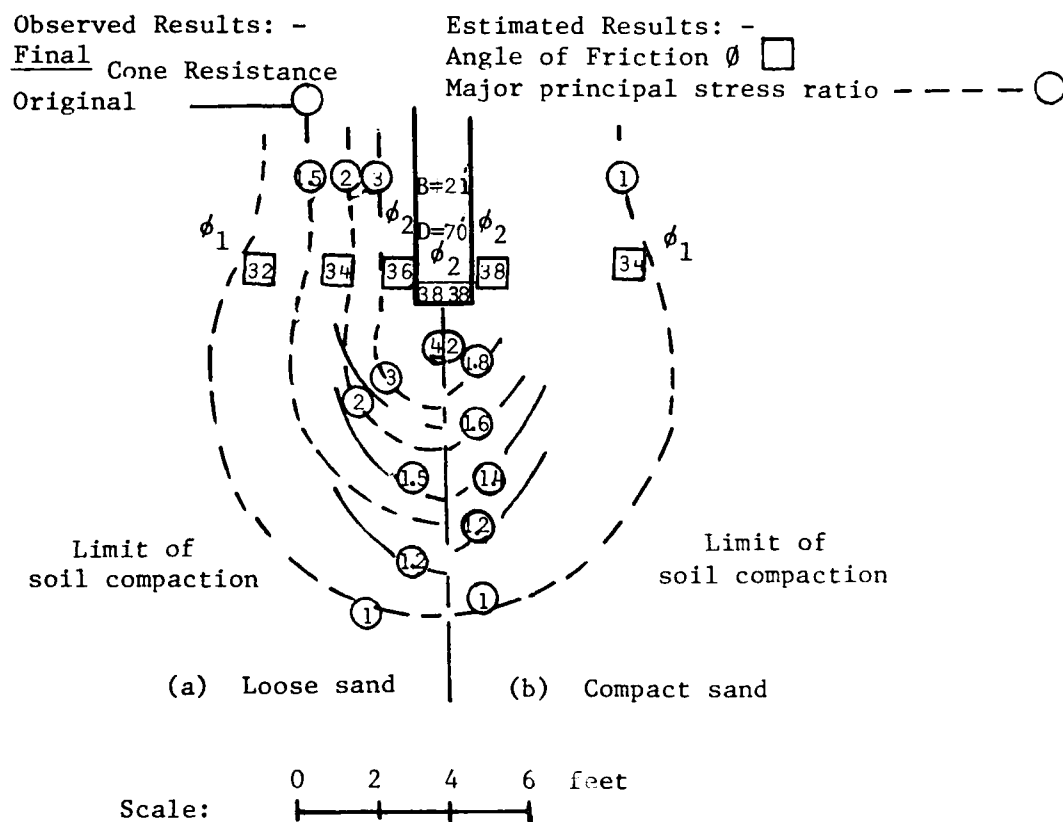
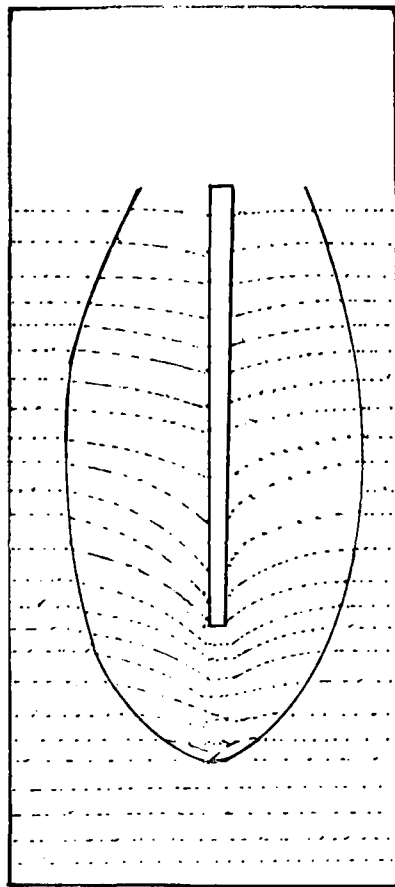


Figure 33. Compaction of Sand Near Driven Pile (After Meyerhof 1959)

(a)
SAND - LOOSE
DEPTH - 20 IN.



(b)
SAND - MEDIUM DENSITY
DEPTH - 20 IN.

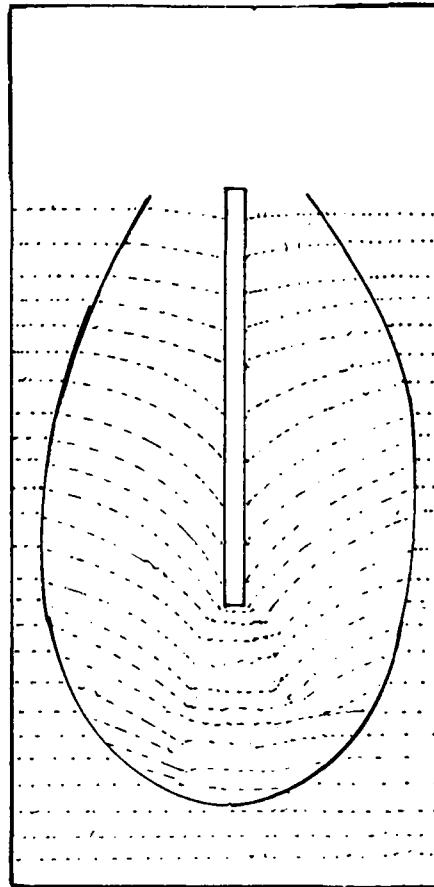
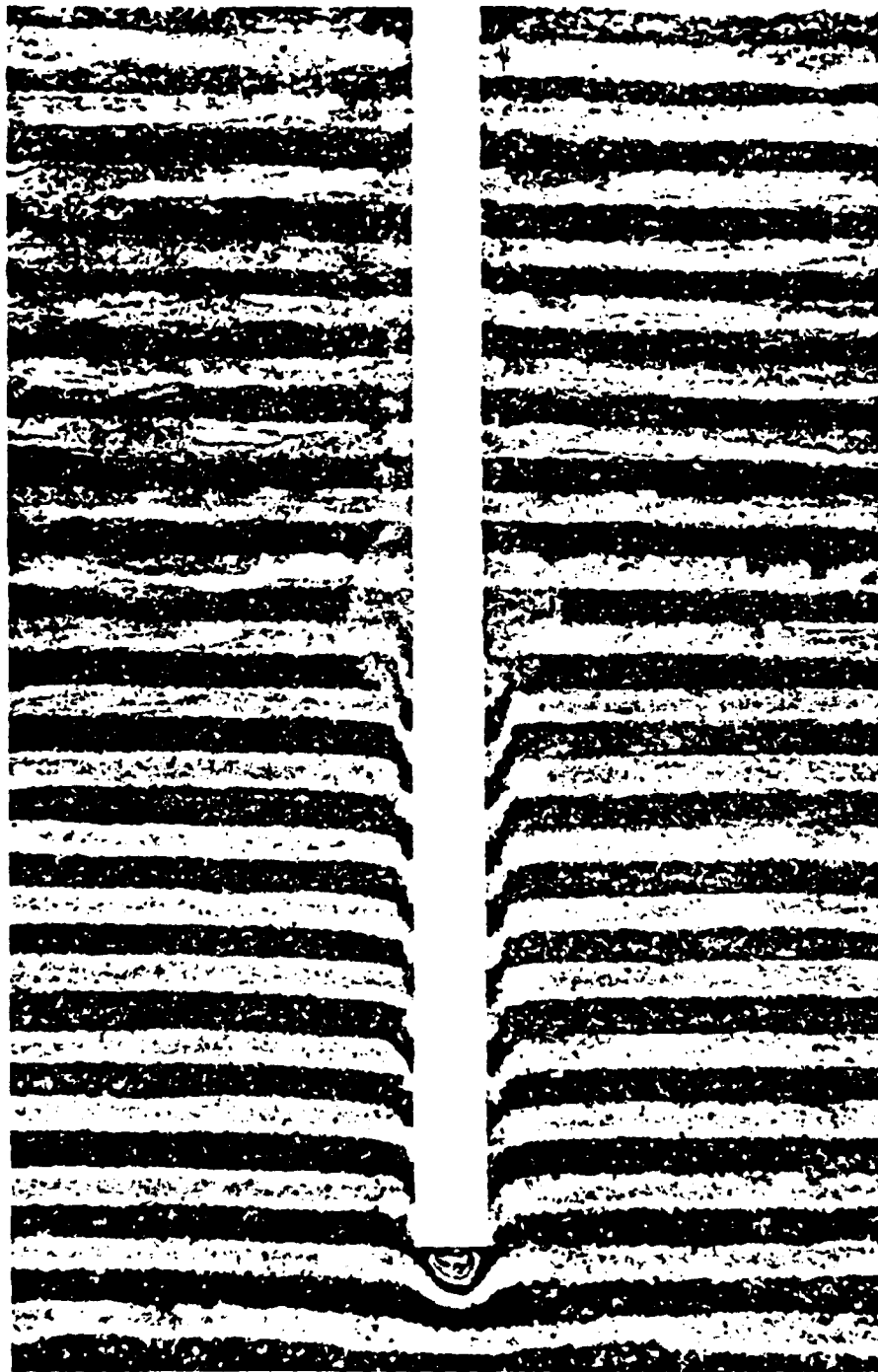


Figure 34. Radiographs of Model Pile Test (After Robinsky and Morrison 1964)

sequence of density changes was discovered from the sand displacement beneath and around the tip. Robinsky and Morrison (1964) described the sequence as two zones:

- (1) A zone approximating the shape of a cone is found beneath the pile extending downwards and outwards from the edge of the pile point. This appears to be the main compaction zone. Within the zone vertical compression and two directional horizontal expansion takes place accompanied by radial downward translation.
- (2) At the zone limits vertical compression ceases and vertical extension begins to take place. It is found that by the time the pile has passed any two points, the vertical distance between them becomes approximately equal to the vertical distance between them, prior to pile driving. Also horizontal radial compression and/or tangential expansion accompanied by additional radial downward translation occur. The vertical extension is caused by the downward movement of soil below the point away from the previously compressed soil to each side and immediately above the pile point.

An additional vertical expansion was measured along the pile walls. This phenomenon was also found by Vesic (1967) as shown in Figure 35. This is attributed to the down drag effect of the pile wall on the surrounding sand particles as the pile moves downwards. The down drag did not occur uniformly along the pile shaft. It was less pronounced near the surface. This coincides with the narrowing of the envelope as it approaches the surface. So as the depth increased the vertical downward movement increased. The most pronounced vertical movement generally occurred about a fourth of a pile diameter from the wall. This resulted in an increase in the void ratio of the sand adjacent to the pile shaft. This creates a thin sleeve or cylinder of loose sand adjacent to the pile shaft which sets



TEST NO. 104 $D/B=10$ CIRCULAR FOUNDATION $B=1$ IN. $D_R \sim 0.9$

Figure 35. Shear Pattern Under a Circular Foundation Placed at Greater Depth in Very Dense Sand (Vesic 1967)

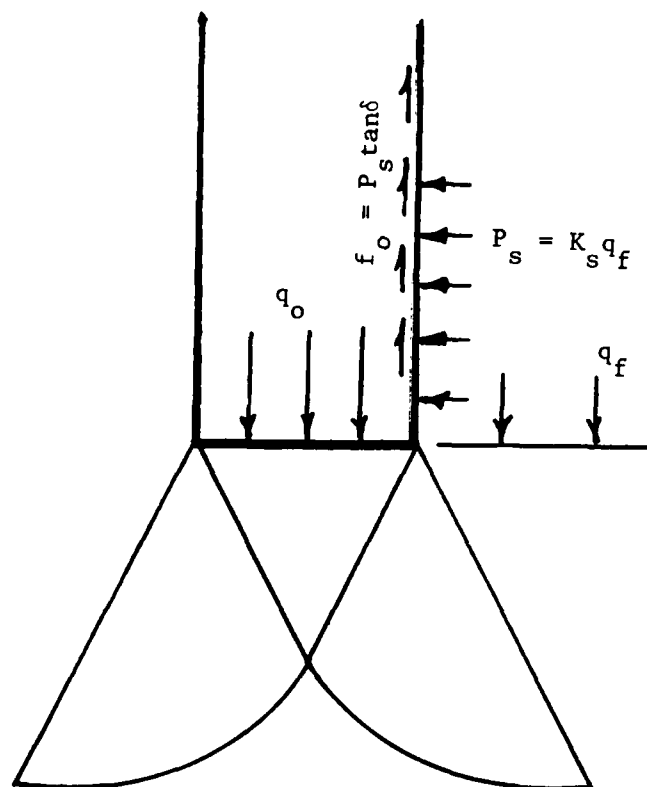
up ideal conditions for arching. The cylinder of loose sand is surrounded by much denser sand that was created from driving. This is denser than the sand in its in situ form. The shear transfer from the pile to the soil is thus developed through arching due to a looser soil directly adjacent to the pile shaft surrounded by a much denser sand. The arching makes it impossible to determine the relationship between the lateral earth pressure applied on the shaft and the vertical overburden pressure, making it is impossible to predict the actual normal earth pressure adjacent to the pile shaft. Other observations in their study were that the model tests showed a drop of load transfer at or near the tip regardless of the depth of embedment of the piles. The load transfer along the pile is irregular in shape; this is attributed to the buildup and breakdown of the arching system. The lateral earth pressure is apparently carried by the cylinder of dense sand surrounding the sleeve of the loose sand adjacent to the pile shaft.

Kerisel (1964) found from his laboratory experiments that the tip resistance reaches a maximum value at a critical depth and only increases slightly with increased depth. He attributed its occurrence to the bearing capacity factor, N_q , being a complex function of the angle of internal frictional, ϕ , depth of penetration to base width ratio at the tip, D/B , and the base width, B . Vesic (1968) also made a similar observation, but offered another explanation for its occurrence. Vesic first considered the assumption of the normal stress used to compute the unit tip resistance being proportional to

$$q_{\max} = \sigma_v N_q \quad (25)$$

the overburden. Under this assumption, however, a limited plastic zone (shear zone) forms beneath the pile tip. The tip resistance will always increase as the overburden pressure increases, if the soil properties remain constant with depth. The bearing capacity factor, N_q , is dependent only on the angle of internal friction, ϕ . As the pile is loaded, the sand will undergo physical changes from the degradation and crushing of the soil grains. The angle of internal friction, ϕ , of this newly formed material will remain greater than zero, so the bearing capacity factor, N_q , will be greater than zero. Consequently, the tip resistance will increase with continued increases in overburden pressure. Vesic (1968) concluded that the decrease in the rate of change of tip resistance is due not to a decrease in N_q but rather to a change in the normal pressure at the tip. He further stated that the in situ normal pressure, q_f , at the tip is not proportional to the overburden pressure before driving (Figure 36).

To state that the theoretical solutions are inadequate or incorrect may be premature. In the formulation of the different theories for bearing capacity, the stress, q_f , is only defined as the normal stress at failure. It has been previously assumed that the normal stress at failure was proportional to the overburden pressure. This was not stated in the development of the method but rather has been assumed by those applying the method.



$$\frac{q_o}{q_f} = N_q = \frac{q_o}{f_o} K_s \tan \delta$$

Figure 36. Stress Conditions in Vicinity of the Pile Tip
(After Vesic 1967)

Vesic proposed a procedure to determine the N_q value from pile tests or model tests that would be independent of use of the vertical overburden pressure as the normal stress. If the point resistance and side resistance are assumed to increase linearly with the normal stress, then the normal stress is assumed to be the effective normal stress at failure acting at the tip. The effective normal stress for an instrumented pile test may be eliminated from the determination of N_q , (Figure 36):

$$q_o = q_f N_q \quad (26)$$

$$f_o = q_f K_s \tan \delta \quad (27)$$

where q_o = unit tip stress

f_o = unit shear stress of the shaft of the pile

Eliminating q_f ,

$$N_q = \frac{q_o}{f_o} K_s \tan \delta \quad (28)$$

where f_o and q_o can be obtained from the pile test.

Ellison (1969) performed an analytical study using finite elements on tests performed by Vesic on large-scale models. Ellison found that the dense sand behaved as an incompressible material, as the vertical stress increased and the horizontal stress also increased appreciably. This was due to the fact that the horizontal strains are high, which results in the small volumetric change as would be found in an incompressible material. The higher confining pressures and lower deviatoric stresses resulted in a higher Young's modulus and yield for the sand. This was not found in the medium or loose sands. A plastic zone was found directly beneath the tip. The

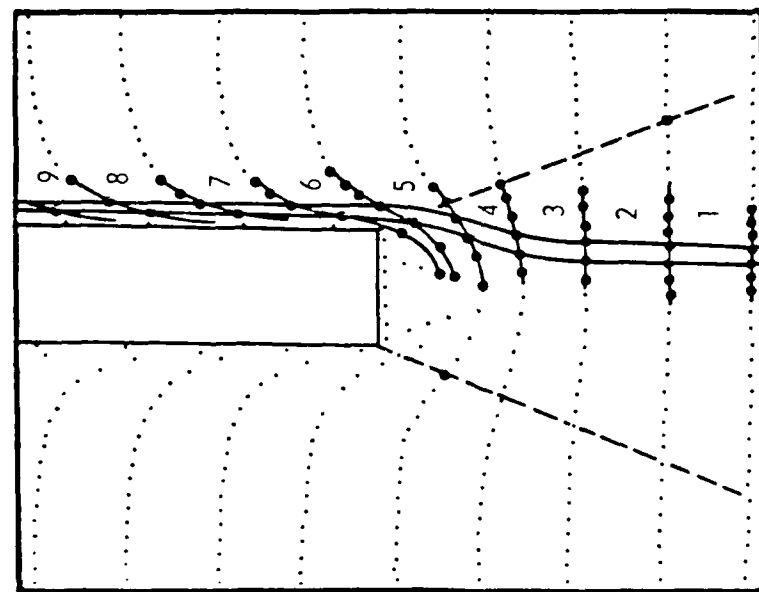
plastic zone for dense sands is larger than that for medium sands. This is in agreement with the classical plasticity theories which assume the size of the plastic zone to be proportional to the angle of internal friction.

Ellison (1969) in his finite element studies discovered that tension failure zones developed at the tip of the pile in the sand. The zones in the dense sand extended diagonally from the edge of the pile tip down and outward from the pile (Figure 37).

Similar observations were made by Robinsky and Morrison (1964) in their model tests (Figure 38). This indicates that arching is also occurring at the pile tip. This phenomenon was also found in the medium sand but to a lesser extent (Figure 37b). A tension crack was found to extend from the edge of the pile horizontally out (Figure 37 and 39). The length of that tension crack was dependent on the density of the sand.

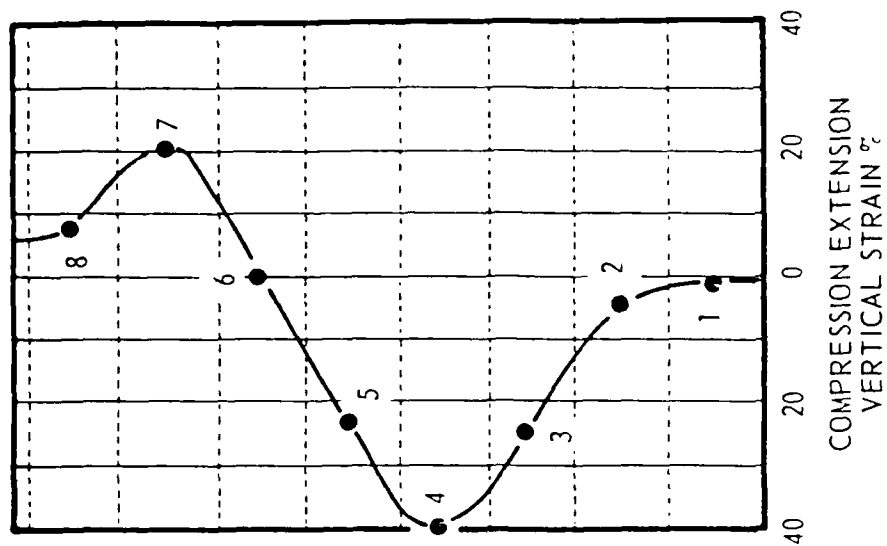
Ellison (1969) was unable to simulate the load-displacement relationships found in Vesic's models. This was attributed to the horizontal pressure distribution used in the finite element analysis. The distribution was linearly increasing with depth or proportional to the overburden pressure. This is contrary to Vesic's explanation for the behavior of his piles reported in his study and to the work done by Robinsky and Morrison (1964) on their model tests. The finite element analysis was unable to model the loosening of the soil adjacent to the pile that resulted in the arching action.

A review of the literature reveals that the arching system established along the shaft from driving and at the tip due to tensile



(AFTER ROBINSKY AND MORRISON)

(a)



(b)

Figure 38. Strain Pattern Around Point of a Deep Foundation

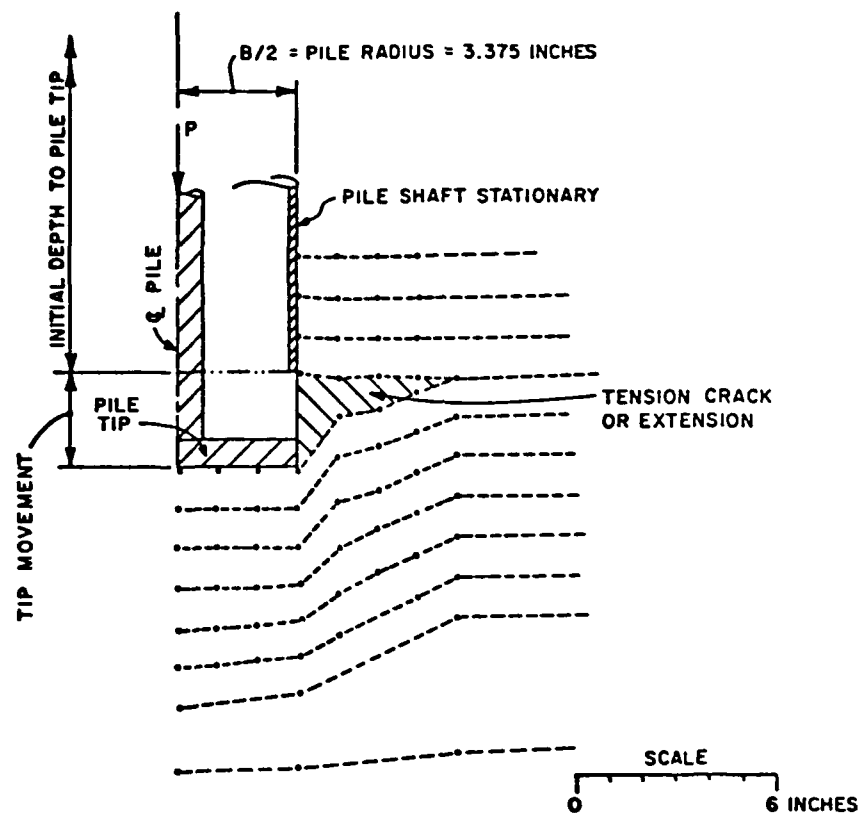


Figure 39. Tension Crack at Tip from Finite Element Analysis (Ellison 1969)

stress is the most important phenomenon affecting the behavior of a pile. Until a procedure to determine its effects is found, theoretical approaches are inadequate for estimating pile capacity.

Summary

Pile foundations have been utilized in the construction of facilities for thousands of years. Yet engineers have been unable to predict the capacity of piles with any reliability. New analytical and numerical approaches have lessened the number of simplifying assumptions in the analysis of the pile-soil system. These new approaches give the displacement compatibility between the pile shaft, the pile tip, and the soil. They allow the engineer to develop the load-displacement response of the pile-soil system.

A review of the literature clearly points out the drastic changes the soil undergoes as the pile is driven and the inadequacy of designing pile foundations based totally on prior soil conditions. The installation of piles by driving causes a permanent rearrangement of the sand particles in the vicinity of the pile. This develops a zone of compacted sand in the vicinity of the pile. As the pile tip penetrates, the shaft of the pile causes a down drag on the surrounding sand particles that results in a vertical displacement of the sand particles. The sand that moves vertically loosens and creates a thin sleeve or cylinder of loose sand adjacent to the pile shaft which sets up ideal conditions for arching. This arching system reduces the lateral pressure applied to the pile shaft, thus reducing the shear

transfer between the pile and soil. The arching of the sand in the vicinity of the pile has been shown by a number of investigations. The arching makes it impossible to determine the relationship between the lateral earth pressure applied to the shaft and the vertical overburden pressure. Tensile stresses produced at the tip cause soil arching to occur which leads to cracks forming horizontally from the tip. The normal stress at the tip is then no longer dependent on the vertical overburden pressure.

Based on these observations, a highly theoretical approach is unwarranted. A semi-empirical or empirical correlation to actual field pile tests will yield good reliable results if a large quantity of high-quality observations can be obtained for a data base. The next chapter will examine the published correlations for side and tip resistance versus pile movement.

CHAPTER 3: LOAD-DEFORMATION CRITERIA

Review of Criteria

The lack of an accepted theoretical approach for determining the load-deformation behavior of soil has required foundation engineers to rely on semi-empirical and empirical criteria to describe the phenomenon of load transfer in the pile-soil system. This type of methodology has been used very successfully for laterally loaded piles. The criteria are generally correlations between field tests and laboratory test data and/or in situ tests. For axially loaded piles in sands, four different criteria were found in a review of the literature. In this chapter these criteria will be presented and reviewed.

Coyle-Sulaiman Criteria

Coyle and Sulaiman (1967) were the first to develop criteria for skin friction versus pile movement for sands. Their approach was to relate field pile test data to model tests in the laboratory. Three of the field pile tests conducted for the Arkansas River Lock and Dam No. 4 project were used as the basis of their correlation. From the report by Fruco and Associates (1964), they reduced the load-distribution curves and load-settlement curves to obtain the skin friction versus pile movement curves (Figure 40). They pointed out

AD-A139 236

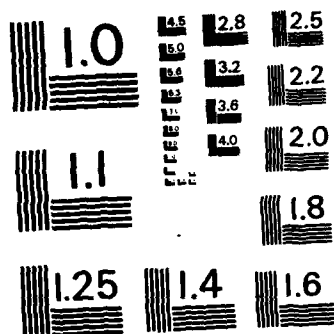
LOAD-TRANSFER CRITERIA FOR NUMERICAL ANALYSIS OF
AXIALLY LOADED PILES IN. (U) ARMY ENGINEER WATERWAYS
EXPERIMENT STATION VICKSBURG MS R L MOSHER JAN 84
WES-TR-K-84-1 F/G 13/1

2/5

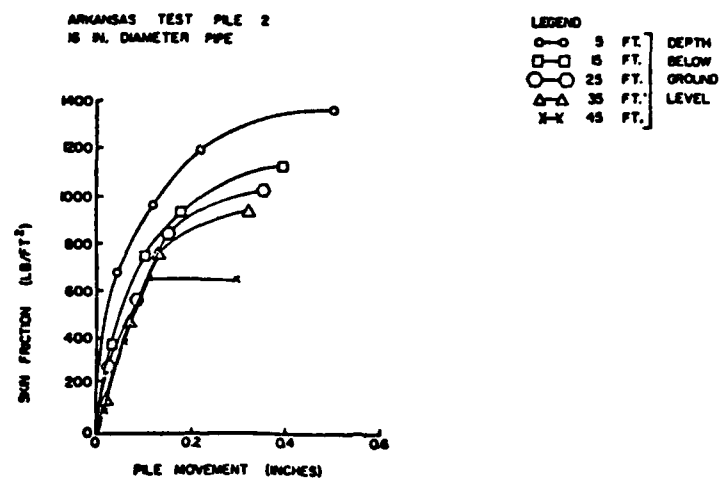
UNCLASSIFIED

JAN 84
F/G 13/13

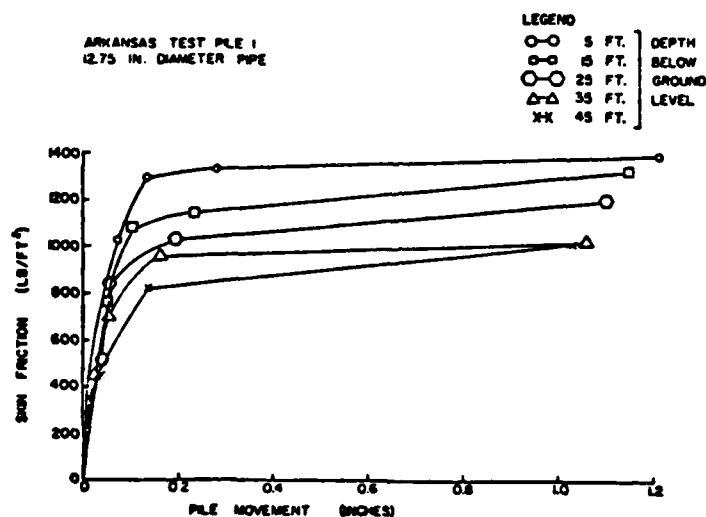
NL



MICROCOPY RESOLUTION TEST CHART
NATIONAL BUREAU OF STANDARDS-1963-A



a. 16-in. Pipe



b. 12.75-in. Pipe

Figure 40. Skin Friction versus Movement for Arkansas River Tests (Coyle and Sulaiman 1967)

that for their initial portions the curves were almost linear, and the magnitude of the maximum shear transfer values decreased as depth increased. No consideration was given to residual stresses in the pile as a result of driving due to the lack of information on how to treat these stresses.

They normalized these curves for skin friction versus pile movement by dividing the skin friction by the shear strength, s , of the sand at the pile-soil interface. They defined the shear strength as

$$s = \bar{\sigma}_n \tan \phi \quad (29)$$

where

$$\bar{\sigma}_n = \text{the effective normal stress}$$

The effective normal stress at a given depth is

$$\bar{\sigma}_n = K\gamma D \quad (30)$$

where

K = the coefficient of lateral earth pressure

γD = the overburden pressure

The coefficient of lateral earth pressure, K , was assumed to be equal to 1.0 and constant with respect to depth. The normalized curves are shown in Figure 41.

The magnitude of the curve for 5 ft is out of line with all other curves. Coyle and Sulaiman (1967) attributed the increase in the curve at 5 ft to the assumption of $K = 1$. They felt that this may be due to the arching in the sand. These conclusions were drawn by Coyle and Sulaiman: (1) the ratio decreases with increasing depth, and (2) the ratio reaches a limiting value at approximately 0.5 for the

ARKANSAS TEST PILES 1, 2, AND 10

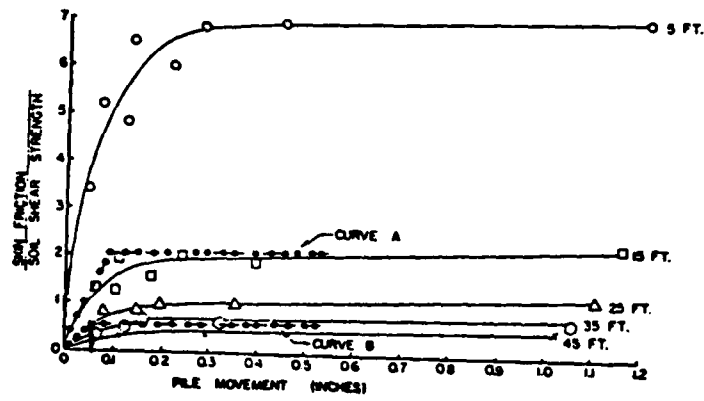
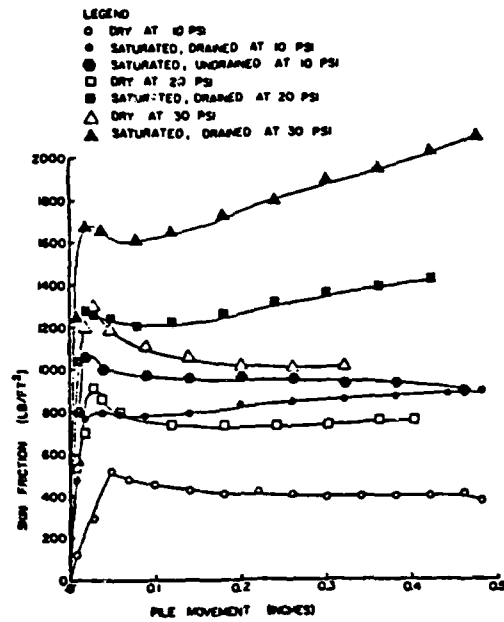


Figure 41. Ratio of Skin Friction to Soil Shear Strength Versus Pile Movement for Piles 1, 2, and 10 (Coyle and Sulaiman 1967)

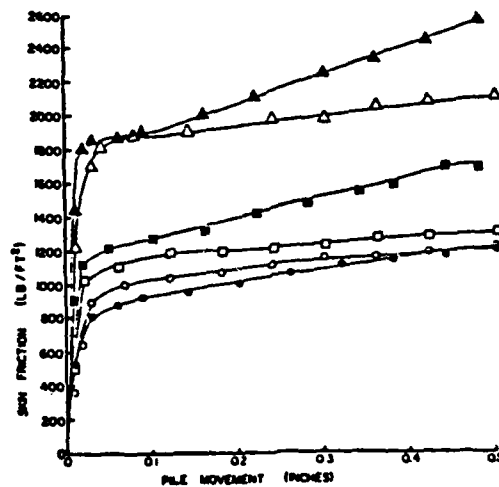
greatest depths (curve B, Figure 41). This is not supported by the data plotted in Figure 41.

The model tests used to evaluate the pile-soil interactions consisted of a 7-in. long steel pile embedded in a saturated sand in a triaxial shear device. The testing program was composed of a test on soil having two different densities which were controlled by the void ratio. The confining pressures were varied to simulate the overburden pressures at various depths. The results are shown in Figure 42. These were normalized by the same procedure as the field tests (Figure 43). Also the angle of wall friction was evaluated by dividing the skin friction by the confining pressure (Figure 44).

The skin friction versus pile movement curves for the model tests (Figure 42) do not exhibit the same trend of decreasing resistance with increasing depth. Coyle and Sulaiman (1967) ascribed this to the field data being influenced by the load capacity in the tip. If the normalized curves for the model tests are compared to the field tests, the high ratio for the shallow depth in the field curves is out of line. As stated earlier by Coyle and Sulaiman (1967), this is probably due to the use of $K = 1$. They felt it was possible to obtain a higher K value due to densification of driving at the surface. This assumption was based on the fact that the model tests only reached a confining pressure of 1.3 psi compared to 7 psi at the 5-ft mark in the field test and 2 psi at the 15-ft mark in the field test for comparable confining pressures. The model curves (Figure 43) exhibit the same trend of decreasing ratio with increasing depth or confining pressure. In Figure 43 a limiting value of approximately



a. $e_o = 0.63$



b. $e_o = 0.53$

Figure 42. Laboratory Miniature Pile Test Curves
 (Coyle and Sulaiman 1967)

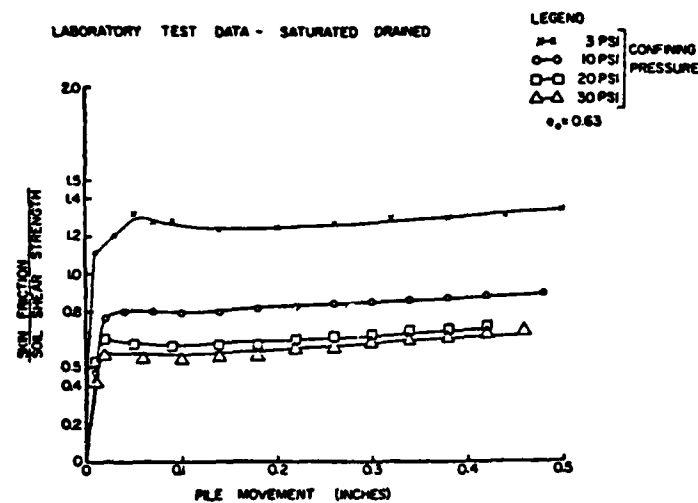


Figure 43. Ratio of Skin Friction to Soil Shear Strength Versus Pile Movement for Laboratory Tests, $e_o = 0.63$ (Coyle and Sulaiman 1967)

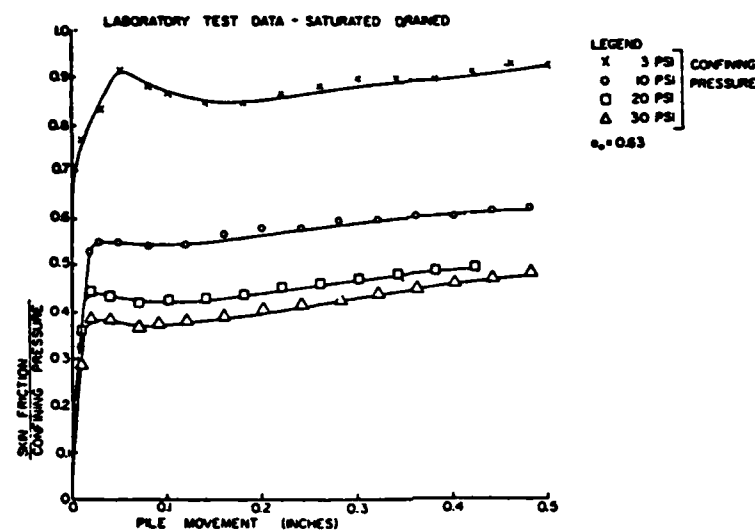


Figure 44. Ratio of Skin Friction to Confining Pressure Versus Pile Movement For Laboratory Tests, $e_o = 0.63$ (Coyle and Sulaiman 1967)

0.5 was reached at a confining pressure of 20 psi, which is equivalent to a depth of 25 ft or greater. This was also found in the normalized field curves.

Coyle and Sulaiman (1967) used an analytical procedure similar to the one described previously in this report to compute a load-settlement curve for one of the axially loaded piles for the Arkansas River site. They used curve A from Figure 41 for 0 to 20 ft and curve B for 20 ft and greater to define the skin friction versus pile movement.

They drew the following conclusions from their investigation:

- (1) The field tests indicated that the skin friction increases approximately linearly until pile movement reaches 0.1 to 0.2 in.
- (2) Skin friction decreases with increasing depth.
- (3) Skin friction increases with increasing density (Figure 41).
- (4) The ratio of skin friction to shear strength has a lower value of 0.5.
- (5) The angle of wall friction decreases with increasing confining pressure.

Vijayvergiya Criteria

Vijayvergiya (1977) presented a paper on load-movement characteristics of piles in which he included criteria for both skin friction versus pile movement and tip load versus tip movement. These were based on his review of the literature and his personal experience. When examining the skin friction, tip resistance, and movement required to develop these, he found that the skin friction reaches a peak value at a small movement and remains constant beyond

the critical displacement but that the tip resistance continues to increase although at a decreasing rate (Figure 7). The gradual tip resistance is the reason that plunging failure is not found during a load pile test in sand. He proposed criteria that exhibited these trends.

The proposed analytical relationship that states the load transfer or unit skin friction mobilized at a given pile movement can be expressed as a function of the maximum skin friction (Figure 45) by

$$f = f_{\max} \left(A_o \sqrt{\frac{z}{z_c}} - B_o \frac{z}{z_c} \right) \quad (31a)$$

where

f = unit skin friction mobilized along the pile shaft segment at movement z

f_{\max} = maximum unit skin friction

z_c = the critical movement of the pile shaft segment when f_{\max} is mobilized, $z < z_c$ (inches)

Vijayvergiya (1977) gave the values of A_o and B_o as 2 and 1, respectively. Substituting these values for A_o and B_o gives

$$f = f_{\max} \left(2 \sqrt{\frac{z}{z_c}} - \frac{z}{z_c} \right) \quad (31b)$$

In his review of the literature on pile tests in sands, he found that the maximum displacement required to reach the maximum skin friction was independent of the size of the pile if the pile was greater than 12 in. in diameter. The movement to reach maximum

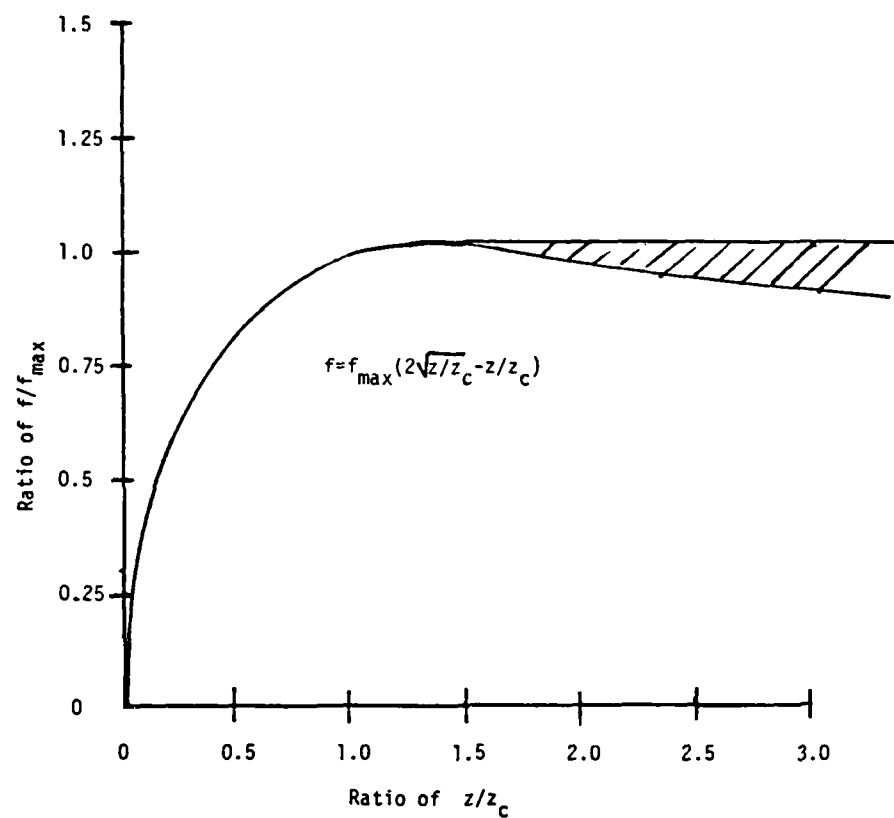


Figure 45. Normalized f-z Curve for Clay and Sand
(After Vijayvergiya 1977)

side resistance, f_{\max} , has a range between 0.2 and 1.0 in. (Table 1).

The value of maximum side resistance, f_{\max} , for the proposed criteria is computed from

$$f_{\max} = K \overline{\sigma}_v \tan \delta \quad (32)$$

where

K = coefficient of lateral earth pressure

$\overline{\sigma}_v$ = effective overburden pressure

δ = angle of friction between soil and pile surface

K in the above equation is difficult to determine accurately. It may range from an active K in loose sands to a passive K in very dense sands.

Available data suggest that large movements are required to mobilize the maximum tip resistance. The critical displacement, z_c , is a function of the dimensions of the pile tip. Table 1 presents variables from 0.04 to 0.09 times the base width. The mobilized value of q at given tip movement z can be obtained from:

$$q = \left(\frac{z}{z_c} \right)^{1/3} q_{\max} \quad (33)$$

Table 1
Summary of Critical Pile Movement Data in Sand
 (After Vijayvergiya 1977)

Reference	Pile Diameter in.	Movement Required to Mobilize f_{max} , in.	Movement Required to Mobilize q_{max} , in
Coyle et al. (1973)	16	0.20-0.40	0.05B*
Coyle and Sulaiman (1967)	12-3/4	0.30-0.40	-
Darragh and Bell (1969)	12-3/4	0.25	0.04B-0.05B
McCammon and Golder (1970)	24	0.40	0.08B
Mansur and Hunter (1970)	16	0.20-0.40	0.04B-0.06B
Vesic (1967)	18	-	0.07B-0.09B
Vijayvergiya (1969)	18	0.5-1.0	-
* B = Base width or diameter of pile			

where q_{\max} = maximum tip resistance

z_c = critical displacement corresponding to q_{\max}

q = tip resistance mobilized when $z < z_c$

The slightly modified curve for $z > z_c$ is shown in Figure 46. The value of q_{\max} is computed as in the static formula:

$$q_{\max} = \overline{\sigma_v} N_q \quad (34)$$

Parker and Reese Criteria

Parker and Reese (1969) proposed a third method based on the performance of laboratory tests on two 90-in.-long instrumented piles with 2-in. diameters. These piles were buried in a homogeneous sand under controlled conditions. The shear transfer performance of these tests was correlated with stress-strain characteristics from triaxial tests on undisturbed specimens from the model test chamber.

The correlation that Parker and Reese (1969) obtained between the shear transfer and the deviatoric stress is

$$f = \frac{U_c}{C_f} \Delta \overline{\sigma} \quad (35)$$

where U_c = correlation coefficient for compression loading

C_f = correction factor for maximum load transferred

$\Delta \overline{\sigma}$ = deviatoric stress

f = shear transfer in compression

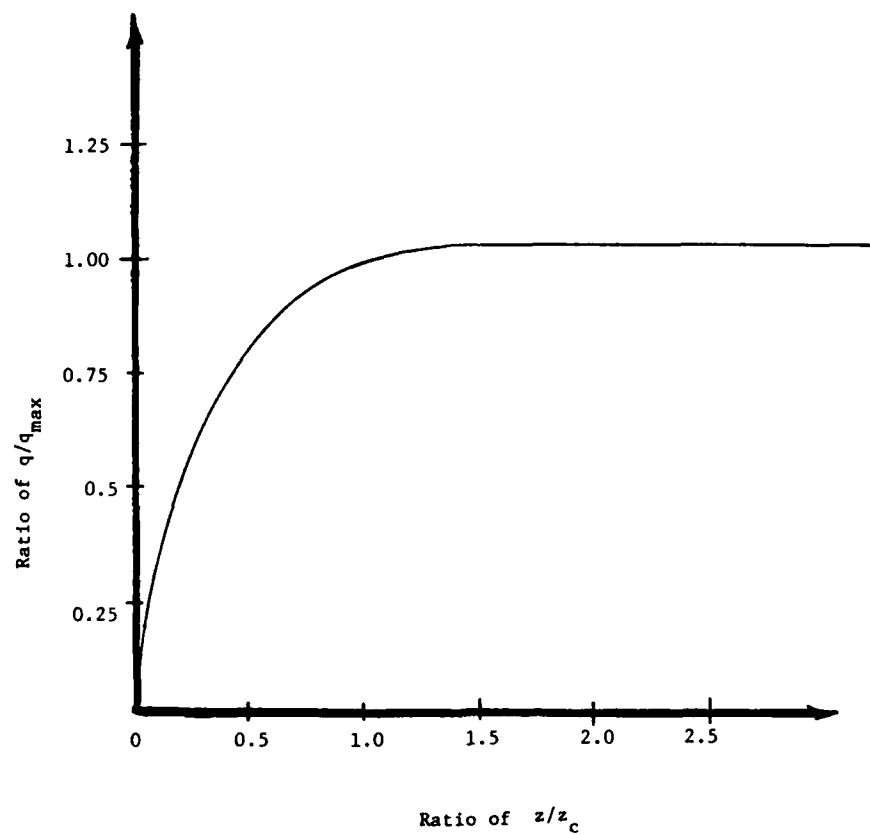


Figure 46. Normalized q-z Curve for Clay and Sand
(After Vijayvergiya 1977)

Correlation coefficients for compression loading for deviatoric stress to shear stress are:

$$U_c = \frac{N_c}{\tan^2(45 + \frac{\phi}{2}) - 1} \quad (36)$$

where

$$N_c = 7.0 - 0.04X$$

X = depth, in.

The correction factor for maximum shear transfer is

$$C_f = -\frac{17.5}{80} (D_R) + \frac{87.5}{4.0} \quad (37)$$

where D_R is the relative density. Pile movement correlations to axial strain from a triaxial test are determined from:

$$z = \epsilon R_c B C_f \quad (38)$$

where

ϵ = axial strain

R_c = correction for compression loading

B = pile diameter (in.)

z = pile movement (in.)

Correction coefficients for compression loading for axial strain to pile movement are

$$R_c = 0.4 + 0.016X \quad (39)$$

where X is depth in inches.

These criteria were investigated in detail, because it was believed that the triaxial test data could be used to develop typical curves for the Lower Mississippi Valley. Idealized triaxial data information was developed from series of tests performed over the years by the Geotechnical Laboratory, WES. The stress-strain curves from a triaxial test are nonlinear and cannot be represented by a simple modulus. The nonlinear stress-strain curves can be represented by a hyperbolic function as suggested by Konder and Zelasko (1963). They suggested a procedure to approximate the stress-strain curves (as shown in Figure 47) that has been shown to be reasonably accurate. The hyperbolic representation can be fulfilled by

$$\sigma_1 - \sigma_3 = \frac{\epsilon}{a + b\epsilon} \quad (40)$$

where σ_1 and σ_3 = the major and minor principal effective stresses, respectively

ϵ = the axial strain

a and b = constants

The physical meaning of the constants a and b is shown in Figure 47. They can be determined by performing an axis transformation and plotting axial strain divided by the deviatoric stress versus the actual strain (Figure 48). The constant a is equal to the intercept, and b is equal to the slope of a straight line formed by the plot:

$$\frac{\epsilon}{\sigma_1 - \sigma_3} = a + b\epsilon \quad (40a)$$

Numerically, a is the reciprocal of the initial tangent modulus, and $\frac{1}{b}$ is the line at which the curve becomes asymptotic.

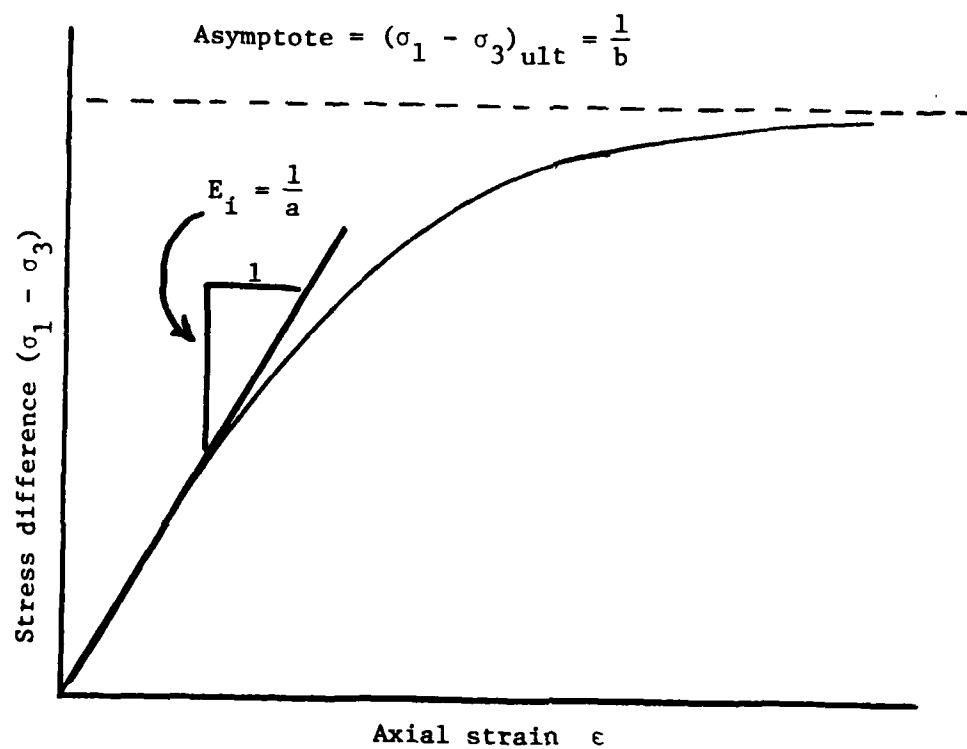


Figure 47. Hyperbolic Curve

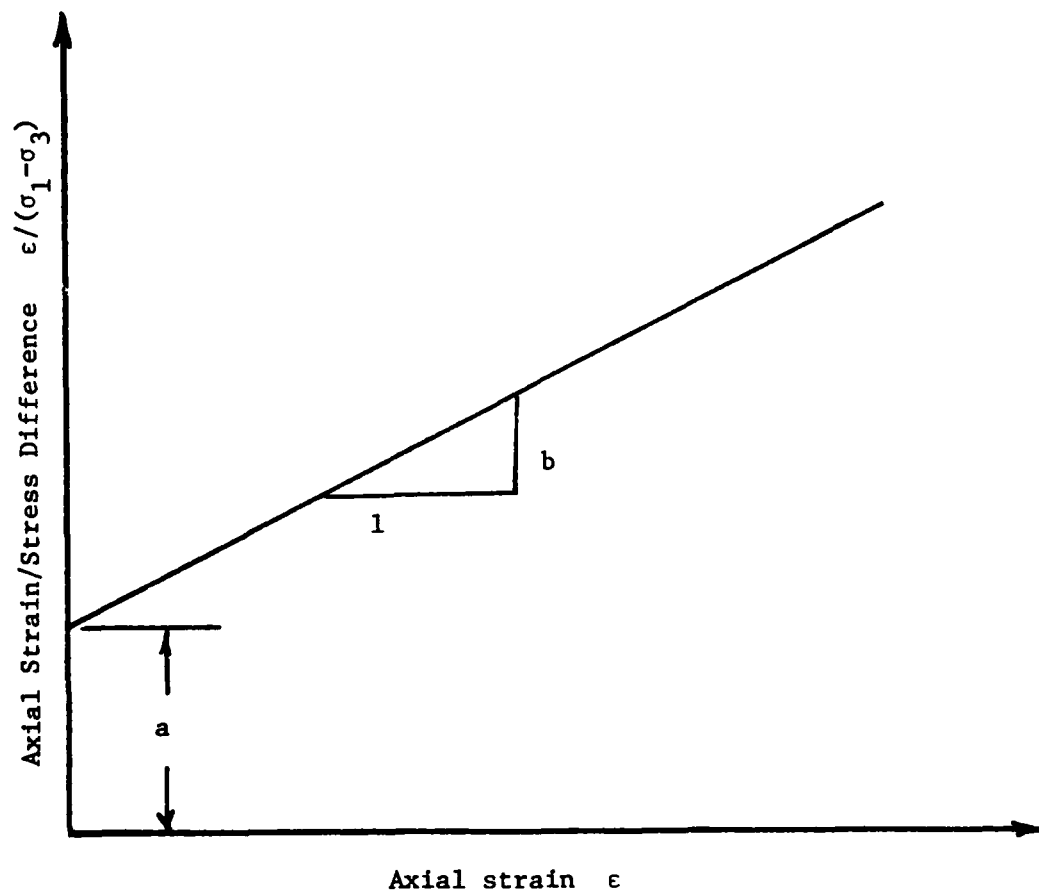


Figure 48. Transformed Axis

$$a = \frac{1}{E_i} \quad (40b)$$

$$b = \frac{1}{(\sigma_1 - \sigma_3)_{ult}} \quad (40c)$$

When triaxial test data are plotted in this fashion, the compressive strength values are slightly lower than the asymptotic value, $(\sigma_1 - \sigma_3)_{ult}$. The asymptotic value may be related to the compressive strength by the following R_f factor:

$$R_f = \frac{(\sigma_1 - \sigma_3)_{failure}}{(\sigma_1 - \sigma_3)_{ultimate}} \quad (41)$$

R_f is always less than 1 and has a range from between 0.75 to 0.9, and it is independent of confining pressure.

Substituting these into Equation 40 yields

$$(\sigma_1 - \sigma_3) = \frac{\epsilon}{\frac{1}{E_i} + \frac{R_f \epsilon}{(\sigma_1 - \sigma_3)}} \quad (41b)$$

Sands are stress-dependent which means that the compressive strength and the initial tangent modulus vary with confining pressure. Janbu (1963) found experimentally that the initial tangent modulus varied with respect to confining pressure based on the expression

$$E_i = K_i P_a \left(\frac{\sigma_3}{P_a} \right)^n \quad (42)$$

where

E_i = initial tangent modulus

P_a = atmospheric pressure

σ_3 = minor principal stress

K_i = a modulus number

n = the exponent determining the rate of variation of E_i with σ_3

where K_i and n are dimensionless numbers that are determined by plotting E_i versus σ_3 on log-log scale and fitting a straight line to the points (Figure 49).

The relationship between compressive strength at failure and confining pressure for sands assumes constant confining pressure during failure, which is

$$(\sigma_1 - \sigma_3)_f = (\tan^2 (45 + \frac{\phi}{2}) - 1) \sigma_3 \quad (43)$$

Substituting this into Equation 40 will yield the following expression for nonlinear stress-strain curves for sand:

$$(\sigma_1 - \sigma_3) = \frac{\epsilon}{\frac{1}{K_i P_a \left(\frac{\sigma_3}{P_a}\right)^n} \frac{R_f \epsilon}{(\tan^2 (45 + \frac{\phi}{2}) - 1) \sigma_3}} \quad (40d)$$

A computer program was written to generate idealized triaxial stress-strain curves based on the parameters in Table 2. Examples of the resulting idealized triaxial stress-strain curves are shown in Figure 50. Figure 51 shows curves for shear transfer versus the dimensionless coefficient, C , which is multiplied times the pile diameter, in inches, to give the pile movement required to produce the shear transfer. The remaining curves are presented in Appendix A.

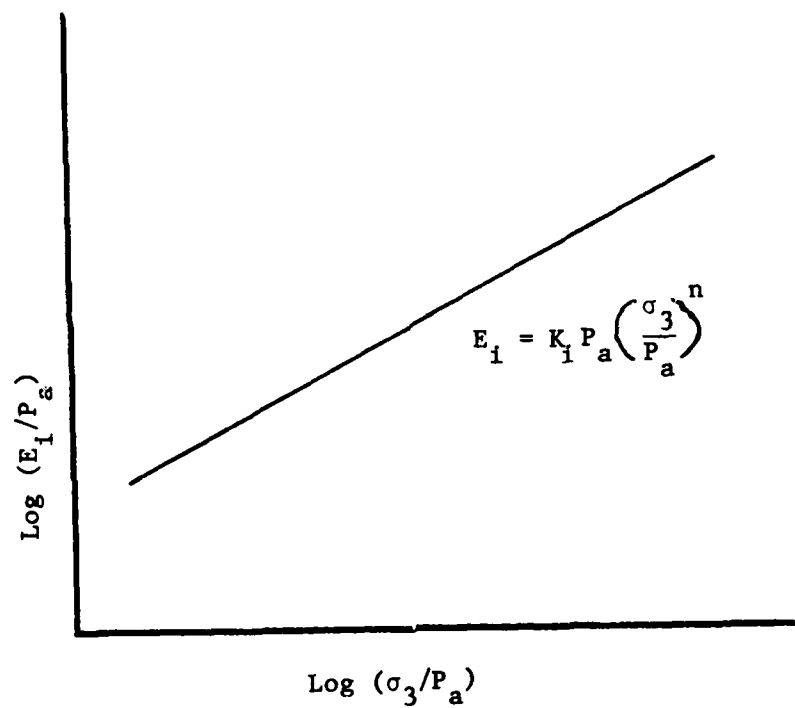


Figure 49. Variation of Initial Tangent Modulus with Confining Pressure

Table 2

Parameters for Hyperbolic Simulation for Sands

<u>ϕ</u>	<u>Relative Density</u>	<u>K_1</u>	<u>n</u>	<u>R_f</u>	<u>γ</u>
30°	Loose 25%	500	0.5	0.80	56.5
33°	Medium 50%	1000	0.6	0.85	61.0
36°	Medium 85%	1500	0.65	0.90	67.5

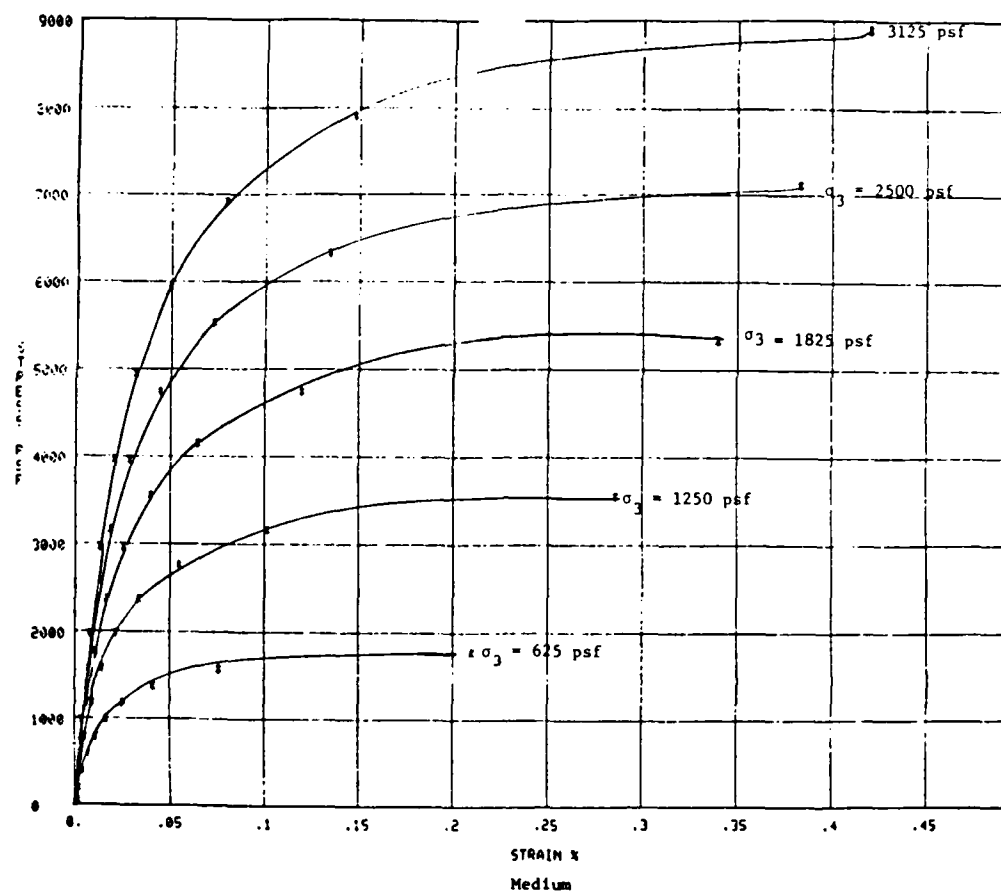


Figure 50. Idealized Triaxial Stress-Strain Curves

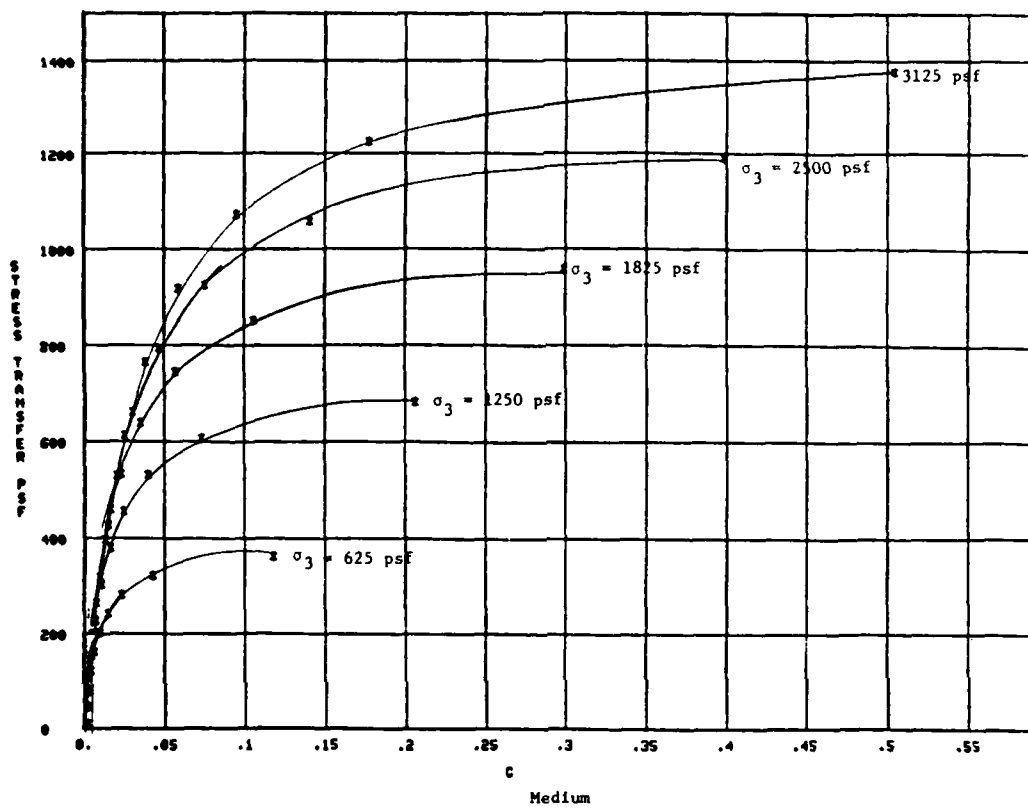


Figure 51. Resulting f-z Curves from Idealized Triaxial Curves

Other Criteria

Coyle (1977) presented another criteria set in his class notes on "Marine Foundation Engineering." For Coyle's (1977) procedure, the maximum side resistance is computed by the same method as Vijayvergiya (1979) proposed, but it has a different displacement function (Figure 52).

Clisby (1970) proposed another procedure for determining load-displacement characteristics of axially loaded piles. His work was founded on the use of laboratory test data to determine these characteristics, direct shear tests for side resistance, and triaxial tests for tip capacity. Obtaining undisturbed samples in sands is expensive and seldom accomplished. For this reason, relating the load-displacement characteristics for axially loaded piles in sands to laboratory tests has been found to be unfeasible. In his later work Clisby (1972) felt that the Dutch cone penetrometer could be used directly to obtain the shear strength parameters of the sand. The Dutch cone penetrometer has shown some promise, but the lack of information on its use in the Lower Mississippi Valley has made this procedure unacceptable at the present time.

Summary of Criteria

The four methods (Coyle-Sulaiman's, Reese and Parker's, Vijayvergiya's, and Coyle's) for determining load-displacement characteristics for pile-soil interaction have a number of

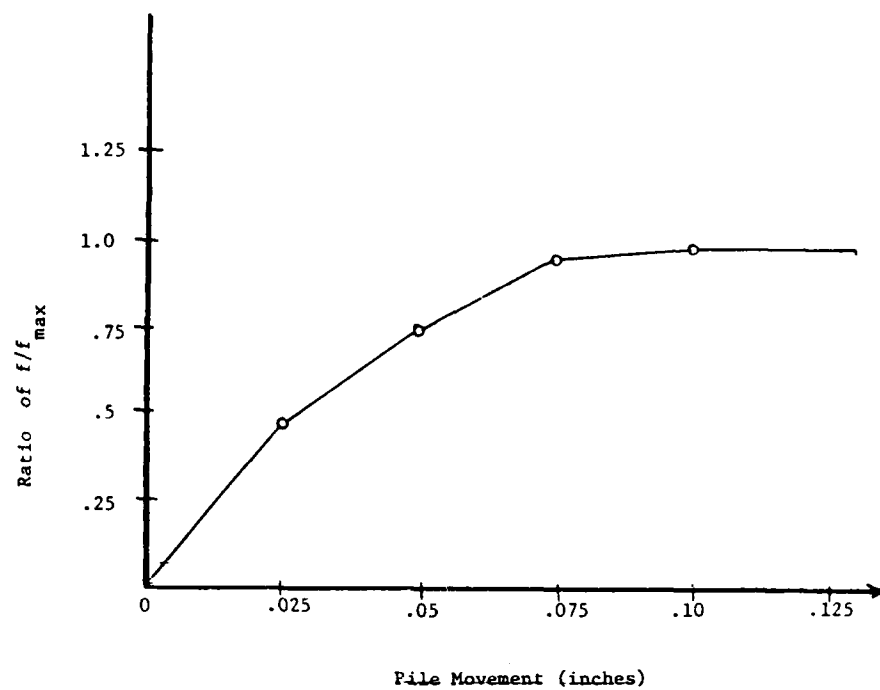


Figure 52. Displacement Function (Coyle 1970)

inadequacies that limit their usefulness. In Coyle and Sulaiman's investigation, their attempt to relate model tests to field performance was unsuccessful. The miniture piles did not show the same trends as the field tests. The field tests showed side resistance decreasing with increasing depth, while the laboratory tests showed increasing side resistance with increasing confining pressure; the confining pressure is comparable to an increase in depth or overburden pressure. They attributed this to the influence of the tip load on the field data. The literature shows no evidence to substantiate this; rather, a review of the literature suggests that two important aspects were not considered. First, residual stresses as a result of driving were not accounted for, as stated in their report, due to the lack of knowledge on how to treat them. The residual stresses may have been the cause of the unusually high values of side resistance near the surface. Second, the normal stress was assumed to be proportional to the overburden pressure. No consideration was given to the arching in the surrounding soil due to driving. Instead of arching, they felt the coefficient of lateral earth pressure and the angle of wall friction varied with depth.

The criteria proposed by Vijayvergiya (1977) and Coyle (1977) have the same limitations as does the static formula. The engineer still must determine a coefficient of lateral earth pressure, K , and use the assumption of the normal stress as being proportional to the overburden pressure. He must also determine a bearing capacity factor, N_q , by some method and again use the normal pressure as being proportional to the overburden stress.

Parker and Reese's (1969) approach was thought to have some promise if used with idealized triaxial test data for typical sands of the Lower Mississippi Valley. A detailed study of this procedure found it to have more limitations than the previous methods. Developing idealized triaxial test data presented the first major problem for the method. Because of the lack of consistency of triaxial test data for the Lower Mississippi Valley and the large variations in the data that was found in the literature, using values in Table 2 for a preliminary study resulted in the shear transfer versus pile movements curves increasing with confining pressure, which is equivalent to increasing depth. The rate was far greater than field evidence substantiated. For this reason, the procedure was unacceptable and was not pursued any further.

The true test of the criteria is their ability to predict the performance of actual field pile tests. In the next chapter, the three remaining criteria will be evaluated against 14 field pile load tests at three different sites.

CHAPTER 4: EVALUATION OF PUBLISHED CRITERIA

The true test of the criteria is to compare them to actual field pile tests. As late as the 1940's, Terzaghi and Peck (1967) stated that the only method available to the foundation engineer to determine the friction capacity of a pile was the field pile load test. The field pile load test has been and still is the principal source of information for the design of large-scale pile foundations. For criteria to be reliable, they must compare favorably to results of field pile tests.

Only instrumented field pile tests were chosen because they can provide the necessary pile-soil interaction information required for a comparison of the criteria. The field pile load tests that were investigated are:

- (1) Arkansas River Lock and Dam No. 4 (6 tests).
- (2) Ascalmore Creek-Tippo Bayou Control Structure (2 tests).
- (3) Red River Lock and Dam No. 1 (6 tests).

Arkansas River Lock and Dam No. 4 Pile Tests

The pile tests were conducted at a site near Lock and Dam No. 4 on the Arkansas River below Pine Bluff, Arkansas. The site is located 1 mile downstream of the Bob Roger Bridge on the St. Louis and Southwestern railroad and about 500 ft east of the bank of the Arkansas River. The pile tests were conducted as part of a comprehensive study to develop information regarding the

characteristics of different types of piles driven into alluvial sands of the Lower Arkansas River Valley.

The typical soil profile in the Lower Arkansas River Valley consists of alluvial deposit strata of loose surface silts, sandy silts, and clays of variable thickness. This is underlain by a stratum of medium to dense sand and silty sand with a thickness ranging from 90 to 150 ft which overlies a stratum of deeply bedded tertiary clays. These conditions are very similar to the Lower Mississippi Valley.

Borings indicated that the soil profile at the site of the test consisted of three major soil strata: a surface blanket of silt and fine sands which extended from the ground surface at el 198 to 185*, a deep stratum of relatively dense medium to fine sand which extended to about el 92, and a base of tertiary clay of undetermined thickness. Some thin seams of silt and clay were present in the deep stratum between el 160 and 137. Two series of borings were made at the test site to determine the subsurface conditions prior to testing. The standard penetration resistance of the upper 60 ft of the deep sand stratum into which the piles were driven showed a general increase with depth, varying from 11 to 50 blows per foot (Appendix B, Figure B1). The average dry density ranged from 90 to 109 pcf but showed no significant trends with depth. Another series of test borings was made to determine the effects of the excavation of 20 ft on the relative density of the subgrade.

*Elevations (el) are in feet referenced to mean sea level.

As mentioned above, after the excavation of 20 ft, the standard penetration results decreased by approximately 15 percent with no measurable change in relative density. A series of borings was made after the pile driving to determine the effect of driving on the relative density. No significant changes were found. Laboratory tests performed on samples from the deep sand stratum consisted of mechanical analysis and several direct shear tests to determine the sliding friction between pile material and foundation sand. The soil was classified as being medium to dense sand and silty sand (SM-SP) with a submerged unit weight equal to 62.8 pcf. The angle of wall friction between the steel ranged from 23 to 30 degrees, the angle of wall friction for mortar ranged from 28 to 36 degrees, and the angle of internal friction ranged from 31 to 35 degrees. Figure B1 shows the profile assumed for the evaluation of load test data.

Load tests were performed on prestressed concrete piles, steel pipe piles, steel H piles, and timber piles. Steel pipe piles and steel H piles were instrumented to develop a comparison between displacement and nondisplacement piles. Strain gages were attached to determine the distribution of load in the piles. Two types of strain gages were used: steel strain rods, and electric-resistance strain gages. On selected piles, both types of strain gages were used to enable a comparison. Table 3 lists the piles that were selected for this study and their properties. The results of the load tests on these piles are shown in Figures B2-B9.

The field data were analyzed as outlined previously in this report and yielded side resistance versus pile movement curves ($f-z$)

Table 3

Pile Types for Arkansas River Tests

Test Pile	Pile Type & Nominal Size	Cross Sectional Area A in ²	Modulus of Elasticity E 10 ⁶ psi	Penetration ft
1	12.75" OD pipe (0.33" wall)	17.12	29.0	53.1*
2	16" OD pipe (0.312" wall)	23.86	29.0	52.8*
3	20" OD pipe (0.375" wall)	27.36	29.0	53.0*
6	14HP73	25.70	29.0	40.
7	14HP73	29.33	29.0	52.1*
9	14HP73	26.28	29.0	53.2*
10	16" OD pipe (0.312" wall)	23.86	29.0	53.1*

*Only the first 50 ft of penetration was used for the side resistance comparisons.

as shown in Figures B10-B17. The tip load versus pile movement curves (P-z) are shown in Figures B18 and B19. The f-z curves for test piles 6, 7, 9, 10 show that these piles never were loaded to their full capacity. The field data did not include the necessary information to perform a rigorous analysis of the residual stresses.

Ascalmore Creek-Tippo Bayou Control Structure Pile Tests

The Ascalmore Creek-Tippo Bayou Control Structure is located approximately 3.4 miles northeast of Philipp, Mississippi, between a Tallahatchie County road and the Tallahatchie River at Mile 207.7. The control structure is for the diversion of flow into the Tallahatchie River from the major drainage outlet of the Ascalmore Creek-Tippo Bayou watershed which is part of the Yazoo Basin of the Mississippi Delta Basin. The control structure consists basically of three reinforced concrete U-frame structures founded on piles. The estimated number of piles was 390 with an estimated total length of 30,900 linear ft.

Ascalmore Creek-Tippo Bayou is located in the Yazoo River Basin, a physiographic subprovince of the Lower Mississippi Valley which is part of the Central Gulf Coastal Plain. The area was formally an active meander belt of the ancient Mississippi and Ohio Rivers. It is characterized by low-relief floodplains and meandering belts of topography. The area is covered by a band of relief alluvial fan material which is deposited from the loess hills to the east. The

Yazoo Basin segment of the Mississippi Alluvial Valley consists of fine- to coarse-grained alluvial sediments over tertiary stiff to hard clays or fine- to medium-grained dense sands. The alluvial sediments can be divided into two distinct units, top stratum and substratum. The top stratum is distinguished by fine-grained clays and silts and silty fine-grained sands. The substratum deposits are generally fine- to medium-grained lignite sands that grade downward into coarser sands and gravels.

The control structure is located in an abandoned channel deposit. The top stratum consists of predominantly thick inorganic clay of high plasticity having a thickness of approximately 55 ft. A large portion of this top stratum will be excavated for the control structure, leaving a minimum of 20 ft ranging up to a maximum of 35 ft of top stratum. After excavation, the material left in the top stratum consisted of approximately 7 ft of inorganic clay with low plasticity, 9 ft of silty material having a low plasticity, and 2 ft of silty sand. The alluvial substratum consists of 20 ft of poorly graded sand, lignite, and gravel which is resting on tertiary deposits consisting of 11 ft of silty sand; 1 ft of high-plasticity inorganic clay; and 1 ft of sand gravel. Four undisturbed sample borings were made along the centerline of the structure and were drilled to the tertiary clay. One of the borings was continuously sampled throughout the entire length of the clay. A split spoon sampler was used in the substratum to obtain the blow count data. No laboratory tests were conducted on the sands of the substratum to determine strength properties. All strength properties were based on blow counts and

experience in the area. The stratification of the profile and results of the standard penetration tests are shown in Figures B20 and B21.

The pile testing was conducted by the F&M Branch of the Corps of Engineer's Vicksburg District after excavation for the foundation was completed. Two HP 14 by 89 steel H piles, one 100 ft long and the other 90 ft long, were tested at the site. Test pile No. 1 was driven at the approximate location of the chamber monolith, and test pile No. 2 at the spillway basin monolith. Cyclic compression loading tests were conducted on both piles, and a cyclic tension loading test was run on pile No. 1. For the tests the piles were spliced, and strain gages and lead hangers were installed. The strain gages located as shown in Figures B20 and B21 were used to provide elastic compression data along the pile. Extensometers were employed to measure pile head movement. The pile tip movements were monitored by a piano wire strung inside a channel from the tip of the pile to a pulley near the pile head. Observations were made from a reference point on the piano wire and a fixed scale. The estimated pile capacities from the static formula were 300 tons in compression and 50 tons in tension for the tests. Pile No. 1 and pile No. 2 both had approximately 280 tons of compression applied before failure. A cyclic test was conducted by loading in increments of 25 tons for two increments and then unloading to 0. For the next cycle, the pile was reloaded to the same level as the last load of the previous cycle and two more increments of 25 tons were applied. The cyclic loading was continued until failure. Measurements of strain and of head and tip movements were made at each increment and at zero butt loading. The rate of load during the tests

was 2 tons per minute. Each increment was held constant for an hour or until the pile head movement was less than 0.01 in./hr. The results from the tests are presented in Figures B22-B27. The test data were reduced by the method described previously in this report.

Figures B28 and B29 present the unadjusted side resistance versus pile movement (f - z) curves for the two pile tests. Figure B30 shows the unadjusted tip load versus tip movement (q - z) curves of the two tests.

Figures 53 and 54 show the load distribution in the piles tested. The loads measured in the top section of the piles for the last three applied loads are greater than the applied loads. This is due to residual loads in the piles. The first evidence of these residual loads was found in a review of the load distribution in the piles at zero butt load. After the last loading cycle was released, the loads measured in the piles were approximately equal to excess loads in them during the last loading increment. These misleading readings are due to zeroing the strain gages after driving. The residual loads were adjusted as described earlier in this report. The new load distribution curves are shown in Figures B31 and B32, and the resulting f - z curves and q - z curves for the sands are presented in Figures B33, B34, and B35, respectively.

Red River Lock and Dam No. 1 Pile Tests

Lock and Dam No. 1 is located in southwestern Louisiana in a 1.7-mile-long cutoff between Miles 42.6 and 51.1, approximately 9 miles

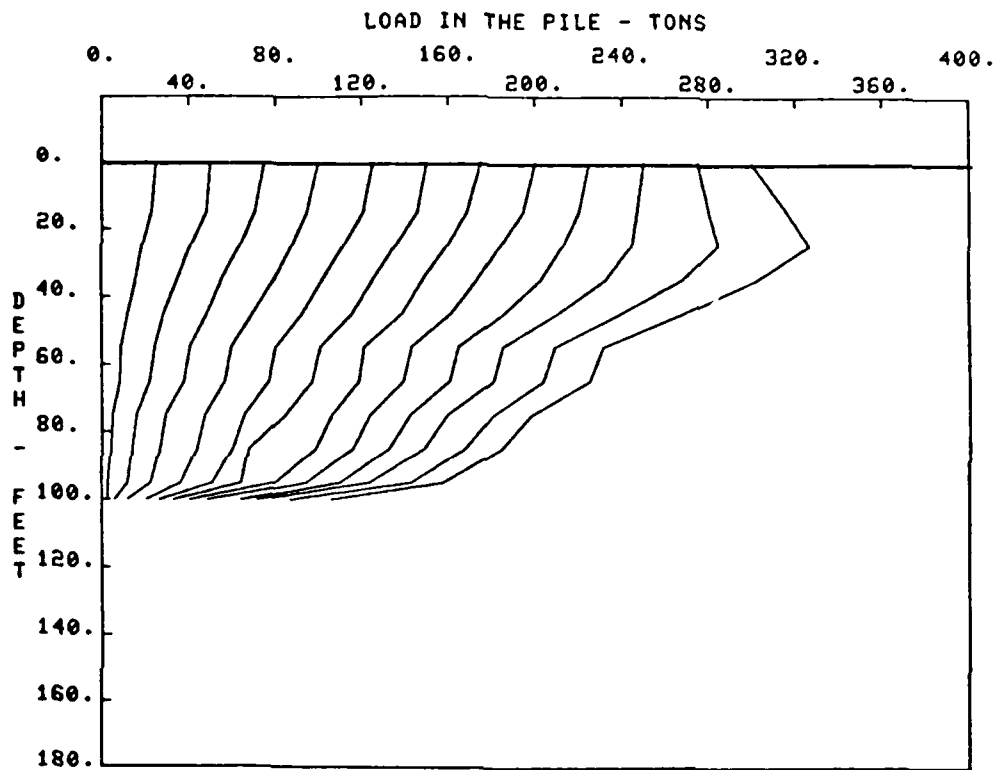


Figure 53. Unadjusted Load Distribution in Pile No. 1, Ascalmore Creek-Tippo Bayou

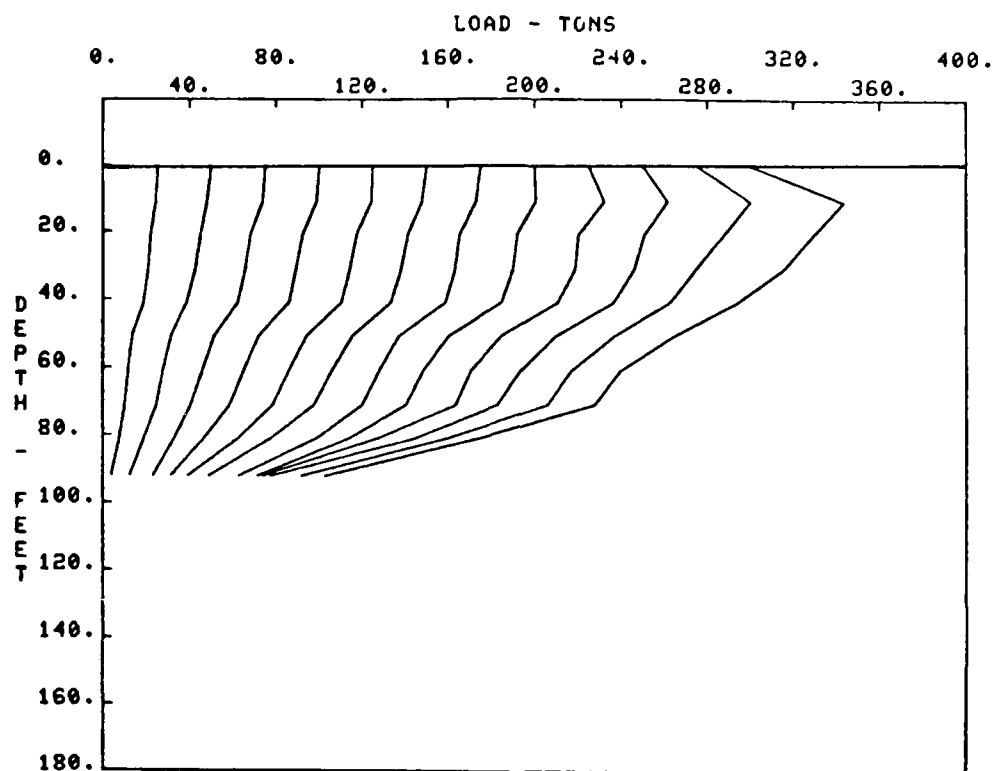


Figure 54. Unadjusted Load Distribution in Pile No. 2, Ascalmore Creek-Tippo Bayou

upstream from the confluence of the Red and Black Rivers. The lock structure is founded on soil, while the dam is placed on H piles. The lock and dam is located within the Gulf Coastal Plain Province near the western edge of the Mississippi River floodplain. The area is characterized by natural levees, backswamps, oxbow lakes, and the bridge and topography of meander scars. The sedimentary history is of the Pleistocene Epoch. Deposits of sand and gravel were laid down as the sea rose to its present level about 5000 years ago. The Mississippi River and its tributaries gave way to a meandering pattern. The sediments laid down during meandering are silts and clays.

The soil conditions under the dam consist of a layer of medium to stiff Holocene backswamp clays from the ground surface at el 28 to the top of the substratum of sands between el -50 and -70. The bottom of the substratum sand layer extends below el -140. The excavation for the dam foundation extends to approximately el -22. Figures B36-B39 show the stratification and SPT results for the test site.

A number of pile tests were performed at the site on H piles and prestressed concrete piles. Six different H piles were instrumented with strain rods. The tests were conducted after excavating approximately 50 ft of overburden material. Two sites were chosen for the tests. At site PT-A four piles were tested, and at site PT-S two piles were tested. Three of these piles were retested, one at site PT-S and two at site PT-A. The piles were driven through approximately 48 to 50 ft of clay and silt into a substratum of sand at site PT-A. The substratum was composed of fine sands and silty

sands. At the second site, PT-S, the piles were driven through approximately 25 ft of clay into the substratum of sand. This substratum was composed of fine, medium, and coarse sands. The range of penetration into the sand for the piles at PT-A was between 10 and 30 ft and at site PT-S between 58 and 78 ft. Borings were made at or near the test piles. SPT results were taken from the nearest boring to determine the strength of the substratum sand. The piles were driven using a vibratory hammer. In analyzing the field data, two of the pile tests showed instrumentation error and were not used in this study. The results of the load tests are shown in Figures B40-B53. The f-z curves for the sands are presented in Figures B54-B60. Since the vibratory hammer places residual loads in the piles as does an impact hammer, the piles tested were adjusted for residual loads. Resulting load distributions are presented in Figures B61-B67, and f-z curves from the adjusted distributions are shown in Figures B68-B74.

In the retested piles, the capacity was substantially increased. This was attributed mainly to the increased tip resistance in the retested piles which can be seen in Figures 55-58. One explanation from these results is that the vibratory hammer does not compact the soil under the tip to the same degree as an impact hammer, thus resulting in less capacity. The increase in capacity for the retested piles would be due to the compaction and densification of the soil under the tip from the first tests on the piles. The higher skin friction from the unadjusted tests can be attributed to residual stresses from the first tests. Another possible explanation is that the vibratory hammer induces high pore water pressures in the soil

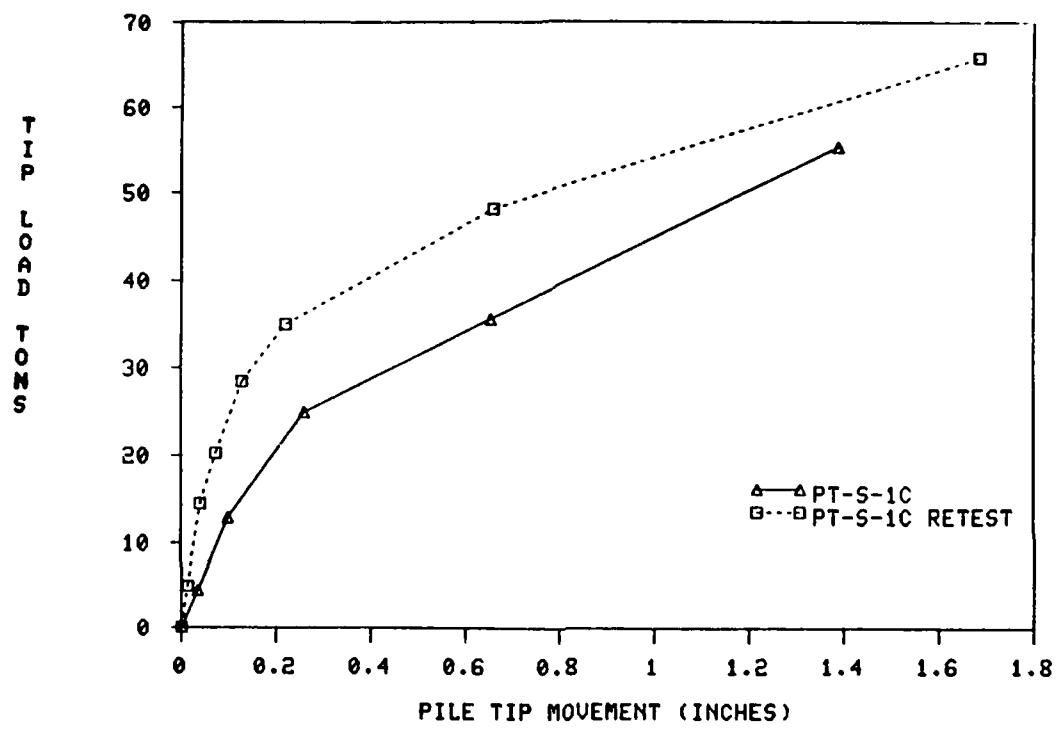


Figure 55. Unadjusted P-z Curves, Red River, H Piles

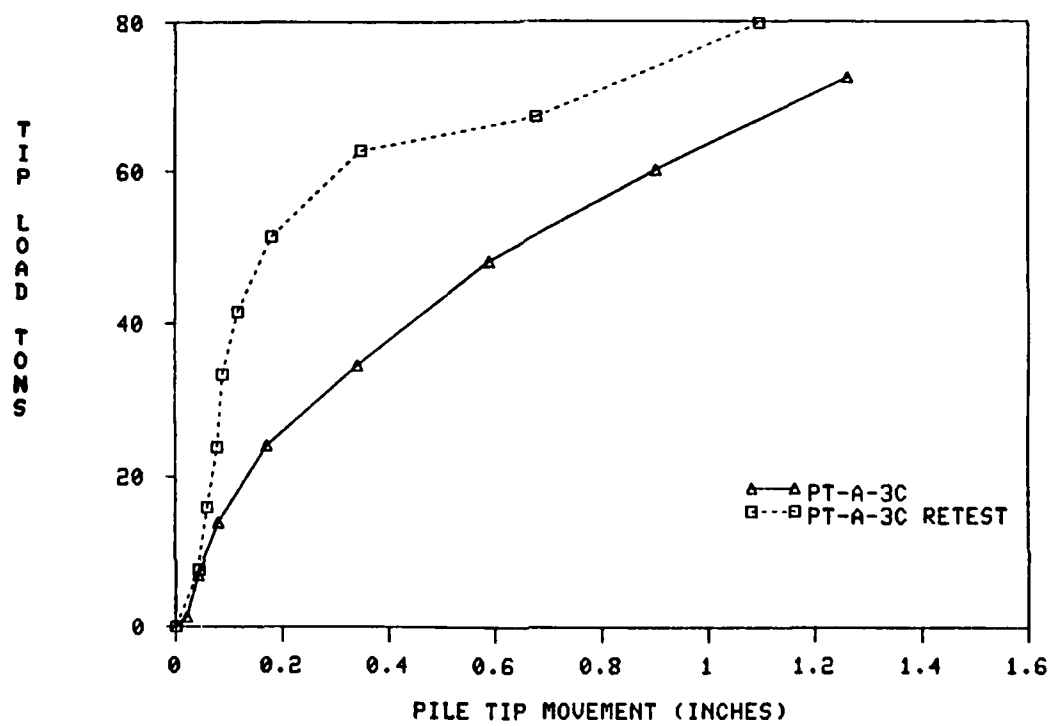


Figure 56 . Unadjusted P-z Curves, Red River, H Piles

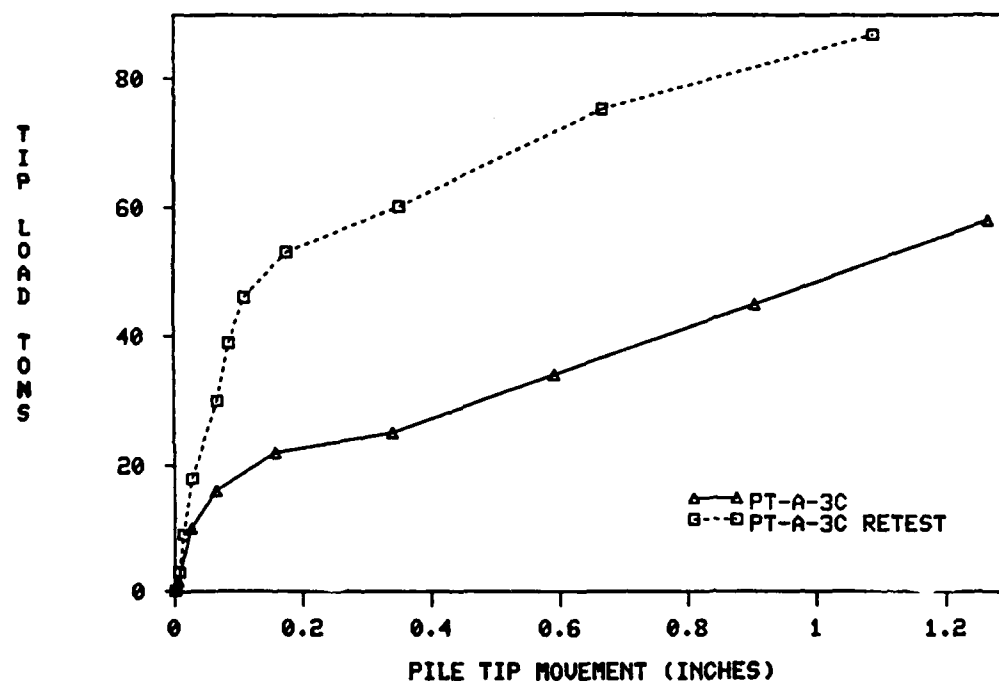


Figure 57. Adjusted P-z Curves, Red River, H Piles

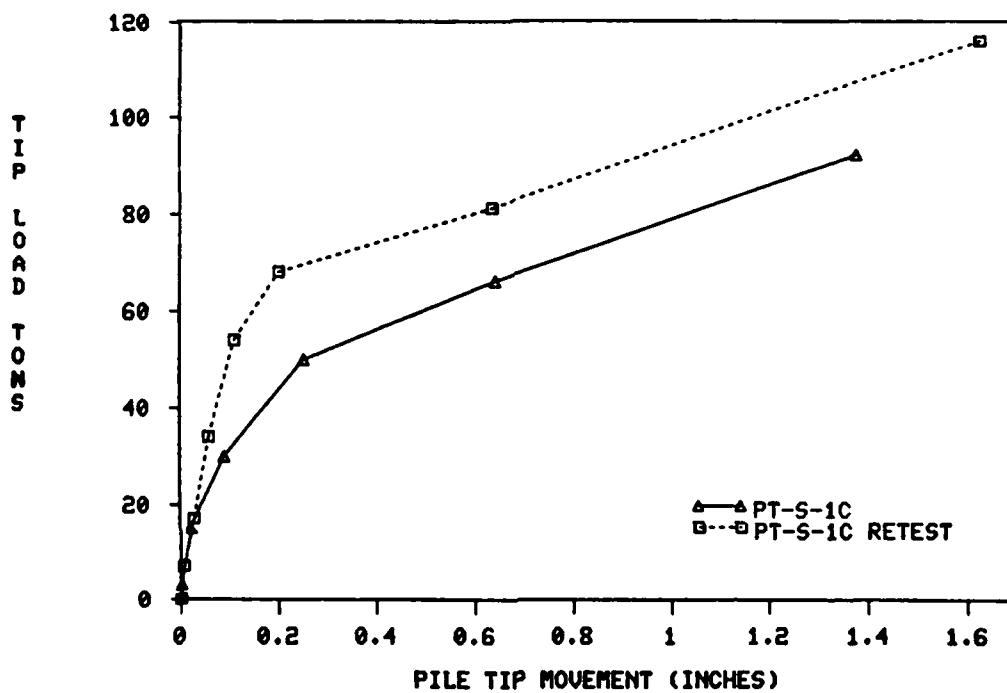


Figure 58. Adjusted P-z Curves, Red River, H Piles

which reduces the effective stress and shear strength of the sand.

Comparison of Criteria with Field Test Results

The first step in conducting a comparison of the available criteria to field pile test results is to determine the shear strength of the sand at each site. The shear strength parameters were based on standard penetration tests (SPT) performed at the sites. The SPT results were corrected as shown previously in this report. The soil description, N values, angle of internal friction, and overburden pressure for the pile tests used in this study are presented in Table 4.

The comparison performed consisted of comparing field f-z curves with computed f-z curves based on the criteria presented by Coyle and Sulaiman (1967), C-S, Vijayvergiya (1977), V, and Coyle (1977), C, referred to previously. The displacement functions are shown in Figures 59, 60, and 61, respectively.

The shear strength used in the Coyle-Sulaiman (1967) criteria was determined from

$$S = \bar{\sigma}_n \tan \phi' \quad (44)$$

where $\bar{\sigma}_n$ = effective normal stress

ϕ' = effective angle of internal friction

The maximum side resistance for the Vijayvergiya (1977) and Coyle (1970) criteria was determined from

Table 4

Soil Properties

Test Site	Substratum Soil Description	Test Pile	Depth ft	σ_v tsf	N_f	N_c	ϕ deg
Ascalmore Creek-Tippo Bayou	Fine to medium sand (SP) w/some Silty sand (SM)	#1	43.0-53.0	1.6	44	20	33
			53.0-63.0	1.9	48	20	33
			63.0-73.0	2.3	48	19	32
			73.0-83.0	2.7	95	21	34
		#2	20.0-30.0	.67	42	21	33
			30.0-40.0	.93	42	20	33
			40.0-50.0	1.2	67	24	36
			50.0-60.0	1.6	55	19	33
			60.0-70.0	1.9	34	13	30
			70.0-80.0	2.2	80	25	35
			80.0-90.0	2.5	77	22	34
Arkansas River	Fine silty sand (SP-SM) to medium sand (SP)	All Tests	0-15	.24	30	23	34
			15-25	.63	33	23	34
			25-33	.91	30	19	32
			33-40	1.15	34	21	33
			40-47	1.37	36	20	33
			47-53	1.57	43	23	33
Red River	Find sand (SP) and silty sand w/clay strata (SM)	PT-A -1C	34.0-50.2	.91	40	20	32
			50.2-58.2	1.27	44	20	32
		3C, 2C	32.9-54.1	.96	44	20	32
			54.1-67.1	1.45	53	21	33
		PT-S -1C	39.7-69.0	1.39	30	19	32
			69.0-84.2	2.03	65	20	32

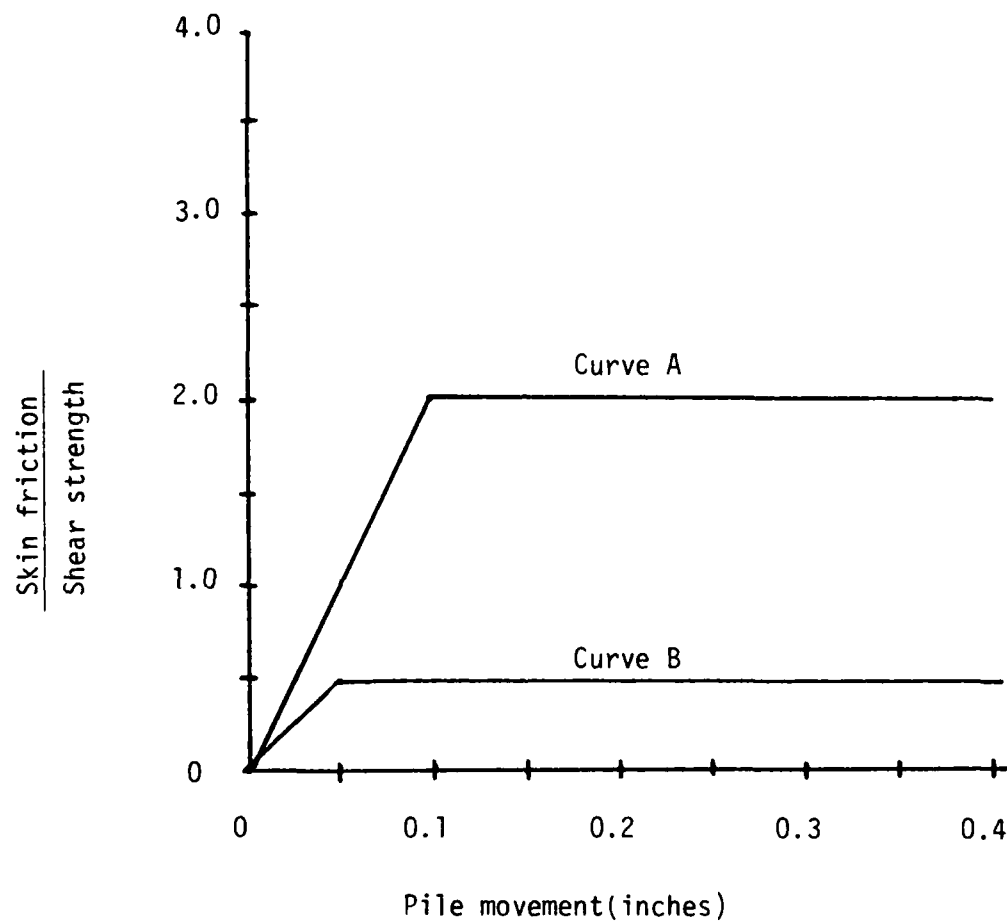


Figure 59. Displacement Function (After Coyle-Sulaiman 1970)

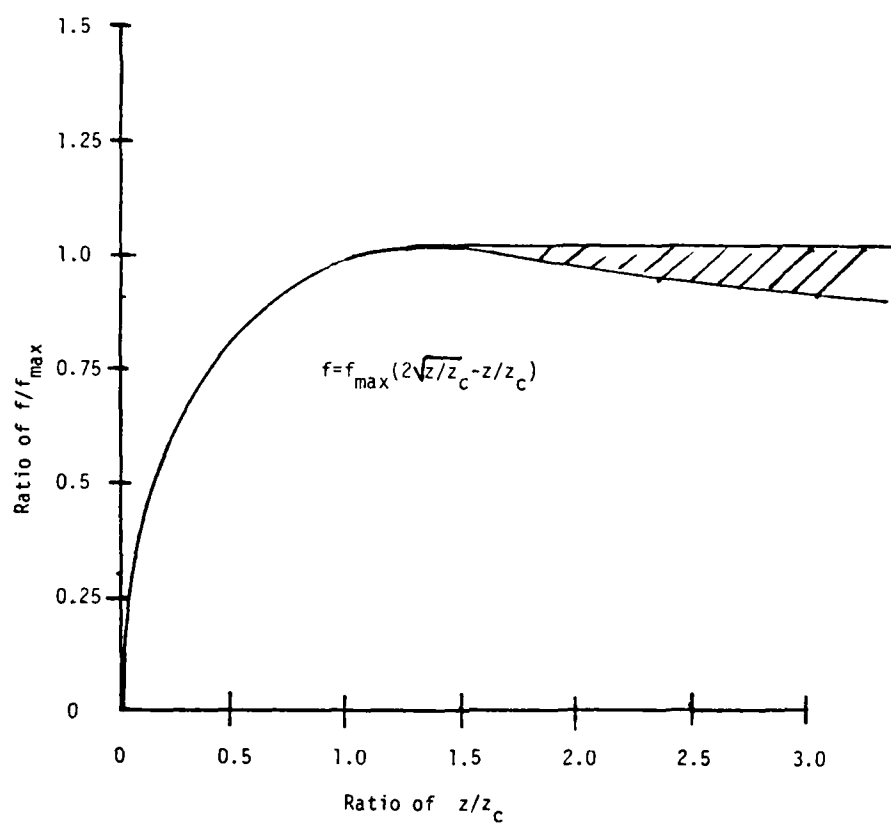


Figure 60. Normalized f - z Curve for Clay and Sand
(After Vijayvergiya 1977)

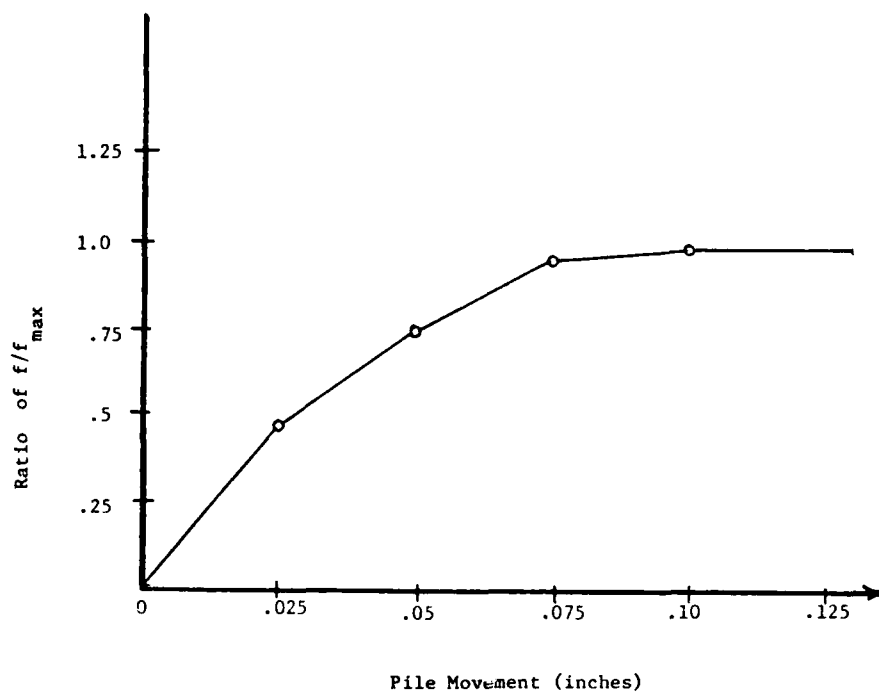


Figure 6L Displacement Function by Coyle (1970)

$$f_{\max} = K \bar{\sigma}_n \tan \delta \quad (45)$$

where K = coefficient of lateral earth pressure

$\tan \delta$ = coefficient of friction between the pile and soil

A value of 1 was used for the coefficient of lateral earth pressure, K , in the comparison. Complete results of the comparison are presented in Appendix C. On the field f - z curves, the symbols indicate the measured values; the computed f - z curves are plotted as smooth curves. In the next section, the results of this comparison will be used to evaluate these criteria.

Evaluation of Criteria

In evaluating the three criteria, two characteristics were observed: the magnitude of the maximum side resistance, f_{\max} , and the shape of the f - z curves with respect to the shape of the field curves. The magnitudes of the side resistance for the V and C criteria were calculated by a simple procedure; they will be examined first. At the Arkansas River site, the two criteria grossly underestimated the maximum side resistance in the upper portion of the pile while overestimating it in the lower portion. An example of this is shown in Figure 62. For the Ascalmore-Tippo tests, the V and C criteria produced a maximum side resistance that was close to the field curves for the midsection (30 to 60 ft from the ground surface)

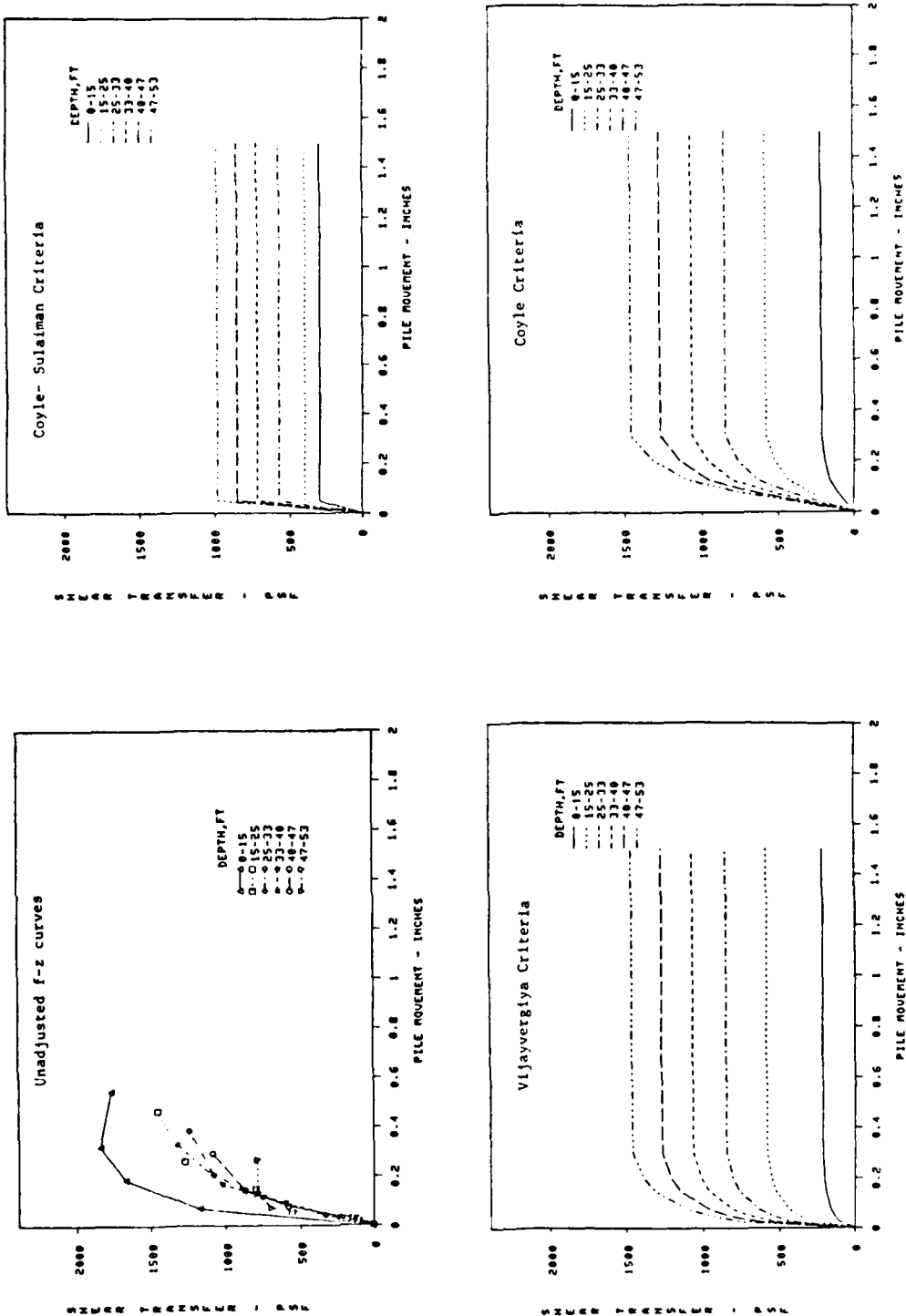


Figure 62. Comparison of f-z Criteria to Unadjusted Field Curves, Arkansas River, Test Pile No. 2

of the pile, but for the lower section they produced a side resistance more than twice the reported field maximum. An example demonstrating this is shown Figure 63. In the Red River tests, the V and C criteria produced maximum side resistance values that compared more closely with the field curves except at depths greater than 50 ft from the surface, examples of which are shown in Figures 64-67. At depths greater than 50 ft, the V and C criteria grossly overestimated maximum side resistance. The overestimations by the two criteria are due to linear dependence of side resistance on the overburden pressure.

The C-S criteria give better correlation with the field curves for the lower portion (40 to 80 ft below the surface) of the piles in the deep substratums of sand, but for depths 10 to 30 ft below the surface, the C-S criteria underestimated the side resistance. Examples of this are shown in Figure 62 for the Arkansas River tests, Figure 63 for the Ascalmore Creek-Tippo Bayou tests, and Figures 68 and 69 for the Red River tests. As with the other criteria, the C-S are linearly dependent on the overburden pressure. It can be seen from the field curves and from the review of the literature that the side resistance is not linearly dependent and may even be independent of overburden pressure.

For the second characteristic, shape, the C-S criteria yielded the poorest result. The curves have a linearly increasing portion and a horizontal straight line at maximum side resistance, f_{\max} , which causes them to be the least representative of the three criteria. The initial portion of curves produced by the V criteria are much steeper

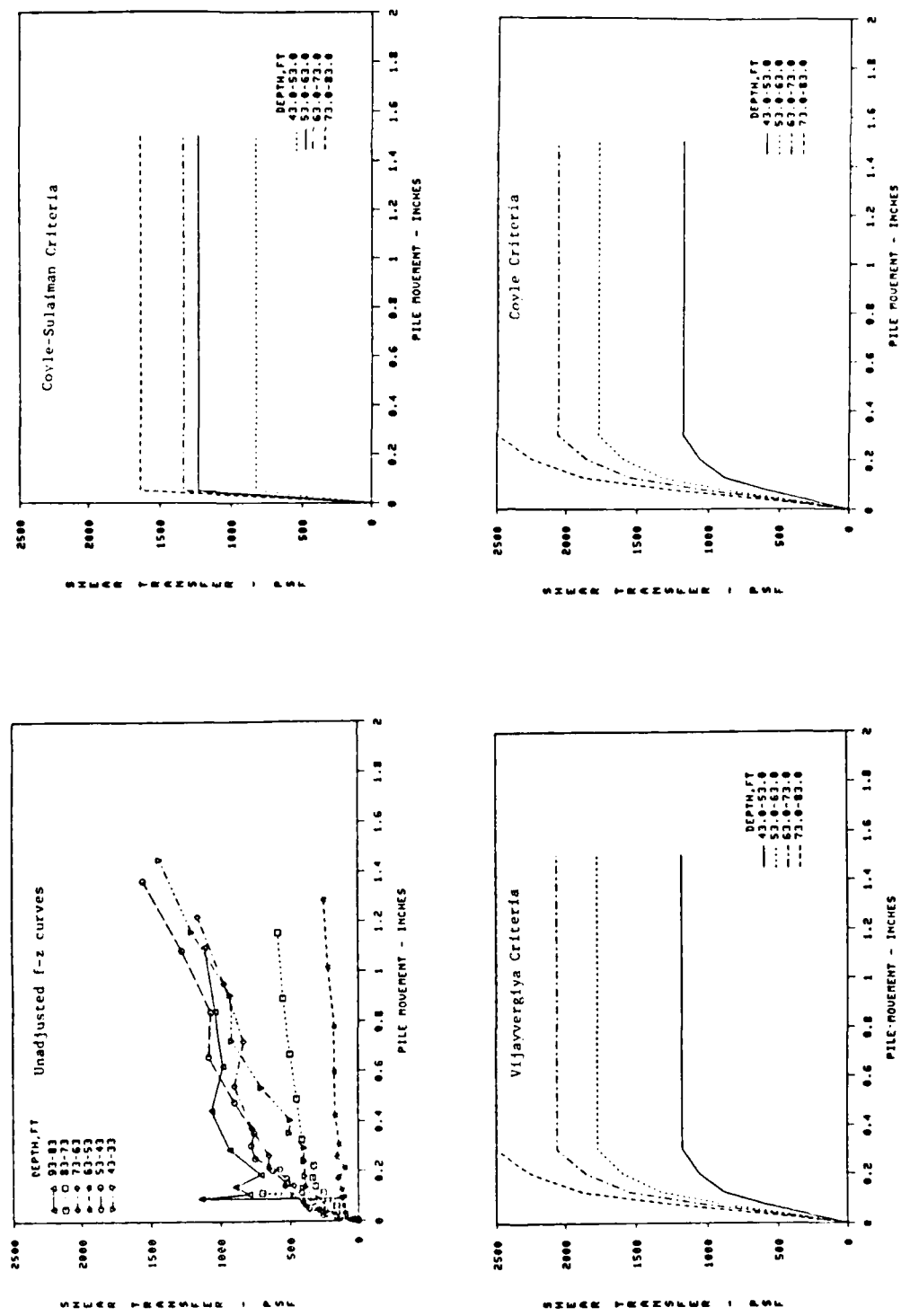


Figure 63. Comparison of f-z Criteria to Unadjusted Field Curves, Ascalmore Creek-Tippo Bayou, Test Pile No. 1

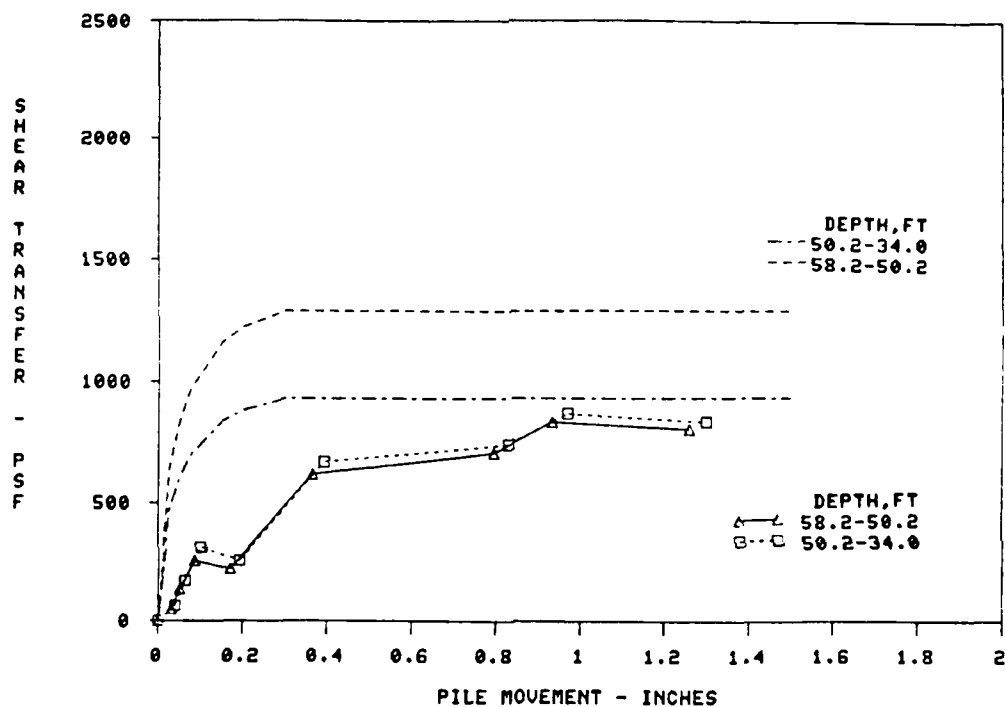


Figure 64. Comparison of f-z Criteria to Unadjusted Field Curves, Red River, Test Pile No. PT-A-1C, Vijayvergiya Criteria

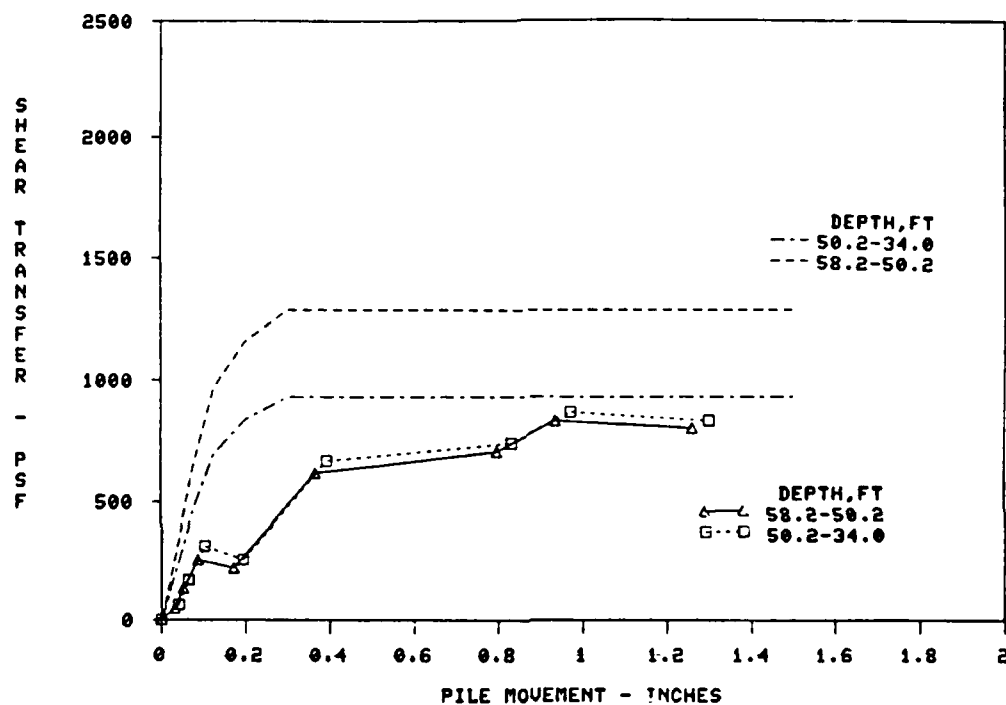


Figure 65. Comparison of f-z Criteria to Unadjusted Field Curves, Red River, Test Pile No. PT-A-1C, Coyle Criteria

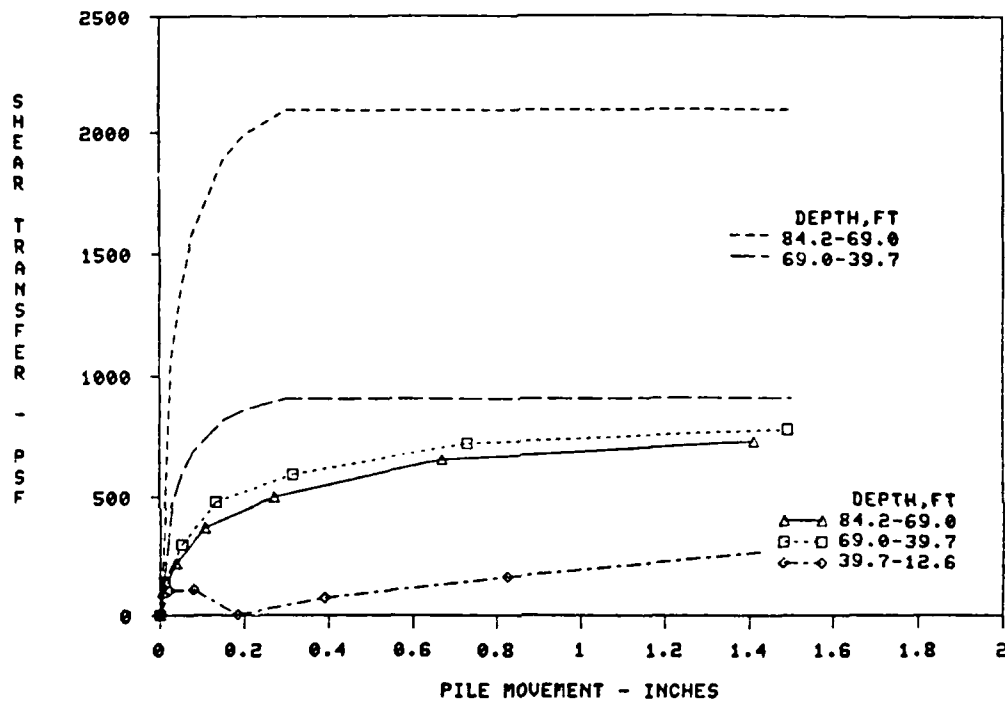


Figure 66. Comparison of f-z Criteria to Unadjusted Field Curves, Red River, Test Pile No. PT-S-1C, Vijayvergiya Criteria

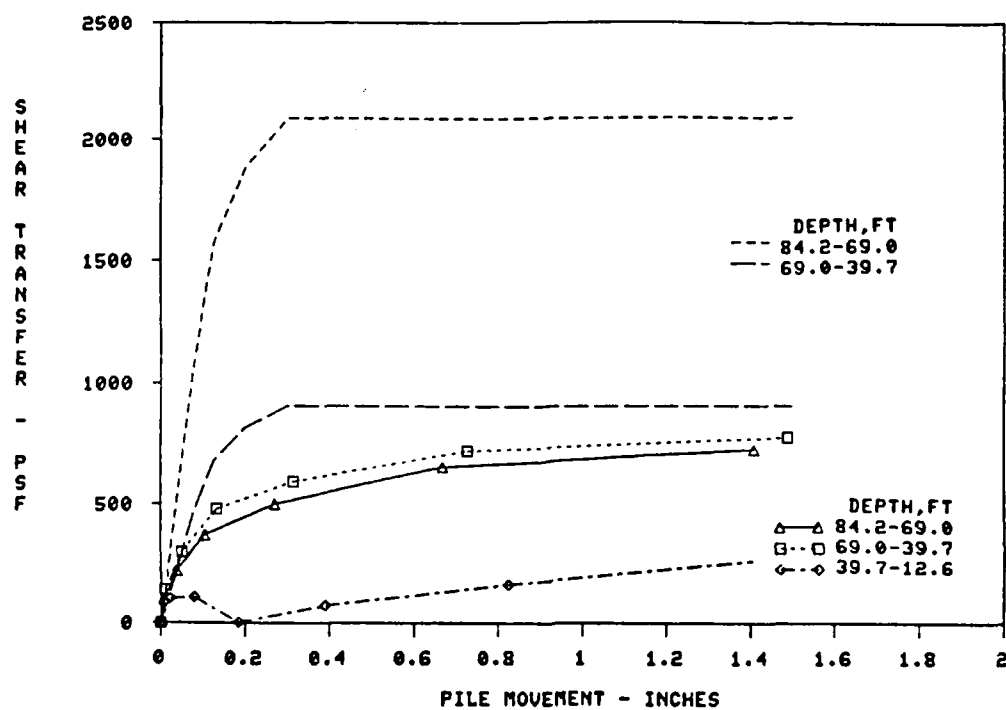


Figure 67. Comparison of f-z Criteria to Unadjusted Field Curves, Red River, Test Pile No. PT-S-1C, Coyle Criteria

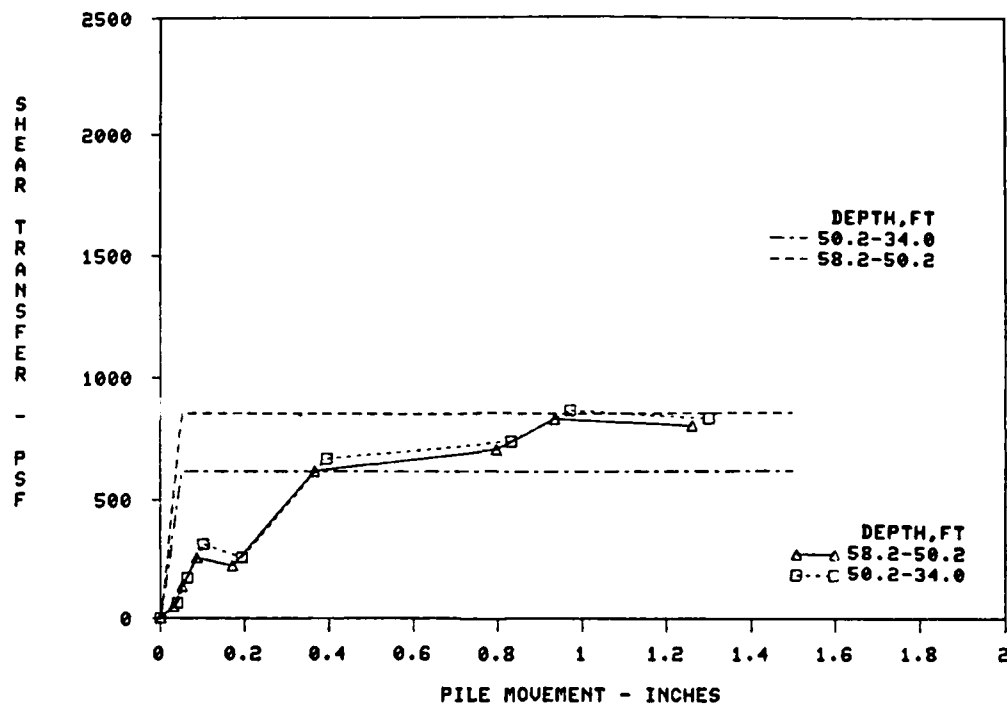


Figure 68. Comparison of f-z Criteria to Unadjusted Field Curves, Red River, Test Pile No. PT-A-1C, Coyle-Sulaiman Criteria

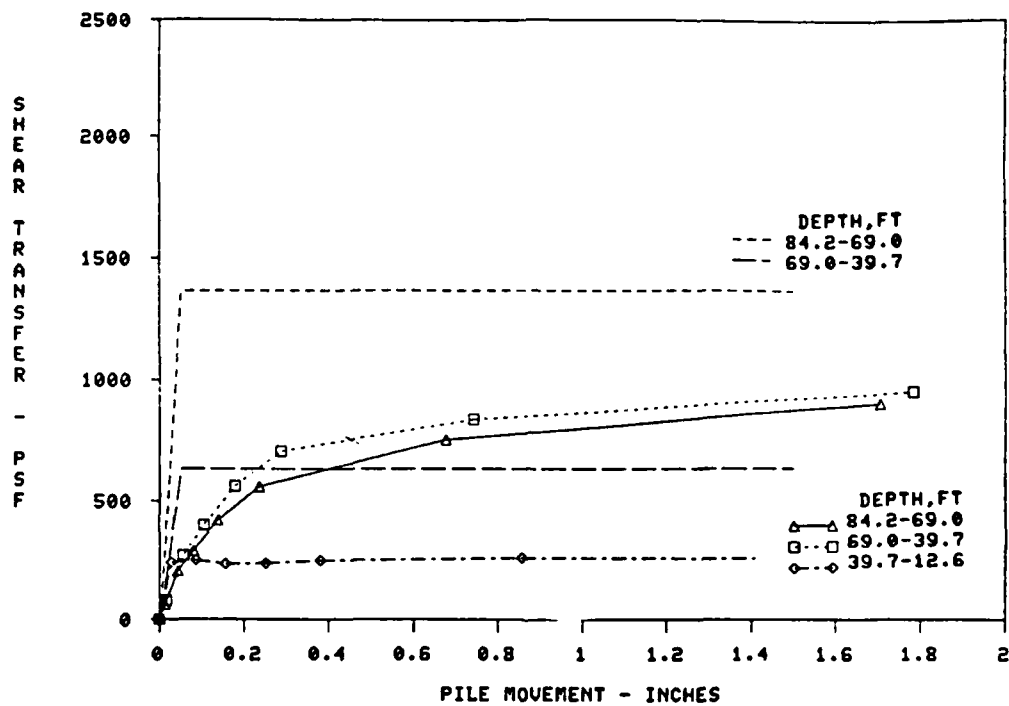


Figure 69. Comparison of f-z Criteria to Unadjusted Field Curves, Red River, Test Pile No. PT-S-1C
Coyle-Sulaiman Criteria

than the field curves causing the curve to level off at lesser pile movement. The C criteria give the best match to the shape of the field curve, but the initial portion was steeper than the field curves. The initial slope of the field curves seems to be dependent on the densities of the sand and may depend on whether the pile was a displacement or nondisplacement pile. This dependence on pile type was seen in the Arkansas River tests where pipe piles and H piles were tested. It will be investigated in the next chapter.

Summary

The three criteria for determining side resistance versus pile movement investigated in this chapter have demonstrated a lack of agreement with field results in several ways. First, and most important, is their inability to predict the magnitude of the maximum side resistance, f_{\max} . These criteria give acceptable values for depths of penetration in the range 30 to 50 ft, but show no consistent trend for the shallower or deeper depths of penetration. The lack of consistency severely limits the reliability of the criteria for estimating the pile capacity. Second, the shape of the curves produced by these criteria does not accurately simulate the field curves in this study. The curves produced by these criteria have a steeper initial slope which results in them reaching the maximum side resistance with smaller pile movement, resulting in the computed pile head movements being less than the actual field movements for the same loads.

From this study, it is obvious that these criteria are insufficient for establishing a design procedure. Any estimation of pile capacity from the use of these criteria would be suspect because of poor performance compared to actual field tests. In the next chapter, the work by Castello (1980) for estimating maximum side and tip resistance will be utilized to develop new criteria. A displacement function will be established based on the data from these field tests.

CHAPTER 5: PROPOSED CRITERIA

Castello (1980) recently published a paper on the bearing capacity of driven piles in sand. He investigated 34 pile load tests to determine the pile geometry and soil parameters that most significantly affect the tip and side resistance of driven piles. These field pile tests were adjusted for residual stresses to determine that effect on the results. Tip and side resistance, bearing capacity factors, and the coefficients of lateral earth pressure, were computed from the 34 field pile tests. These factors were correlated with the most significant pile and soil parameters.

In the static formula for axially loaded piles in sands, the primary parameter is the angle of internal friction. Castello (1980) felt that other parameters such as pile size and shape, depth of penetration, and relative density of the sands would also influence the capacity of piles. He investigated these parameters and their influence on a number of instrumented pile tests. From these tests, the unit skin friction and unit tip resistance were evaluated to determine their relationship to these pile and soil parameters.

The depth of penetration to diameter ratio was found to have a significant influence along with the angle of internal friction and the relative density of the sand. Castello (1980) developed curves for tip and side resistance, bearing capacity factor, N_q , and the coefficient of lateral earth pressure, K , versus depth of penetration to diameter ratio for different relative densities which were

distinguished by angle of internal friction (Figures 70-73). The bearing capacity factors and the coefficients of lateral earth pressure have little meaning, as explained in previous discussions in this paper, due to the normal stress computations used in Castello's study. The normal stress was taken as being proportional to the overburden pressure. The curves for tip and side resistance are felt to be the most meaningful representation of the information. These curves are based on pile tests that were adjusted for residual stresses.

The ultimate tip and side resistance curves developed by Castello (1980) coupled with a displacement function will become the focus for the development of load-displacement criteria for axially loaded piles in sands. The displacement function will be developed from correlations with the field curves. This approach follows the same methodology as Castello followed with his development of ultimate tip and side resistance. The field pile tests that were used in the evaluation of the criteria in the previous chapter will be used in the development of the displacement function.

Displacement Function for Side Resistance

The stress-strain behavior of sands can often be described by a hyperbolic expression of the form

$$\sigma = \frac{\epsilon}{a + b\epsilon} \quad (46)$$

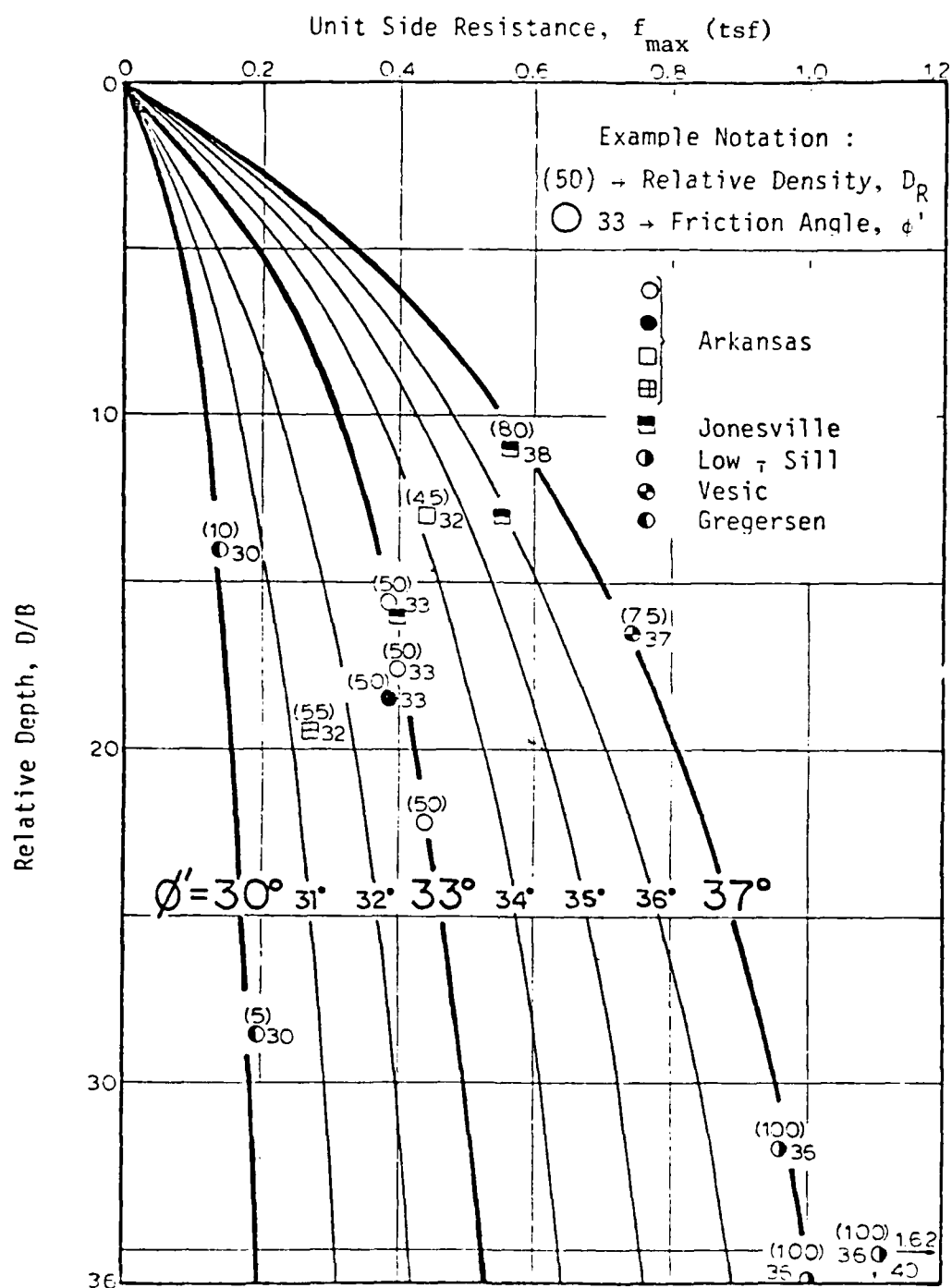
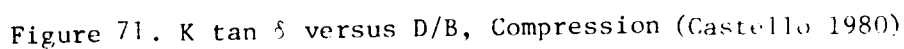
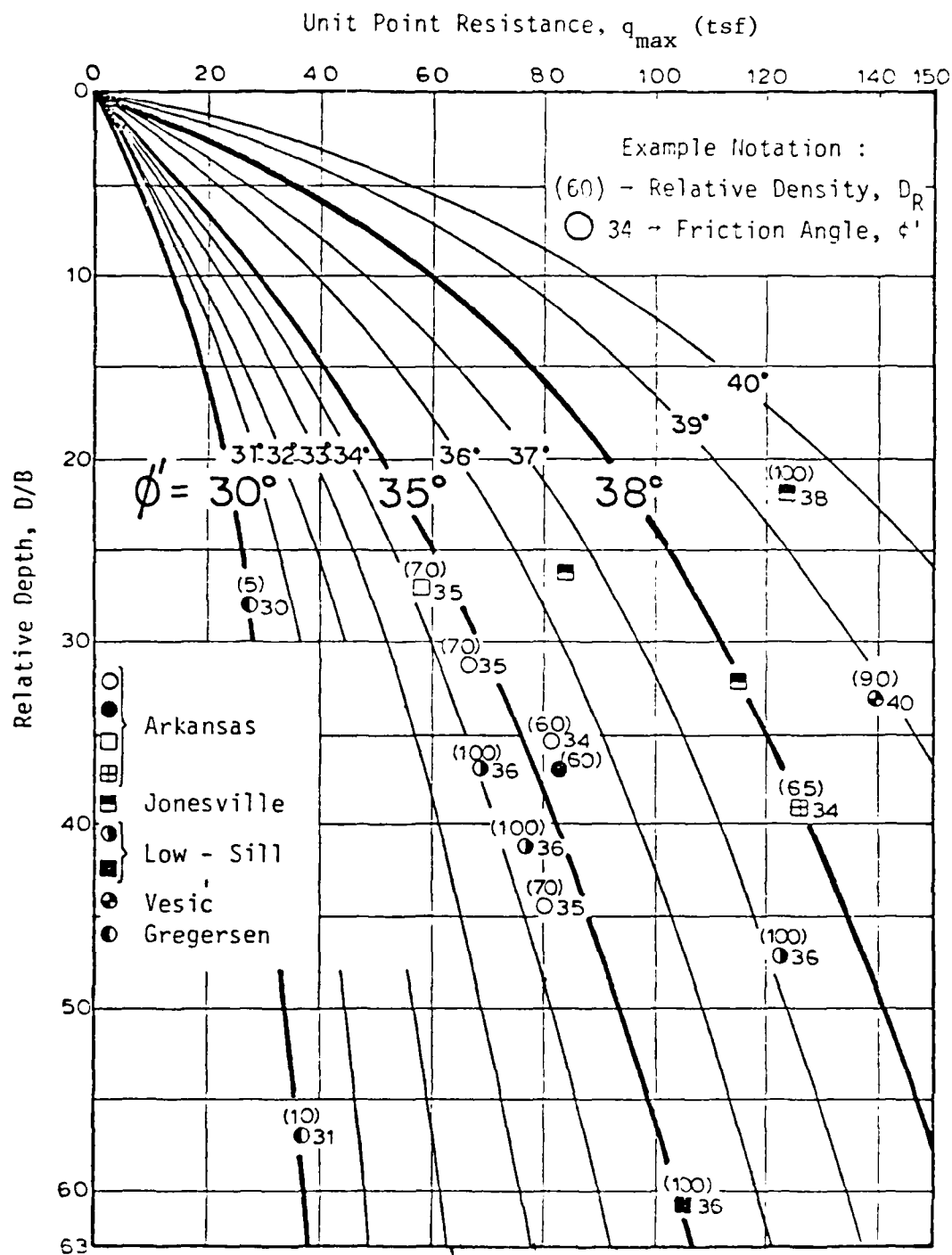


Figure 70. f_{\max} versus D/B , Compression
 (1 tsf = 95.76 kN/m²) (Castello 1980)





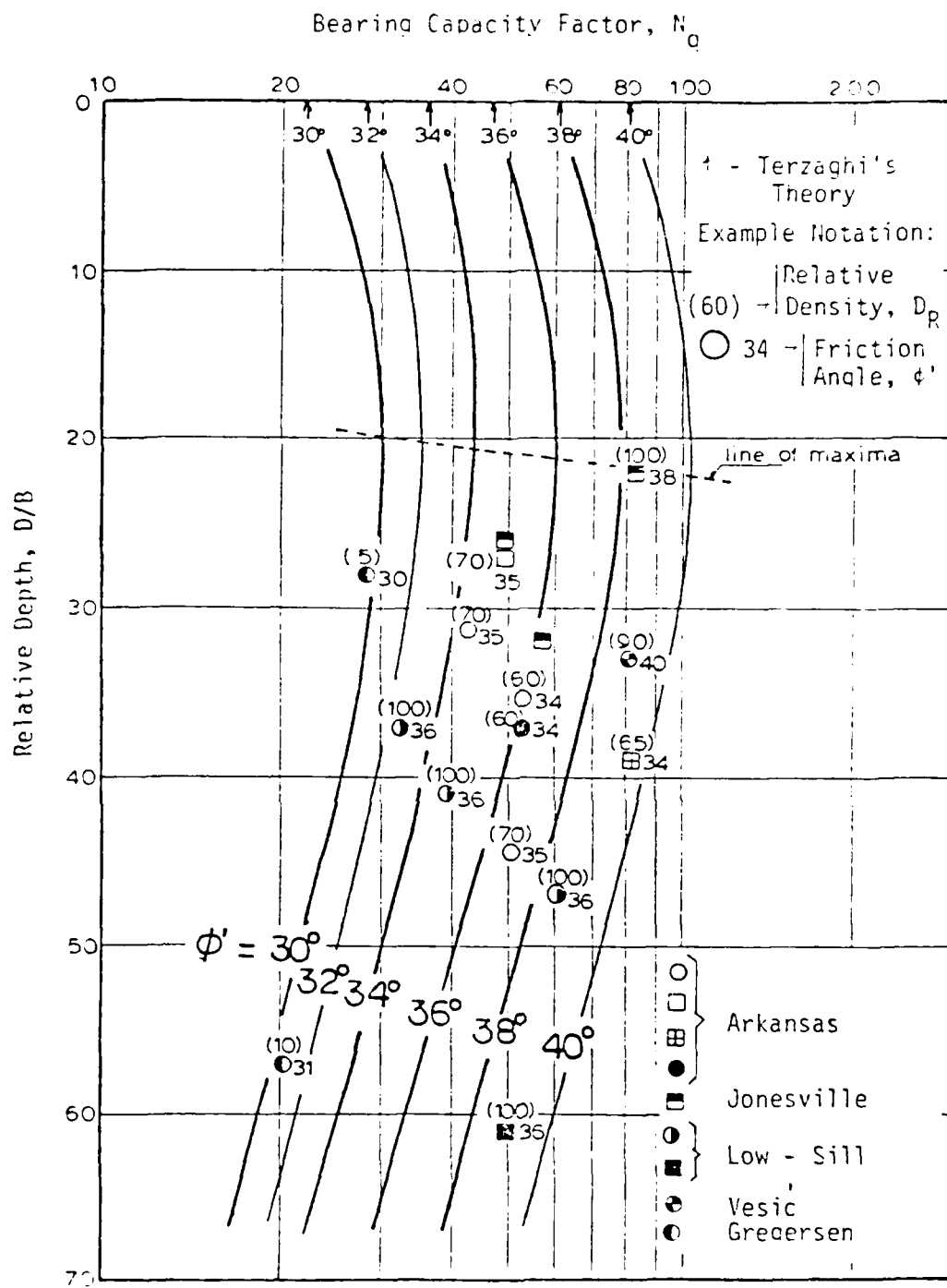


Figure 73 N_q versus D/B , Compression (Castello 1980)

The characteristics of the use of this expression for stress-strain behavior of sands have been presented previously in this report.

The hyperbolic expression has been proposed by Kraft et al. (1981) for the general description of the shear transfer behavior of axially loaded piles. Kraft et al. (1981) based the coefficients in the expression on soil properties obtained from laboratory tests on undisturbed samples. Their work was centered more on the shear transfer of clays for which obtaining undisturbed samples for laboratory tests is much easier than for sands. For sands, the most practical correlations of the coefficients are with field tests. The hyperbolic expression for shear transfer is

$$f = \frac{z}{a + bz} \quad (47)$$

The coefficients a and b , as described earlier, have a physical meaning which is illustrated in Figure 74. The coefficient a is the reciprocal of the initial tangent modulus, E_f , and b is the reciprocal of the asymptotic value of maximum side resistance, f_{\max} . Rewriting the expression including the term described above yields

$$f = \frac{z}{\frac{1}{E_f} + \frac{1}{f_{\max}}}(z) \quad (47a)$$

Using the data from the field tests, the values of the initial modulus, E_f , and the maximum side resistance, f_{\max} , can be determined by plotting the field data on a transformed axis system (Figure 75) with the pile movement, z , divided by side resistance, f , as the ordinate and the pile movement, z , as the abscissa. The initial modulus, E_f , is the reciprocal of the slope intercept of the straight line formed by connecting the data points. Appendix D show che

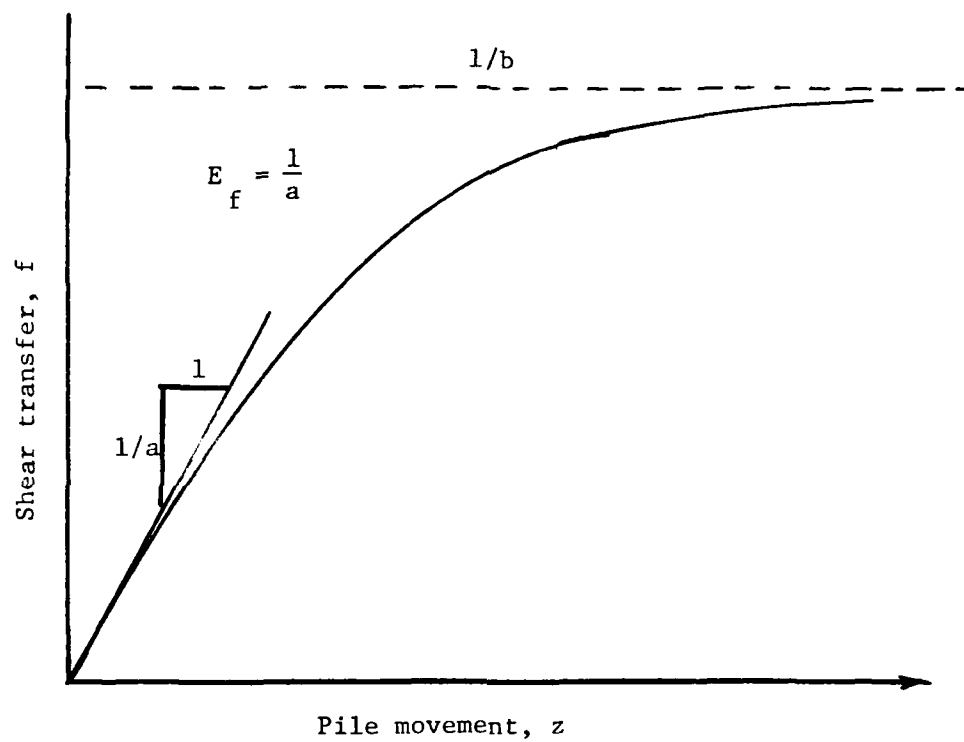


Figure 74. Proposed Hyperbolic Equation

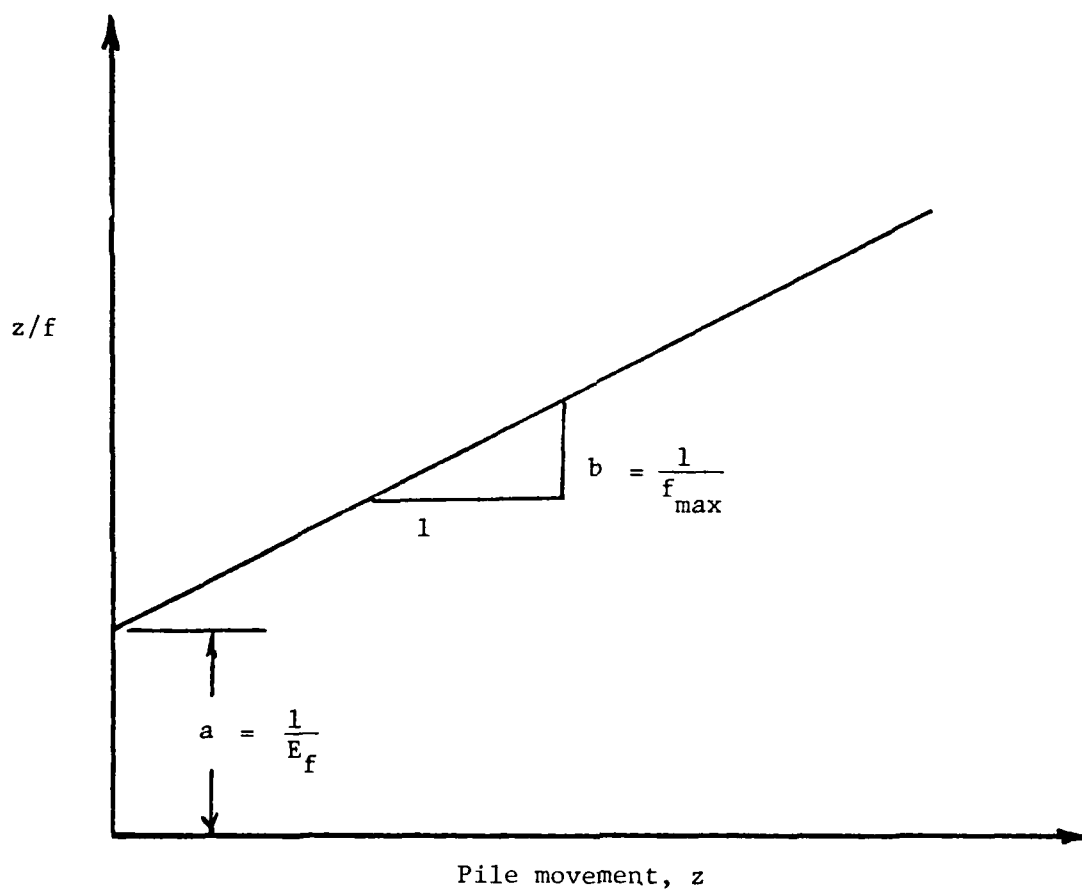


Figure 75. Transformed Axis

results of plotting the field data on this transformed axis. The purpose of this investigation was to obtain a check on the maximum side resistance, f_{\max} , from Castello's (1980) correlation and the field tests, and to obtain values for the initial modulus, E_f , of side resistance. Table 5 show the ranges that were developed for the initial modulus of side resistance.

From a review of the data, the initial modulus, E_f , is independent of the pile diameter. Values of initial modulus were within the same range for similar densities, except for the 12-in. pipe pile in the Arkansas River tests. The initial modulus for this pile was unrealistically high and was not used in establishing the recommended values for initial modulus, E_f , in Table 6.

In the Arkansas River tests, the average standard error of the side resistance between the field data and the Castello adjusted value was approximately 32 percent. Using the values that were unadjusted for residual stresses presented by Castello (Figures 76 and 77) for side resistance, the error was approximately 25 percent. The field data for the Arkansas River tests were insufficient to make a good evaluation of the residual loads in the pile, and failure was not completely reached in a number of tests. The Ascalmore Creek-Tippo Bayou and Red River tests had standard errors of approximately 23 and 18 percent, respectively, for the unadjusted values and 16 and 11 percent, respectively, for the adjusted values.

The average standard errors were greater than had been anticipated, but given that the average standard error was 50 percent or more for the other three criteria investigated, the proposed

Table 5

Initial Modulus of Side Resistance from Field Tests

Relative Density/ Pile Type	Initial Modulus of Side Resistance, E_f (psf/in.)		
	30° Loose	33° Medium	36° Medium-Dense
12" pipe	-	40,000-50,000	50,000-60,000
16" pipe	-	8,000-13,000	12,000-18,000
20" pipe	-	10,000-15,000	13,000-20,000
12" H pile	6,000-9,000	10,000-13,000	12,000-18,000
14" H pile	5,000-10,000	8,000-12,000	10,000-16,000

Table 6
Initial Modulus of Side Resistance

<u>Relative Density</u>	<u>ϕ</u>	<u>Initial Modulus of Side Resistance, E_f, psf/in.</u>
Loose	28°-31°	6,000-10,000
Medium	32°-34°	10,000-14,000
Medium-Dense	35°-38°	14,000-18,000

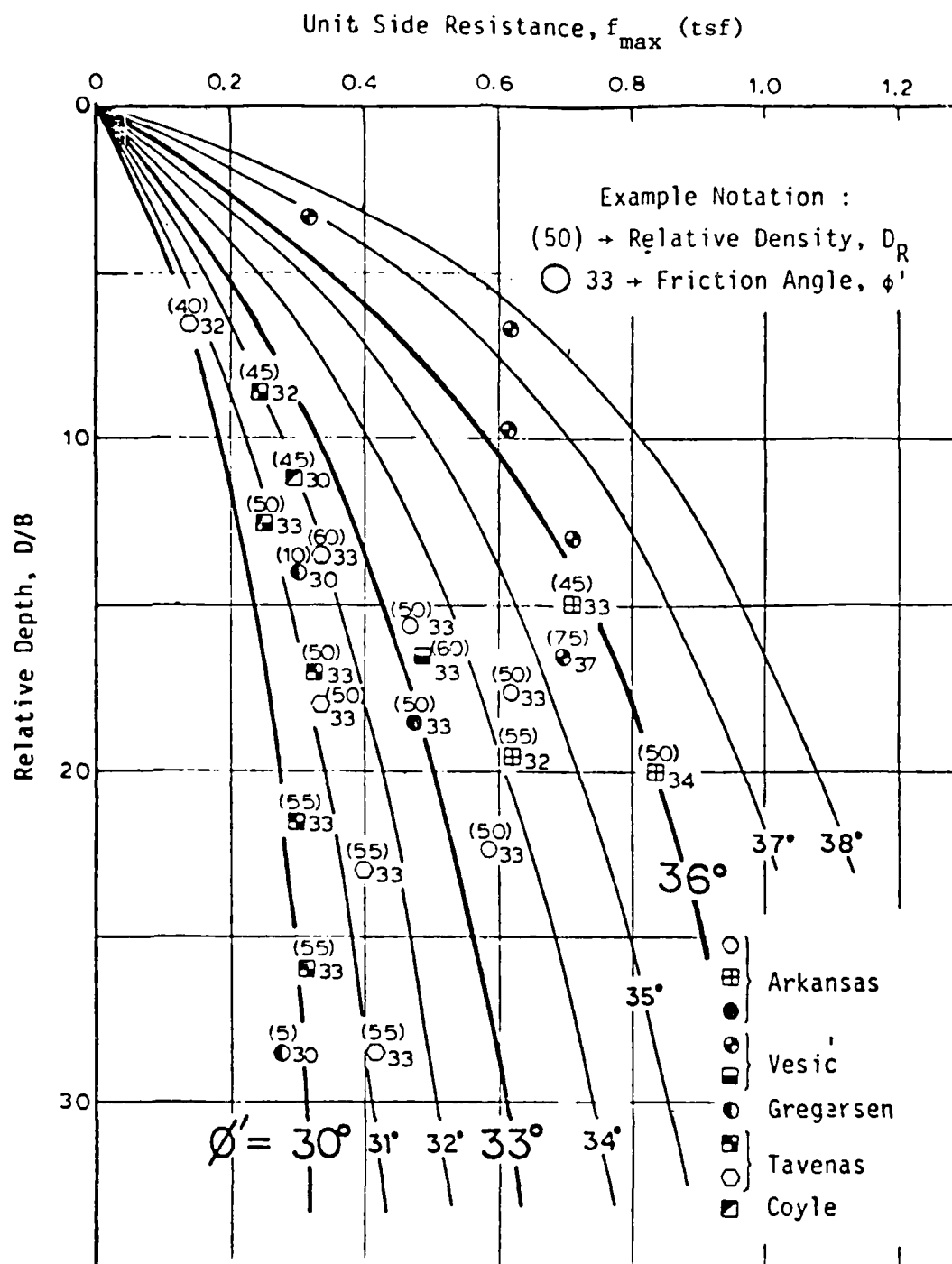


Figure 76. f_{\max} versus D/B, Unadjusted Compression (1 tsf = 95.76 kN/m²)

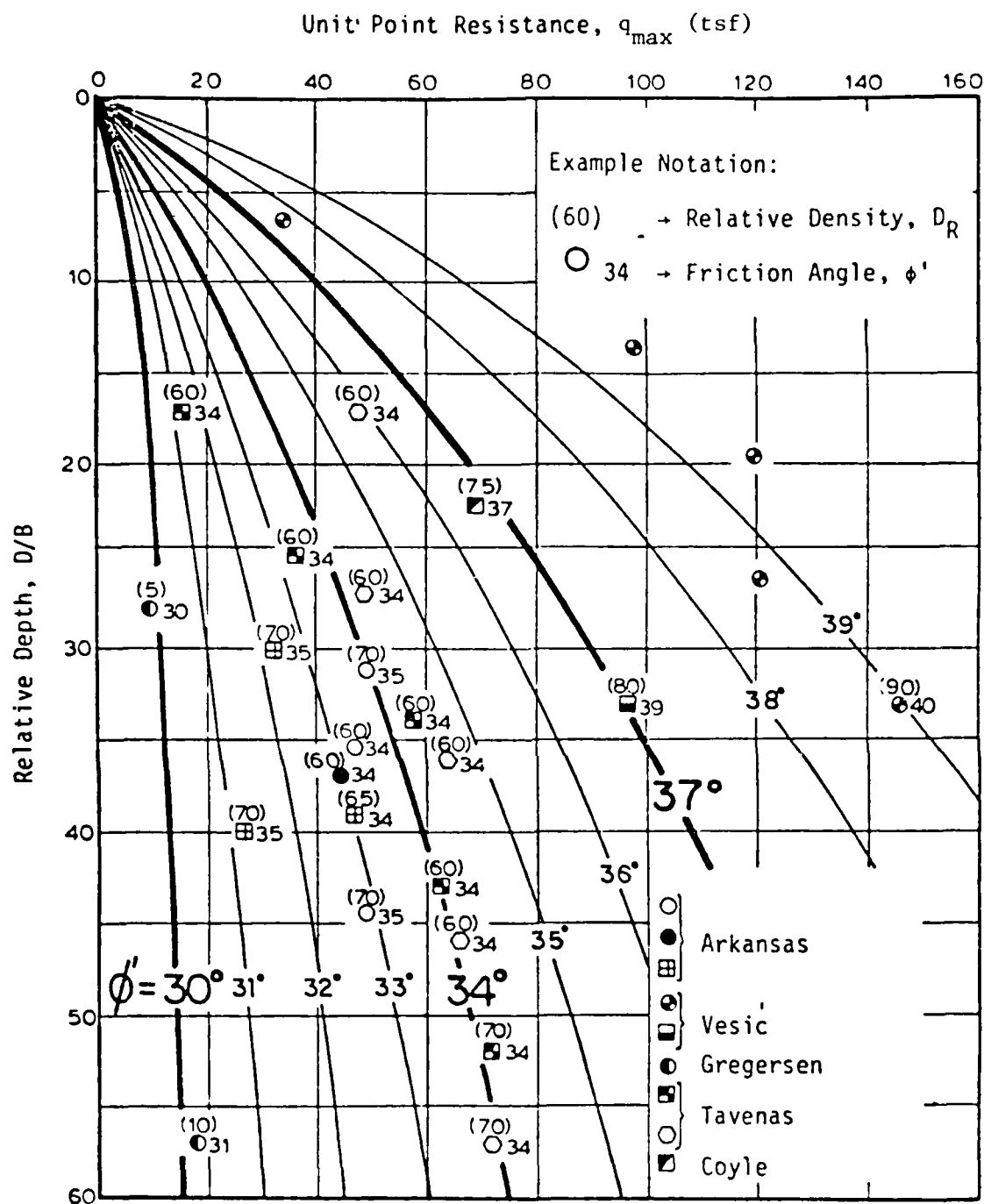


Figure 77. q_{\max} versus D/B , Unadjusted Compression (1 tsf = 95.8 kN/m^2)

criteria are acceptable. One must keep in mind that an error of 20 percent in estimating soil performance is generally considered reliable.

Displacement Function for Tip Resistance

Vijayvergiya (1977) was the only source presenting criteria for tip resistance. Vijayvergiya (1977) gives the displacement function as

$$q = \left(\frac{z}{z_c} \right)^{1/3} q_{\max} \quad (48)$$

where the maximum bearing capacity, q_{\max} , is

$$q_{\max} = \bar{\sigma}_v N_q \quad (49)$$

and $\bar{\sigma}_v$ is the effective vertical stress which is equal to the overburden pressure. The greatest limitation of use of the maximum bearing capacity is its dependence on overburden pressure which has been discussed previously in this report.

Vijayvergiya (1977) linked the critical displacement, z_c , to the width of the pile tip. For displacements, z , greater than the critical displacement, z_c , the tip resistance is taken as being constant. This is contrary to early statements in his paper, that for sands the tip resistance continued to increase with displacement.

Another approach for defining the maximum tip resistance would be to define it as the yield point; that is, the soil beneath the tip is assumed to behave similarly to an elastic-plastic material with strain hardening, as shown in Figure 78. The yield point is then defined as the point of transition between elastic and plastic strain hardening

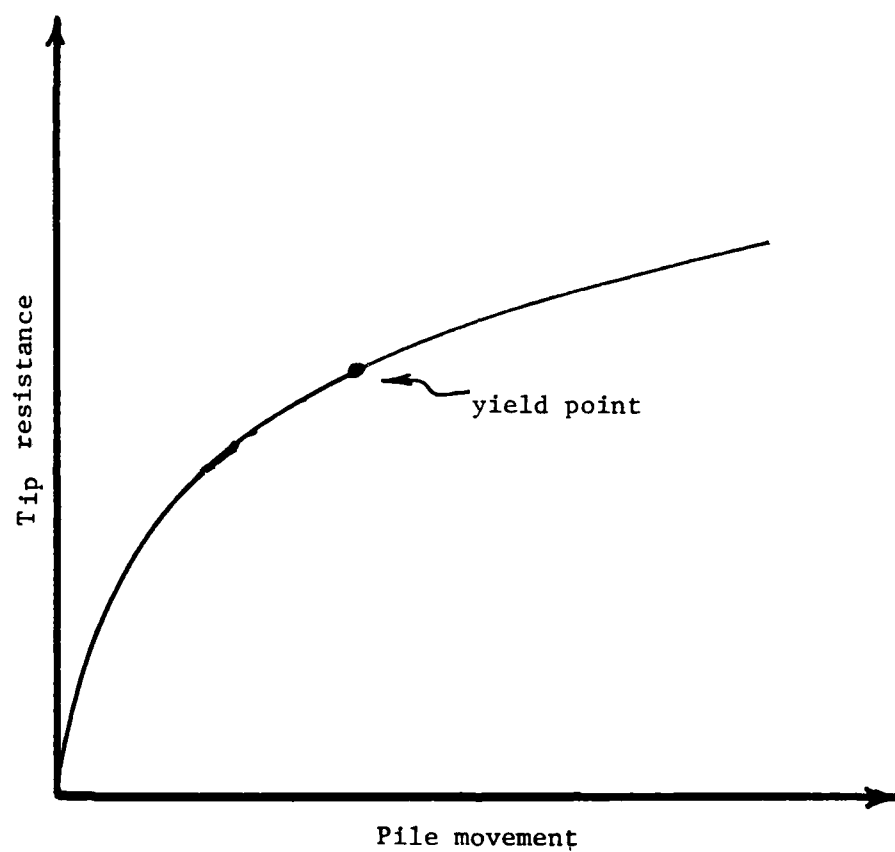


Figure 78 . Tip Resistance-Displacement Function

behavior. The yield capacity of a pile has been assumed to be reached when the tip displacement is 0.25 in. Substituting 0.25 in. in Vijayvergiya's expression for displacement yields

$$q = (4 z)^{1/3} q_{\max} \quad (49)$$

This displacement function showed better agreement with field data. It was further altered to reflect the field data for different densities:

Loose	$q = (4 z)^{1/2} q_{\max}$	(49a)
-------	----------------------------	-------

Medium	$q = (4 z)^{1/3} q_{\max}$	(49b)
--------	----------------------------	-------

Medium-dense	$q = (4 z)^{1/4} q_{\max}$	(49c)
--------------	----------------------------	-------

where the maximum yield tip resistance, q_{\max} , is determined from Castello's curves for ultimate tip resistance.

Comparisons were made between field P-z curves and the computed P-z curves using Equation 49 and maximum tip resistances, q_{\max} , from Figure 72 for adjusted pile tests and Figure 77 for unadjusted pile tests. The results are presented in Figures 79-88, where the field curves are those plotted with symbols and the computed curves are the smooth curves. Using the angle of internal friction, ϕ , established previously, for determining the maximum tip resistance, q_{\max} , from Figures 72 and 77 yielded computed curves with higher values of tip resistance, q , than field curves for the same pile movement. By reducing the angle of internal friction, better agreement was

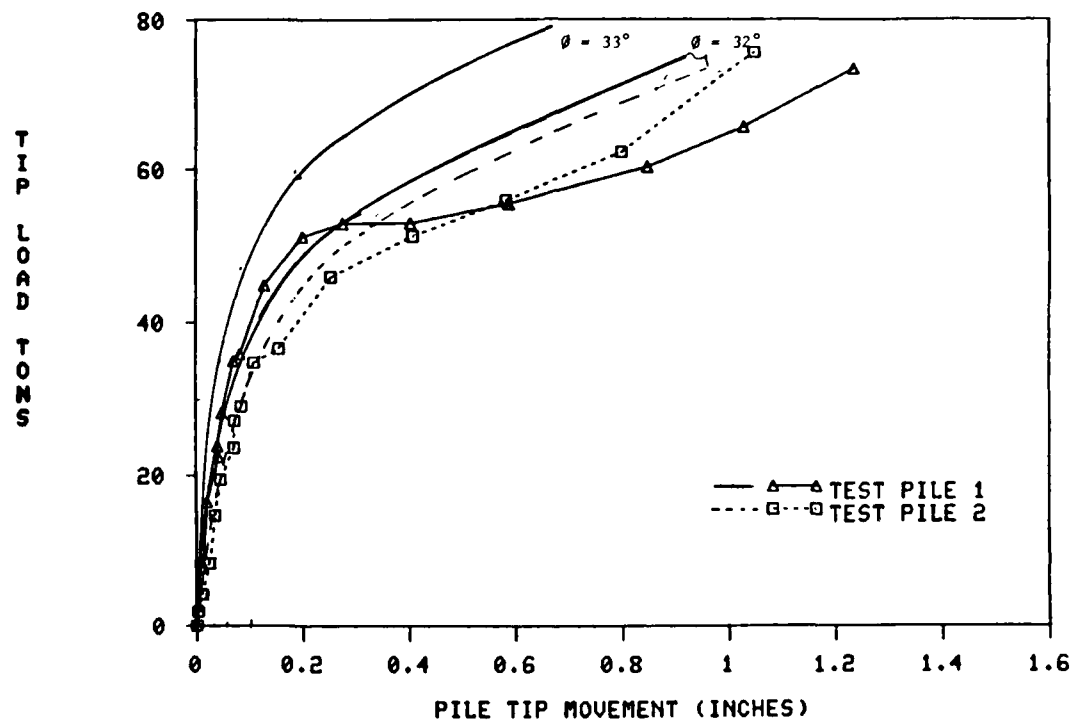


Figure 79. Computed P-z curves Comparison to Unadjusted Field Curves, Ascalmore Creek-Tippo Bayou, H Piles

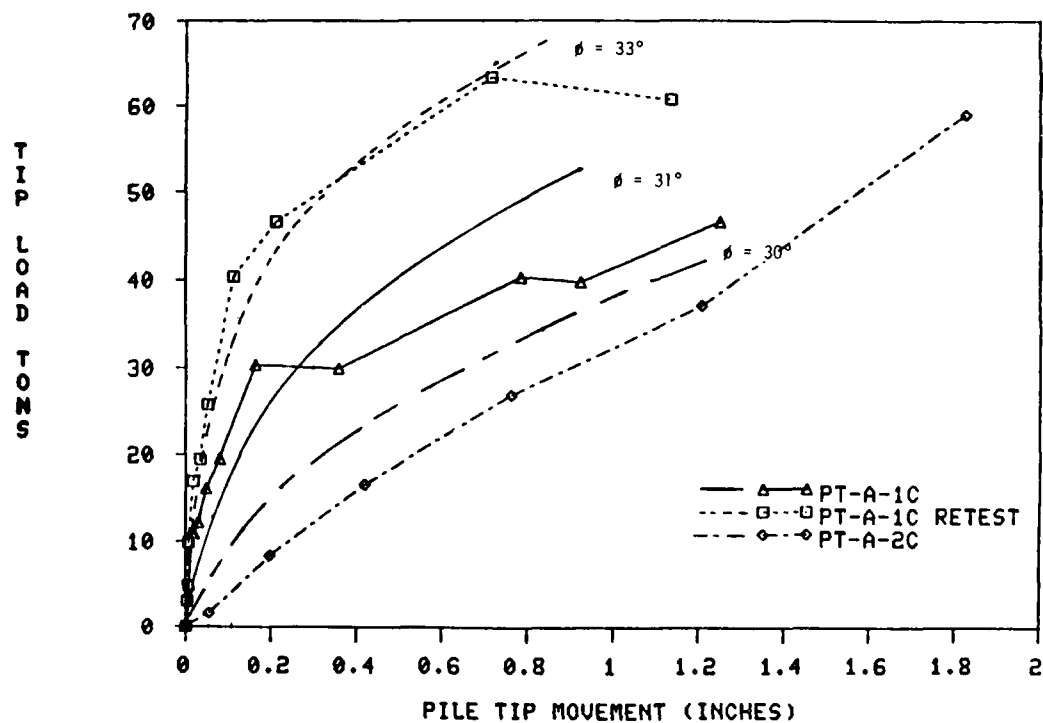


Figure 80. Computed P-z Curves Comparison to Unadjusted Field Curves, Red River, H Piles

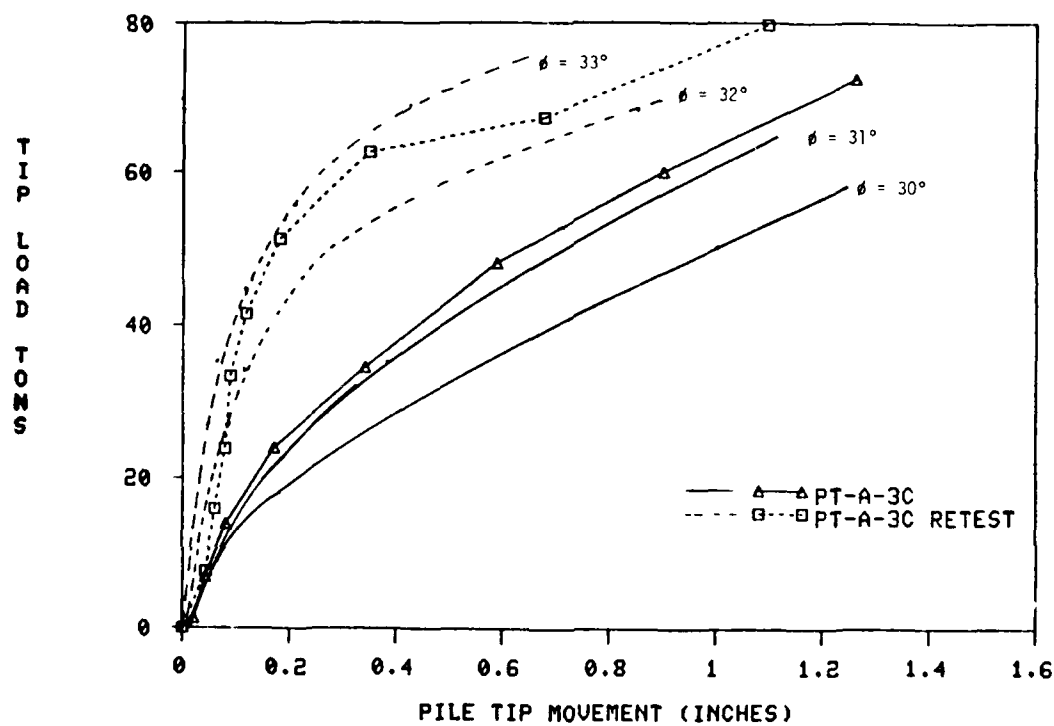


Figure 81. Computed P-z Curves Comparison to Unadjusted Field Curves, Red River, H Piles

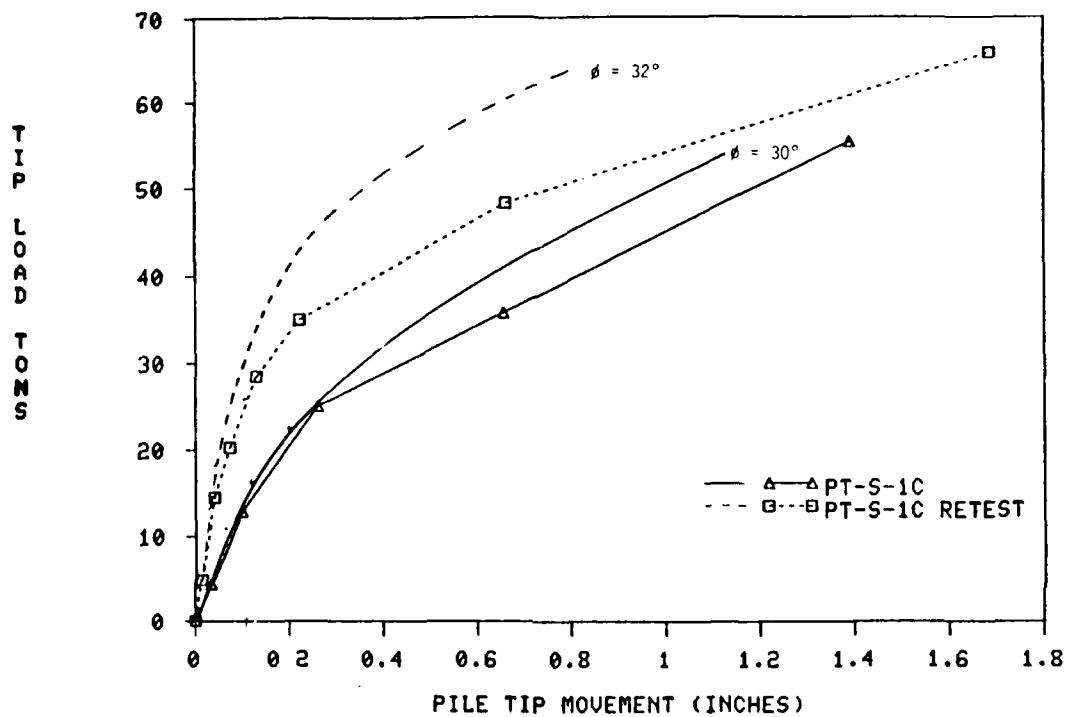


Figure 82. Computed P-z Curves Comparison to Unadjusted Field Curves, Red River, H Piles

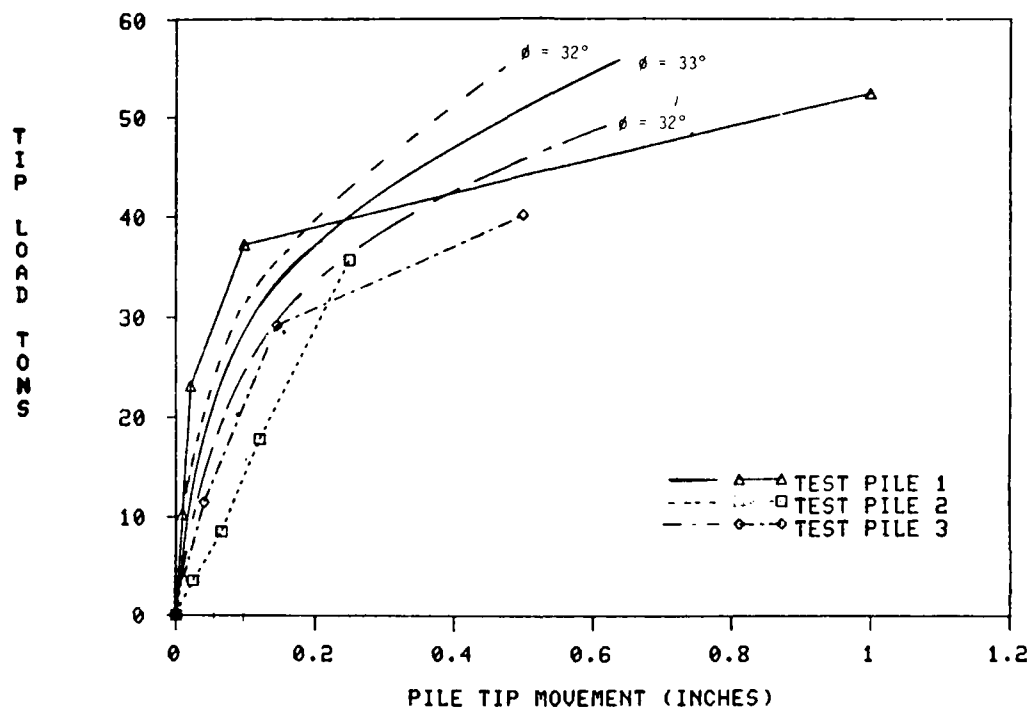


Figure 83. Computed P-z Curves Comparison to Unadjusted Field Curves, Arkansas River, Pipe Piles

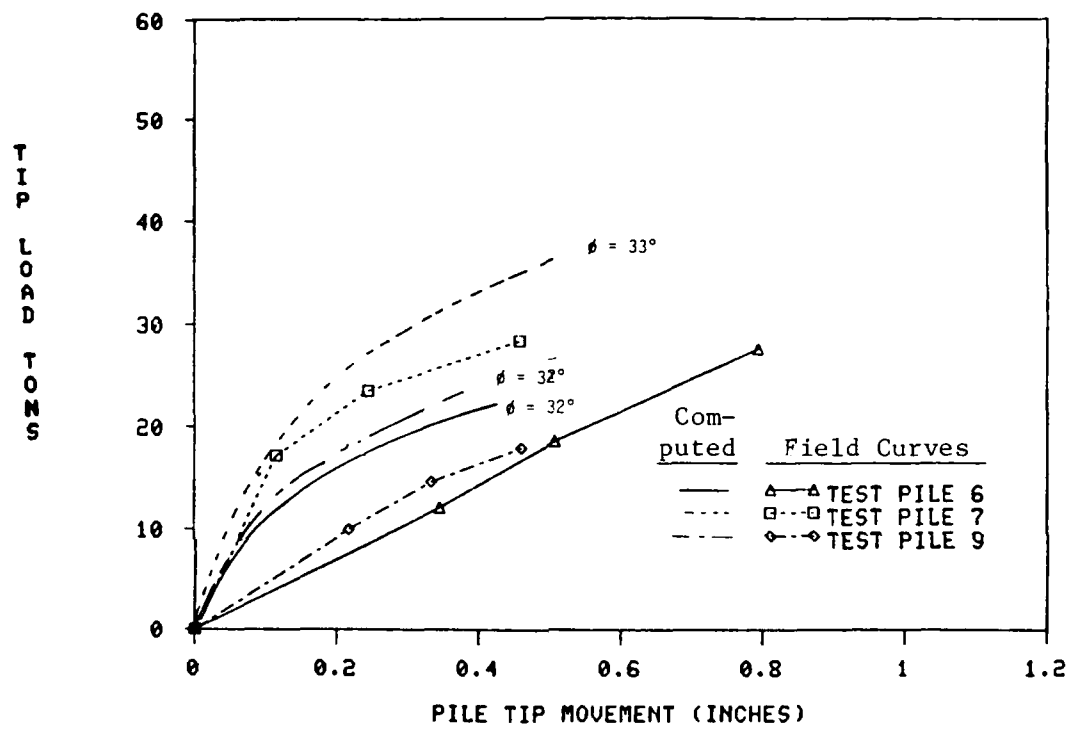


Figure 84. Computed p-z Curves Comparison to Unadjusted Field Curves, Arkansas River, H Piles

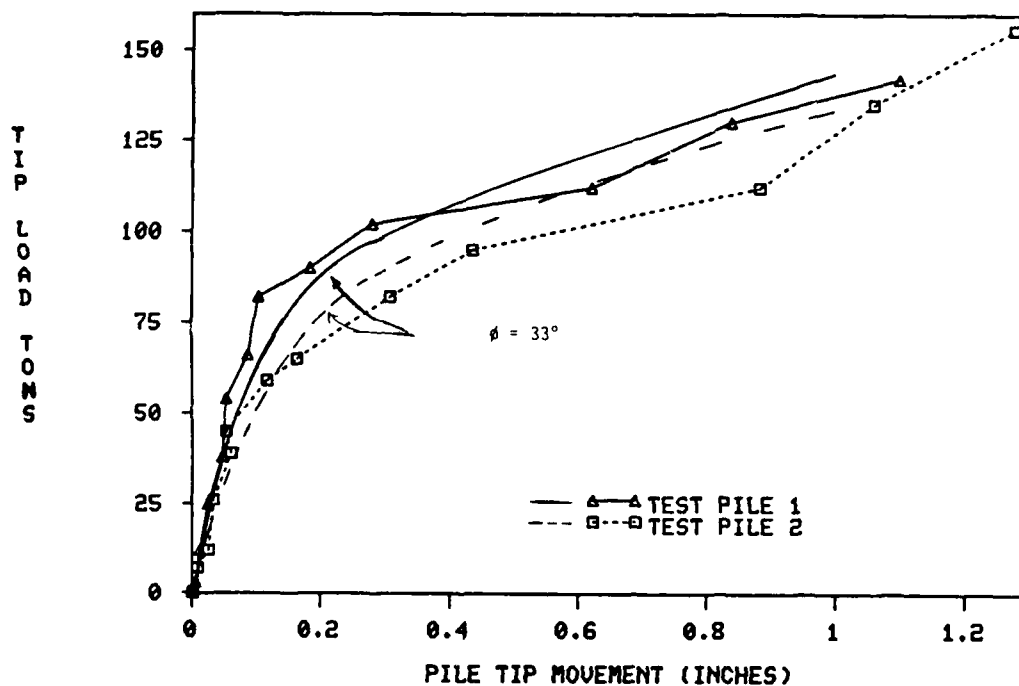


Figure 85. Computed P-z Curves Comparison to Adjusted Field Curves, Ascalmore Creek-Tippo Bayou, H Piles

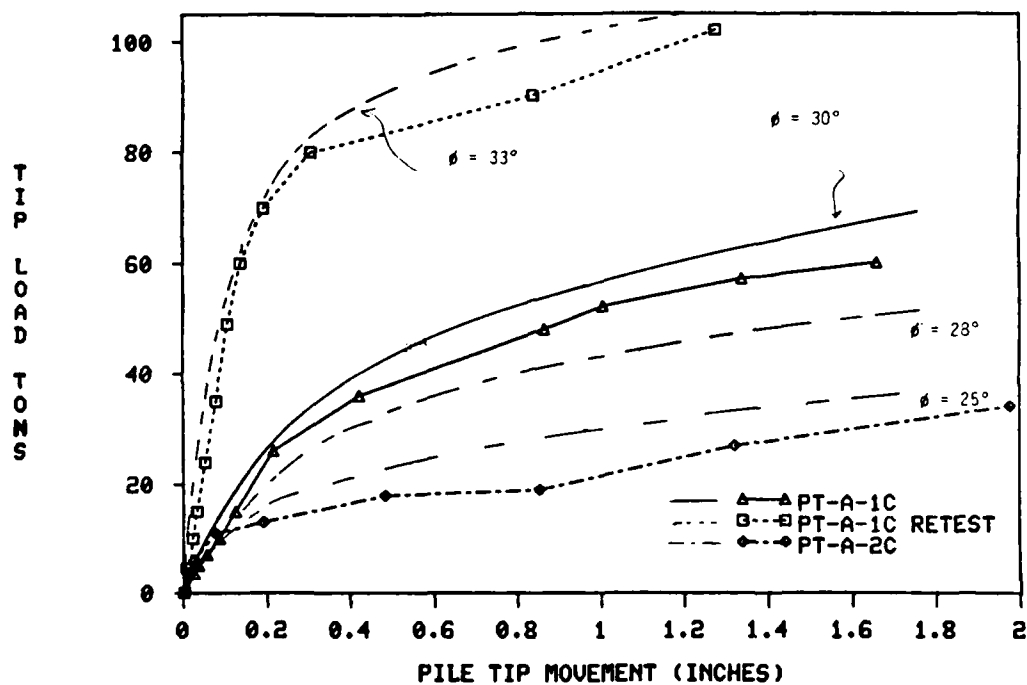


Figure 86. Computed P-z Curves Comparison to Adjusted Field Curves, Red River, H Piles

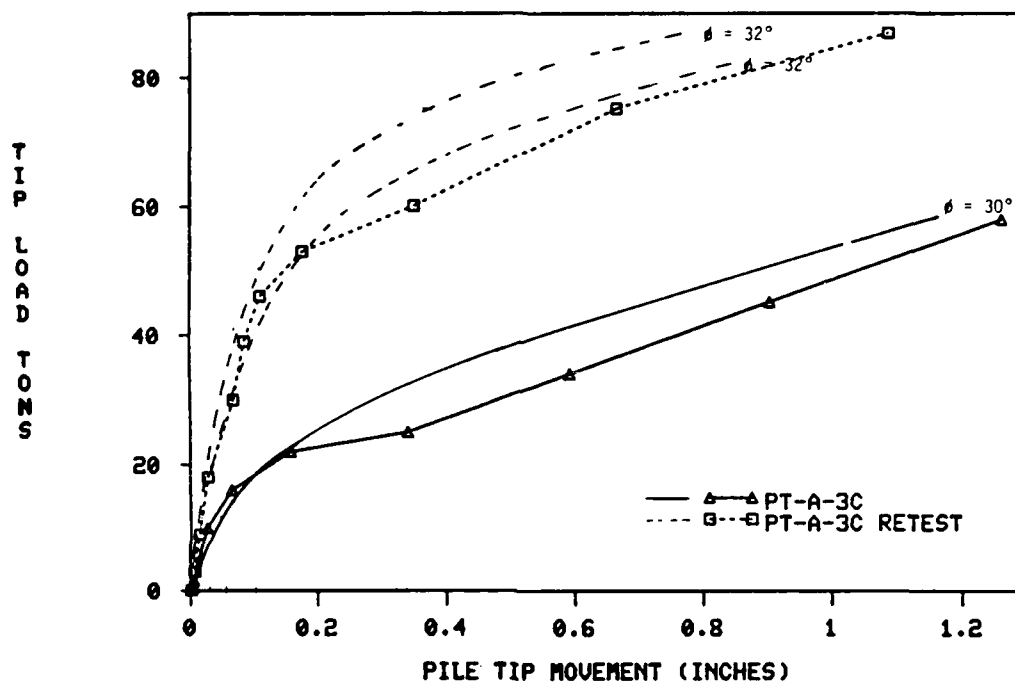


Figure 87. Computed P-z Curves Comparison to Adjusted Field Curves, Red River, H Piles

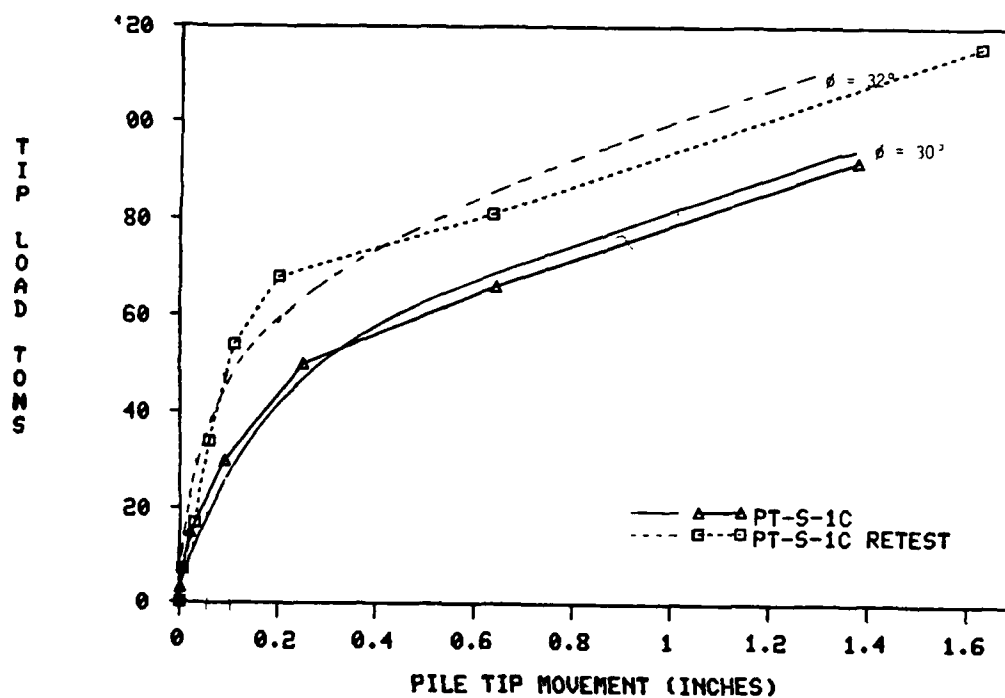


Figure 88. Computed P-z Curves Comparison to Adjusted Field Curves, Red River, H Piles

obtained, as shown in Figures 79-88. The reason for this is that Castello defines the ultimate capacity of the pile as the load at the head of the pile resulting from a movement of 10 percent of the diameter. For pile design in the Corps of Engineers' Lower Mississippi Valley Division (LMVD), this is considered excessive. In LMVD, a pile for which a movement of approximately 1/4 in. at the tip occurs is considered as a limit. Based on the field data, new sets of curves were developed and are shown in Figures 89 and 90. The shapes of the curves produced by the displacement were in good agreement with those of the field curves.

Comparison of Computed and Actual Butt and Tip Performance

The Ascalmore Creek-Tippo Bayou and Red River tests were selected for the comparison. The Arkansas River tests had insufficient data to provide a good comparison. For the piles that penetrated clay layers, the actual field f-z curves were used for the comparison. The results of the comparison are presented in Figures 91-99. The agreement between the computed and actual load-movement behavior was found to be very good up until the pile-soil system began to yield. Beyond the yield point, the computed values from the criteria were greater than the respective field values. This is attributed to the tip resistance criteria overestimating the tip resistance at large displacements.

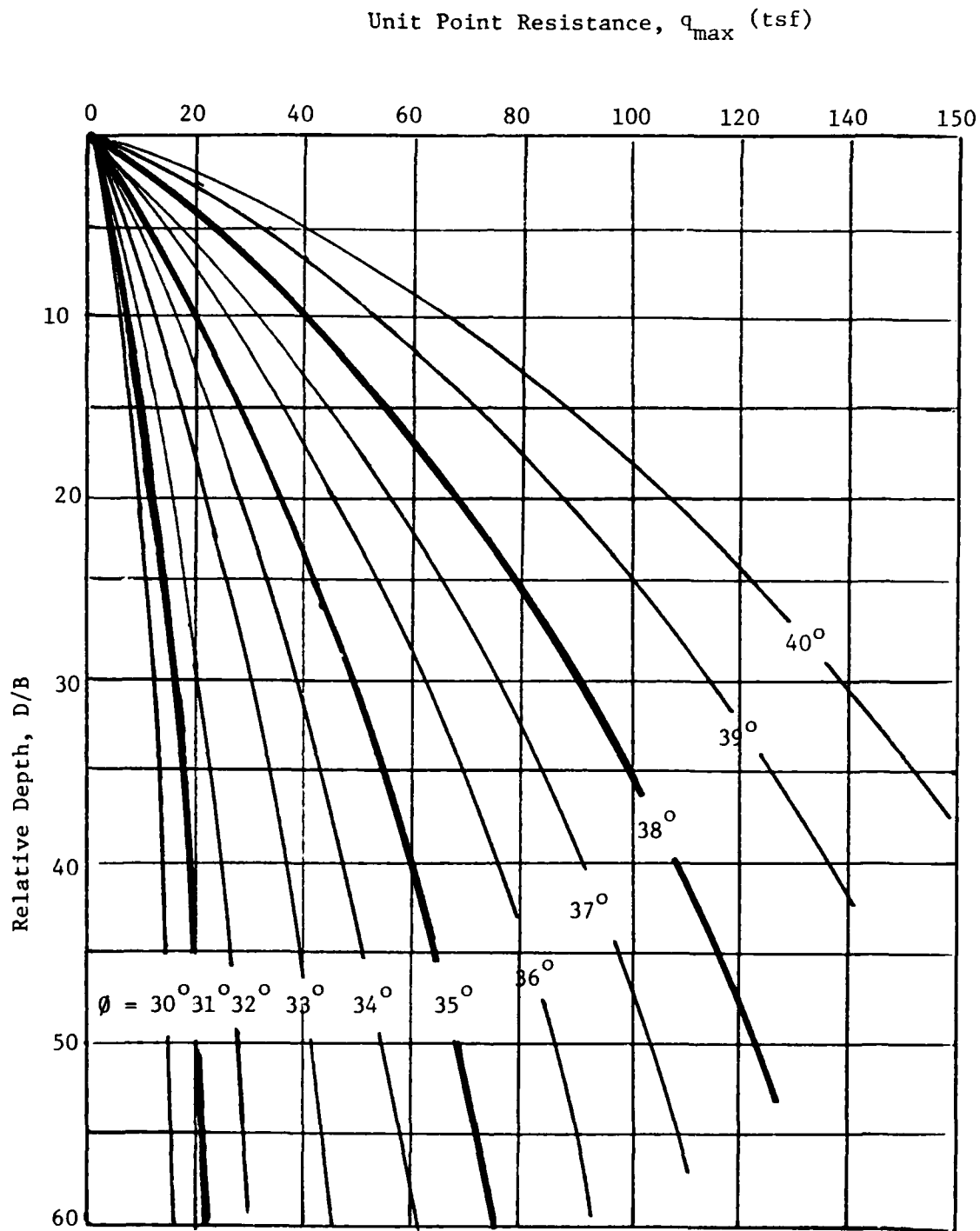


Figure 89. q_{\max} versus D/B , Unadjusted Compression (1 tsf = 95.8 kN/m^2)

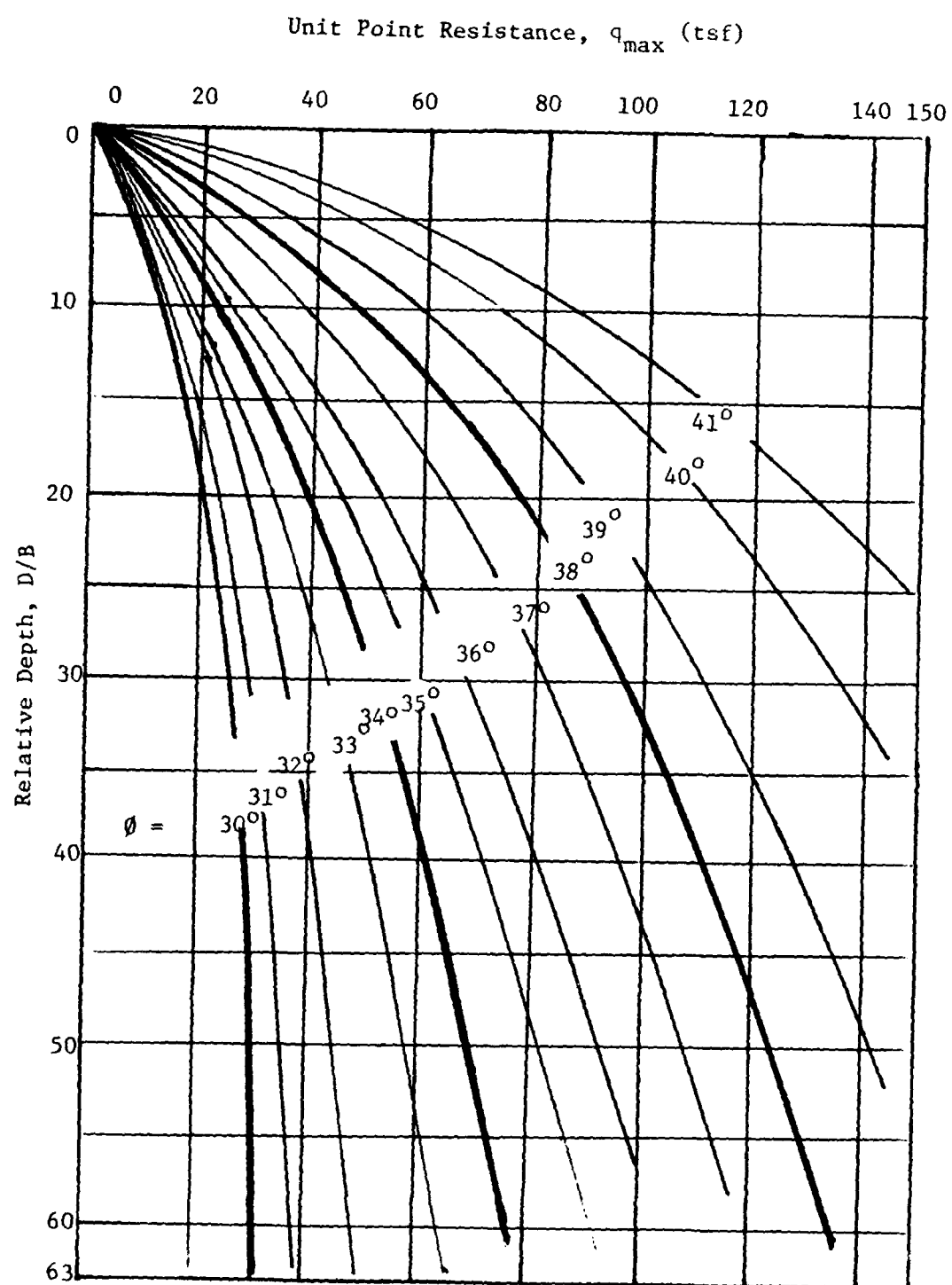


Figure 90. q_{\max} versus D/B , Compression (1 tsf = 95.76 kN/m²)

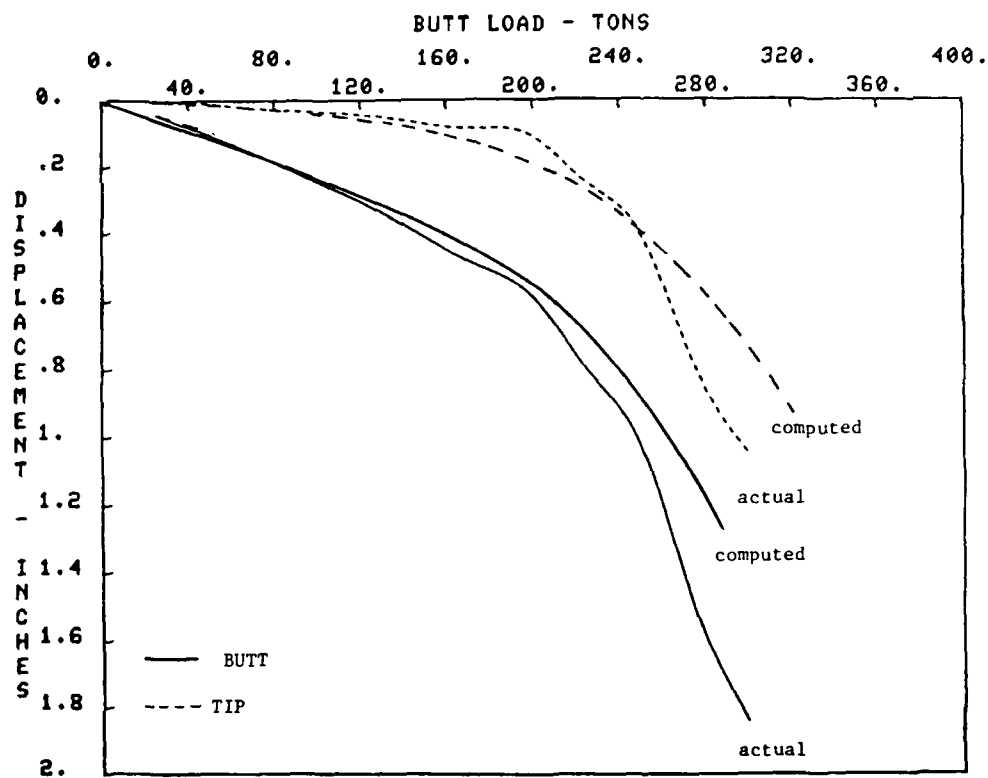


Figure 91. Computed and Actual Butt and Tip Load-Movement Curves, Ascalmore Creek-Tippo Bayou, Test Pile No. 1

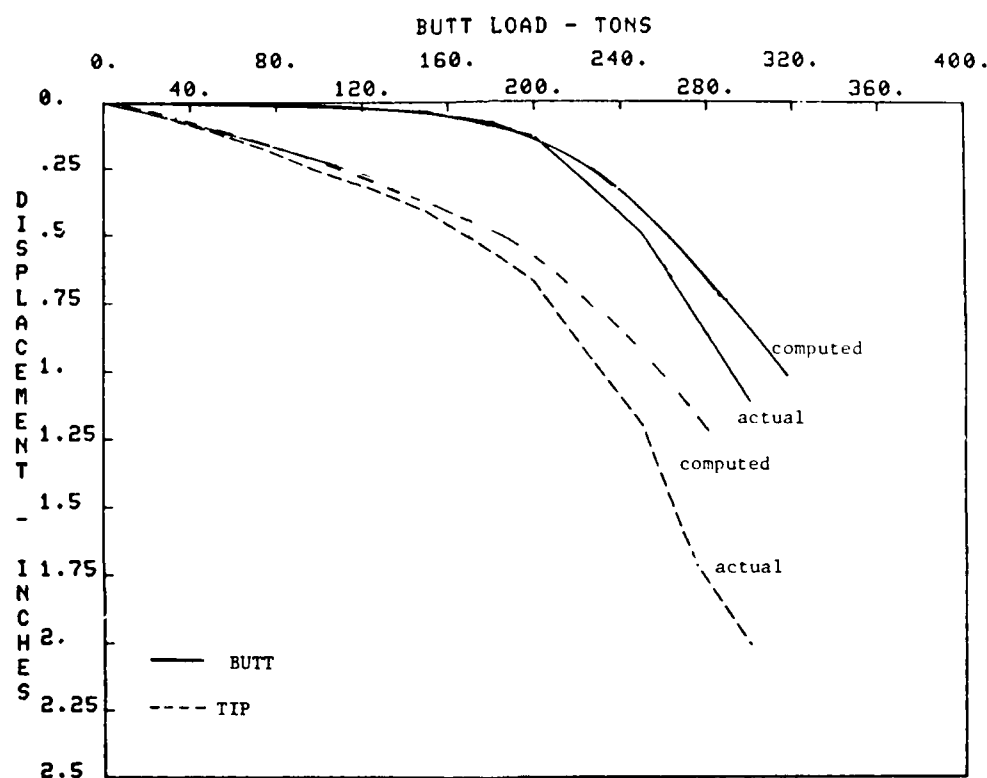


Figure 92. Computed and Actual Butt and Tip Load-Movement Curves, Ascalmore Creek-Tippo Bayou, Test Pile No. 2

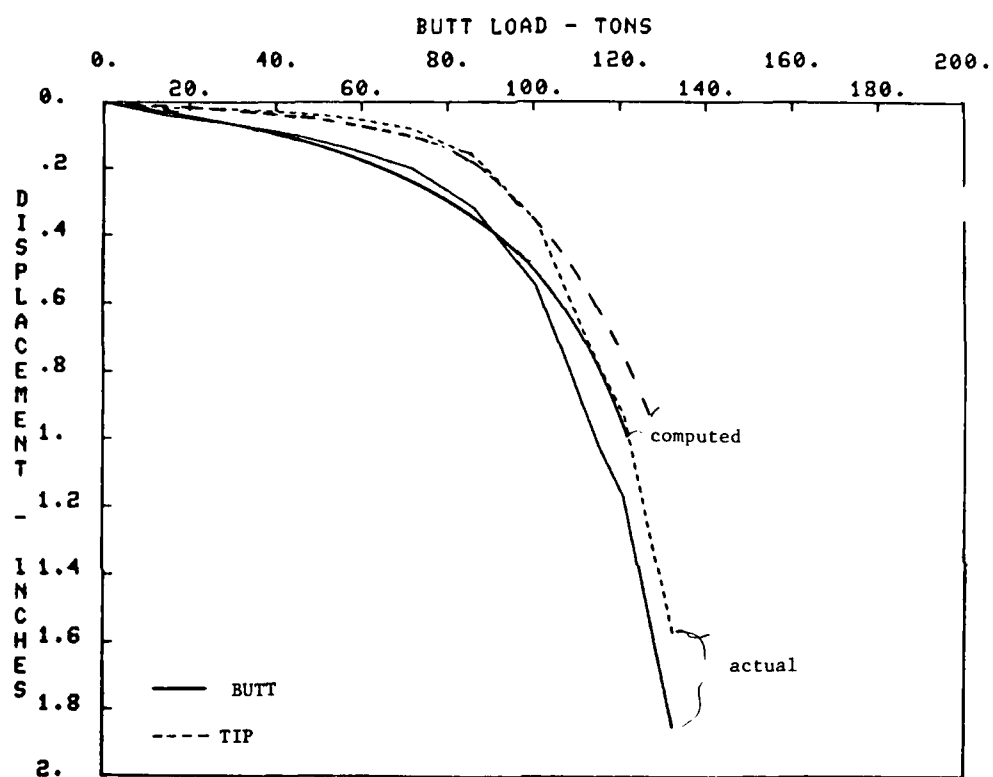


Figure 93. Computed and Actual Butt and Tip Load-Movement Curves, Red River, Test Pile No. PT-A-1C

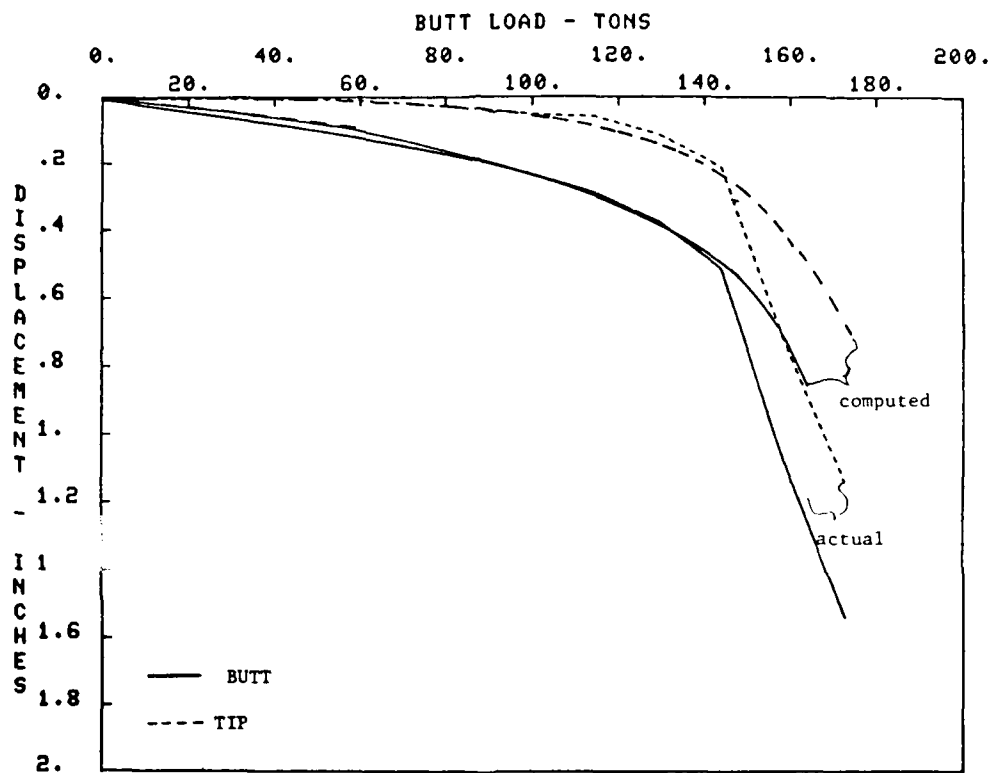


Figure 94. Computed and Actual Butt and Tip Load-Movement Curves, Red River, Test Pile No. PT-A-1C Retest

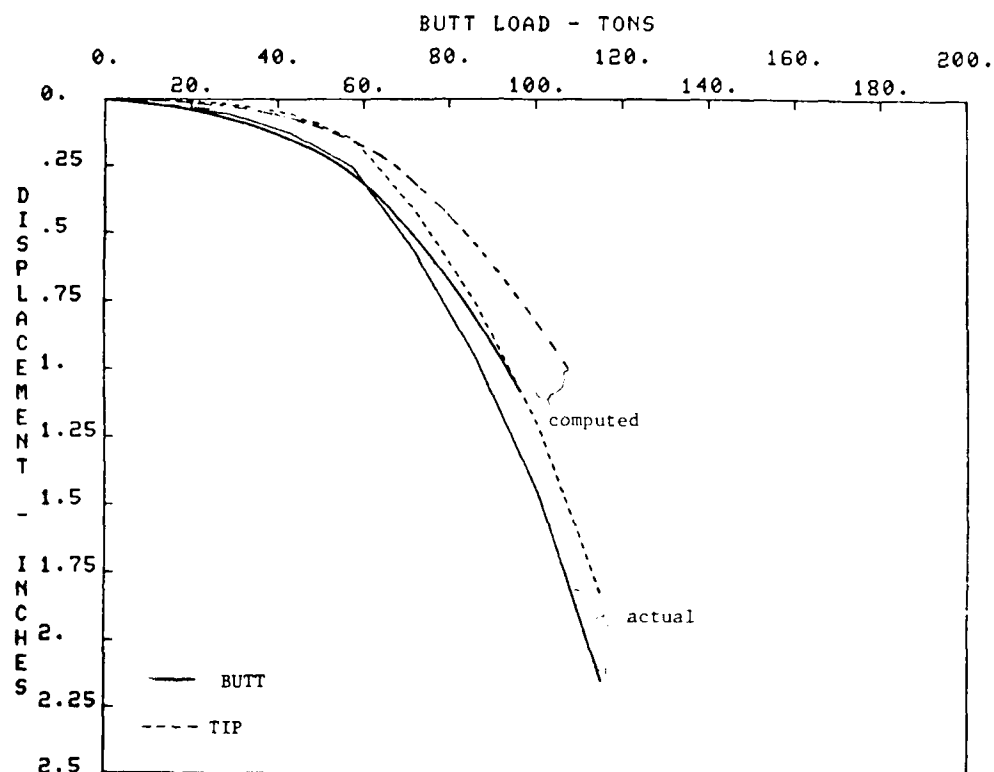


Figure 95. Computed and Actual Butt and Tip Load-Movement Curves, Red River, Test Pile No. PT-A-2C

AD-A139 236

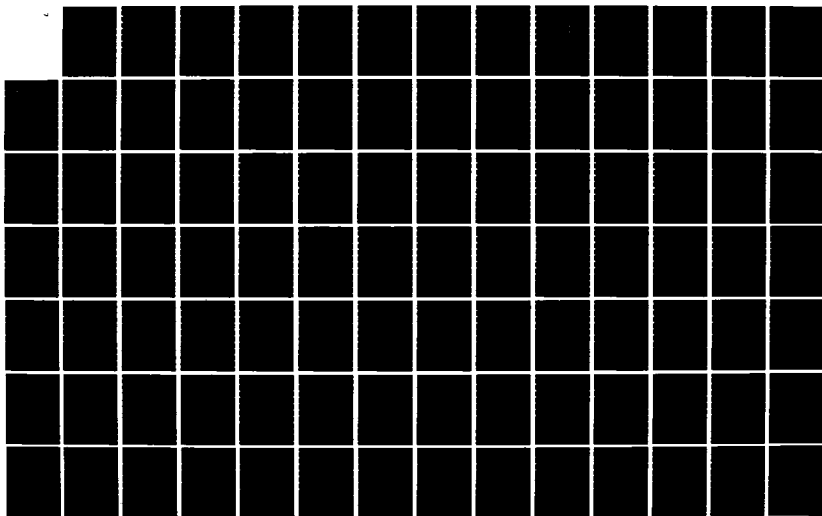
LOAD-TRANSFER CRITERIA FOR NUMERICAL ANALYSIS OF
AXIALLY LOADED PILES IN (U) ARMY ENGINEER WATERWAYS
EXPERIMENT STATION VICKSBURG MS R L MOSHER JAN 84
WES-TR-K-84-1

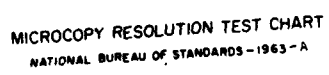
3/5

UNCLASSIFIED

F/G 13/13

NL





MICROCOPY RESOLUTION TEST CHART
NATIONAL BUREAU OF STANDARDS-1963-A

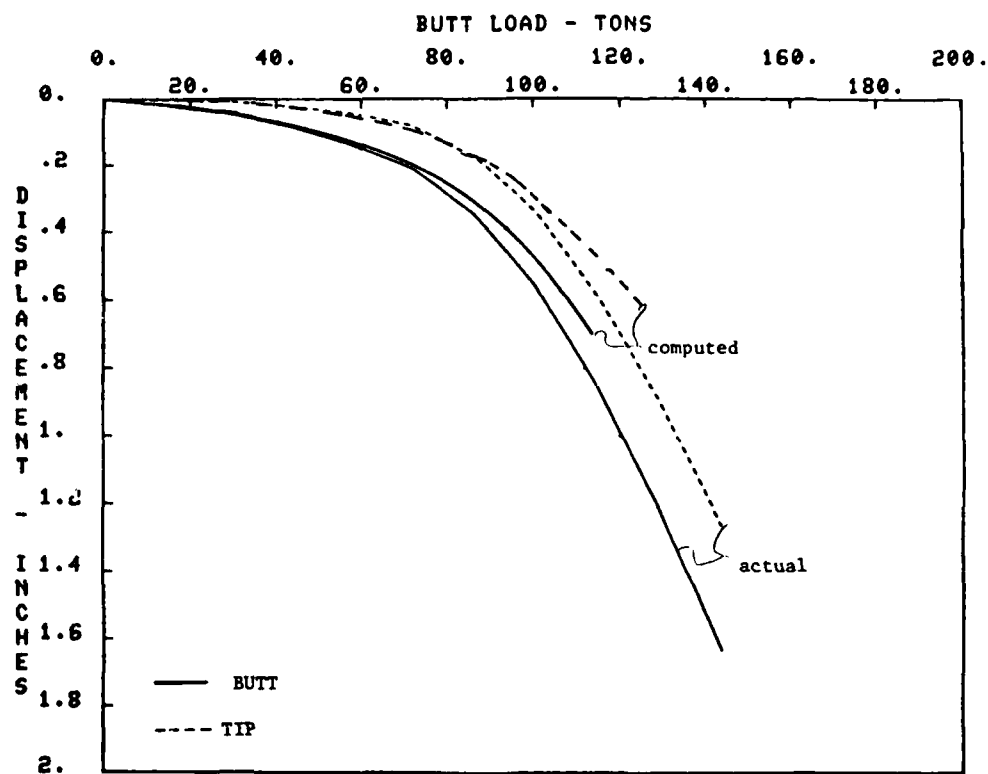


Figure 96. Computed and Actual Butt and Tip Load-Movement Curves, Red River, Test Pile No. PT-A-3C

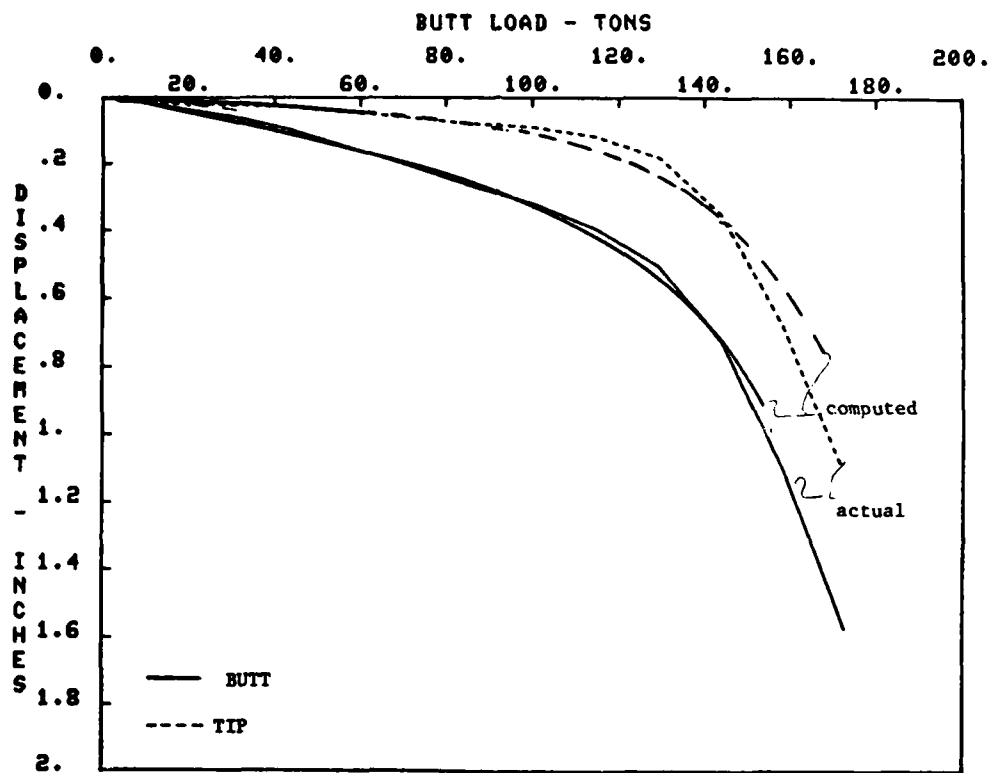


Figure 97. Computed and Actual Butt and Tip Load-Movement Curves, Red River, Test Pile No. PT-A-3C Retest

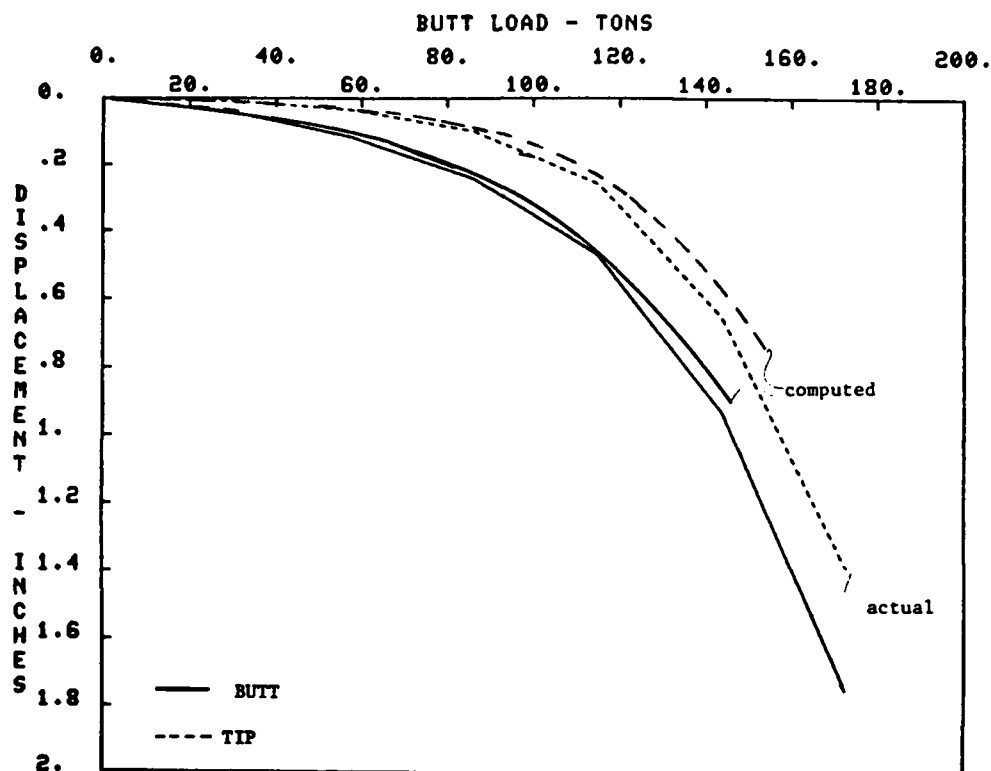


Figure 98. Computed and Actual Butt and Tip Load-Movement Curves, Red River, Test Pile No. PT-S-1C

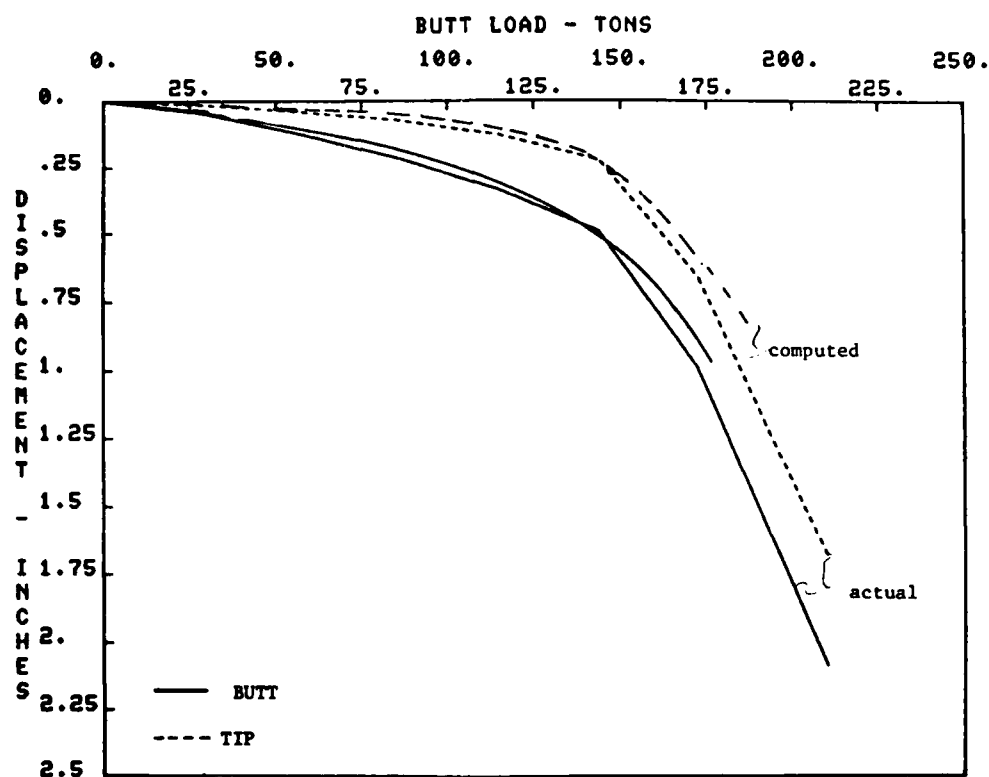


Figure 99. Computed and Actual Butt and Tip Load-Movement Curves, Red River, Test Pile No. PT-S-1C Retest

Comments

Two sets of curves for maximum tip resistance and shear transfer have been shown in this chapter; one based on pile tests that were adjusted for residual stresses (compression), and the other based on pile tests that weren't adjusted (unadjusted compression). For design work the values from adjusted (compression) are recommended. The values from the unadjusted are recommended for evaluating pile tests with insufficient data to determine residual stresses.

The allowable pile load using a conventional pile design procedure is obtained by dividing the ultimate capacity of the pile by a specified factor of safety. In the conventional pile design procedure, the displacement of the pile butt for the allowable pile load is generally not considered in determining the performance of the structure. For example, consider the butt load-movement curve presented in Figure 91. The capacity of the pile is approximately 240 tons for a tip movement of 0.25 in. For a factor of safety of 1.5, the allowable pile load would be 160 tons with a butt displacement of approximately 0.40 in. If these piles were for a pumping station which has a number of pipes entering it from outside, a displacement of 0.40 in. may not be tolerable.

Thus, being able to determine the load-movement curve is very important in determining whether or not the pile head displacement for the design load is within allowable limits. The available Soil-Structure Interaction (SSI) procedures can be used to compute the pile load-movement curves. The reliability of these existing procedures

can be improved by employing the relationships for shear-transfer and tip load presented in this report. These are based on actual pile tests and reflect the true behavior of piles driven into sand deposits. The computed load-movement performance using the new criteria has shown good agreement with the actual load-movement performance of field pile tests. A step-by-step illustration for using this procedure is presented in the next section.

Outline of Analysis Procedure

Figure 100 shows a typical boring log and SPT result found at a construction site in the Lower Mississippi Valley. The facility being constructed is being founded on piles after excavating the first 20-ft layer of clay. The pile and its properties are described in Figure 101. The following is a step-by-step procedure employing SSI analysis and shear-transfer and tip load criteria presented in this report:

1. Determine the average blow count for each soil layer:

<u>Depth, ft</u>	<u>Layer, ft</u>	<u>N Value</u>
30	20-40	18
50	40-60	28
75	60-90	30

2. Correct N values for removal of overburden; a 1 percent reduction for each foot of overburden removed: 20 ft of excavation - 20 percent reduction.

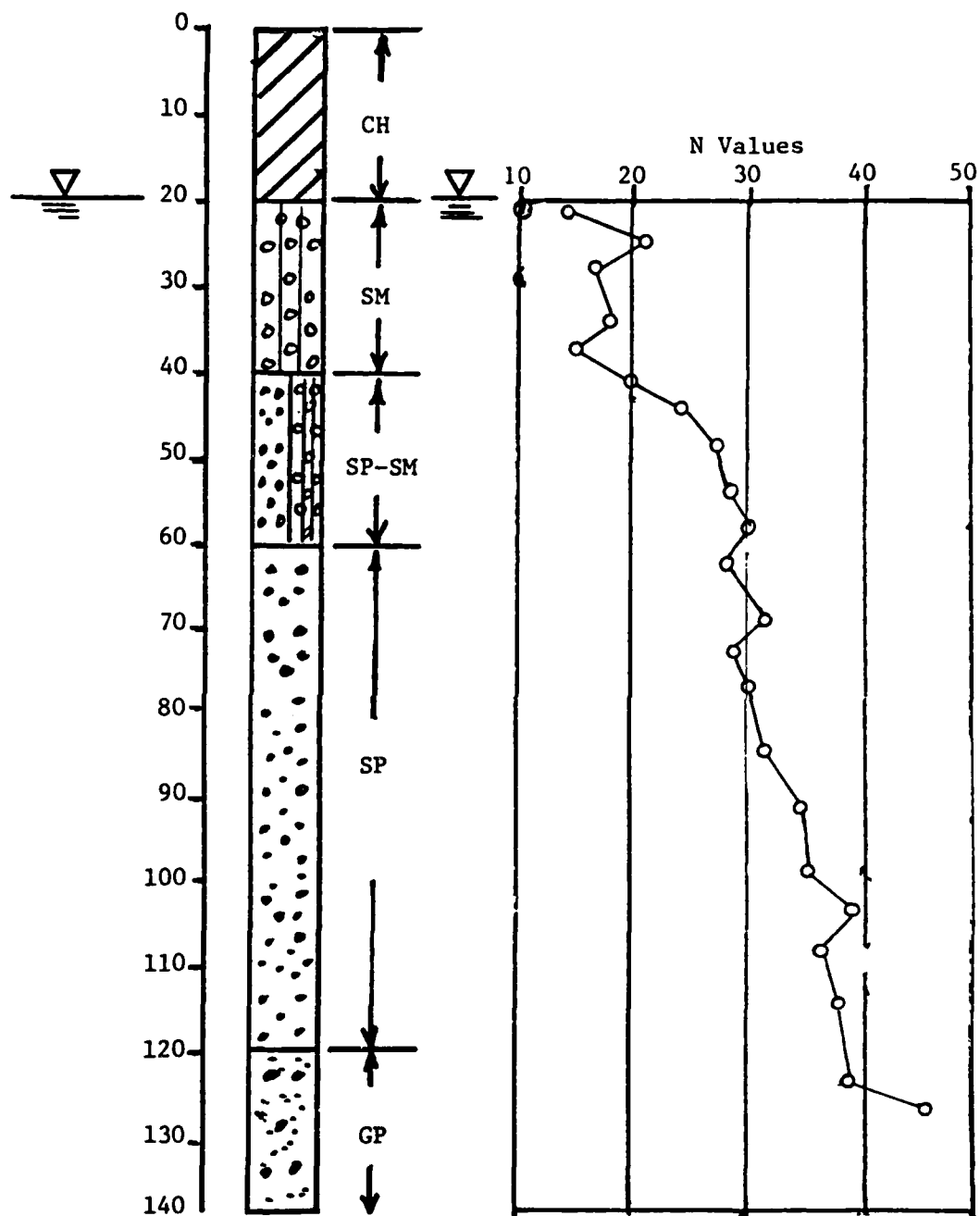


Figure 100. Soil Stratification and SPT Results

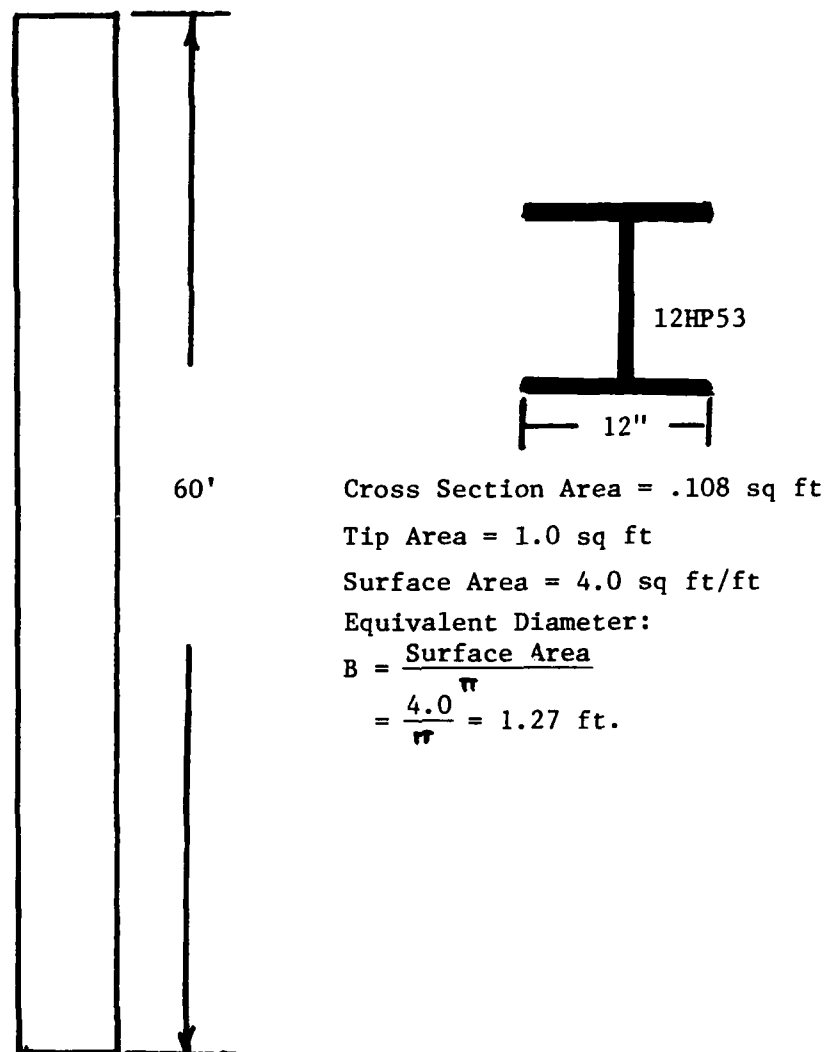


Figure 101. Pile and Pile Properties

<u>Depth, ft</u>	<u>Layer, ft</u>	<u>N Value</u>	<u>Reduced N Value</u>
30	20-40	18	15
50	40-60	28	23
75	60-90	30	25

3. Correct N values for penetration into fine sand or silty sand below the water table using the expression

$$N' = \frac{1}{2}(N - 15) + 15 \quad (21 \text{ bis})$$

<u>Depth, ft</u>	<u>Layer, ft</u>	<u>N Value</u>	<u>Reduced N Value</u>
30	20-40	15	15
50	40-60	23	19
75	60-90	35	25

4. Correct N values for effective overburden pressure using the correction factor, C_N , determined by

$$C_N = 0.77 \log \frac{20}{\bar{\sigma}_v} \quad (23 \text{ bis})$$

where $\bar{\sigma}_v$ is the effective overburden pressure (based on excavated ground surface), tsf. The purpose of this correction is to normalize the N values to an effective overburden pressure of 1 tsf on which the angle of internal friction chart shown in Figure 102 is based.

<u>Depth, ft</u>	<u>Layer, ft</u>	<u>$\bar{\sigma}_v$, tsf</u>	<u>C_N</u>	<u>N Value</u>	<u>Corrected N Value</u>
30	20-40	0.313	1.39	15	21
50	40-60	0.938	1.02	19	20
75	60-120	1.72	0.820	25	21

5. From Figure 102 determine the angle of internal friction, ϕ .

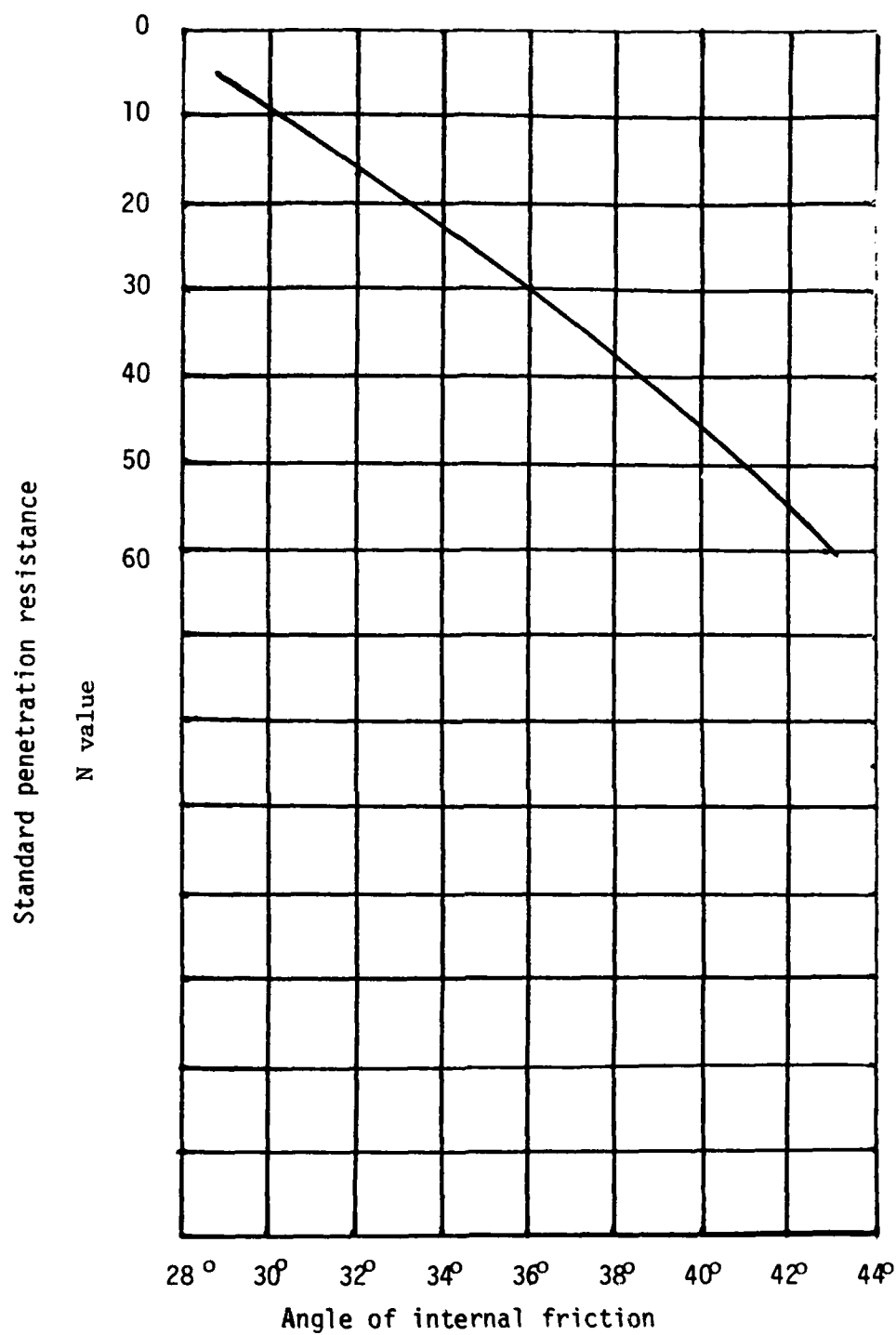


Figure 102. Correlation of N Values with angle of Internal Friction

<u>Depth, ft</u>	<u>Layer, ft</u>	<u>Corrected N Value</u>	<u>ϕ</u>
30	20-40	21	33°
50	40-60	20	33°
75	60-90	21	33°

6. Develop the shear transfer and pile movements, f - z , curves.

a. Find the maximum side and tip resistance from Figures 103 and 104, respectively (Figures 103 and 104 are reprints of Figures 70 and 90, respectively). Extrapolate for depths greater than those shown in Figures 103 and 104. The maximum tip resistance, q_{\max} , is the resistance for 0.25 inch of tip displacement.

<u>Pile</u>		<u>Penetration to Diameter Ratio (D/B)</u>	<u>ϕ</u>	<u>f_{\max} psf</u>	<u>q_{\max} psf</u>
<u>Depth, ft</u>	<u>Equivalent Diameter, ft</u>				
0	1.27	0	33°	0	
5	1.27	3.9	33°	360	
10	1.27	7.9	33°	540	
20	1.27	15.7	33°	780	
30	1.27	23.6	33°	860	
40	1.27	31.5	33°	950	
50	1.27	39.3*	33°	1050*	
60	1.27	47.4*	33°	1100*	112,000

* Approximate values obtained from Figure 103 by smooth extrapolation of appropriate curve.

b. Develop f - z curves using the expression

$$f = \frac{z}{\frac{1}{E_f} + \frac{1}{f_{\max}}} (z) \quad (47a \text{ bis})$$

In the above equation, f is in psf, z is in inches, E_f is in psf/inch, and f_{\max} is in psf. From Table 6 (p. 161), using an angle of internal

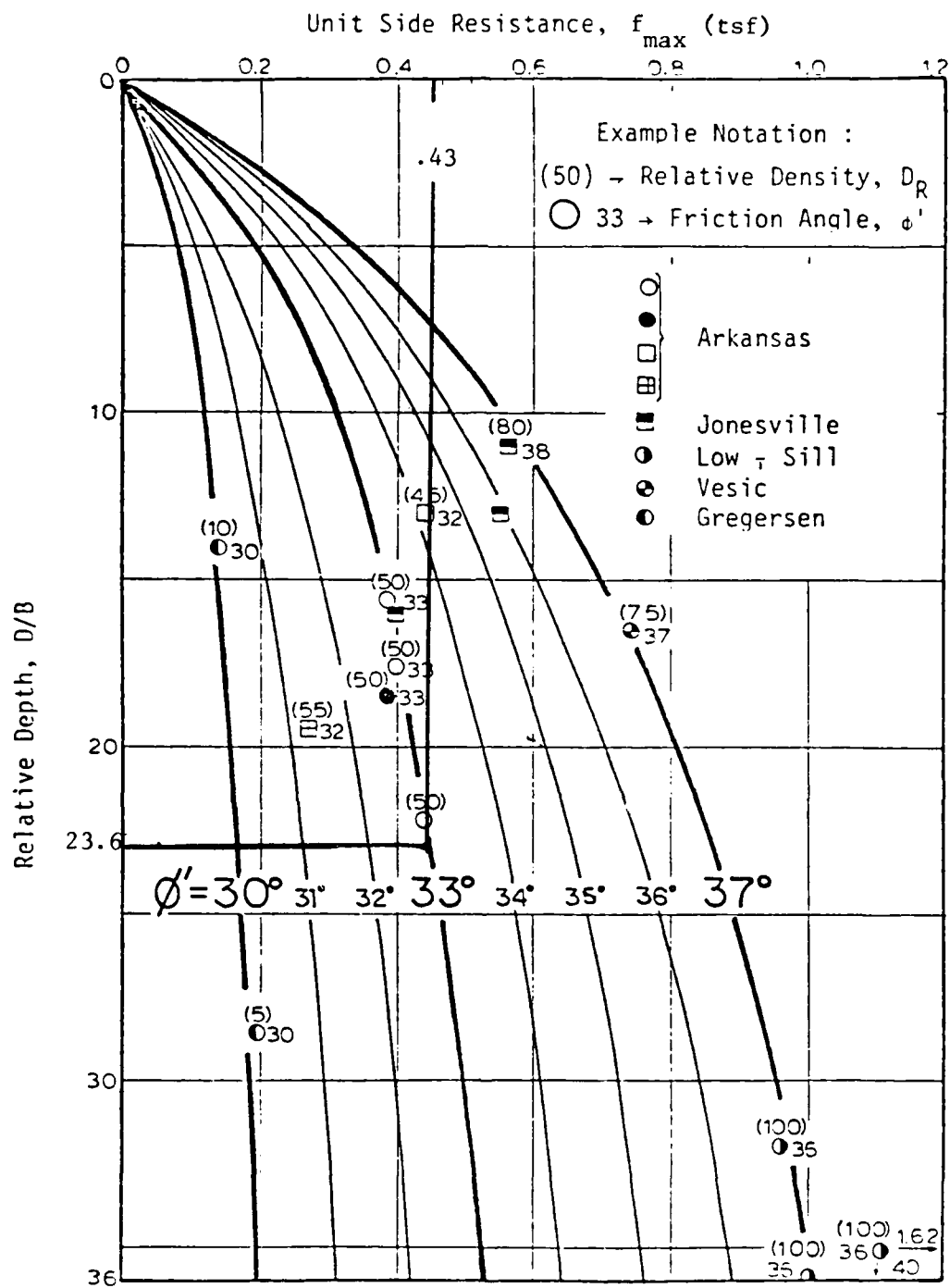


Figure 103. f_{\max} versus D/B, Compression
 (1 tsf = 95.76 kN/m²) (Castello 1980)

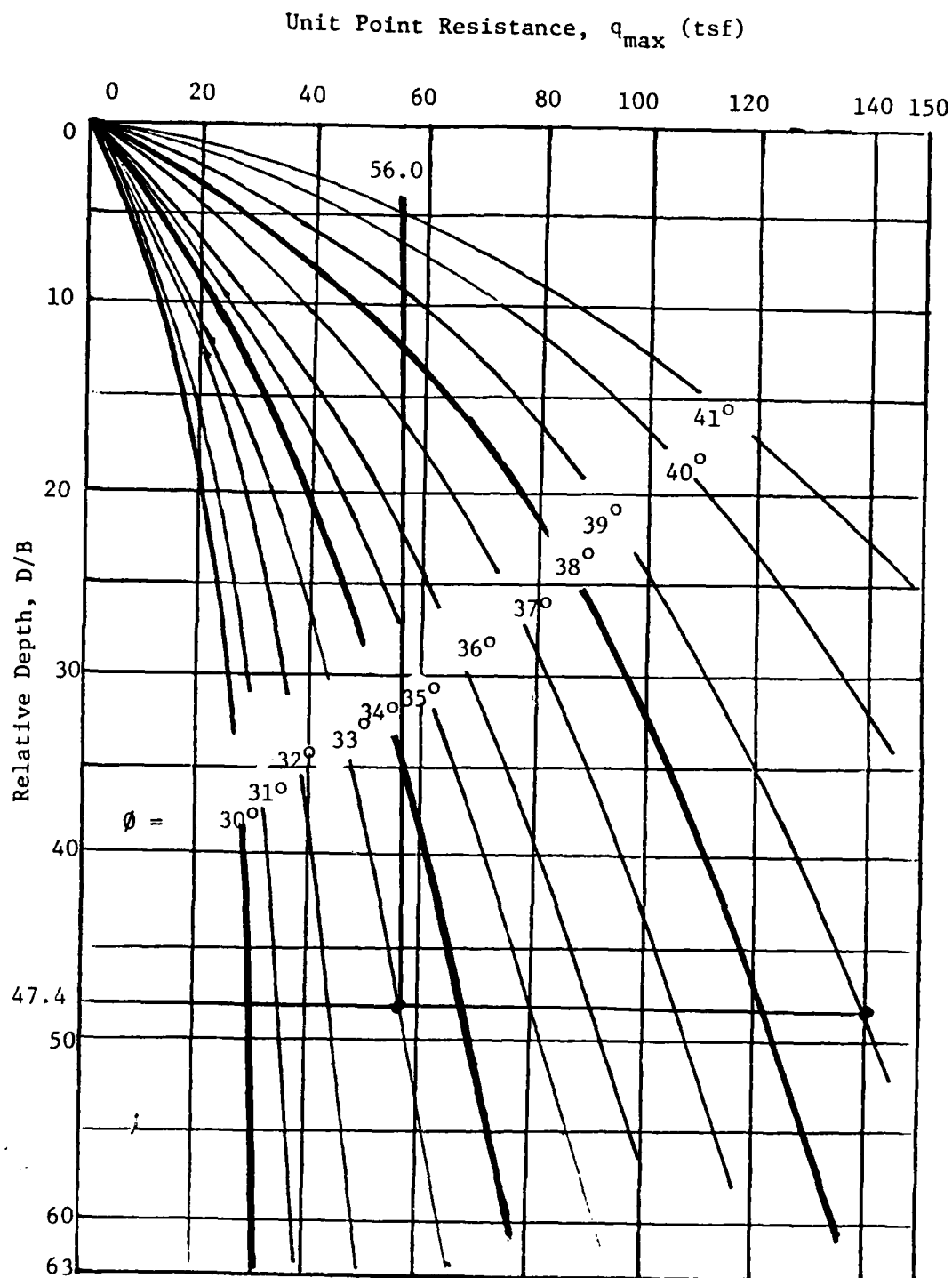


Figure 104. q_{\max} versus D/B , Compression (1 tsf = 95.76 kN/m²)

friction, ϕ , equal to 33° , an initial modulus, E_f , of 12,000 psf/in. is found. Using Equation 47a, shear transfer, f , values are computed and presented in Table 7 for given pile movements, z , at the depths of penetration shown above. These are plotted in Figure 105.

c. Develop q - z curves using the empirical expression for medium sands (see Equations 49a through 49c in Chapter 5 for relations for other sands).

$$q = [4 z]^{1/3} q_{\max}$$

and

$$P_{\max} = q_{\max} \times \text{area of the pile tip}$$

where

q and q_{\max} have units of psf and z is in inches. The q - z values are shown in Table 8 and plotted in Figure 106. Load capacity is predicted based on a tip movement of 0.25 inch. Values of P for tip movement greater than 0.25 inch are used to predict the entire load-settlement curves.

A computer program that analyzes axially loaded piles using the discrete spring soil model described in Chapter 2 (p. 32) is needed to determine the tip and butt load-displacement behavior for this example. An example of such a program is PX4C3, "Axially Loaded Pile Analysis Program," written by Drs. Coyle and Reese at the University of Texas. This program is available on the Conversationally Oriented Read-Time Program-Generating System (CORPS) under program number 10003 and is used for this example. Figure 107 shows a plot of the input data for the program, Figure 108 shows a plot of the load distribution in the pile for given butt loads, and Figure 109 shows the tip and butt

Table 7

Depth Penetration of Pile, Ft

	0	5	10	20	30	40	50	60
f _{max} , psf	0	360	540	780	860	950	1050	1100
Pile Movement z, in.	Shear Transferred, f, psf							
0.00	0	0	0	0	0	0	0	0
.025	0	164	193	214	220	228	233	235
.050	0	224	284	335	350	367	382	388
.075	0	256	337	411	435	462	486	495
.100	0	276	372	464	501	530	561	573
.150	0	299	415	533	582	622	665	682
.200	0	312	441	576	635	681	733	754
.250	0	321	458	605	674	721	781	804
.300	0	326	470	626	690	752	816	842
.400	0	334	486	655	730	793	865	894
.600	0	342	503	686	755	820	921	954
1.000	0	350	517	713	800	880	971	1007
10.000	0	358	538	773	852	943	1047	1090

for a D/B = 23.6, using figure 103;

$$f_{\max} = .43 \text{ tsf} = 860 \text{ psf}$$

for a z = .100 in:

$$f = \frac{z}{\frac{1}{E_f} + \frac{1}{f_{\max}}} = \frac{.10 \text{ in}}{\frac{1}{12000 \text{ psf/in}} + \frac{1}{860 \text{ psf}}} (.10 \text{ in})$$

$$= 501 \text{ psf}$$

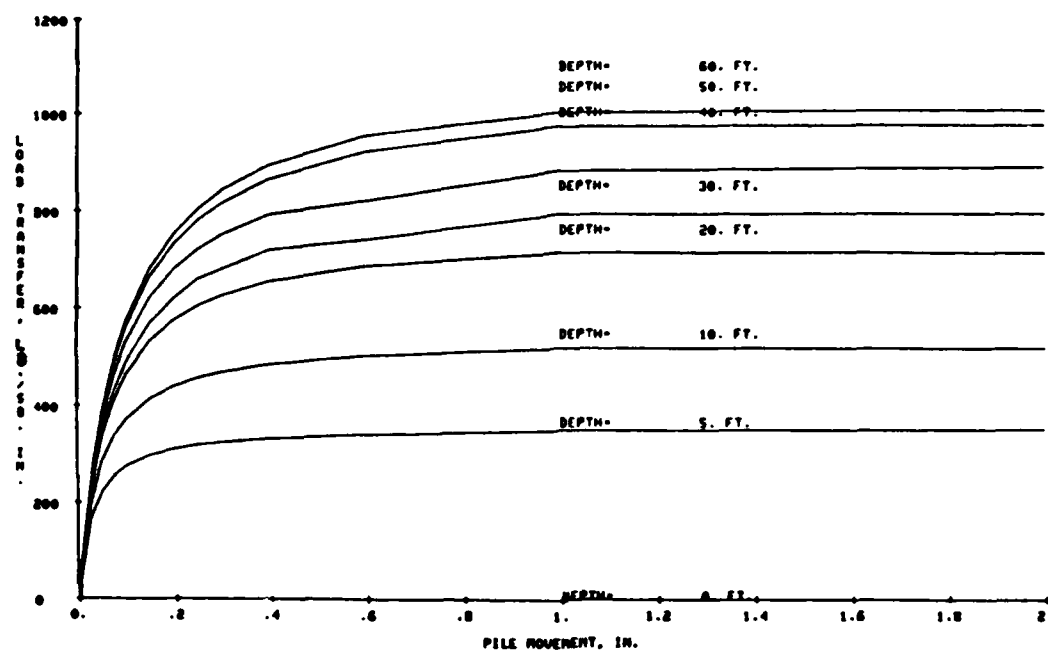


Figure 105. f-z Curves for Example Problems

Table 8

P-z Values

$$q_{\max} = 56.0 \text{ tsf}^*$$

$$P_{\max} = (56.0 \text{ tsf}) (2000.0 \text{ lb/ton}) (1.0 \text{ sq ft})$$

$$= 112,000 \text{ lb}$$

<u>Tip Movements, in.</u>	<u>Tip Load, lb.</u>
0.000	0.0
0.010	38460.0
0.020	48450.0
0.030	55460.0
0.040	61050.0
0.050	65760.0
0.075	75270.0
0.100	82850.0
0.125	89240.0
0.150	94830.0
0.175	99830.0
0.200	104380.0
0.250	112000.0
0.300	119480.0
0.400	131500.0
0.600	150500.0
1.000	178400.0
10.000	178400.0

* q_{\max} is the pressure corresponding to a tip movement of 0.25 inch.

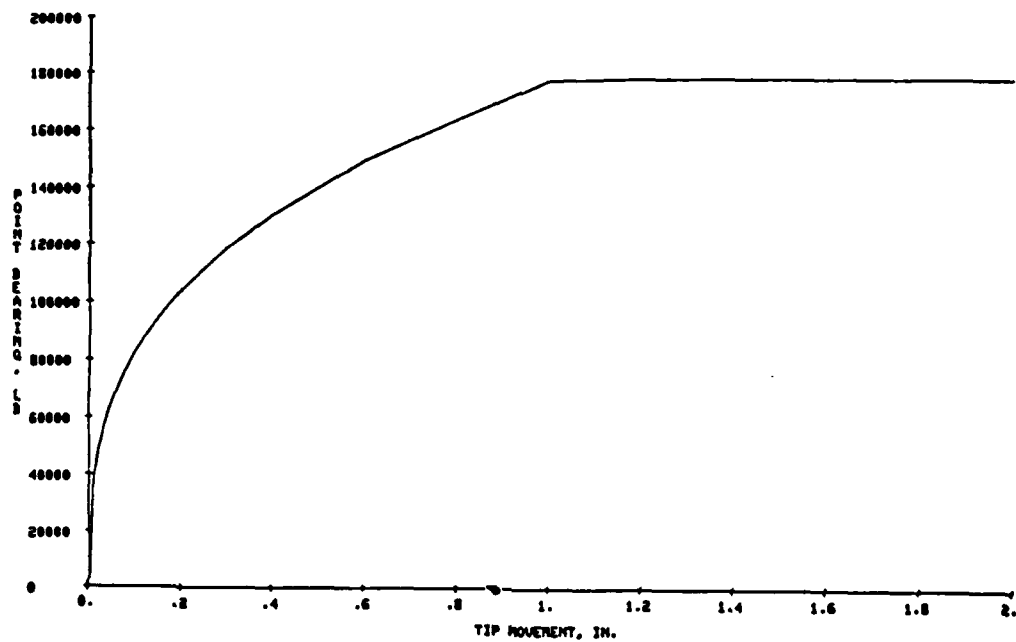


Figure 106. P-z Curve for Example Problems

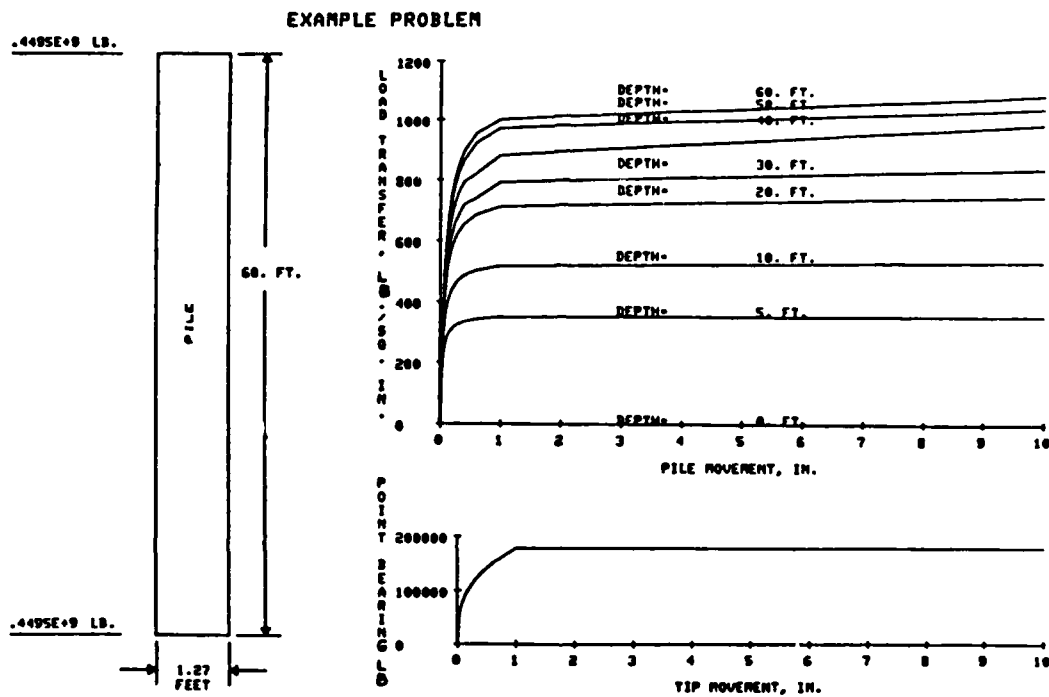


Figure 107. Plot of Data Input to Computer Program

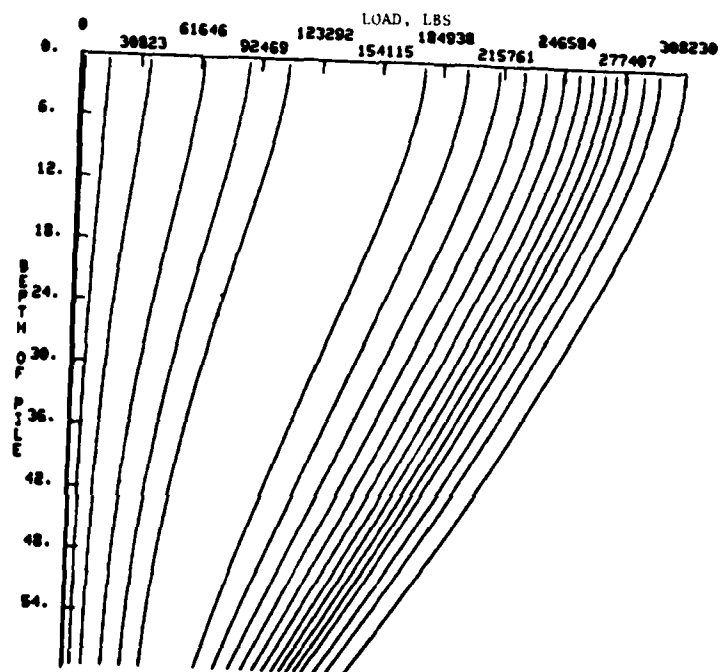


Figure 108. Plot of Load Distribution in Pile

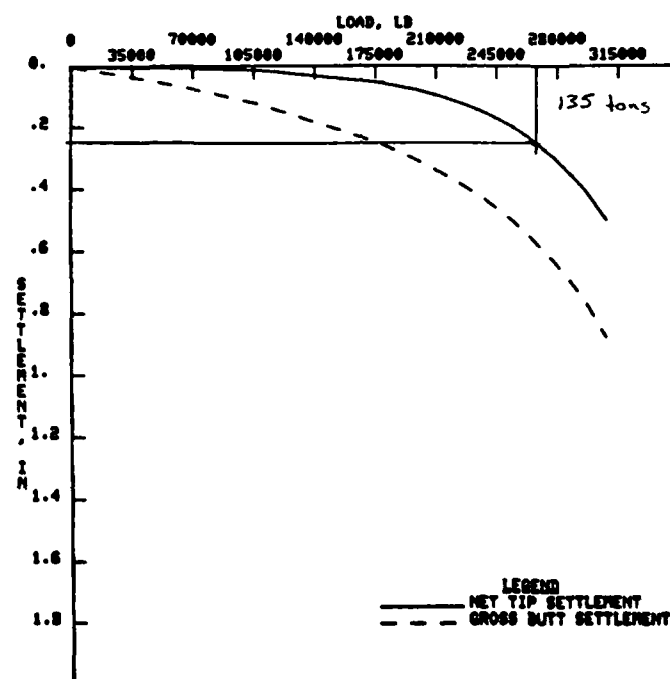


Figure 109. Tip and Butt Load-Displacement Curves for a 12HP53 Pile. $\phi = 33^\circ$

load-displacement curves for this example. Entering Figure 109 with a tip displacement of 0.25 in. yields a pile capacity of approximately 135 tons.

Design Curves

Using the new criteria presented in this chapter, and an axially loaded pile computer program, a set of pile capacity curves was developed for various pile diameters, surcharge loads at the surface, and soil densities. The capacity of a pile was defined as the butt load at a tip movement of 0.25 in. The surcharge loads were accounted for by computing an equivalent depth and using that depth to determine the maximum tip and side resistance. Samples of these design curves are presented in Figures 110-115. A complete set of design curves for H piles, concrete piles, steel piles (closed) and steel piles filled with concrete for ϕ values of 30° , 33° , 35° , and 37° is included in Part II of this report.

The pile capacity is found by entering the set of curves for a given pile type with a pile length and surcharge load and matching the desired pile length with the curve for the appropriate surcharge load. Using the pile length type, and angle of internal friction, ϕ , for the previous example, the pile capacity would be determined by entering Figure 111 for a 12 HP by 53, finding the pile length (60 ft), matching it with the curve of zero surcharge load, and reading down to find the pile capacity (135 tons). A comparison of this value with the value determined in the previous example reveals that they are identical, as they should be.

The pile capacity curves developed in this report are for

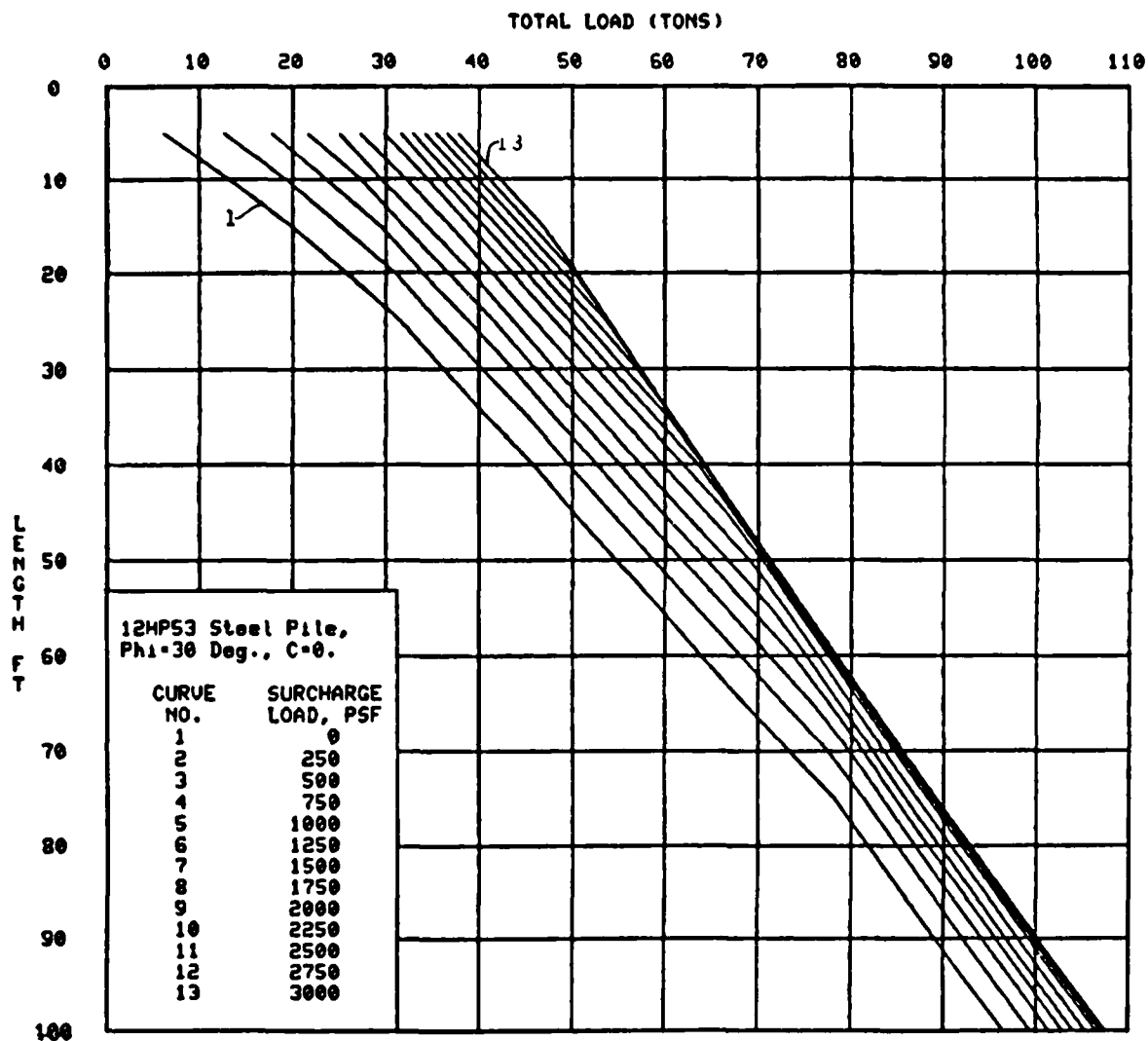


Figure 110. Total Pile Capacity for a 12HP53 Steel Pile, Submerged Condition, 1/4-in. Tip Movement, Phi = 30 Deg., C = 0

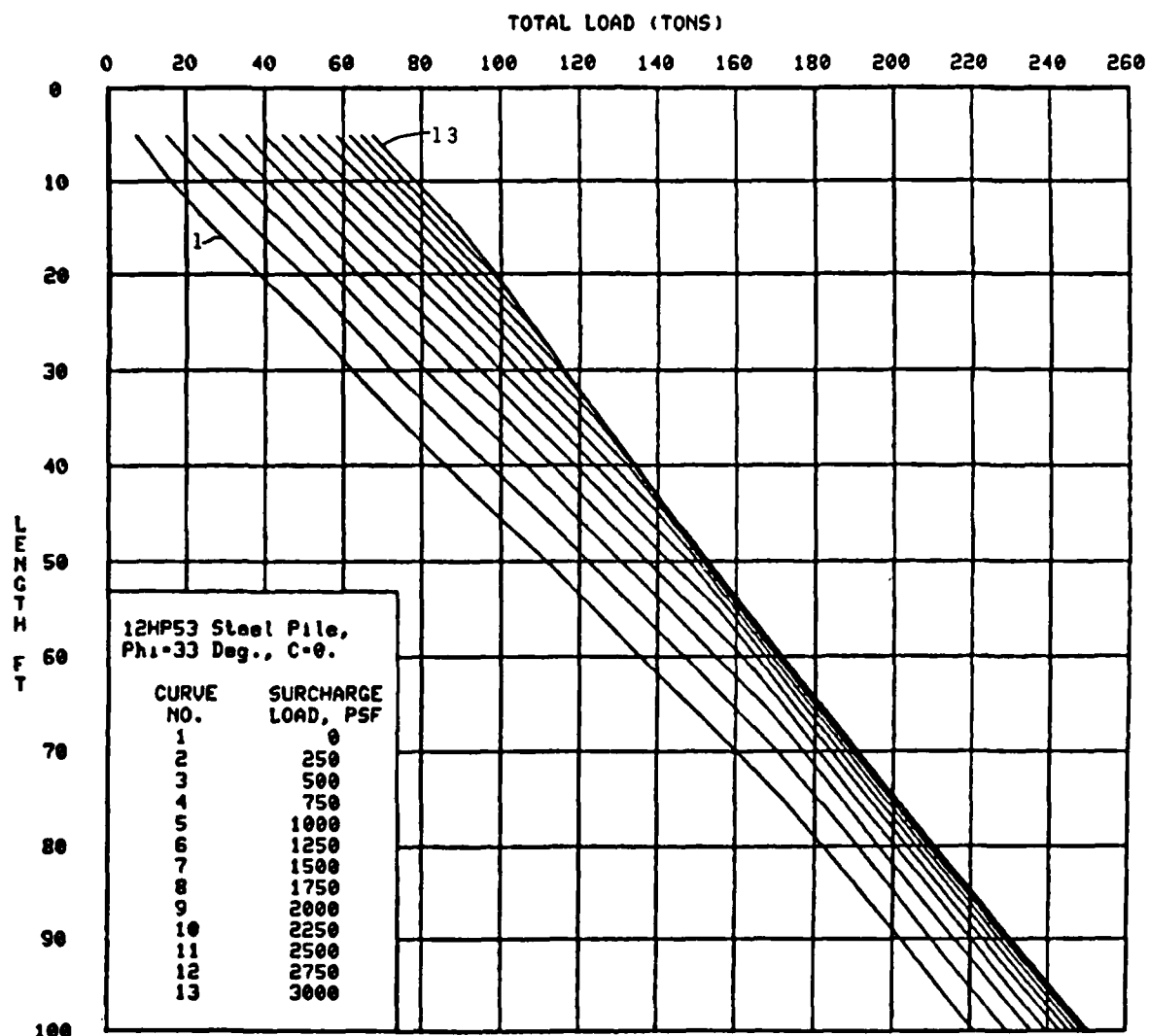


Figure 111. Total Pile Capacity for a 12HP53 Steel Pile, Submerged Condition, 1/4-in. Tip Movement, $\Phi = 33$ Deg., $C = 0$

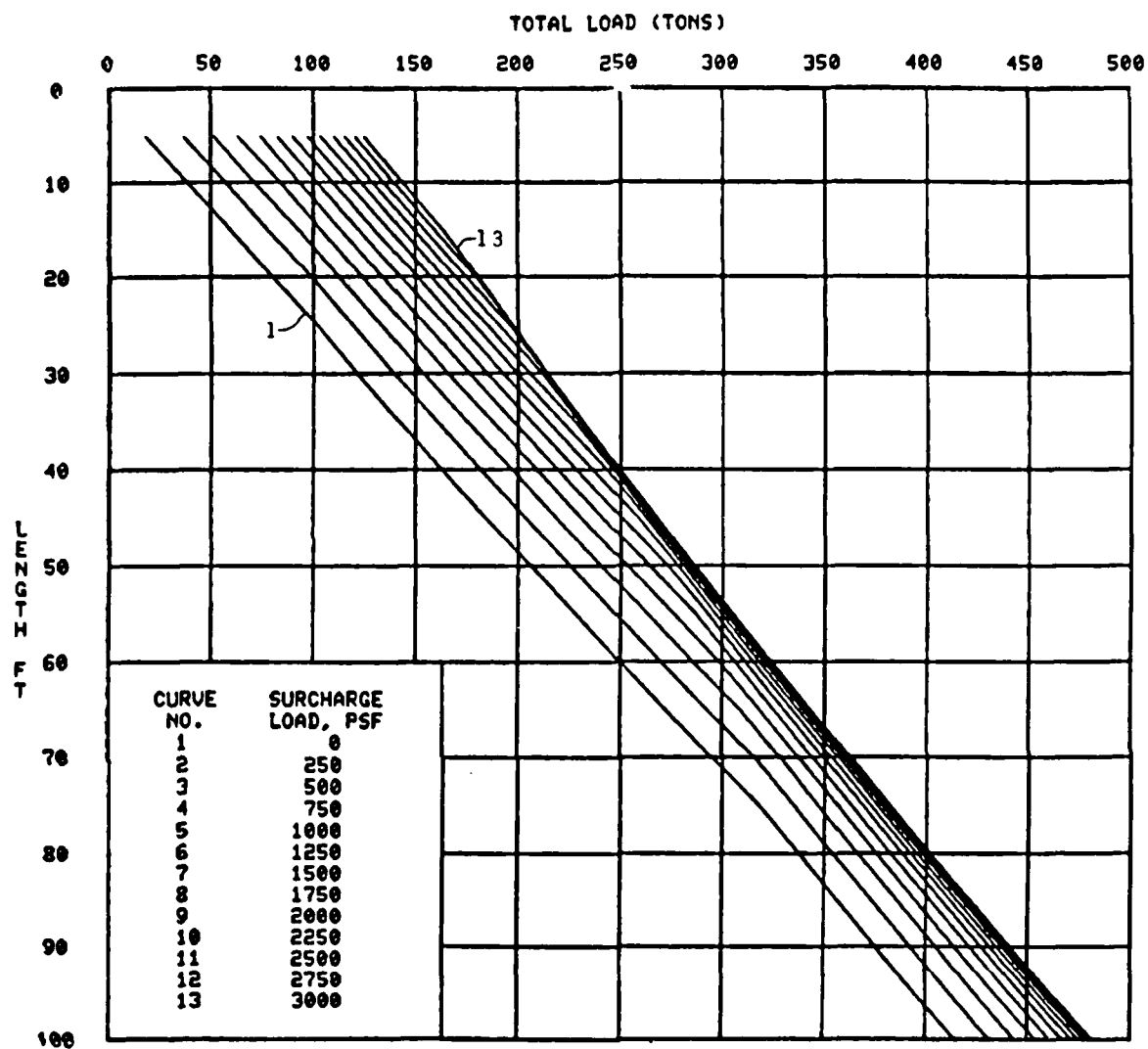


Figure 112. Total Pile Capacity for a 12HP53 steel Pile, Submerged Condition, 1/4-in. Tip Movement, $\Phi = 37$ Deg., $C = 0$

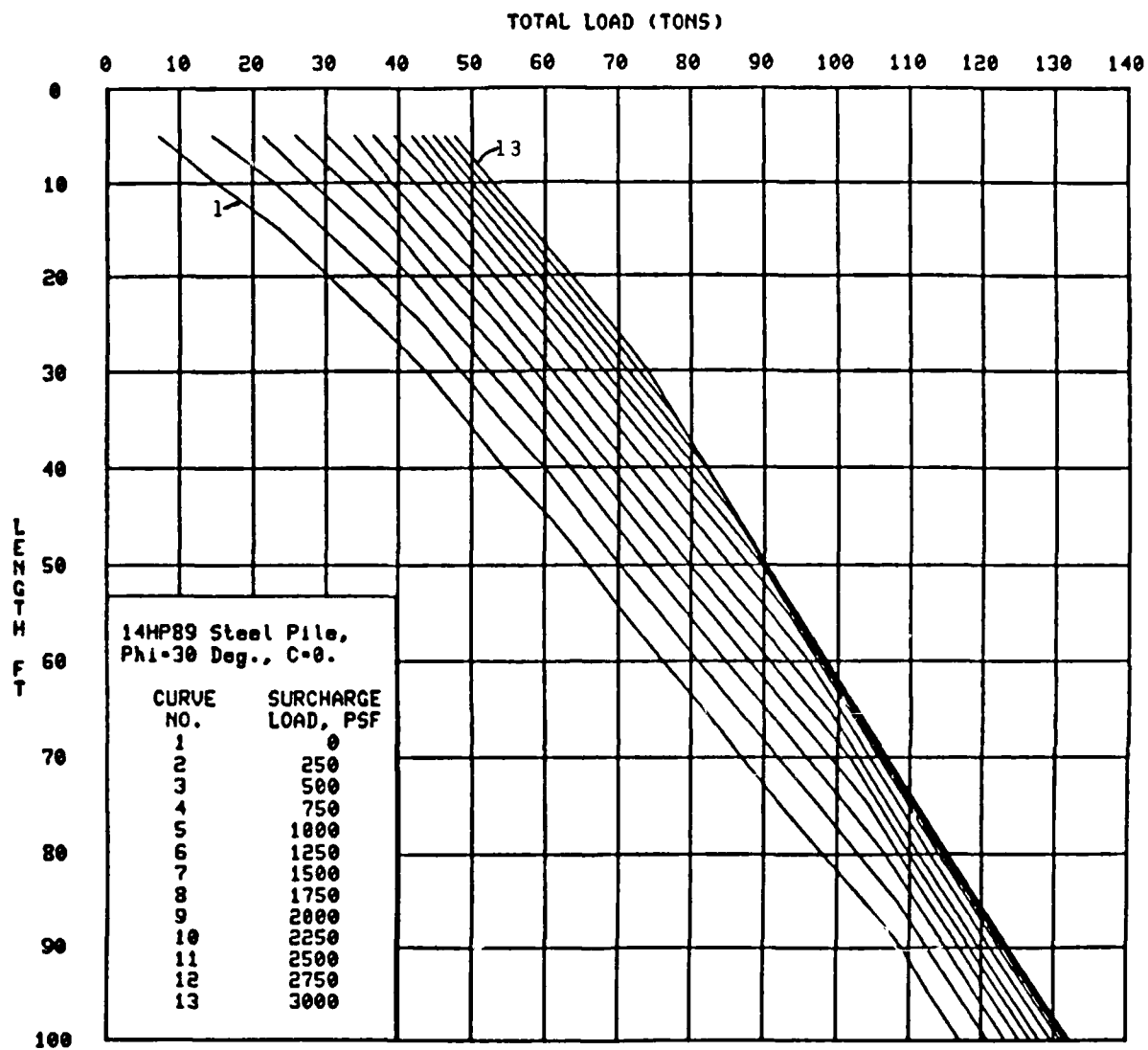


Figure 113. Total Pile Capacity for a 14HP89 Steel Pile, Submerged Condition, 1/4-in. Tip Movement, $\Phi = 30$ Deg., $C = 0$

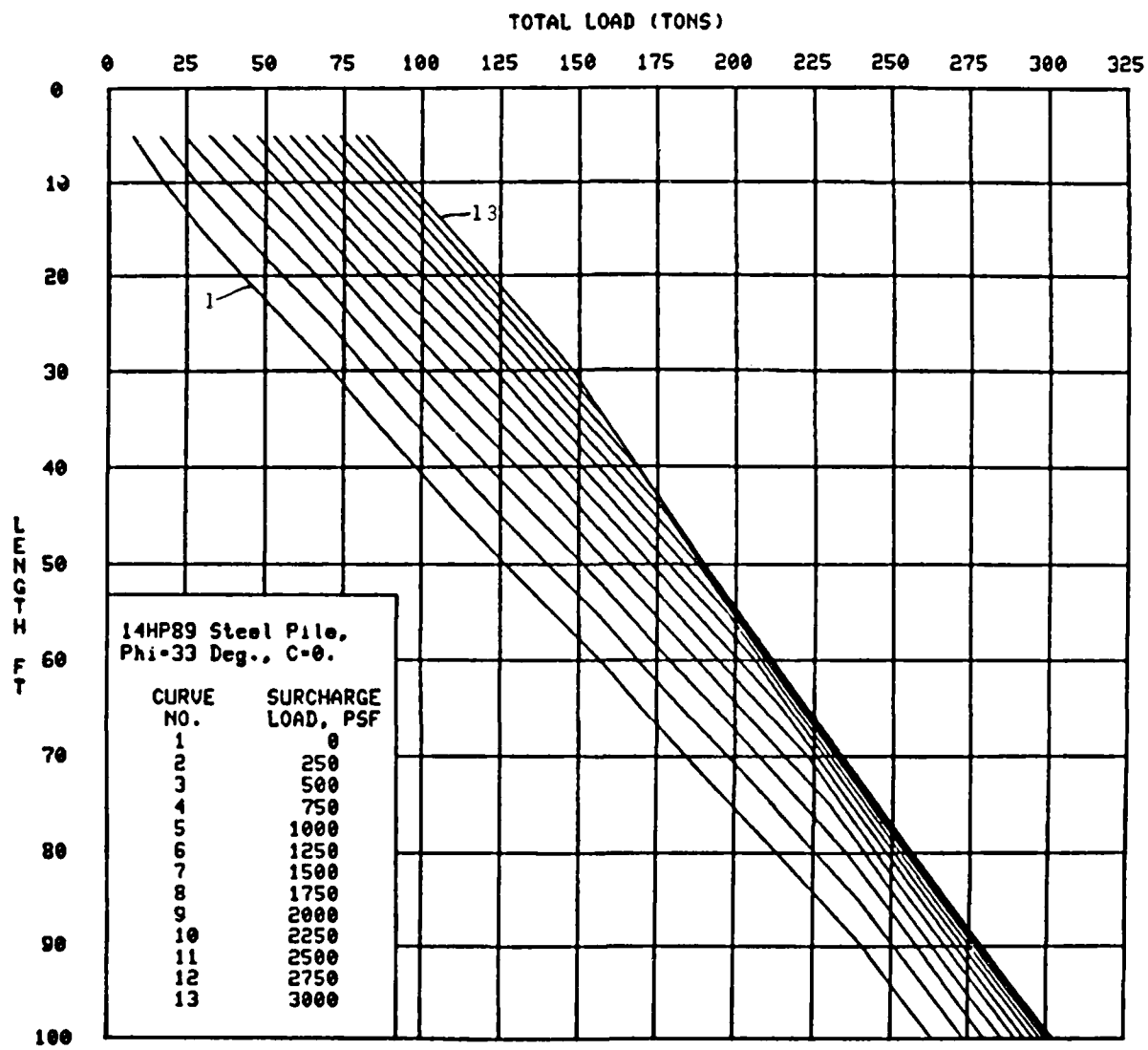


Figure 114. Total Pile Capacity for a 14HP89 Steel Pile, Submerged Condition, 1/4-in. Tip Movement, $\Phi = 33$ Deg., $C = 0$

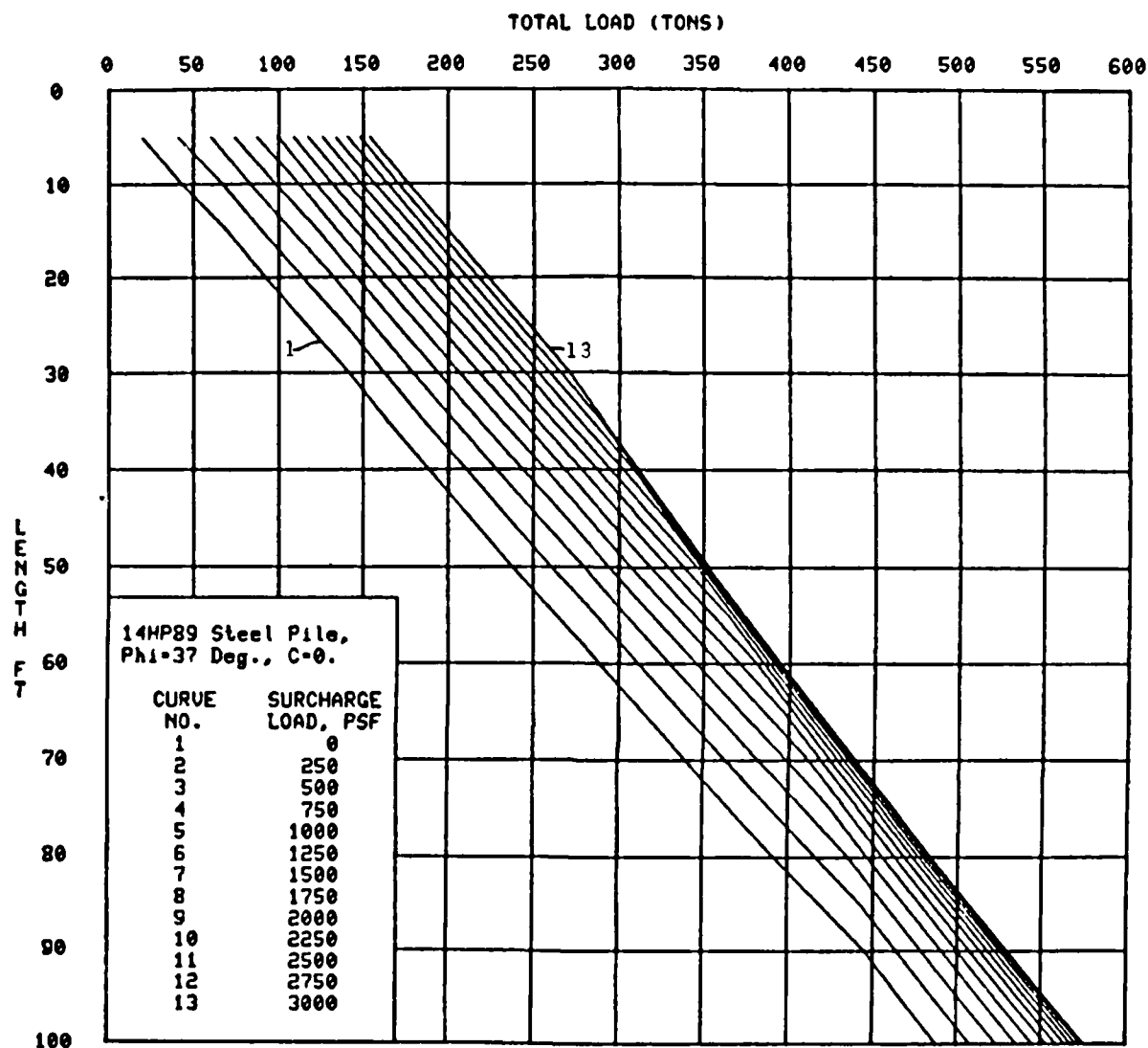


Figure 115. Total Pile Capacity for a 14HP89 Steel Pile, Submerged Condition, 1/4-in. Tip Movement, Phi = 37 Deg., C = 0

homogeneous soils. The pile capacity curves may give misleading results for a nonhomogeneous soil. The example presented previously will be reexamined, but instead of having the tip resting in the same soil stratum, it is to rest on denser sand. The soil at the tip has an angle of internal friction of 39° . The tip resistance obtained from Figure 104 is 140 tsf, and the resulting points for the P-z curves are shown in Table 9 and are plotted in Figure 116. The tip and butt load-displacement curves from the computer analysis are shown in Figure 117. The pile capacity for this example is 240 tons, approximately 100 tons greater than the pile capacity curves would give for a homogeneous soil. The pile capacity curves should not be used without careful consideration of the soil conditions. If the soil profile is highly nonhomogeneous, a detailed computer analysis should be performed using the side and tip resistance curves for the appropriate soil conditions.

Summary

The proposed criteria have been formed by drawing on the work of Castello (1980) for establishing the maximum side and tip resistance. This approach reflects the newest and latest research in this area. Castello's work has been verified and refined in this investigation to yield more representative results for the soil conditions encountered in the Lower Mississippi Valley. The displacement functions for the side and tip resistance have been based on the results of field tests.

The criteria are established through correlations to actual field performance of piles in the Lower Mississippi Valley. They demonstrate the consistency of resistance versus depth penetration that was found in the investigation of field tests. The proposed criteria are a

Table 9

P- z Values

$$q_{\max} = 140 \text{ tsf}$$

$$P_{\max} = (140 \text{ tsf}) (2000.0 \text{ lbs/ton})(1.0 \text{ sq ft})$$

$$= 280,000 \text{ lbs}$$

<u>Tip Movements, in</u>	<u>Tip Load, lbs</u>
0.000	0.0
0.010	125200.0
0.020	148900.0
0.030	164800.0
0.040	177100.0
0.050	187200.0
0.075	207200.0
0.100	222700.0
0.125	235500.0
0.150	246400.0
0.175	256100.0
0.200	264800.0
0.250	280000.0
0.300	293000.0
0.400	314900.0
0.600	392000.0
1.000	395000.0
10.000	396000.0

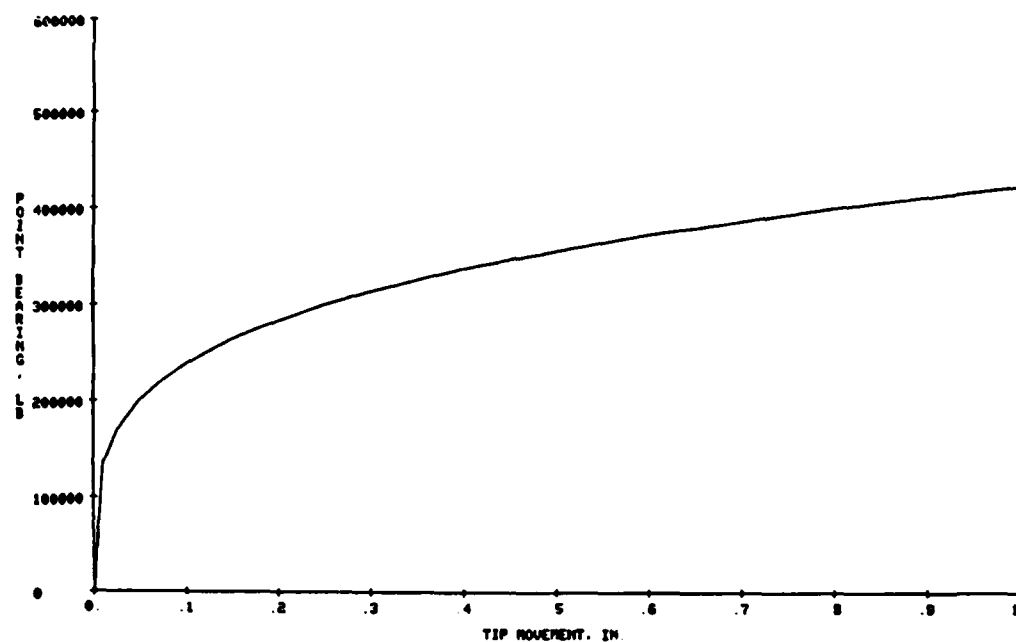


Figure 116. P-z Curve for $\phi = 39^\circ$

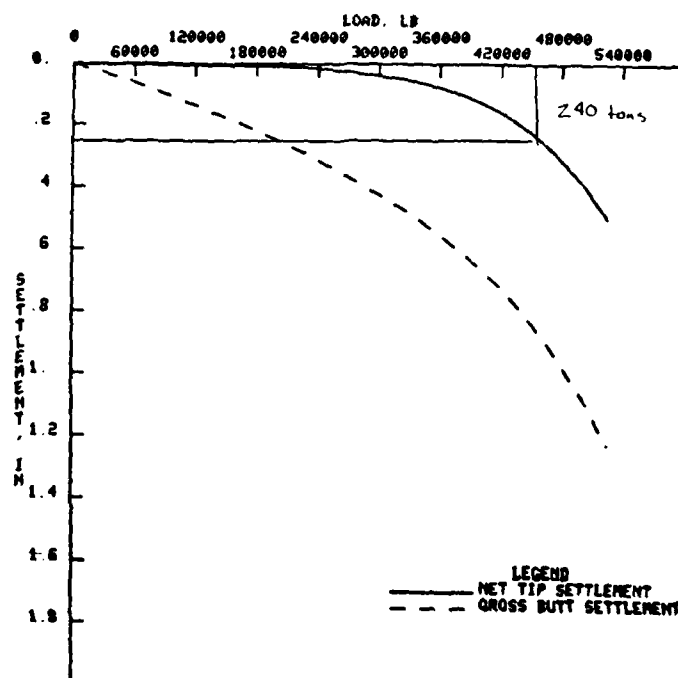


Figure 117. Tip and Butt Load-Displacement Curves

fuction of the angle of internal friction and the ratio of depth of penetration to pile diameter. They are independent of overburden pressure. The earth pressure effect and the arching system formed in the vicinity of the pile from installation are implicitly accounted for in the ratio of depth of penetration to pile diameter. The criteria demonstrate the ability to predict the load-deformation behavior of axially loaded piles in sand with reasonable accuracy for the soil conditions in the Lower Mississippi Valley.

The correlations for maximum side and tip resistance presented here appear valid for similar type soils in the Lower Mississippi Valley. They may be used in other regions, if they are cross-checked with previous pile tests results for that region. If they yield different results, adjustments should be made to the curves to reflect the result of the field tests.

CHAPTER 6: SUMMARY AND CONCLUSIONS

The ultimate capacity of a pile in a conventional pile design procedure is based on the assumption that the pile has enough displacements at every point for the soil to reach its maximum resistance. No consideration is given to the displacement compatibility of the pile-soil system, but in the design of a pile foundation based on an actual field pile test, the ultimate capacity is determined by an allowable displacement.

The most important reason for utilizing a pile foundation is to limit relative displacements. Thus, it would seem logical that a design procedure for determining the capacity should be based on allowable displacement.

Soil-structure interaction analysis techniques provide an analytical tool for exploring the performance of the pile-soil system. They have advantages over conventional methods in that they can consider the displacement compatibility of the pile and the surrounding soil along with the nonlinear load-deformation characteristics of the soil. A more realistic determination of pile capacity can be made based on the computed displacements of the pile.

The difficulty with any pile design procedure for piles embedded in sand is obtaining the soil parameters for the computations. In the past, the capacity has been determined based on soil conditions that were measured prior to installation of the piles. The installation by driving alters the soil conditions surrounding the pile resulting in a

permanent change to the soil. The soil is compacted by insertion of the pile and by the impulse from the hammer's impact causing a permanent rearrangement and crushing of the soil particles in the vicinity of the pile. As the pile tip penetrates compacting and crushing the soil particles, the shaft of the pile causes a down drag on the surrounding sand particles that results in a vertical displacement of the sand particles. The vertical displacement of the sand particles along the pile shaft creates a thin sleeve or cylinder of loose sand surrounding the pile. The loose cylinder of sand adjacent to the pile shaft is circumscribed by a much denser sand that was densified under the tip as it was being driven. This condition is ideal for arching and has been well documented in the literature. The result of this phenomenon is that the shear transfer along the shaft is developed through an arching system that redistributes the in situ lateral earth pressure that was present prior to the installation, resulting in a reduction of pressure on the pile shaft. This phenomenon and the arching system at the edges of the pile tip make it virtually impossible to determine the relationship between the vertical overburden pressure and lateral earth pressure along the shaft or normal pressure at the tip.

Theoretical approaches are unavailable for this highly complex and indeterminate system, but with empirical correlations, such as developed in this report, it can be implicitly accounted for. Empirical approaches can yield good, reliable results if a large quantity of high-quality observations are available for a data

base. A large number of instrumented pile tests were used in this study to give a representative cross section of data points.

In the reduction of the pile test data, residual stresses played an important role in the interpretation of the results. Impact driving of piles induces stresses into the pile-soil system before the pile is ever loaded in testing. The ram of the hammer transfers momentum to the pile causing it to compress and penetrate into the soil. After the blow is delivered, the pile rebounds due to the compression force within it. The total rebound is prevented by the soil along the shaft leaving the pile with compression stresses in its lower portion and tensile stresses in its upper portion. The soil will also have a stress build up from the loading action. These stresses are commonly referred to as residual stresses. If the residual stresses are not accounted for, the load distribution measured in the pile from the test can lead to an overestimation of side resistance and an underestimation of tip capacity.

The three published criteria for side resistance versus pile movement evaluated in this report have demonstrated an inconsistency with respect to the field results presented. They lack the ability to predict the magnitude of side resistance and the shape of the function of side resistance versus pile movement.

Because of this lack of agreement in field results for these criteria, new criteria have been proposed in this report. The new criteria were established by combining the ultimate capacity work of Castello (1980) and the development of a displacement function from actual field load tests. The new criteria demonstrate trends that are

found in field tests and not presented in the other criteria. The criteria have proven themselves in comparisons with field results. They provide an engineer with a powerful tool for predicting the load-displacement behavior of piles with reasonable and reliable results. However, the methodology and criteria should only be used in combination with good engineering judgment.

REFERENCES

1. Aihart, T. P., Coyle, H. M., Hirsch, T. J., and Buchanan, S. J. (1969), "Pile Soil System Response in a Cohesive Soil", Performance of Deep Foundation, ASTM, SPT 44, pp. 264-294.
2. Banerjee, P. K., and Davies, T. G., (1977), "Analysis of Pile Groups Embedded in Gibson Soil", Proceedings, 9th International Conference on Soil Mechanics and Foundation Engineering, Vol 1, pp. 381-386.
3. Bazaraa, A. R., (1967), "Use of the Standard Penetration Test for Estimating Settlements of Shallow Foundations On Sand", Ph.D. Thesis, University of Illinois, Urbana, p. 379.
4. Bishop, A. W., Collingridge, V. H., and O'Sullivan, T. P., (1948), "Driving and Loading Tests on Six Precast Concrete Piles in Gravel", Geotechnique, Vol I, June 1948, pp. 49-58.
5. Bowles, J. E., (1977), Foundation Analysis and Design, 2nd ed., McGraw-Hill Book Company, New York, 1977.
6. Brinch Hansen, J., (1961), "A General Formula for Bearing Capacity", Bulletin No. 11, The Danish Geotechnical Institute, Copenhagen, Denmark.
7. Broms, B. B., (1966), "Methods of Calculating the Ultimate Bearing Capacity of Piles: A Summary", Sol-Soils, France, Vol. V, Nos. 18-19, pp. 21-31.
8. Buisman, A. S. K., (1935), "De Weerstand Van Paalpunten in Sand", De Ingenieur 50, pp. Bt. 25-28, 31-35.
9. Buisman, A. S. K., (1940), Grondmechanica, Delft, The Netherlands, pp. 190.
10. Butterfield, R., and Banerjee, P. K., (1971a), "A Note on the Problem of a Pile-Reinforced Half Space", Geotechnique, Vol 20, No. 1, pp. 100-103.
11. Butterfield, R., and Banerjee, P. K., (1971b), "The Problem of Pile Group and Pile Cap Interaction", Geotechnique, Vol 21, No. 2, pp. 135-142.
12. Caquot, A., (1934), Equilibre des massifs afrottement interne, Paris.
13. Caquot A., and Kerisel, J., (1953), "Sur le terme de surface dans le calcul des foundations en milieu pulverulent", Proceedings, Third Intern. Confer. Soil Mech. Found. Engrg., Zurich, Vol I, pp. 336-337.

14. Castello, R. R., (1980), "Bearing Capacity of Driven Piles in Sand", Ph.D. Thesis, Texas A&M University, College Station, Texas.
15. Chellis, R. D., (1961), Pile Foundations, McGraw-Hill, New York, pp. 704.
16. Clisby, M. B., (1970), "An Evaluation of Pile Bearing Capacities Load-Deflection Values of Piles by Interaction Interim Report", Mississippi State University and Mississippi State Highway Department.
17. Clisby, M. B., (1972), "An Evaluation of Pile Bearing Capacities", Interim Report II, Mississippi State University and Mississippi State Highway Department.
18. Clough, G. W., and Duncan, J. M. (1969), "Finite Element Analyses of Port Allen and Old River Locks", Report No. TE 69-13, Office of Research Services, University of California, Berkeley.
19. Clough, G. W., and Duncan, J. M., (1971), "Finite Element Analyses of Retaining Wall Behavior," Journal of the Soil Mechanics and Foundation Division, ASCE, Vol 97, No. SM12.
20. Clough, G. W., (1972), "Application of the Finite Element Method of Earth-Structure Interaction," Proceedings, Symposium on Applications of the Finite Element Method To Problems in Geotechnical Engineering, U. S. Army Engineer Waterways Experiment Station, Vicksburg, Mississippi.
21. Coyle, H. M., and Reese, L. C., (1966), "Load Transfer to Axially Loaded Piles in Clay", Journal of the Soil Mechanics and Foundation Division, ASCE, Vol 92, No. SM2, Proc. Paper 4072, March 1966, pp. 1-26.
22. Coyle, H. M., and Sulaiman, I. H., (1967), "Skin Friction for Steel Piles in Sand", Journal of the Soil Mechanics and Foundation Division, ASCE, Vol. 93, No. SM6, Proc. Paper 5590, pp. 261-278.
23. Coyle, H. M., and Sulaiman, I. H., (1970), "Bearing Capacity of Foundation Piles: State of the Art", Highway Research Record No. 333, p. 87.
24. Coyle, H. M., Bartoskewitz, R. E., and Berger, W. J., (1973), "Bearing Capacity Prediction by Wave Equation Analysis - State of the Art", Research Report No. 125-8, Texas Transportation Institute, Texas A&M University.

25. Coyle, H. M., (1977), "Marine Foundation Engineering", Unpublished Class Notes, Texas A&M University.
26. D'Appolonia, E., and Romualdi, J. P., (1963), "Load Transfer in End-Bearing Steel Hl-Piles," Journal of the Soil Mechanics and Foundations Division ASCE, Vol 89, SM2, pp. 1-25.
27. Darragh, R. D., and Bell, R. A., (1969), "Load Tests on Long Bearing Piles", Performance of Deep Foundations, ASTM, STP-444, pp. 41-67.
28. Desai, C. S., and Abel, J. F., (1972), Introduction to the Finite Element Method, Van Nostrand Reinhold, New York.
29. Desai, C. S., and Holloway, D. M., (1972), "Load-Deformation Analysis of Deep Pile Foundations," Proceedings, Symposium on Applications of the Finite Element Method to Problems in Geotechnical Engineering, U. S. Army Engineer Waterways Experiment Station, Vicksburg, Mississippi.
30. Desai, C. S., (1974), "Numerical Design-Analysis for Piles in Sand", Journal of the Geotechnical Engineering Division, ASCE, Vol 100, No. GT6, pp. 613-635.
31. Duncan, J. M., and Chang, Y-Y., (1970), "Nonlinear Analysis of Stress and Strain in Soils", Journal of the Soil Mechanics and Foundations Division, ASCE, Vol 96, No. SM5.
32. Duncan, J. M., and Clough, G. W., (1971), "Finite Element Analyses of Port Allen Lock," Journal of the Soil Mechanics and Foundations Division, ASCE, Vol 97, No. SM8, Proc. Paper, pp. 1063-1068.
33. Ellison, R. D., (1969), "An Analytical Study of the Mechanics of Single Pile Foundations", Ph.D. Dissertation, Carnegie-Mellon University, Pittsburg, PA.
34. Ellison, R. D., D'Appolonia, E., and Thiers, G.R., (1971), "Load-Deformation Mechanism for Bored Piles", Journal of the Soil Mechanics and Foundations Division, ASCE, Vol 97, SM4, pp. 661-678.
35. Fruco and Associates, (1964), "Pile Driving and Loading Tests", Report for Corps of Engineers, Little Rock, Arkansas.
36. Furlow, C. R., (1968), "Pile Tests, Jonesville Lock and Dam, Quachita and Black Rivers, Arkansas and Louisiana", Technical Report S-68-10, U. S. Army Engineer Waterways Experiment Station, Vicksburg, Mississippi.

37. Gibbs, H. J., and Holtz, W. G., (1957) "Research on Determining the Density of Sands by Spoon Penetration Testing", Proceedings of the IV International Conference on Soil Mechanics and Foundation Engineering, London, Vol 1, pp. 35-38.
38. Gregersen, O. S., Aas, G., and DiBiagio, E., (1973) "Load Tests on Friction Piles in Loose Sand", Proceedings of the VIII International Conference on Soil Mechanics and Foundation Engineering, Moscow, Vol 2.1, pp. 19-27.
39. Headquarters, Department of the Army, (1958), "Design of Pile Structures and Foundations", Engineer Manual 1110-2-2906, Washington, D.C.
40. Hanna, T. H., and Tan, R. H. S., (1973), "The Behavior of Long Piles Under Compressive Loads in Sand", Canadian Geotechnical Journal, Vol 10, No. 3, pp. 311-340.
41. Headquarters, Department of the Army, (1971), "Instrumentation of Earth and Rock-Fill Dams", Engineer Manual 1110-2-1908, Washington, D. C.
42. Hirsch, T. J., et al., (1970), "Instruments, Performance and Method of Installation," Proceedings, Conference on Design Installation of Pile Foundations and Cellular Structures, Lehigh University, Bethlehem, PA, pp. 173-177.
43. Holloway, D. M., (1974) "DUKFOR: Utilization Guidelines", Draft Report submitted for review, U. S. Army Engineer Waterways Experiment Station, Vicksburg, Mississippi.
44. Holloway, D. M., (1974), "User's Guide, Program AXISYM," Draft Report submitted for review, U. S. Army Engineer Waterways Experiment Station, Vicksburg, Mississippi.
45. Holloway, D. M., (1975), "Wave Equation Analyses of Pile Driving," Technical Report, S-75-5, U. S. Army Engineer Waterways Experiment Station, Vicksburg, Mississippi.
46. Holloway, D. M., Clough, G. W., and Vesic, A. S., (1975), "The Mechanics of Pile-Soil Interaction in Cohesionless Soils", Contract Report S-75-5, U. S. Army Engineer Waterways Experiment Station, Vicksburg, Mississippi.
47. Holloway, D. M., Clough, G. W., and Vesic, A. S., (1978), "The Effects of Residual Driving Stresses on Pile Performance Under Axial Loads", Proceedings of 1978 Offshore Technology Conference, Paper No. OTC 3306 Houston, TX, pp. 2225-2236.

48. Hunter, A. A., and Davisson, M. T., (1969), "Measurement of Pile Load Transfer", Performance of Deep Foundations, ASTM, STP 444, pp. 106-117.
49. Janbu, Nilmar, (1963), "Soil Compressibility as Determined by Oedometer and Triaxial Tests", European Conference on Soil Mechanics and Foundation Engineering, Wiesbaden, West Germany Vol 1, pp. 19-25.
50. Kaufman, R. I., and Sherman, W. C., (1957) "Review of Soils Design, Pile Loading Tests, Construction, and Performance Observations, Section 1-B Floodwall, Memphis, Tennessee", Technical Report No. 3-454, U. S. Army Engineer Waterways Experiment Station, CE, Vicksburg, MS.
51. Kerisel, J., (1961) "Fondations Profondes en Milieux Sableux: Variation de la Force Portante Limite en Fonction de la Densite, de la Profondeur, du Diametre et de la Vitesse d'Enfoncement", Proceedings of the V International Conference on Soil Mechanics and Foundation Engineering, Paris, Vol 2, pp. 73-83.
52. Kerisel, J., (1964), " Deep Foundations - Basic Experimental Facts; Proceedings, North American Conference on Deep Foundations, Mexico City.
53. Kerisel, J., L'Herminier, R., and Tcheng, Y., (1965), "Resistance de Pointe en Millieux Pulverulents de Serrages Divers", Proceedings of the VI International Conference on Soil Mechanics and Foundation Engineering, Montreal, Canada, Vol 4, pp. 165-169.
54. Kezdi, A., (1975), "Pile Foundations", Foundation Engineering Handbook, edited by H. F. Winterkorn and H. Y. Fang, Van Nostrand Reinhold Co., New York, pp. 556-600.
55. Kondner, R. L., (1963), "Hyperbolic Stress-Strain Response: Cohesive Soils", Journal of the Soil Mechanics and Foundations Division, ASCE, Vol 89, No. SM1, p. 115.
56. Kondner, R. L., and Zelasko, J. S., (1963), "A Hyperbolic Stress-Strain Formulation of Sands", Proceedings of the 2nd Pan-American Conference on Soil Mechanics and Foundation Engineering, Vol 1, Brazil, p. 289.
57. Kraft, L. M., Jr., Ray, R. R., and Kagawa, T., (1981), "Theoretical t-z Curves", Journal of Geotechnical Engineering Division, ASCE, Vol 107, No. GT11, Proc. Paper 16653, pp. 1543-1561.

58. Kulhawy, F. H., Duncan, J. M. and Seed, H. B., (1969), "Finite Element Analysis of Stresses and Movements in Embankments During Construction", Report No. TE 69-4, Office of Research Services, University of California, Berkeley, California.
59. Kulhawy, F. H., Duncan, J. M., (1972), "Stresses and Movements in Oroville Dam", Journal of the Soil Mechanics and Foundation Division, ASCE, Vol 98, No. SM7, Proc. Paper 9016, pp. 653-665.
60. Lambe, T. W., and Whitman, R. V., (1969), Soil Mechanics, John Wiley & Sons, Inc., New York.
61. Leonards, G. A., (1970), "Summary and Review of Part II", Pile Foundations, Highway Research Record No. 333, pp. 55-59.
62. Mansur, C. I., and Kaufman, R. I., (1958), "Pile Tests, Low-Sill Structure, Old River, Louisiana", Transactions of ASCE, Vol 123, pp. 715-748.
63. Mansur, C. I., and Hunter, A. H., (1970), "Pile Tests - Arkansas River Project", Journal of the Soil Mechanics and Foundation Division, ASCE, Vol 96, No. SM5, pp. 1545-1582.
64. Matlock, H. and Reese, L. C., (1960), "Generalized Solutions for Laterally Loaded Piles", Journal of the Soil Mechanics and Foundations Division, ASCE, Vol 86, No. SM5, pp. 63-91.
65. McCammon, N. R., and Golder, N. G., (1970), "Some Tests on Long Pipe Piles", Geotechnique, Vol 20, No. 2, pp. 171-184.
66. McClelland, B., Focht, J. A., Jr., and Emrich, W. J., (1969), "Problems in Design and Installation of Heavily Loaded Pipe Piles", Journal of the Soil Mechanics and Foundation Division, ASCE, Vol 95, No. SM6.
67. McClelland, B., (1972), "Design and Performance of Deep Foundations", ASCE Specialty Conference on Performance of Earth and Earth Supported Structures, Purdue University, Lafayette, Indiana.
68. Meyerhof, G. G., (1951), "The Ultimate Bearing Capacity of Foundations", Geotechnique, Vol 2, NO. 4, p. 301.
69. Meyerhof, G. G., (1956), "Penetration Tests and Bearing Capacity of Cohesionless Soils", Journal of the Soil Mechanics and Foundations Division, ASCE, Vol 82, No. SM1, pp. 1-17.
70. Meyerhof, G. G., (1959), "Compaction of Sands and Bearing Capacity of Piles", Journal of the Soil Mechanics and Foundation Division, ASCE, Vol 85, No. SM6, Proc. Paper 2292, pp. 1-29.

71. Meyerhof, G. G., (1976), "Bearing Capacity and Settlement of Pile Foundations", Journal of the Geotechnical Engineering Division, ASCE, Vol 102, No. GT3, pp 197-228.
72. Meyerhof, G. G., and Valsangkar, (1977), "Bearing Capacity of Piles in Layered Soils", Proceedings of the IX International Conference on Soil Mechanics and Foundation Engineering, Tokyo, Vol 1, pp. 645-650.
73. Mindlin, R. D., (1936), "Force at a Point in the Interior of a Semi-Infinite Solid", Physics, Vol 7, No. 5.
74. Nair, K., (1967), "Load-Settlement and Load Transfer Characteristics of a Friction Pile Subject to a Vertical Load", Proceedings, Third Pan-American Conference on Soil Mechanics and Foundation Engineering, Vol 1, pp. 565-590.
75. Nordlund, R. L., (1963), "Bearing Capacity of Piles in Cohesionless Soils", Journal of the Soil Mechanics and Foundation Division, ASCE, Vol 89, No. SM3, Proc. Paper 3506, pp. 1-35.
76. Parker, F., Jr., and Reese, L. C., (1969), "Experimental and Analytical Studies of Behavior of Single Piles in Sand Under Lateral and Axial Loading", Research Report 117-2, Center for Highway Research, University of Texas, Austin, TX.
77. Peck, R. B., Hansen, W. E., and Thornburn, T. H., (1974), Foundation Engineering, 2nd Edition, John Wiley & Sons, Inc., New York.
78. Potyondy, J. G., (1961), "Skin Friction Between Various Soils and Construction Materials", Geotechnique, Vol II, No. 4, pp. 339-353.
79. Poulos, H. G., and Davis, E. H., (1968), "The Settlement Behavior of Single Axially-Loaded Incompressible Piles and Piers", Geotechnique, Vol 18, pp. 351-371.
80. Poulos, H. G., and Mattes, N. S., (1969a) "The Behavior of Axially-Loaded End-Bearing Piles", Geotechnique, Vol 19, pp. 285-300.
81. Poulos, H. G., and Mattes, N. S., (1969b), "The Analysis of Downdrag in End-Bearing Piles Due to Negative Friction", Proceedings 7th International Conference Soil Mechanics and Foundation Engineering, Vol 2, pp. 204-209.

82. Poulos, H. G., (1972), "Load-Settlement Prediction for Piles and Piers," Journal of the Soil Mechanics and Foundations Division, Vol 98, SM9, pp. 879-897.
83. Poulos, H. G., and Davis, E. H., (1980), "Pile Foundation Analysis and Design, John Wiley and Sons, New York, pp. 13-15, 52-66, 71-83.
84. Prandtl, L., (1920), "Über die Harte plastischer Körper", Nachrichten Kon. Gesell. der Wissenschaften, Göttingen, Math., Physics Klasse, pp. 74-85.
85. Prandtl, L., (1921), "Über die Eindringungsfestigkeit plastischer Baustoffe und die Festigkeit von Schneiden Zeitschrift für Angewandte Mathematik und Mechanik 1, No. 1, pp. 15-20.
86. Randolph, M. F., and Wroth, C. P., (1978), "Analysis of Deformation of Vertically Loaded Piles", Journal of the Geotechnical Engineering Division, ASCE, Vol 104, No. GT12, pp. 1465-1488.
87. Reese, L. C., (1964), "Load versus Settlement for an Axially Loaded Pile", Proceedings, Symposium on Bearing Capacity of Piles, Part 2, Central Building Research Institute, Roorkee, Roorkee, India, Cement and Concrete, New Delhi, India, pp. 18-38
88. Reese, L. C., Hudson, W. R., and Vijayvergiya, V. N., (1969), "An Investigation of the Interaction between Bored Piles and Soil", Proceedings, Seventh International Conference on Soil Mechanics and Foundation Engineering, Mexico City, Vol 2, pp. 211-215.
89. Reese, L. C., (1979), "Design and Evaluation of Load Tests on Deep Foundations", ASTM STP 670, Raymond Lundgren, Ed., American Society for Testing and Materials, pp 4-26.
90. Reissner, H., (1924), "Zum Erddruckproblem", Proceedings, First Intern. Conference Applied Mechanics, Delft, The Netherlands, pp. 295-311.
91. "Results of Tests in Foundation Materials, Lock and Dam No. 4, Arkansas River Navigation Project, Little Rock District", U.S. Army Engineer Division Laboratory, Southwestern, CE, Reports No. 7920 and 7932, Dallas, Texas.
92. Robinsky, E. I., and Morrison, C. F., (1964), "Sand Displacement and Compaction Around Model Friction Piles", Canadian Geotechnical Journal, Vol 1, No. 4, pp. 189-204.

93. Robinsky, E. I., Sagar, W. L., and Morrison, C.F., (1964), "Effect of Shape and Volume on the Capacity of Model Piles in Sand", Canadian Geotechnical Journal, Vol 1, No. 4, pp. 189-204.
94. Schultze, E., and Menzenbach, E., (1961), "SPT and Compressibility of Soils", Proceedings of the V International Conference on Soil Mechanics and Foundation Engineering, Paris, Vol 1, pp. 527-532.
95. Scott, R. F., (1963), Principles of Soil Mechanics, Addison-Wesley.
96. Sherman, W. C., and Trahan, C. C., (1968), "Analysis of Data from Instrumentation Program, Port Allen Lock", Technical Report S-68-7, U. S. Army Engineer Waterways Experiment Station, CE, Vicksburg, Mississippi.
97. Sherman, W. C., Holloway, D. M., and Trahan, C. C., (1974), "Analysis of Pile Tests," Technical Report S-74-3, U. S. Army Engineer Waterways Experiment Station, Vicksburg, Mississippi.
98. Smith, A. E. L., (1960), "Impact and Longitudinal Wave Transmission", American Society of Mechanical Engineers.
99. Smith, A. E. L., (1960), "Pile Driving Analysis by the Wave Equation", Journal of the Soil Mechanics and Foundations Division, ASCE, Vol 86, No. SM4.
100. Snow, R., (1965), "Telltale", Foundation Facts, Vol I, No. 2, pp. 12-13.
101. Sowers, G. B., and Sowers, G. F., (1970), Introductory Soil Mechanics and Foundations, 3rd. ed., MacMillan Publishing Co., New York, p. 446.
102. Szechy, C., (1961), "The Effects of Vibration and Driving Upon the Voids in Granular Soils Surrounding a Pile", Proceedings of the V International Conference on Soil Mechanics and Foundation Engineering, Paris, Vol 2, pp. 161-164.
103. Tavenas, F. A., (1971), "Load Tests on Friction Piles in Sand", Canadian Geotechnical Journal, Vol. 8, No. 7, pp. 7-22.
104. Terzaghi, K., (1943), Theoretical Soil Mechanics, John Wiley and Sons, Inc., New York.
105. Terzaghi, K., and Peck, R. B., (1967), Soils Mechanics in Engineering Practice, 2nd ed., John Wiley & Sons, Inc., New York.

106. Thurman, A. G., and D'Appolonia, E., (1965), "Computed Movement of Friction and End-Bearing Piles Embedded in Uniform and Stratified Soils", Proceedings, The Sixth International Conference on Soil Mechanics and Foundation Engineering, pp. 323-327.
107. Tomlinson, M. J., (1977), Pile Design and Construction Practice, Viewpoint Publications by Cement and Concrete Association, London.
108. U. S. Army Engineer Waterways Experiment Station, (1956), "Mississippi River and Tributaries, Old River Control Low-Sill Structure: Pile Loading Tests", Design Memorandum 1-B Supplement No. 3, Vicksburg, Mississippi.
109. Vesic, A. S., and Barksdale, R. D., (1963), "On Shear Strength of Sand at Very High Pressures, American Society of Testing and Materials", Symposium on Laboratory Shear Strength Testing of Soils, Ottawa, Canada.
110. Vesic, A. S., (1964), "Model Testing of Deep Foundations in Sand and Scaling Laws, Panel Discussion, Session II", Proceedings, North American Conference on Deep Foundations, Mexico City.
111. Vesic, A. S., (1966), "A Study of Bearing Capacity of Deep Foundations", Project B-189, (Final Report), Georgia Institute of Technology, Atlanta, Georgia.
112. Vesic, A. S., (1967), "Ultimate Loads and Settlement of Deep Foundations in Sand", Proceedings of the Symposium on Bearing Capacity and Settlement of Foundations, Duke University, Durham, North Carolina.
113. Vesic, A. S., (1968), "Load Transfer, Lateral Loads, and Group Action of Deep Foundations", Performance of Deep Foundations, ASTM, STP, pp. 5-14.
114. Vesic, A. S., (1970), "Tests on Instrumented Piles, Ogeechee River Site", Journal of the Soil Mechanics and Foundation Division, ASCE, Vol 96. No. SM2, pp. 561-583.
115. Vesic, A. S., (1972), "Expansion of Cavities in Infinite Soil Mass", Journal of the Soil Mechanics and Foundation Division, ASCE, Vol 98, No. SM3, Proc. Paper 8790, pp. 265-290.
116. Vesic, A. S., (1977a), "Design of Pile Foundations", NCHRP Synthesis of Highway Practice No. 42, Transportation Research Board.

117. Vesic, A.S., (1977b), "On Significance of Residual Loads for Load Response of Piles", Contribution presented at Main Session 2: "Behavior of Foundations and Structures", Proceedings of the IX International Conference on Soil Mechanics and Foundation Engineering, Tokyo, Vol 3, pp. 374-379.
118. Vijayvergiya, V. N., (1977), "Load-Movement Characteristics of Piles", Proceedings, The Port Allen 1977 Conference, Long Beach, CA.
119. Zienkiewicz, O. C., (1971), The Finite Element Method in Engineering Science, McGraw-Hill, London.

APPENDIX A

LOAD-TRANSFER CURVES FROM IDEALIZED TRIAXIAL
CURVES BASED ON PARKER AND REESE CRITERIA

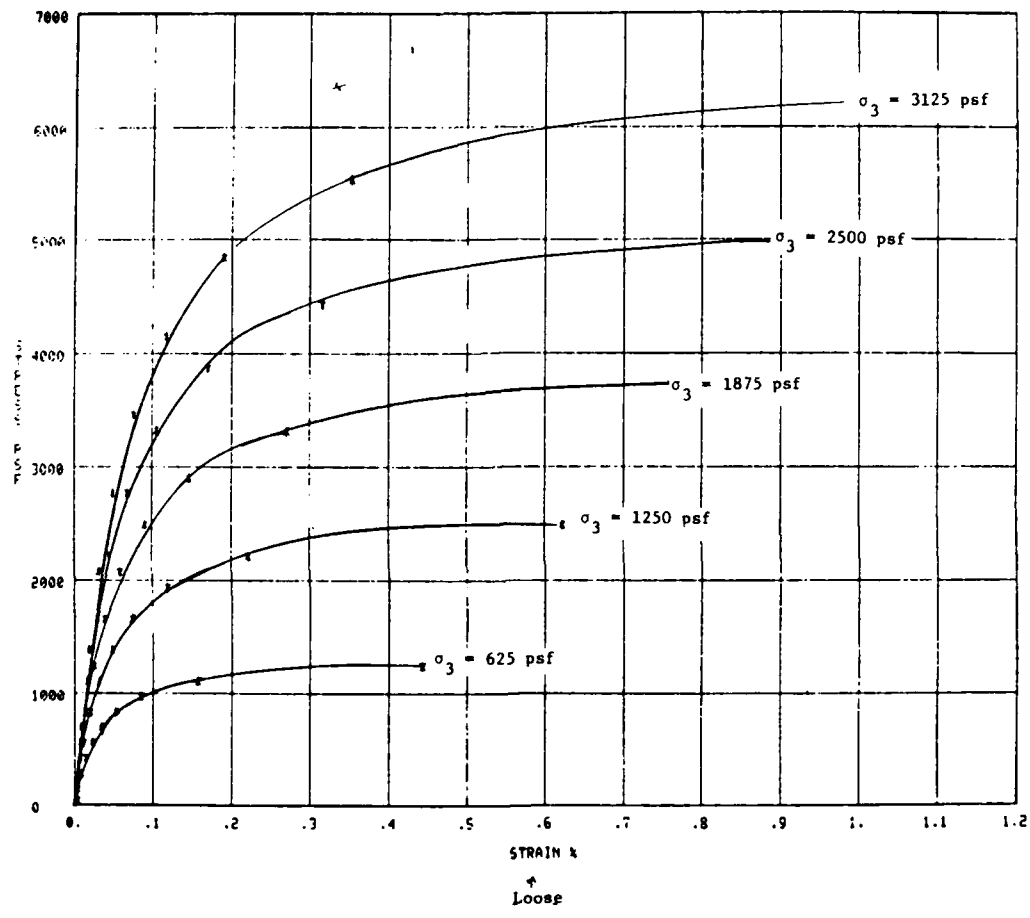


Figure A1. Idealized Triaxial Results (Sheet 1 of 2)

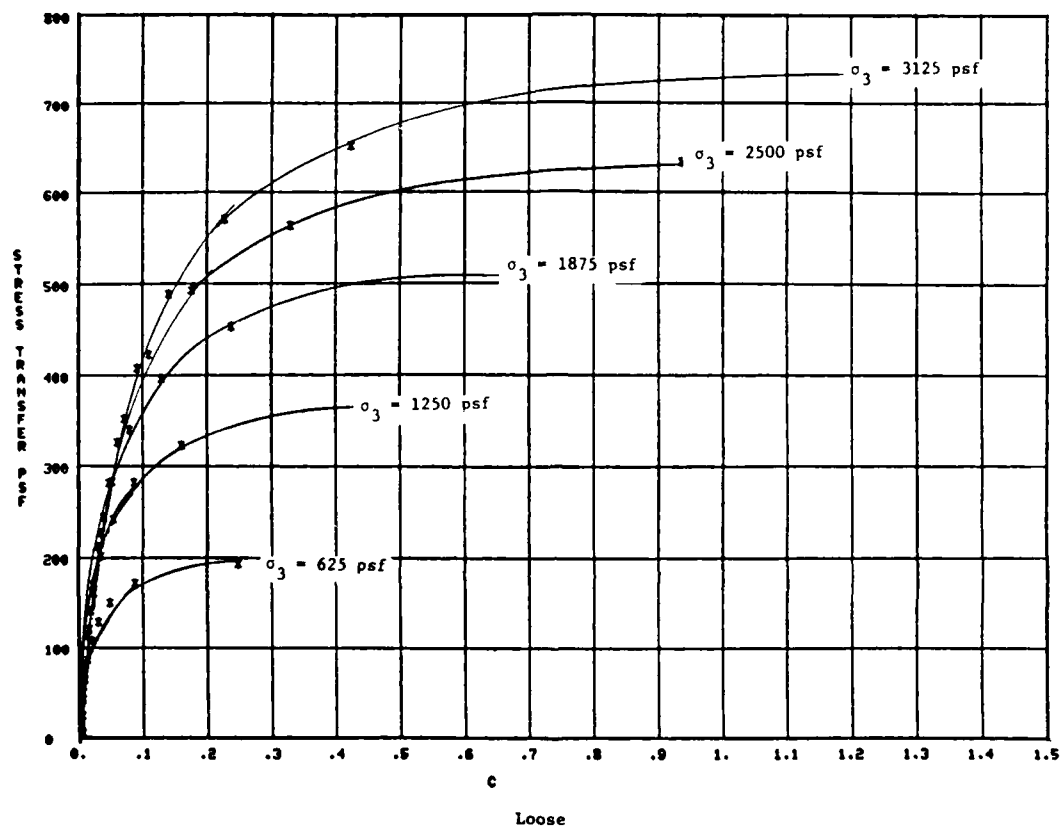


Figure A1. (Sheet 2 of 2)

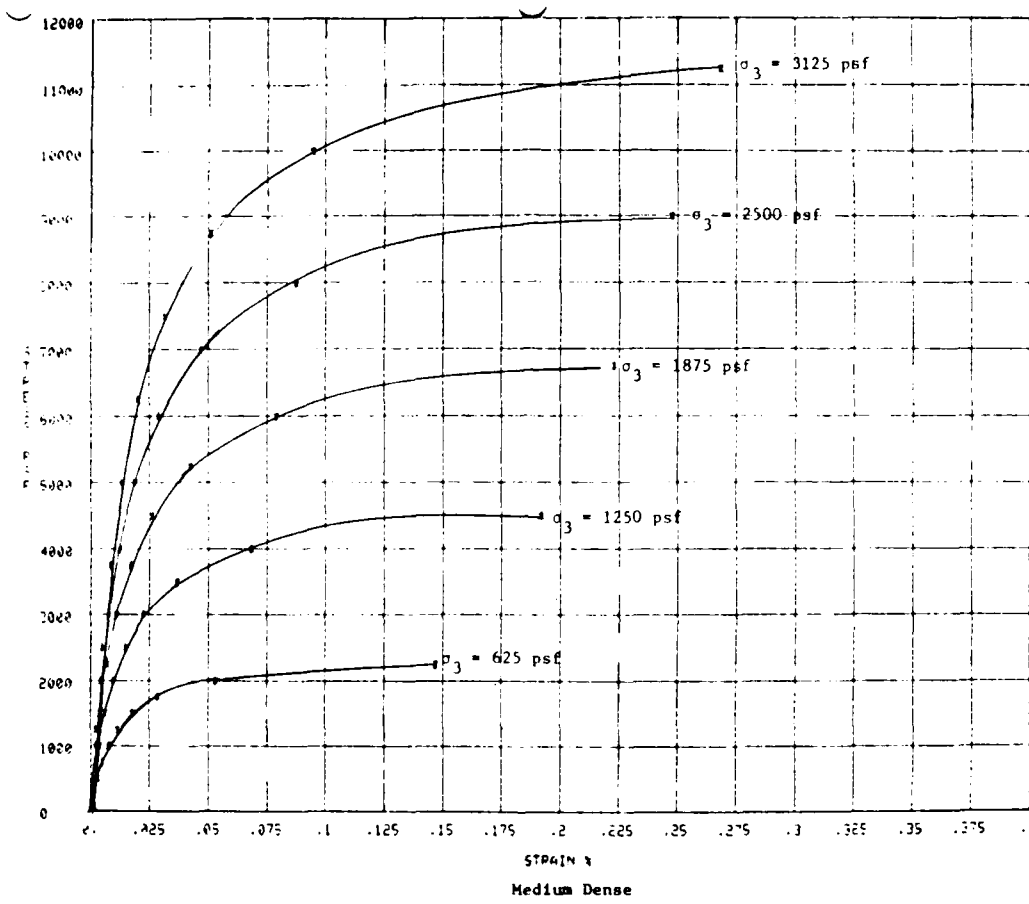


Figure A2. T-z Curves from Idealized Triaxial Results (Sheet 1 of 2)

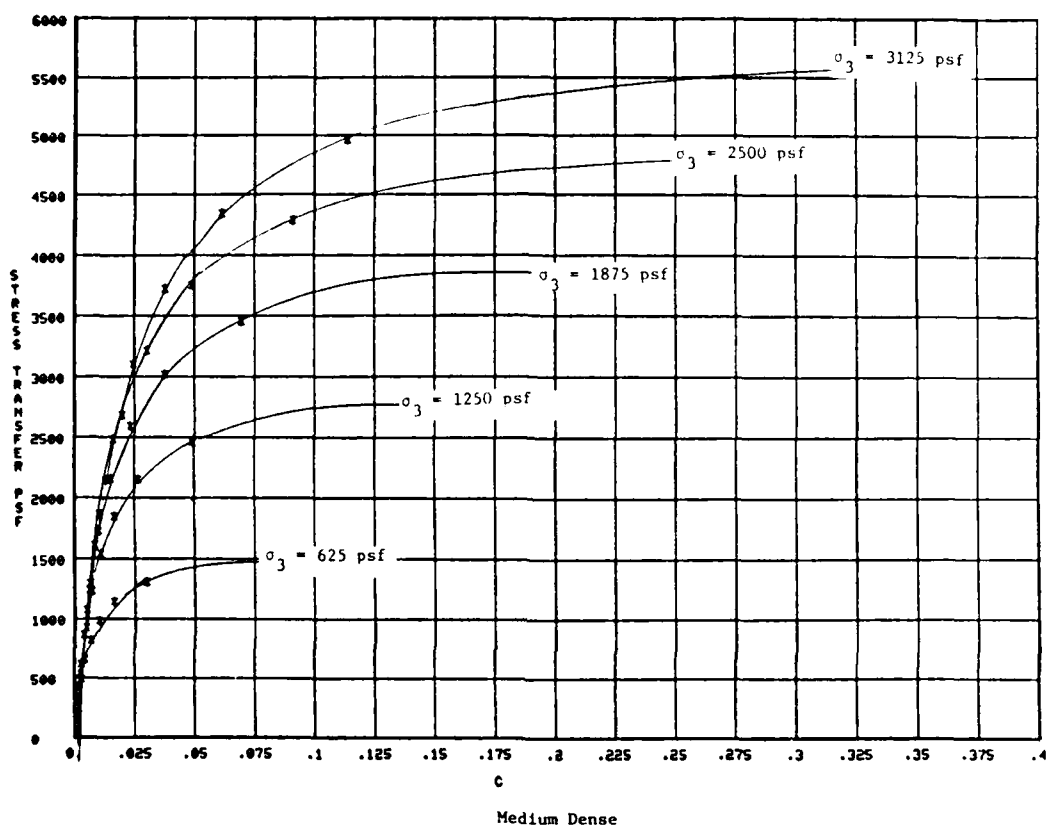


Figure A2. (Sheet 2 of 2)

APPENDIX B
RESULTS OF FIELD PILE TESTS

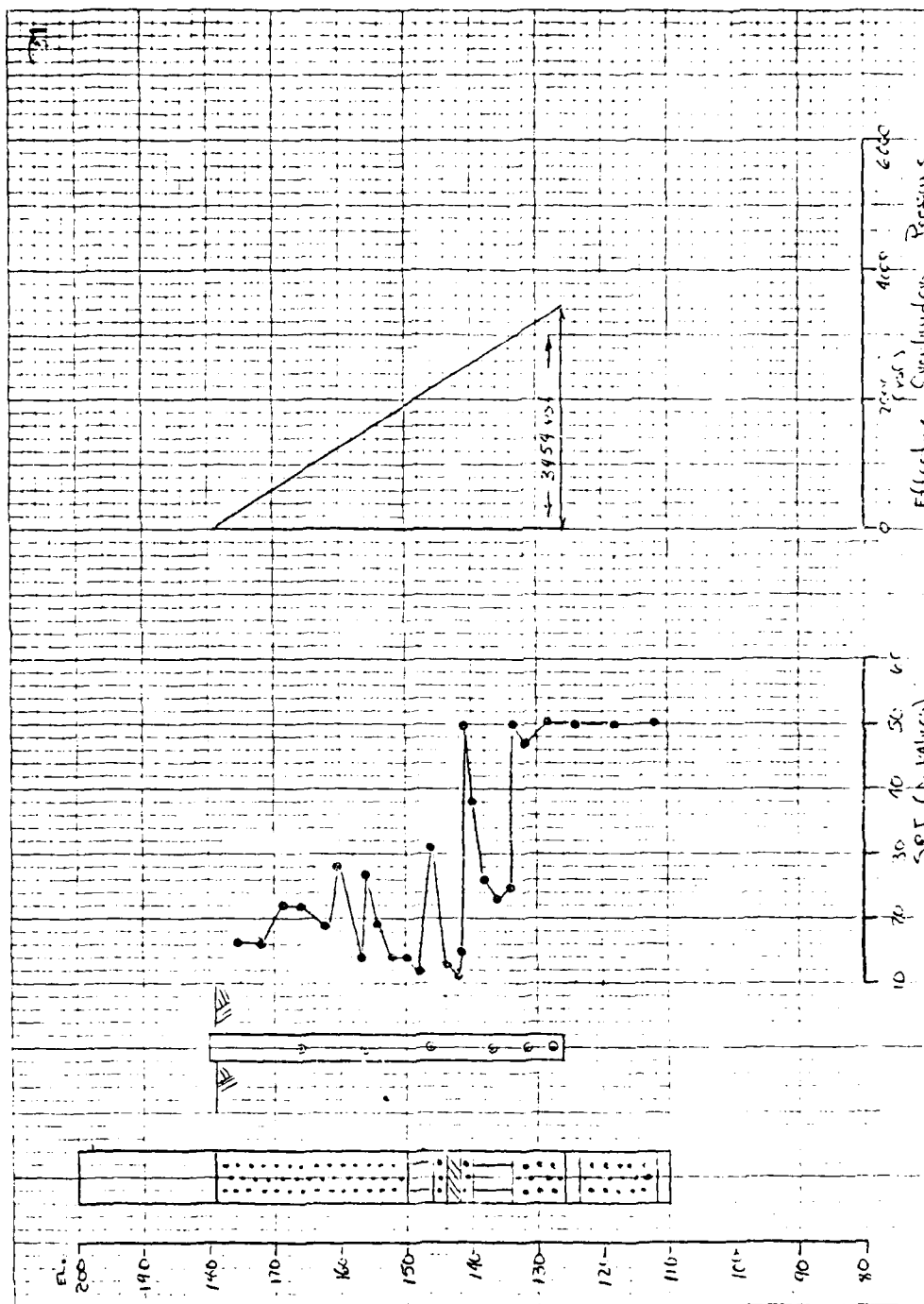


Figure B1. Arkansas River L&D No. 4 Soil Boring Data

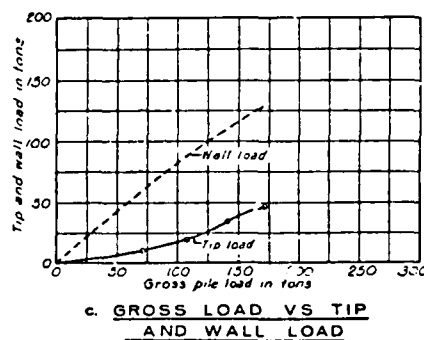
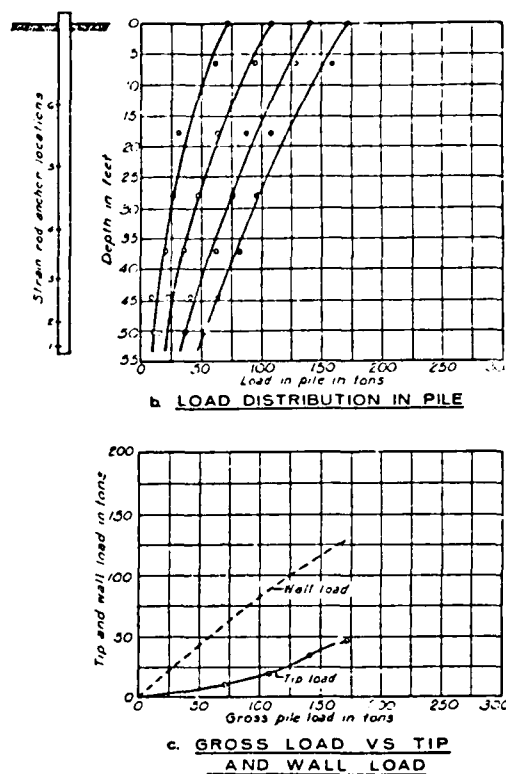
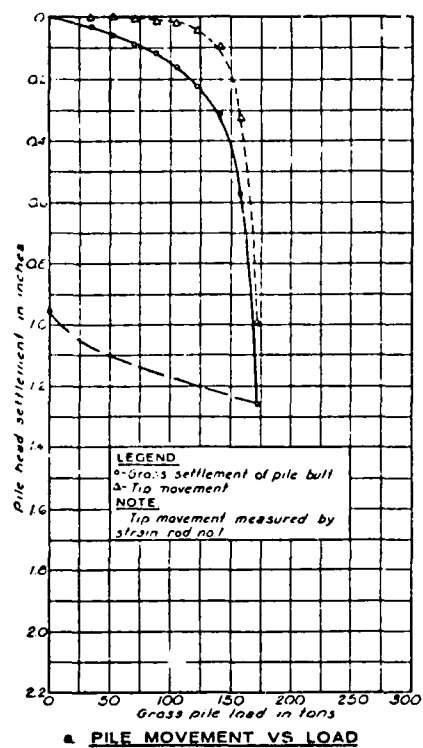


Figure B2. Compression Test Results, Arkansas River, Test Pile No. 1, 12.75-in.-Diameter Pipe

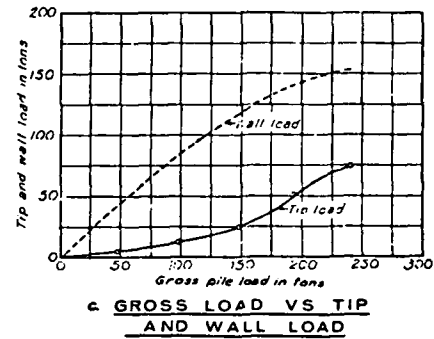
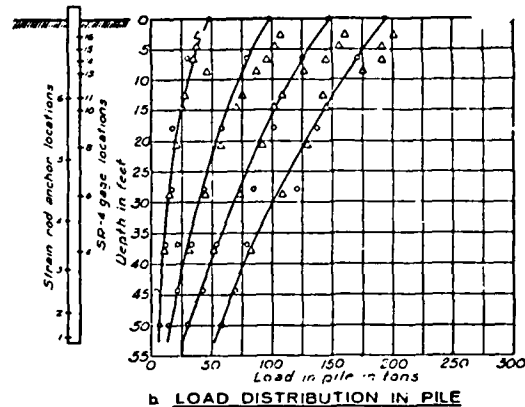
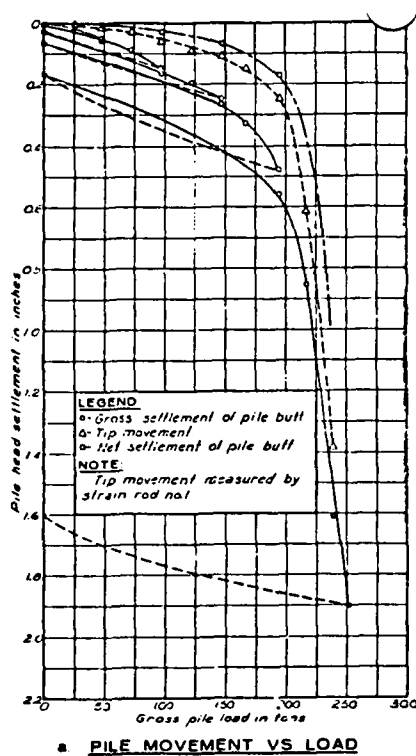
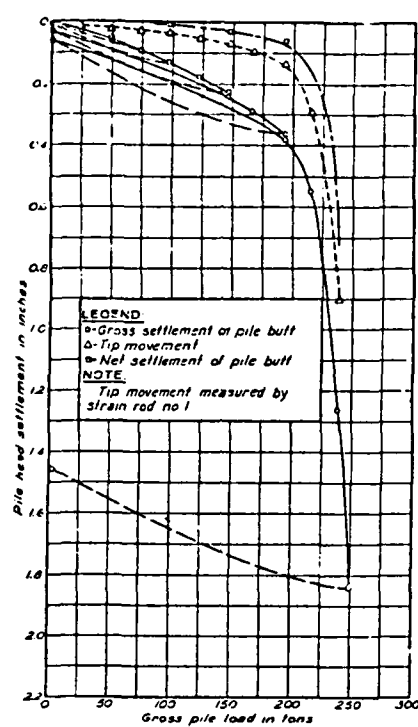
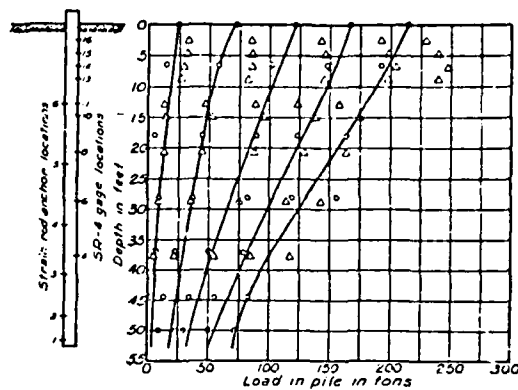


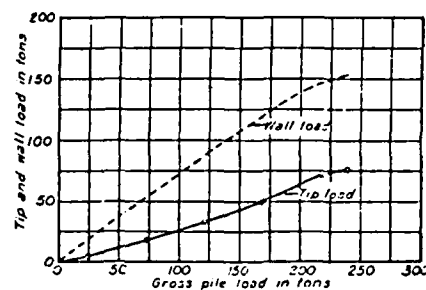
Figure B3. Compression Test Results, Arkansas River, Test Pile No. 2, Test 1, 16-in.-Diameter Pipe



a. PILE MOVEMENT VS LOAD

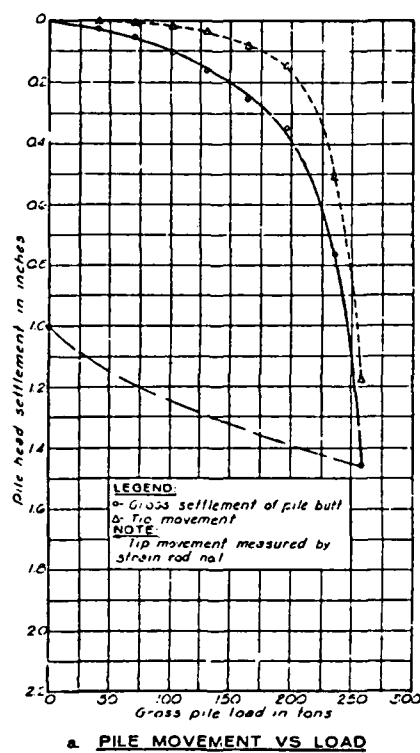


b. LOAD DISTRIBUTION IN PILE

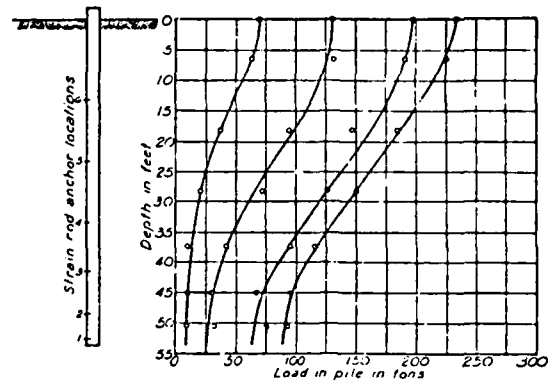


c. GROSS LOAD VS TIP AND WALL LOAD

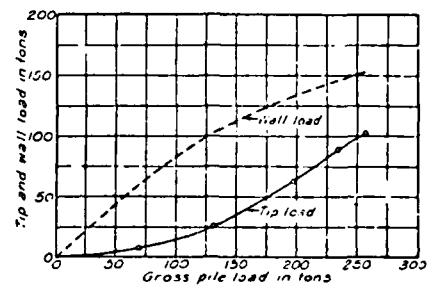
Figure B4. Compression Test Results, Arkansas River, Test Pile No. 2, Test 2, 16-in.-Diameter Pipe



a. PILE MOVEMENT VS LOAD

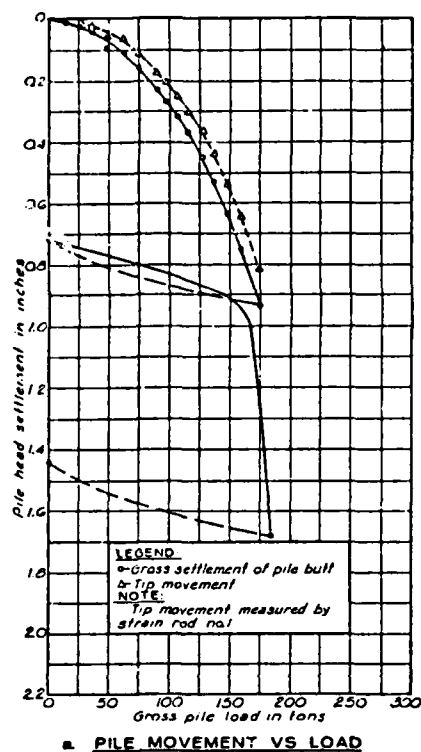


b. LOAD DISTRIBUTION IN PILE

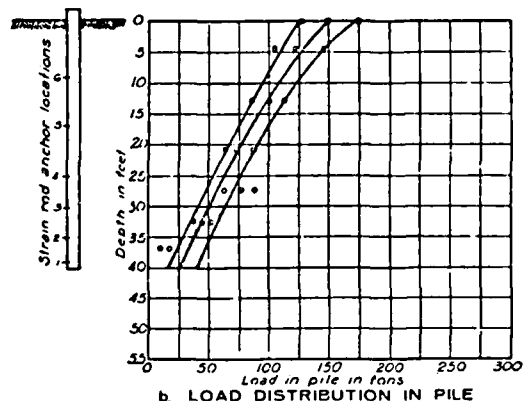


c. GROSS LOAD VS TIP AND WALL LOAD

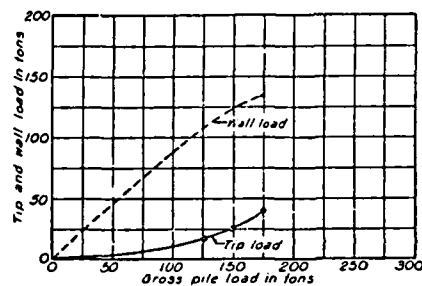
Figure B5. Compression Test Results, Arkansas River, Test Pile No. 3, 20-in.-Diameter Pipe



a. PILE MOVEMENT VS LOAD



b. LOAD DISTRIBUTION IN PILE



c. GROSS LOAD VS TIP AND WALL LOAD

Figure B6. Compression Test Results, Arkansas River, Test Pile No. 6, 14BP73

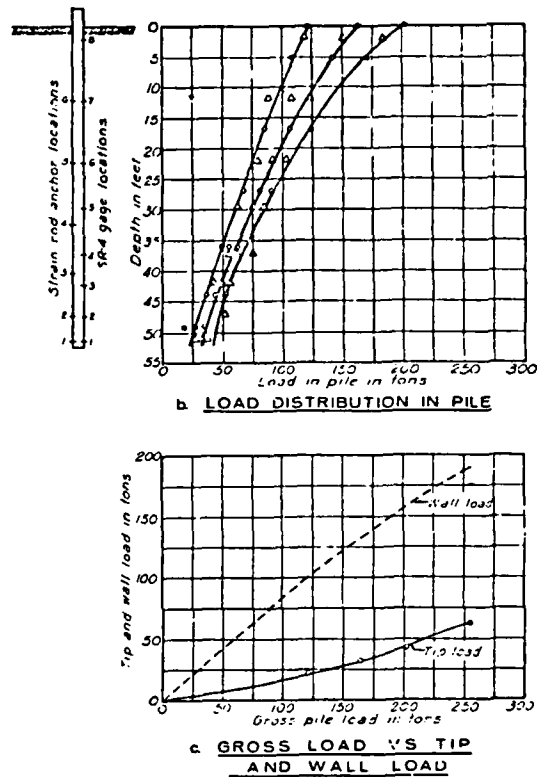
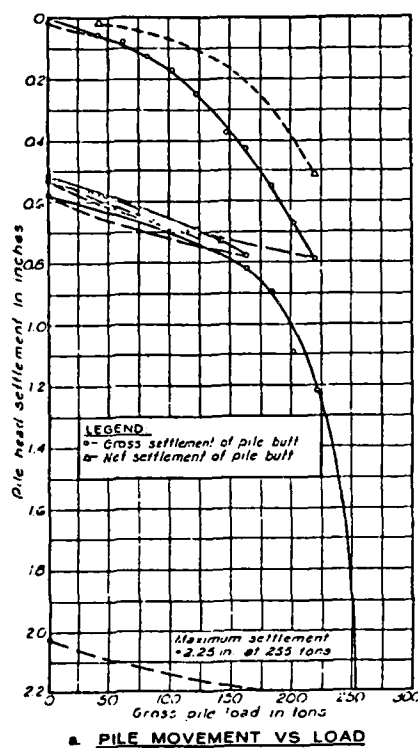


Figure B7. Compression Test Results, Arkansas River, Test Pile No. 7, 14BP73

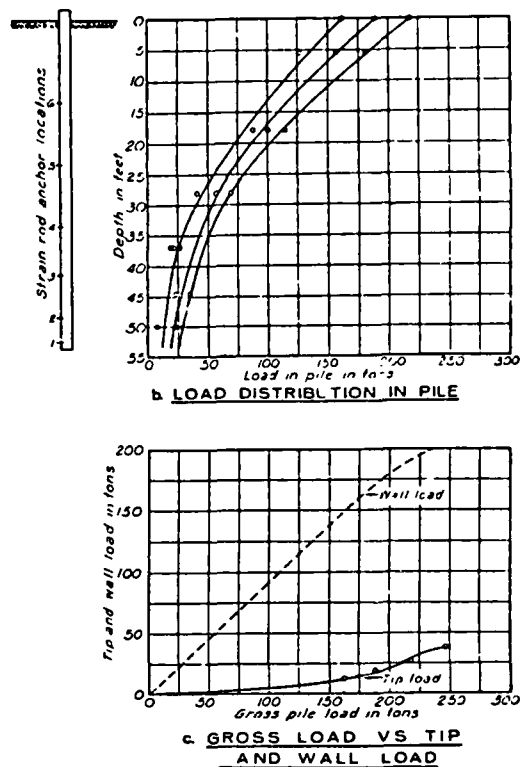
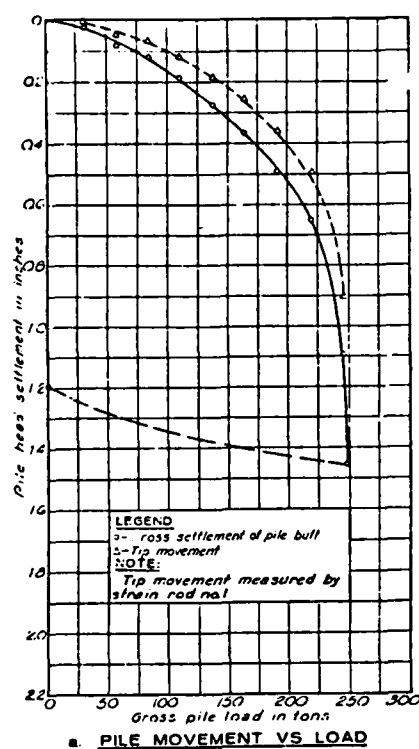
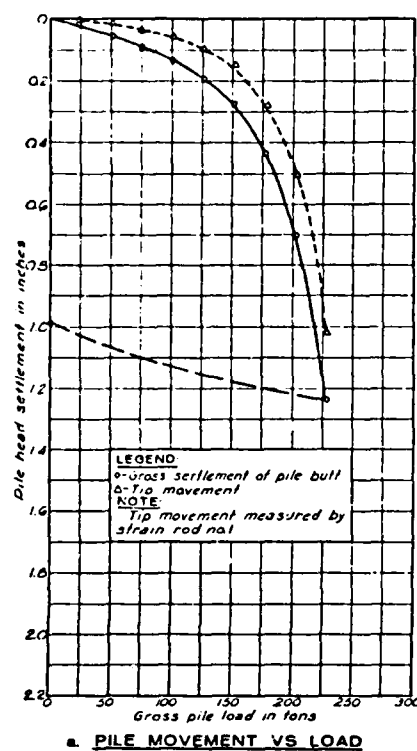
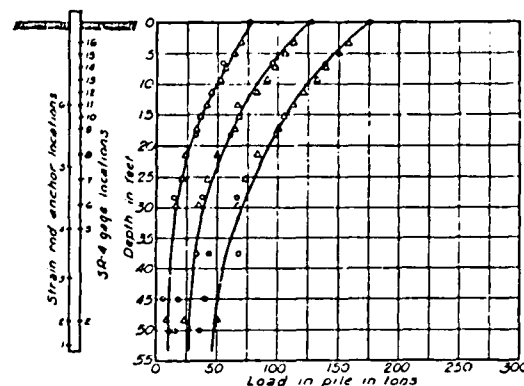


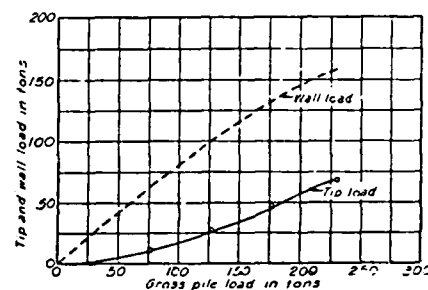
Figure B8. Compression Test Results, Arkansas River, Test Pile No. 9, 14BP73



a. PILE MOVEMENT VS LOAD



b. LOAD DISTRIBUTION IN PILE



c. GROSS LOAD VS TIP AND WALL LOAD

Figure B9. Compression Test Results, Arkansas River, Test Pile No. 10, 16-in.-Diameter Pipe

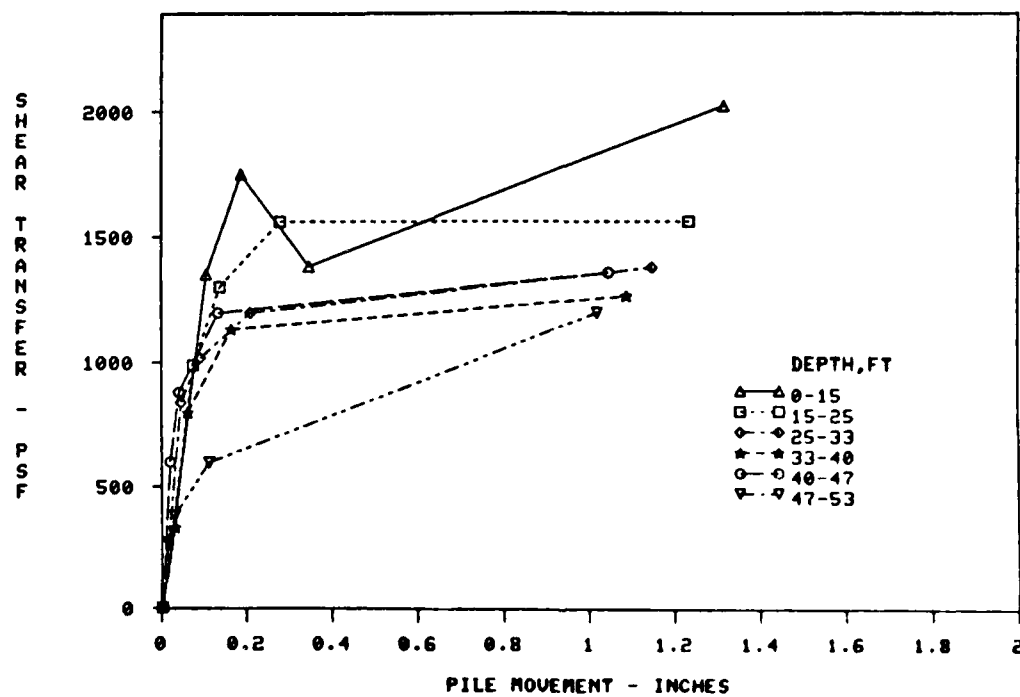


Figure B10. f-z Curves, Arkansas River, Test Pile No. 1

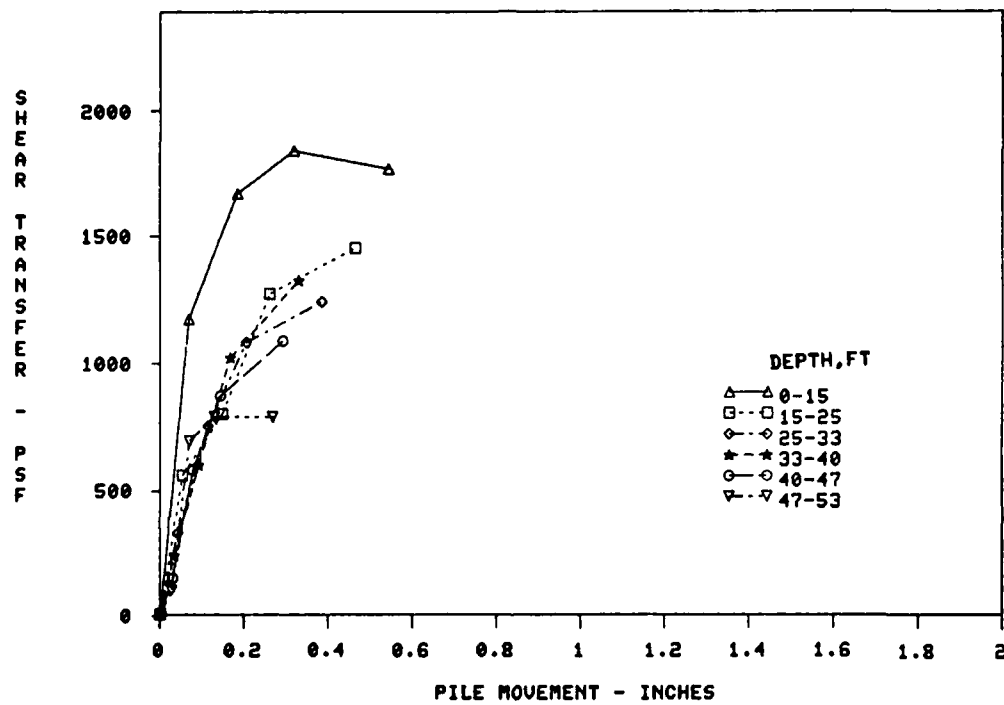


Figure B11. Unadjusted f - z Curves, Arkansas River, Test Pile No. 2

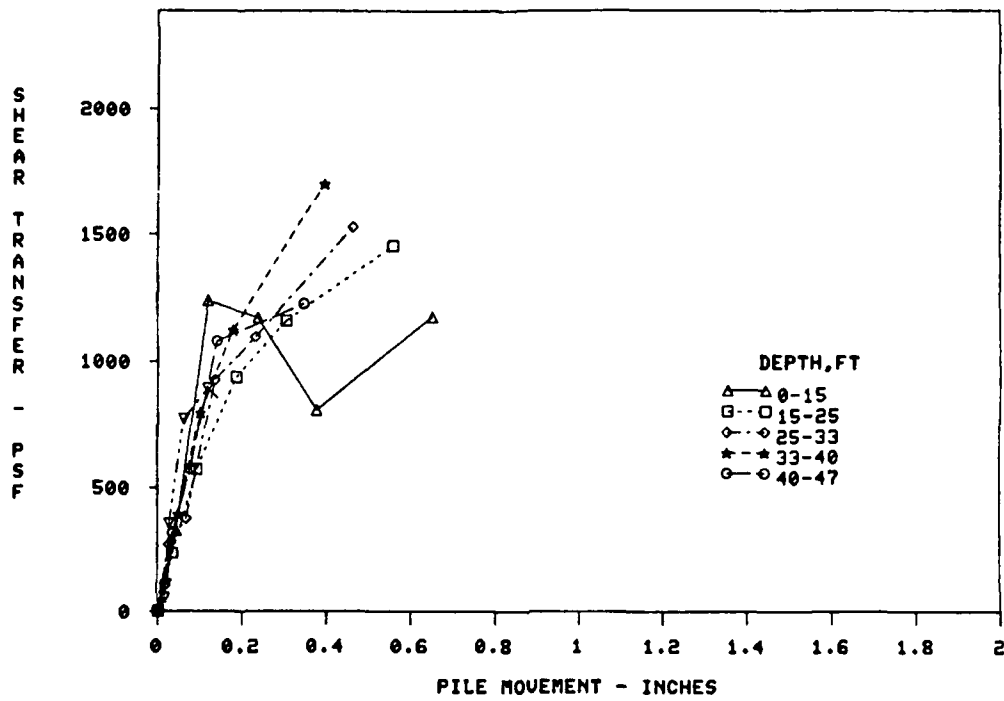


Figure B12. Unadjusted f-z Curves, Arkansas River, Test Pile No. 2 Retest

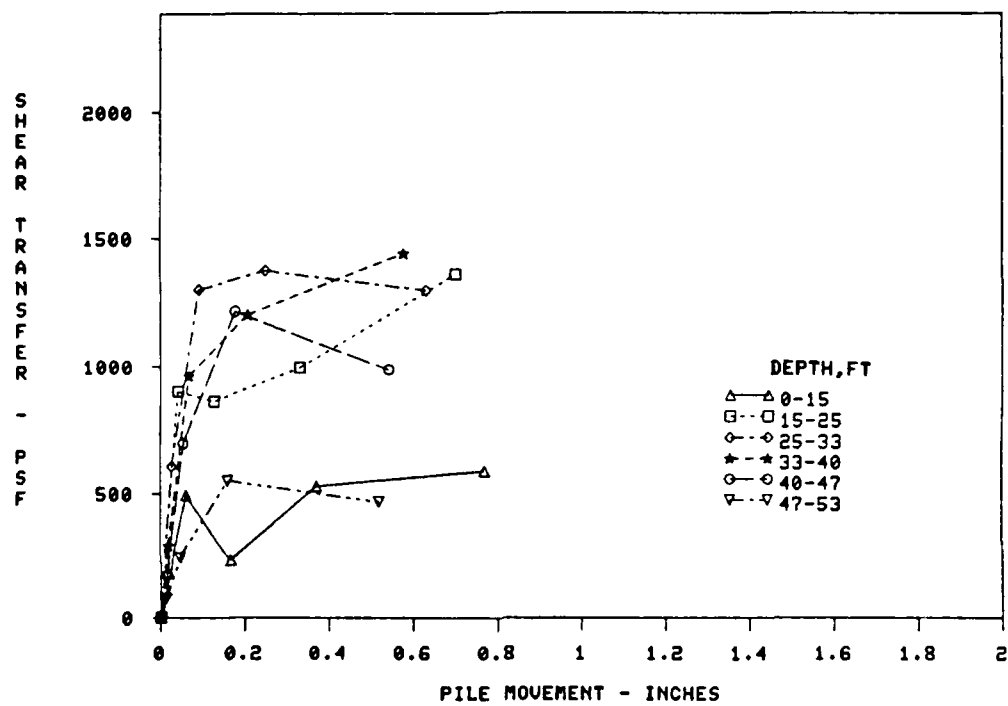


Figure B13. Unadjusted f-z Curves, Arkansas River, Test Pile No. 3

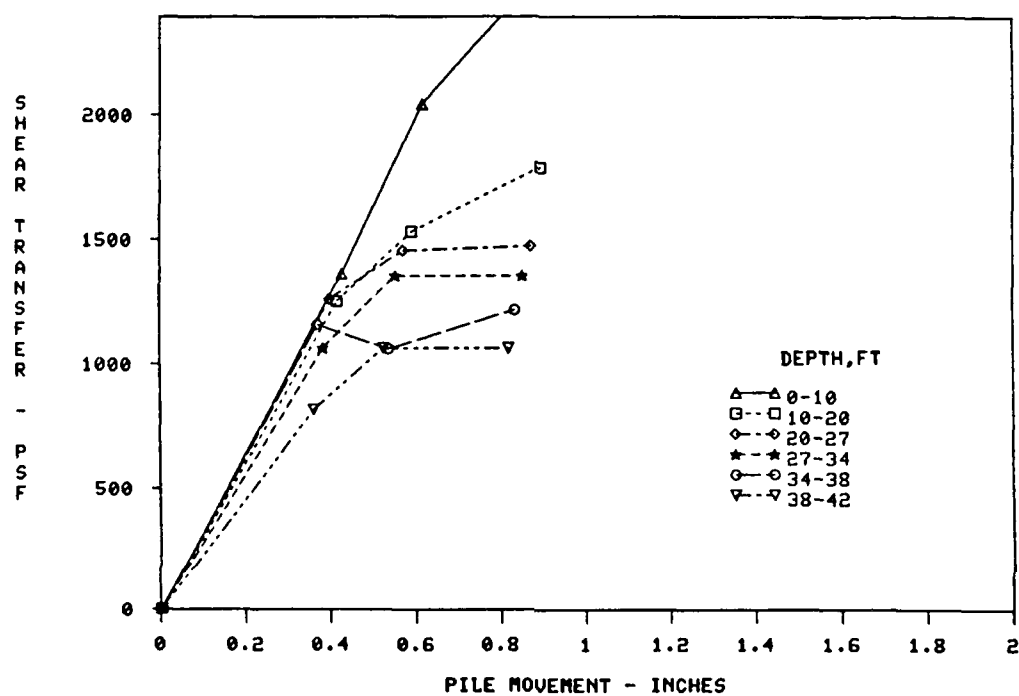


Figure B14. Unadjusted f-z Curves, Arkansas River, Test Pile No. 6

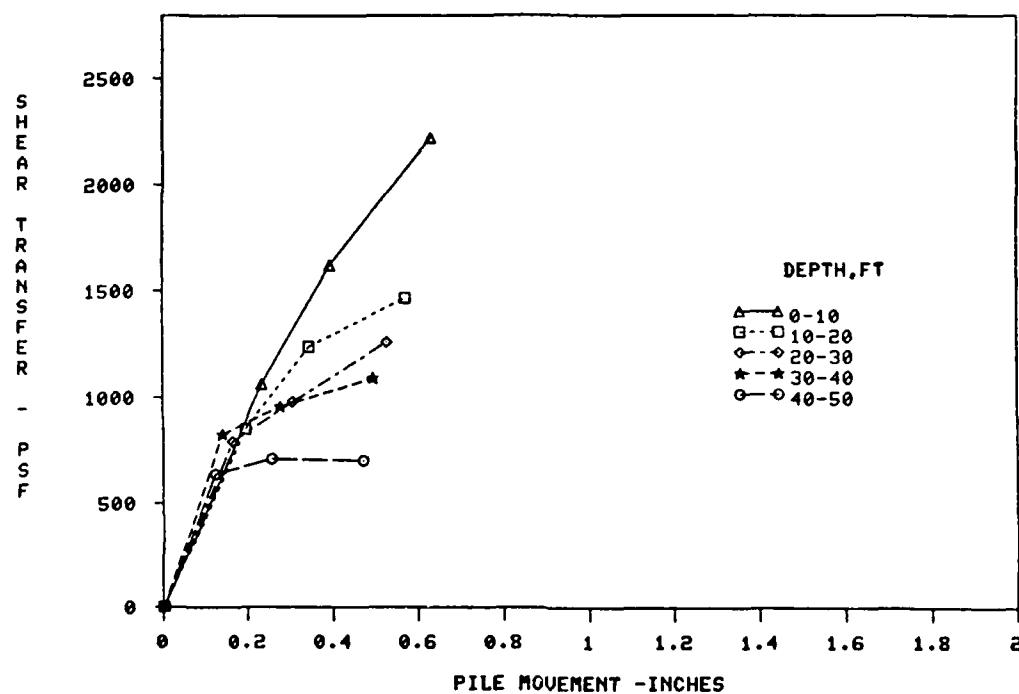


Figure B15. Unadjusted f-z Curves, Arkansas River, Test Pile No. 7, 14HP73

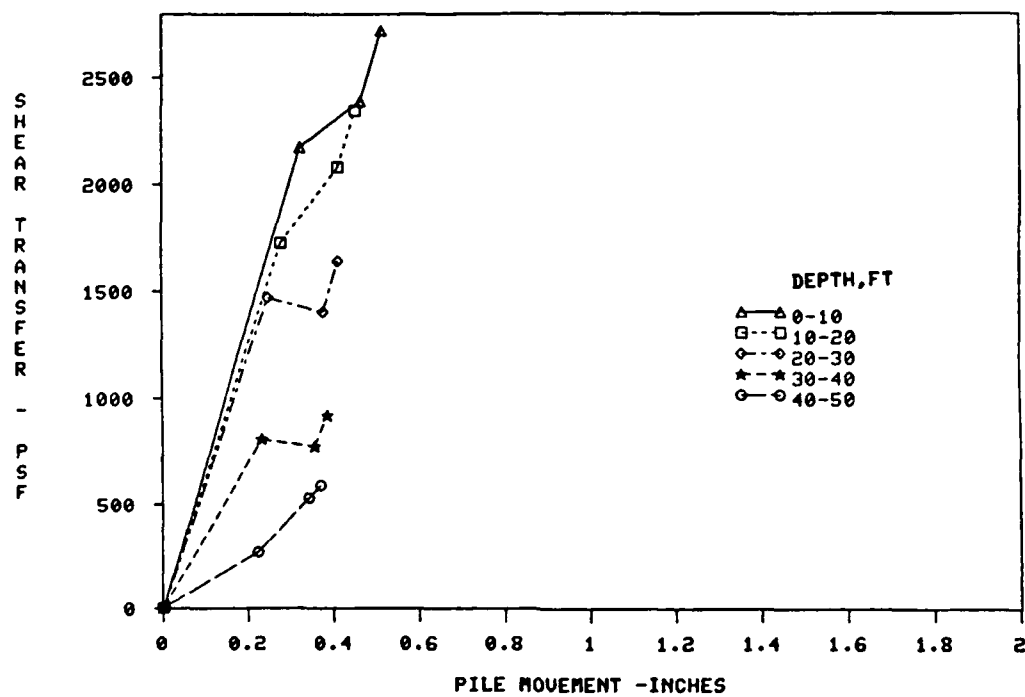


Figure B16. Unadjusted f-z Curves, Arkansas River, Test Pile No. 9, 14HP73

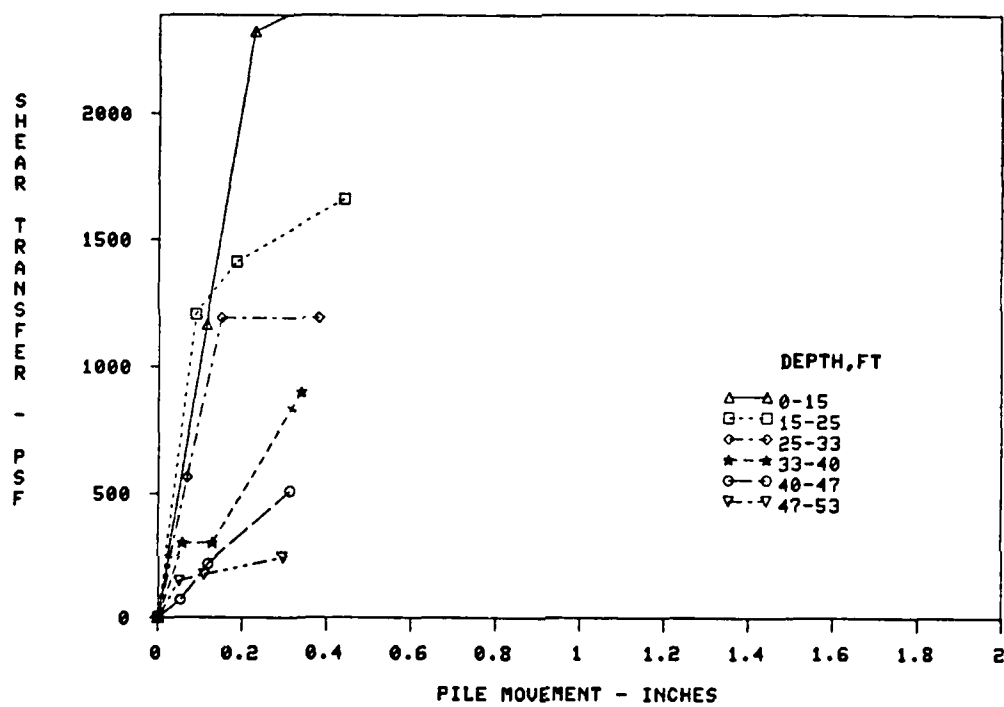


Figure B17. Unadjusted f-z Curves, Arkansas River, Test Pile No. 10

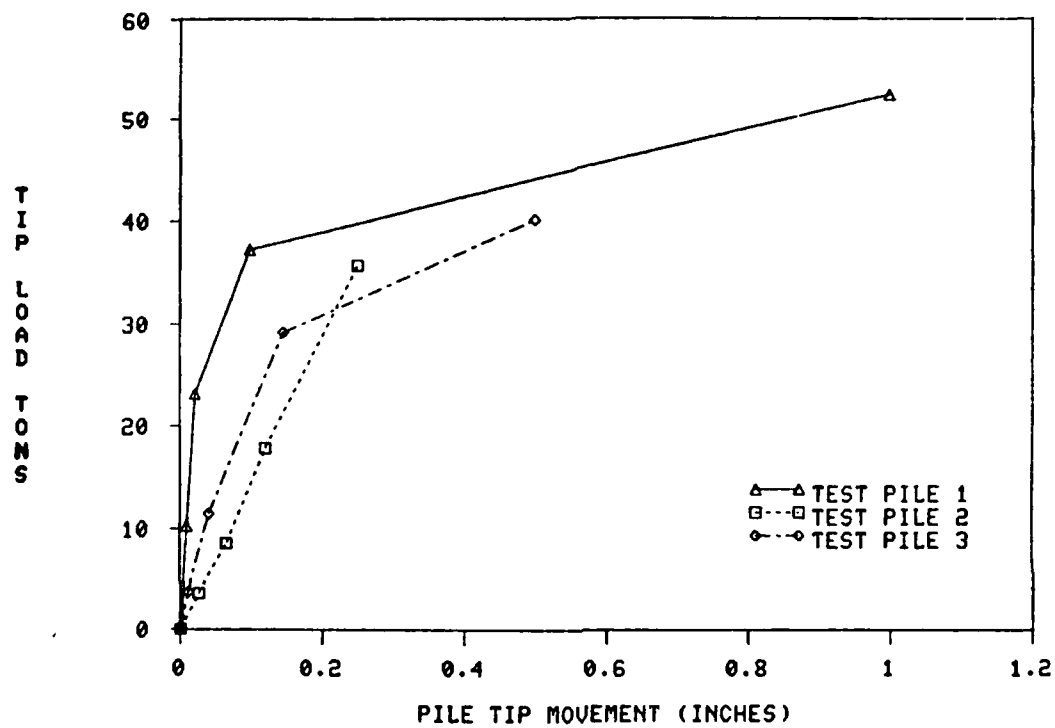


Figure B18. P-z Curves, Arkansas River, Pipe Piles

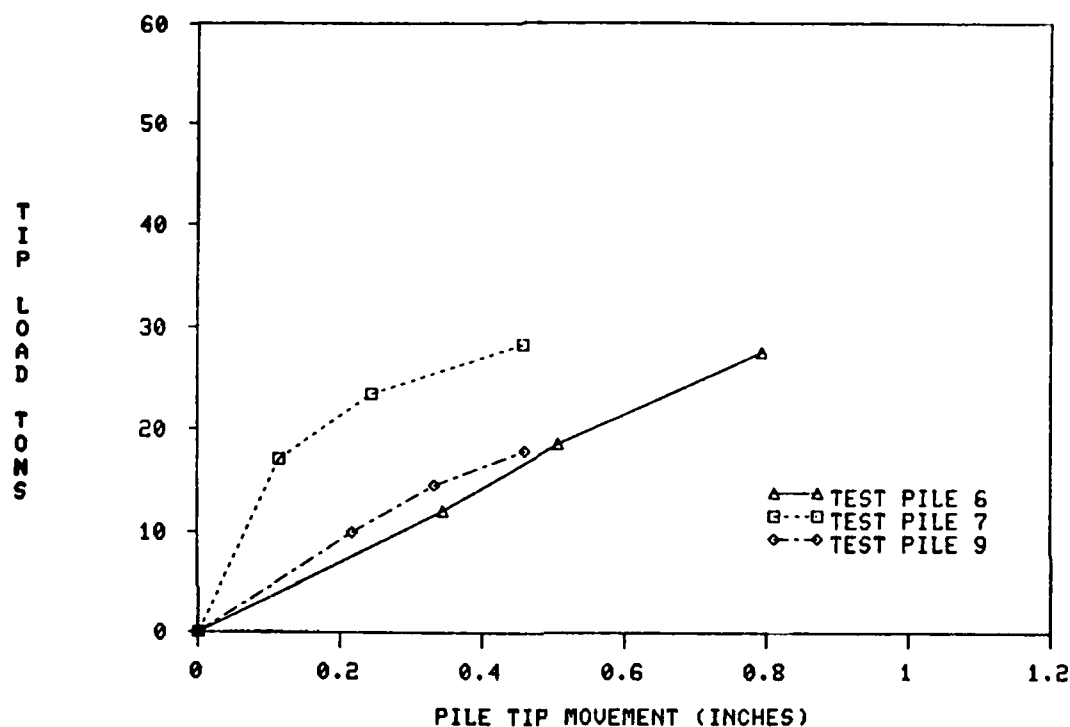


Figure B19. P-z Curves, Arkansas River, H Piles



Figure B20. Stratification and SPT Results, Ascalmore Creek-Tippo Bayou,
Test Pile No. 1

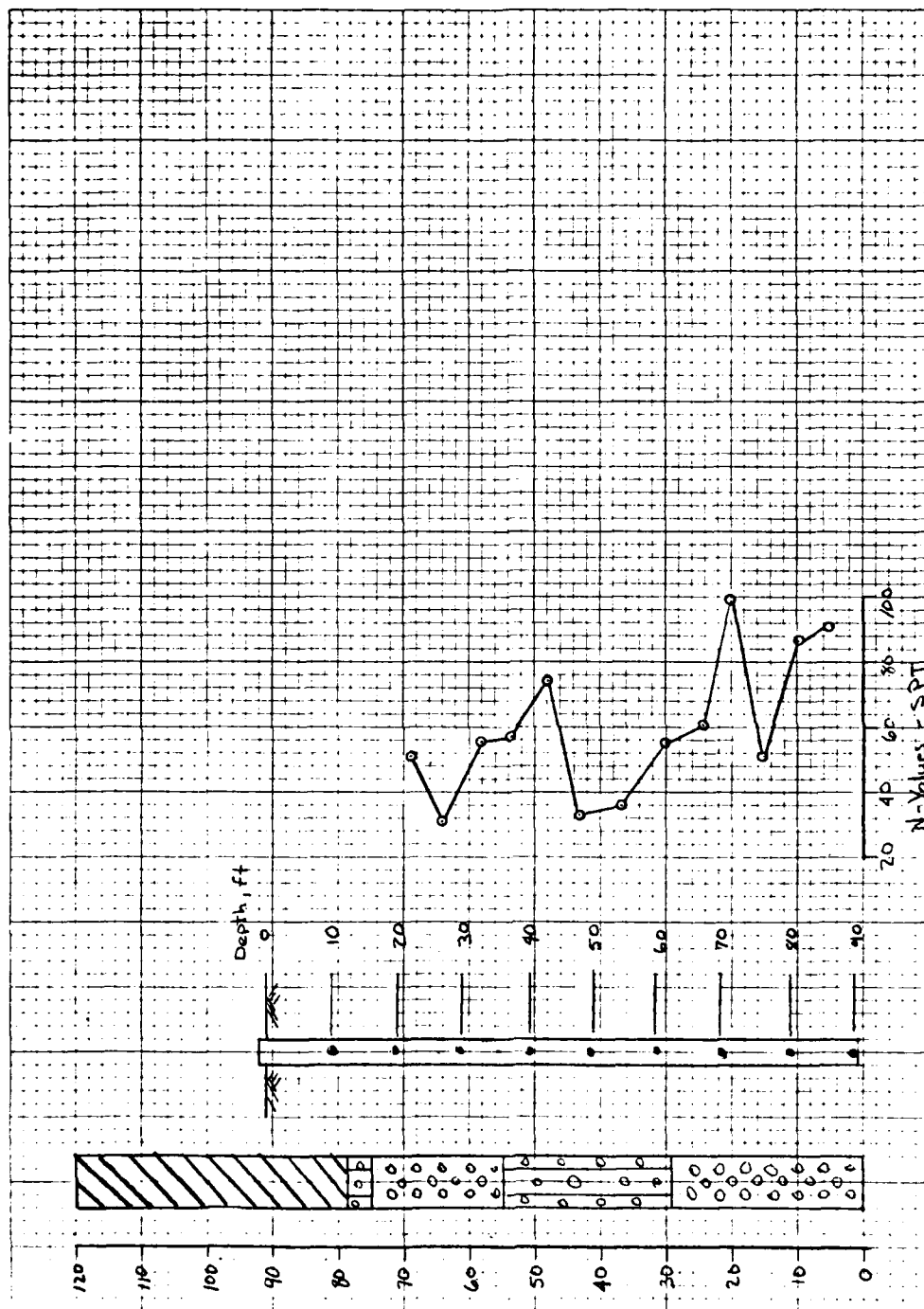


Figure B21. Stratification and SPT Results, Ascalmore Creek-Tippo Bayou, Test Pile No. 2

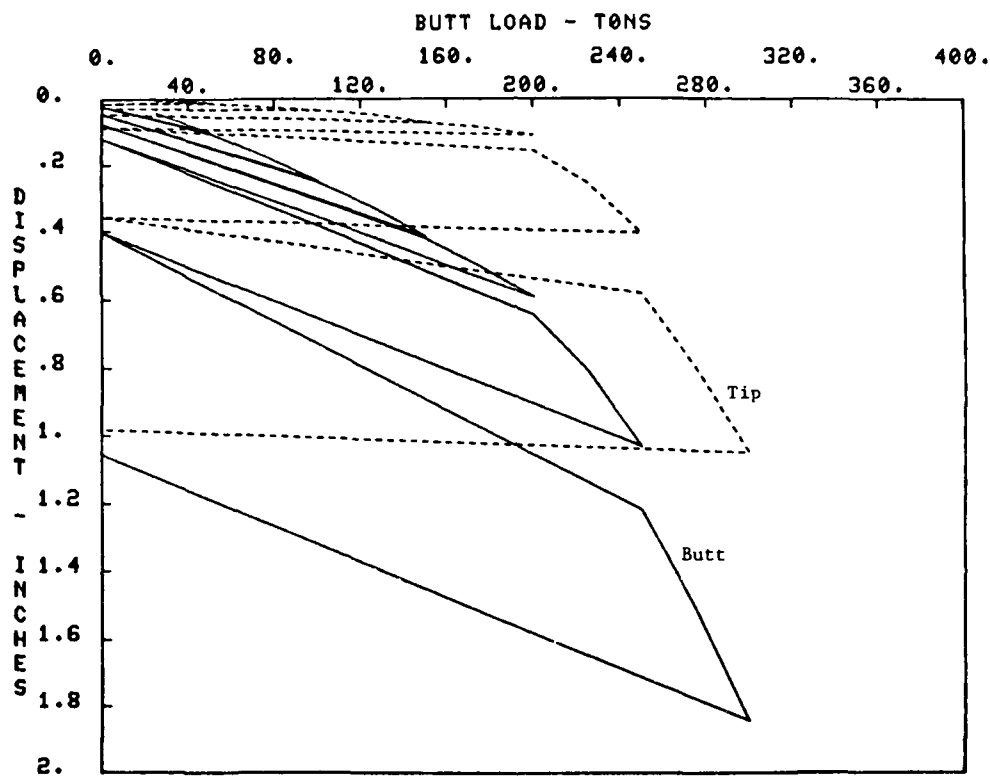


Figure B22. Unadjusted Butt and Tip Performance,
Ascalmore Creek-Tippo Bayou, Test Pile No. 1

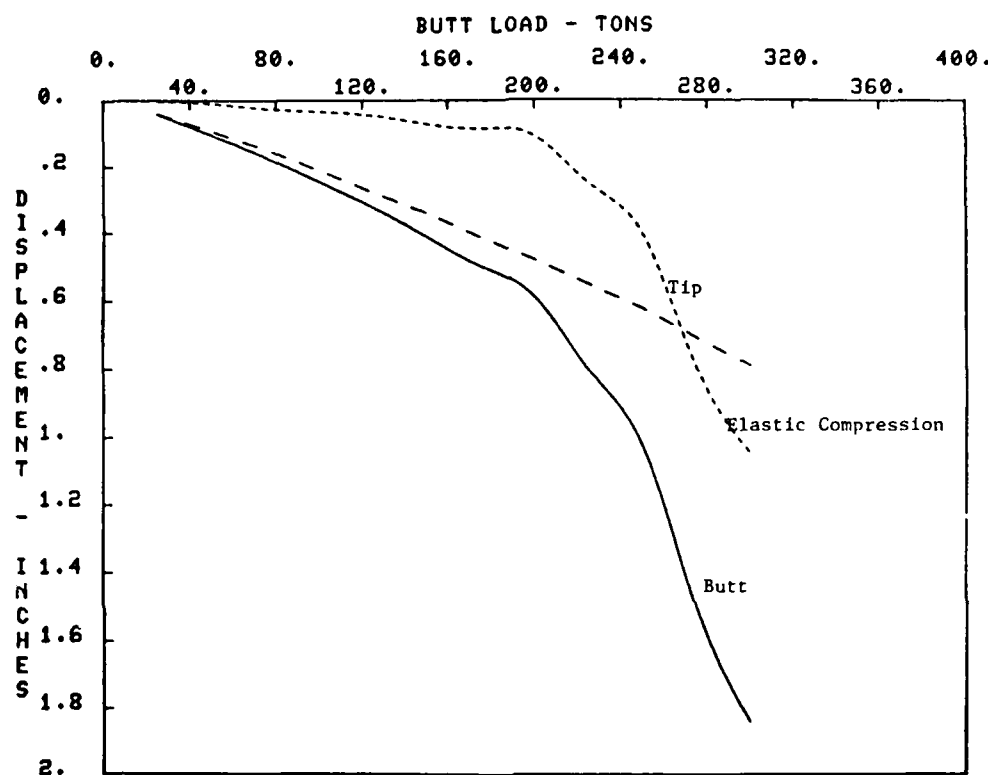


Figure B23. Butt and Tip Performance After Adjustment for Cyclic Loading, Ascalmore Creek-Tippo Bayou, Test Pile No. 1

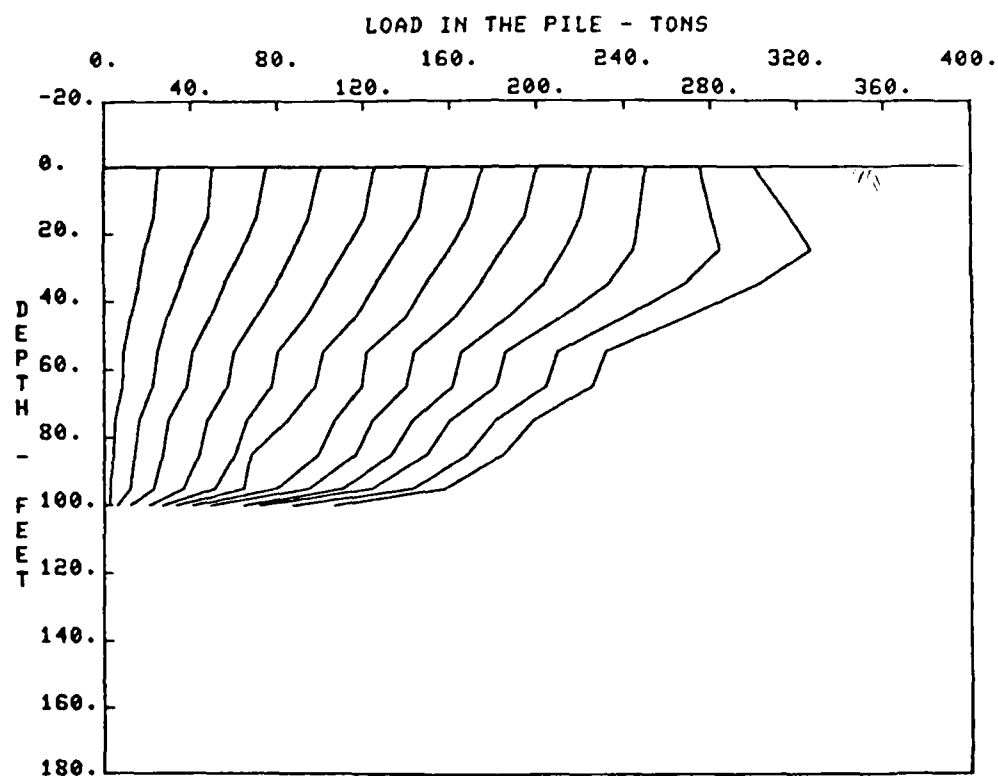


Figure B24. Load Distribution in Pile, Ascalmore Creek-Tippo Bayou, Test Pile No. 1

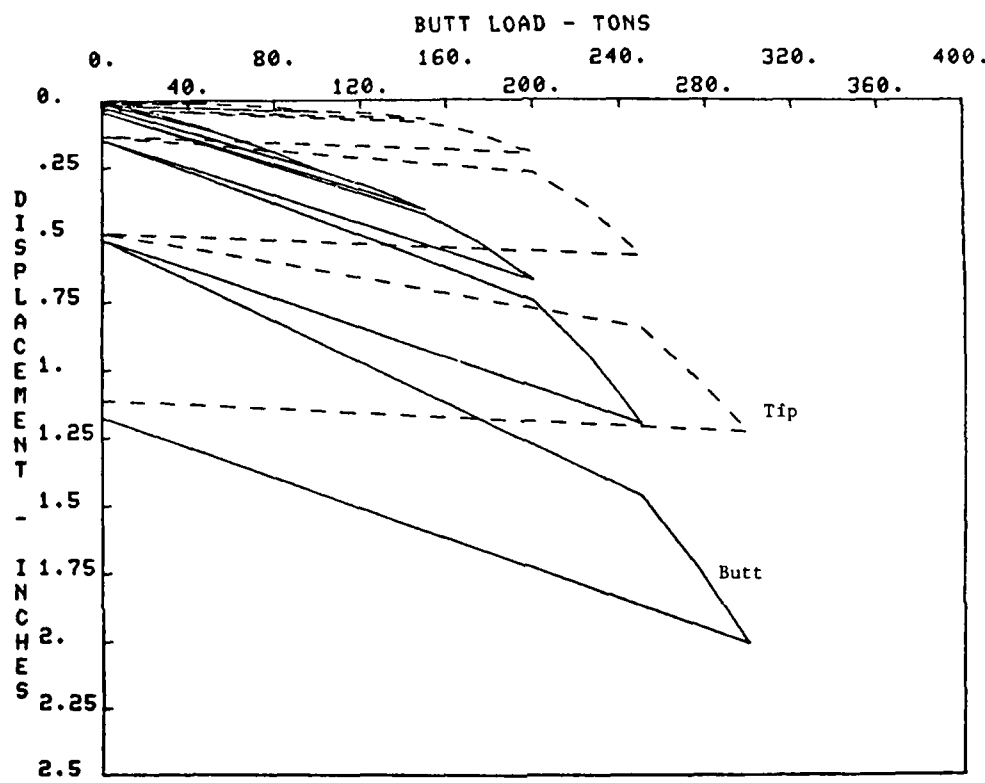


Figure B25. Unadjusted Butt and Tip Performance,
Ascalmore Creek-Tippo Bayou, Test Pile No. 2

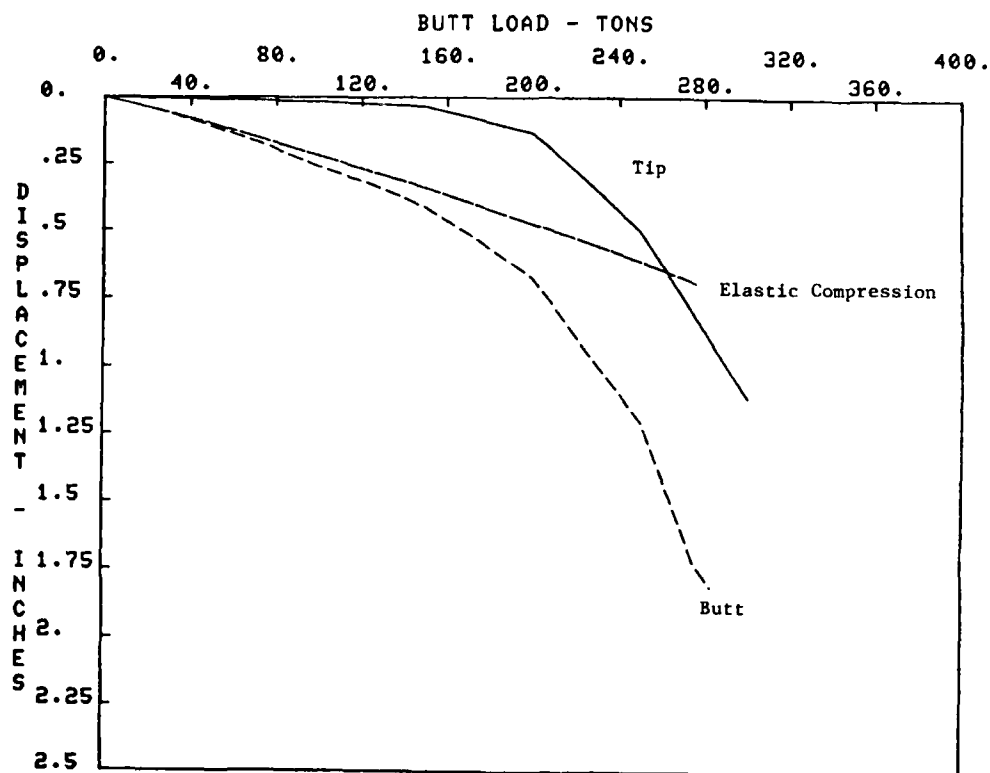


Figure B26. Butt and Tip Performance Adjusted for Cyclic Loading, Ascalmore Creek-Tippo Bayou, Test Pile No.2

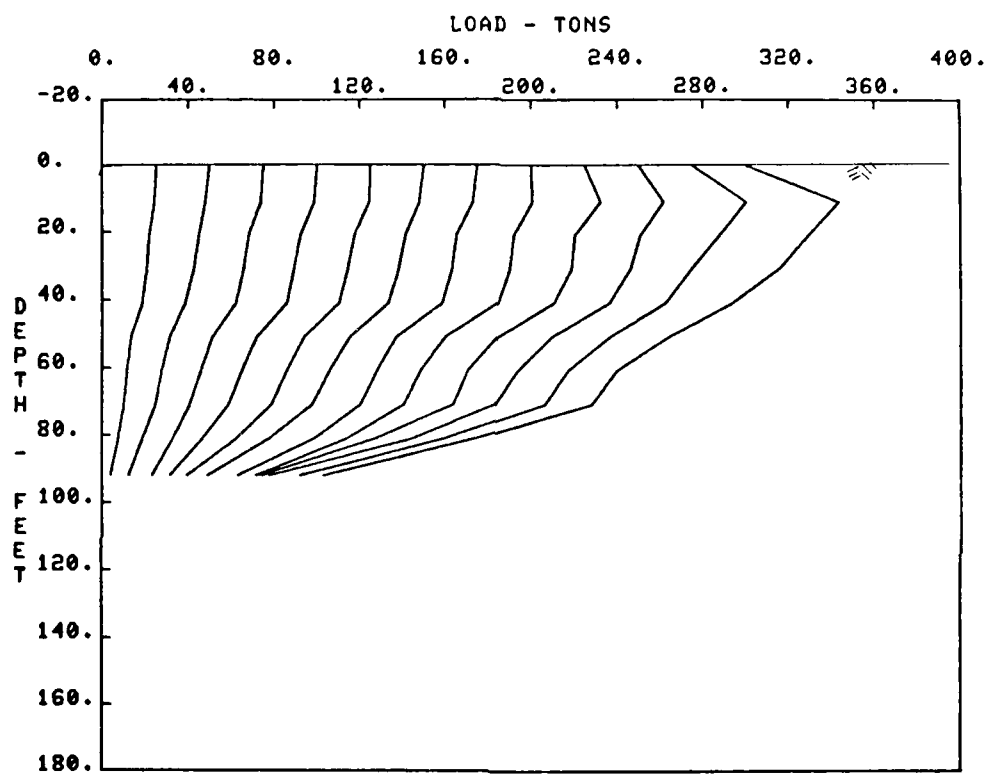


Figure B27. Load Distribution in Pile, Ascalmore Creek-Tippo Bayou, Test Pile No. 2

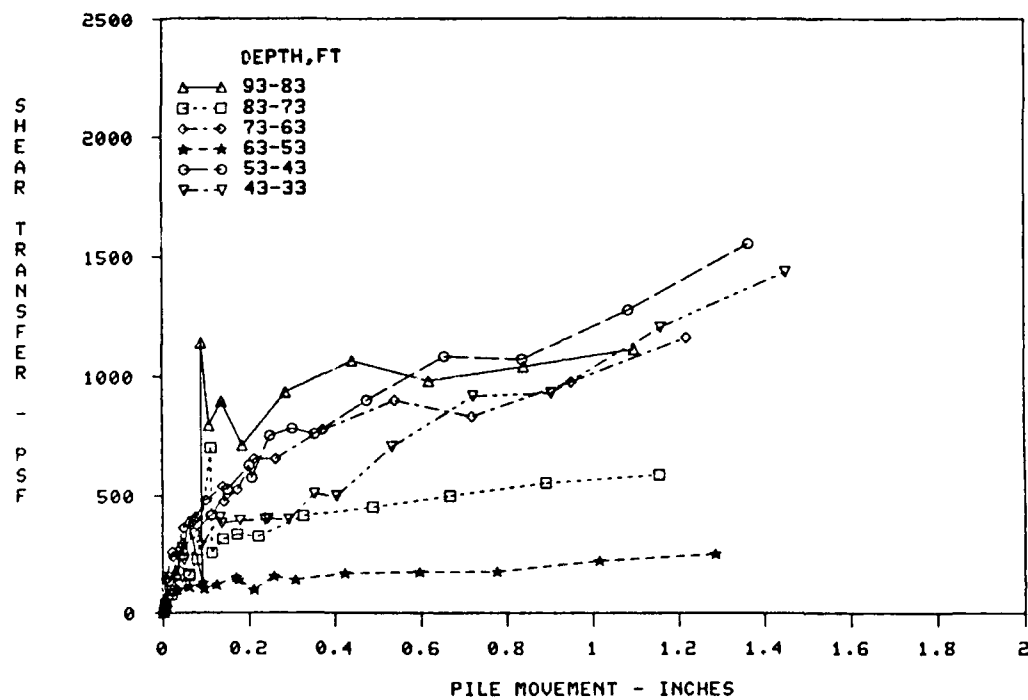


Figure B28. Unadjusted f-z Curves, Ascalmore Creek-Tippo Bayou, Test Pile No. 1

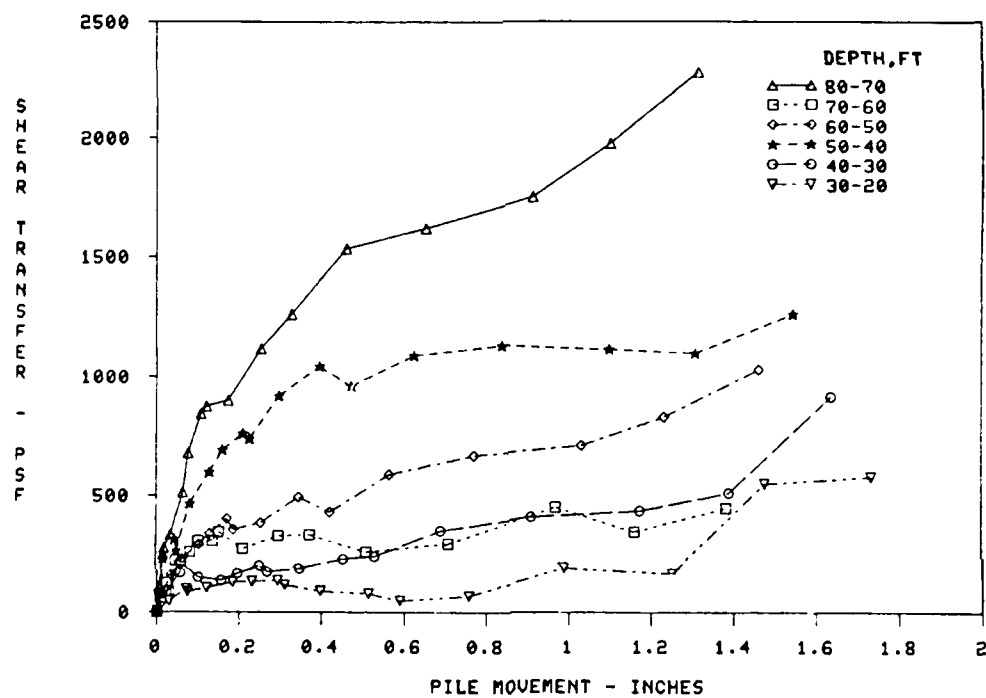


Figure B29. Unadjusted f-z Curves, Ascalmore Creek-Tippo Bayou, Test Pile No. 2

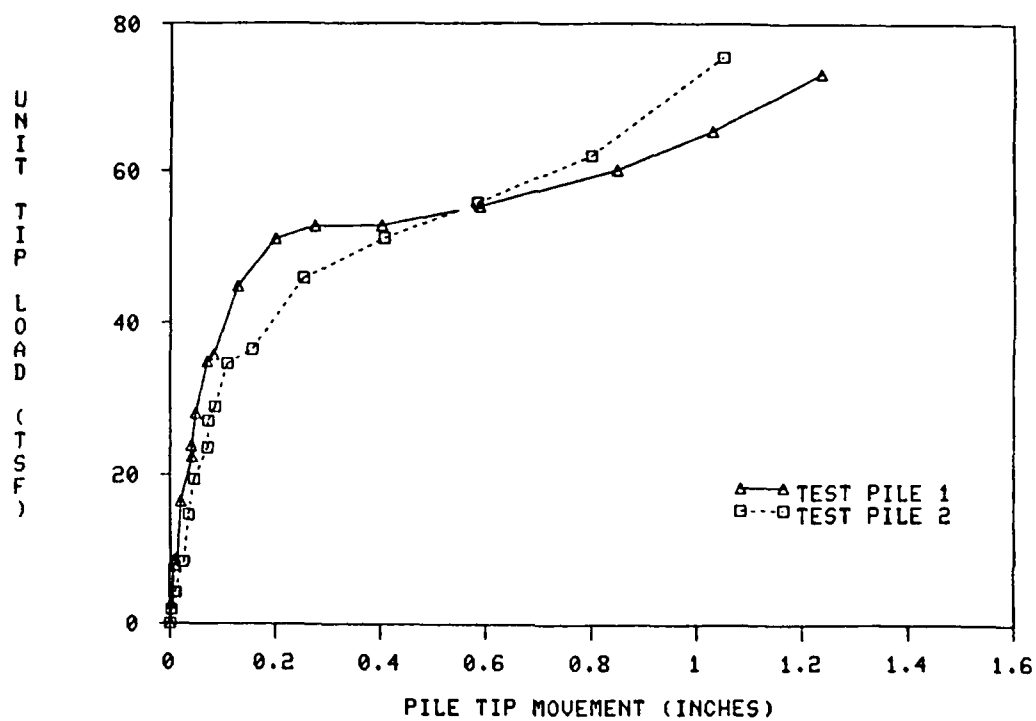


Figure B30. Unadjusted Tip Load Versus Movement,
Ascalmore Creek-Tippo Bayou, H Piles

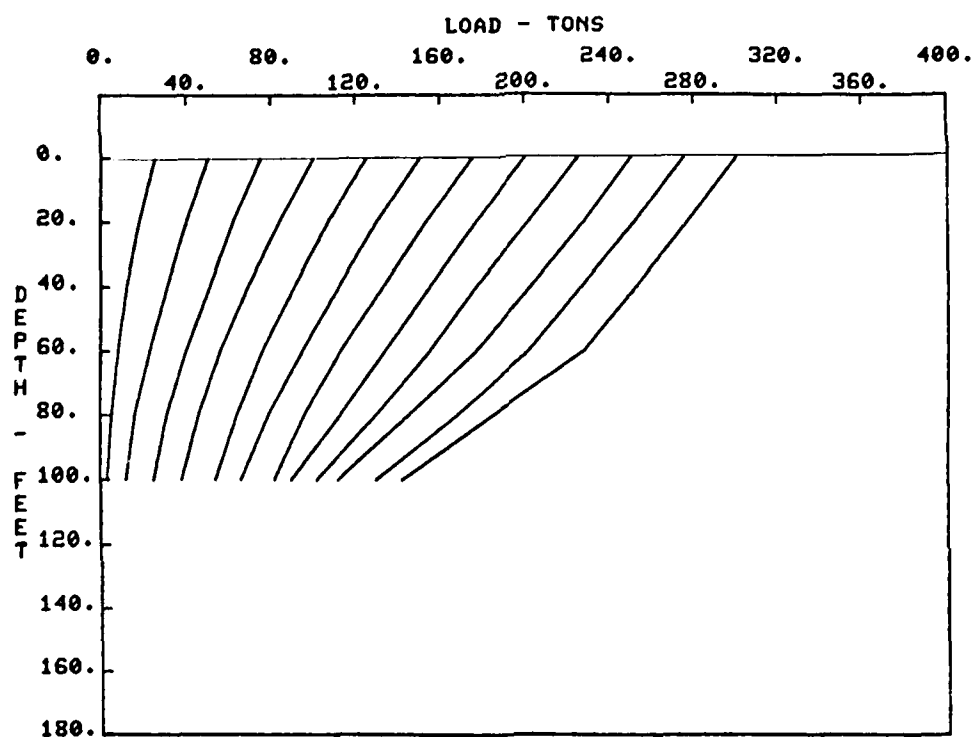


Figure B31. Load Distribution Curves Adjusted for
Residual Loads, Ascalmore Creek-Tippo Bayou,
Test Pile No. 1

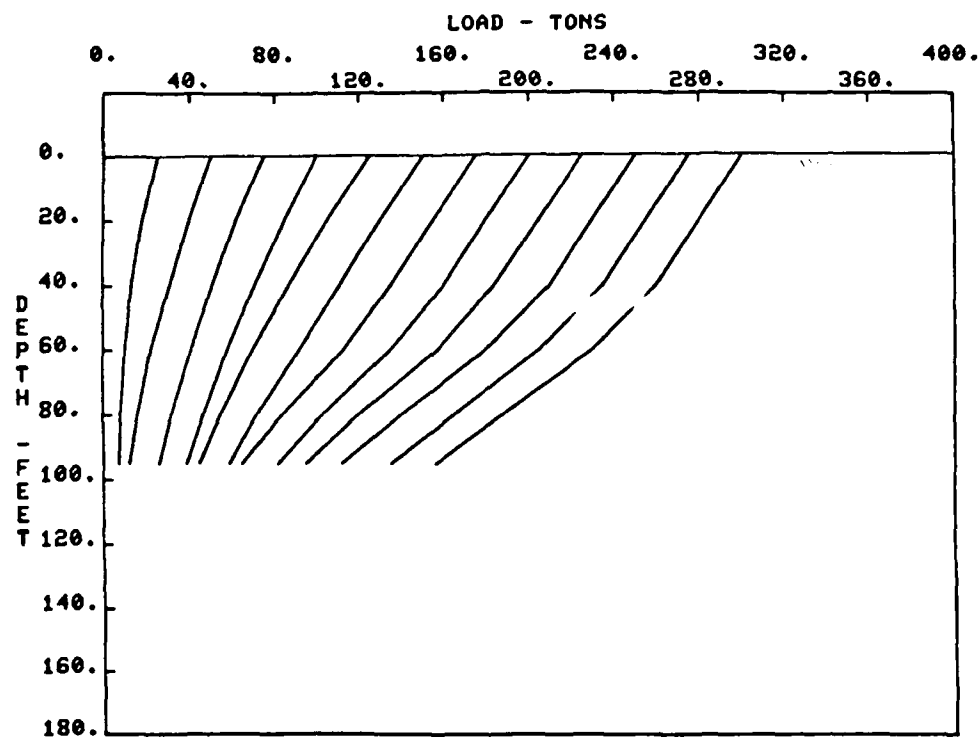


Figure B32. Load Distribution Curves Adjusted for Residual Loads, Ascalmore Creek-Tippo Bayou, Test Pile No. 2

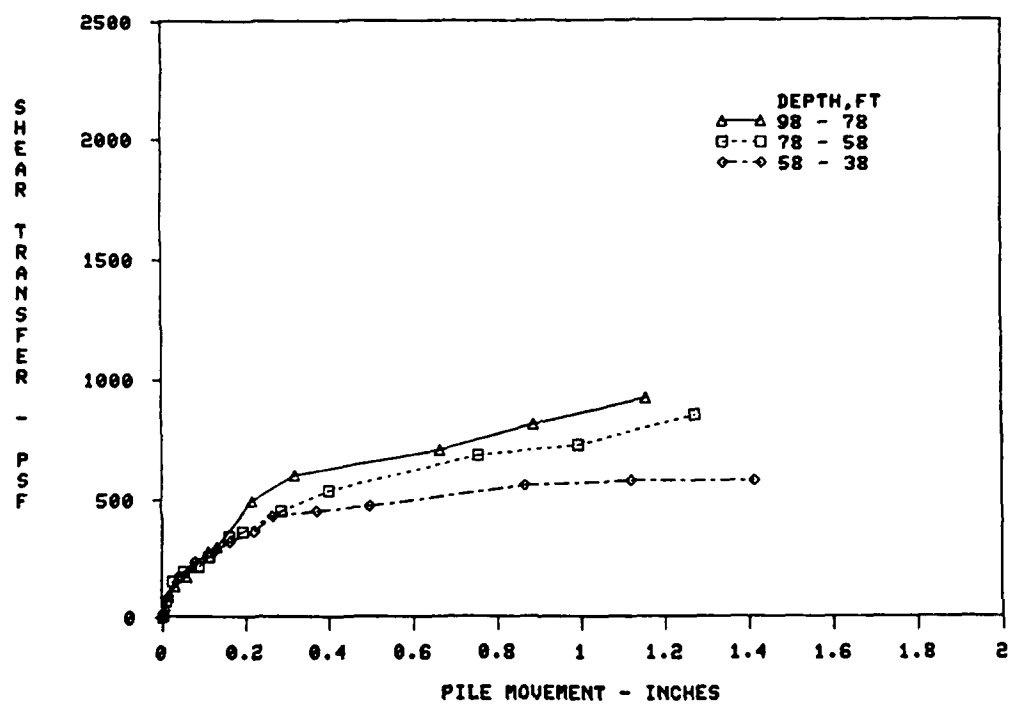


Figure B33. Adjusted f-z Curves, Ascalmore Creek-Tippo Bayou, Test Pile No. 1

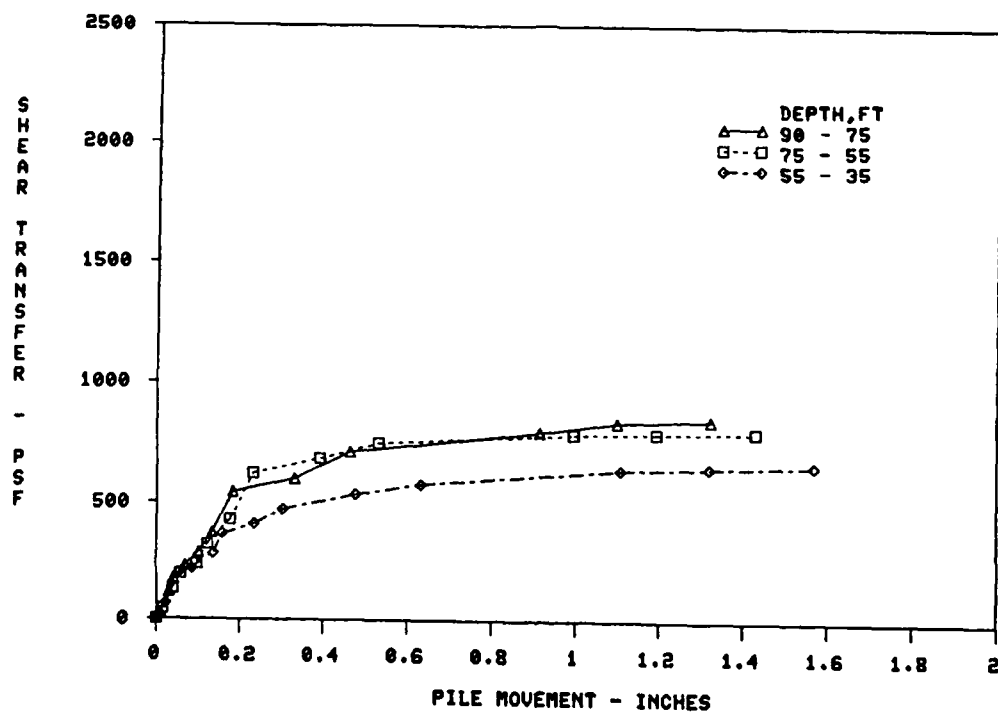


Figure B34. Adjusted f-z Curves, Ascalmore Creek-Tippo Bayou, Test Pile No. 2

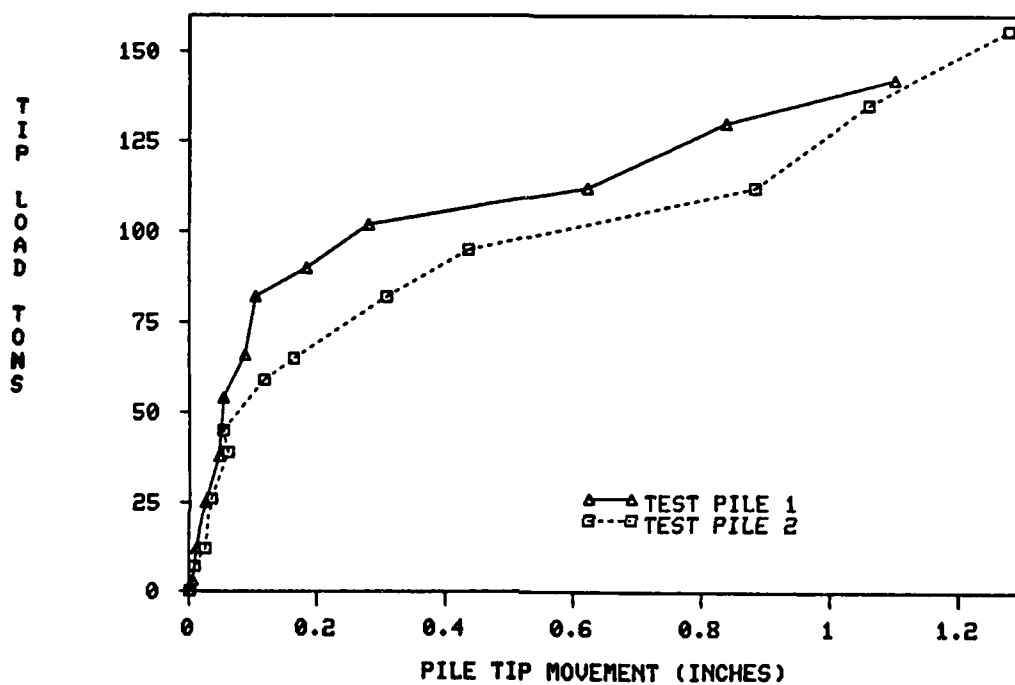


Figure B35. Adjusted $P-z$ Curves, Ascalmore Creek-Tippo Bayou, H Piles

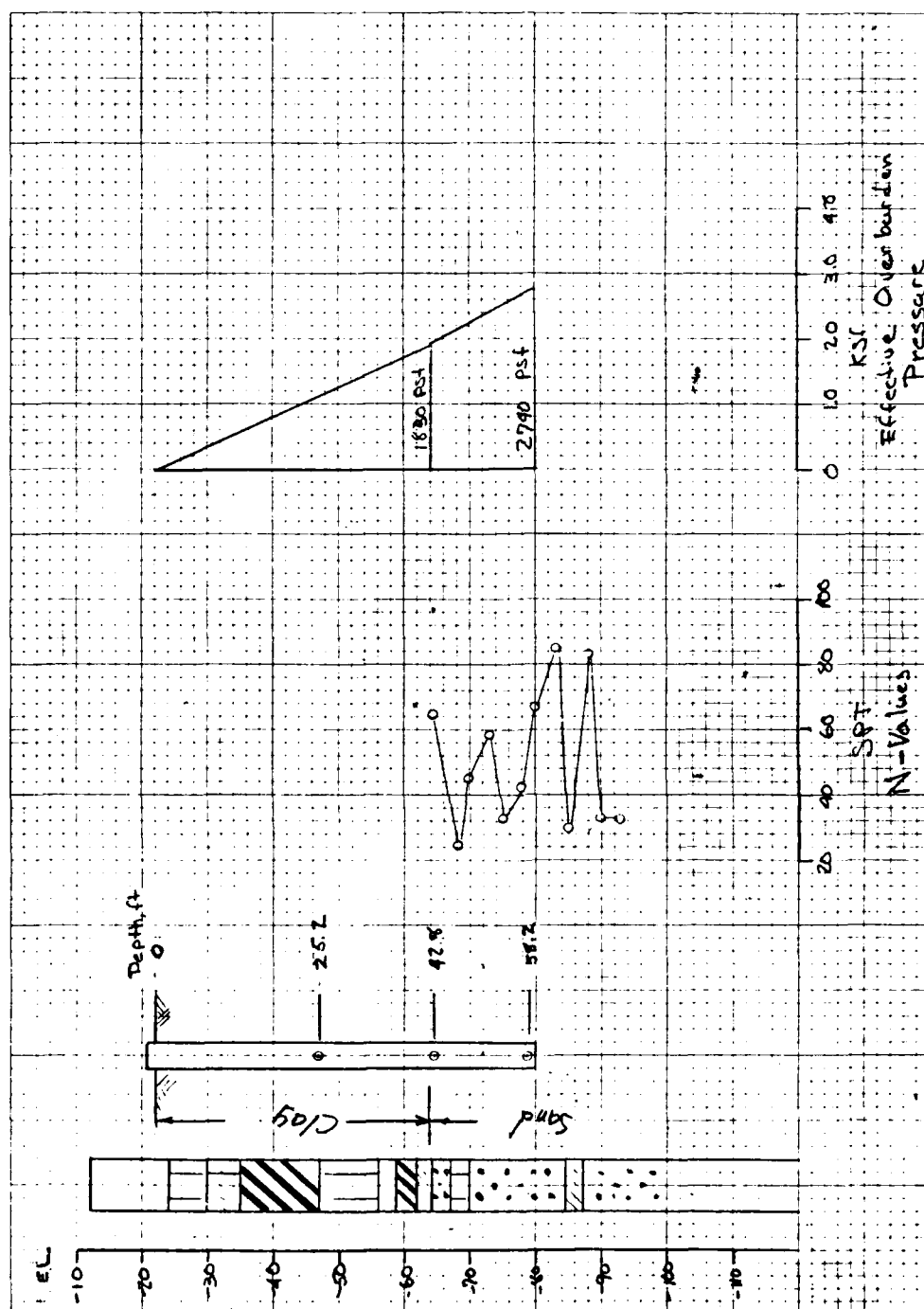


Figure B36. Stratification and SPT Results, Red River, Test Pile No. PT-A-1C

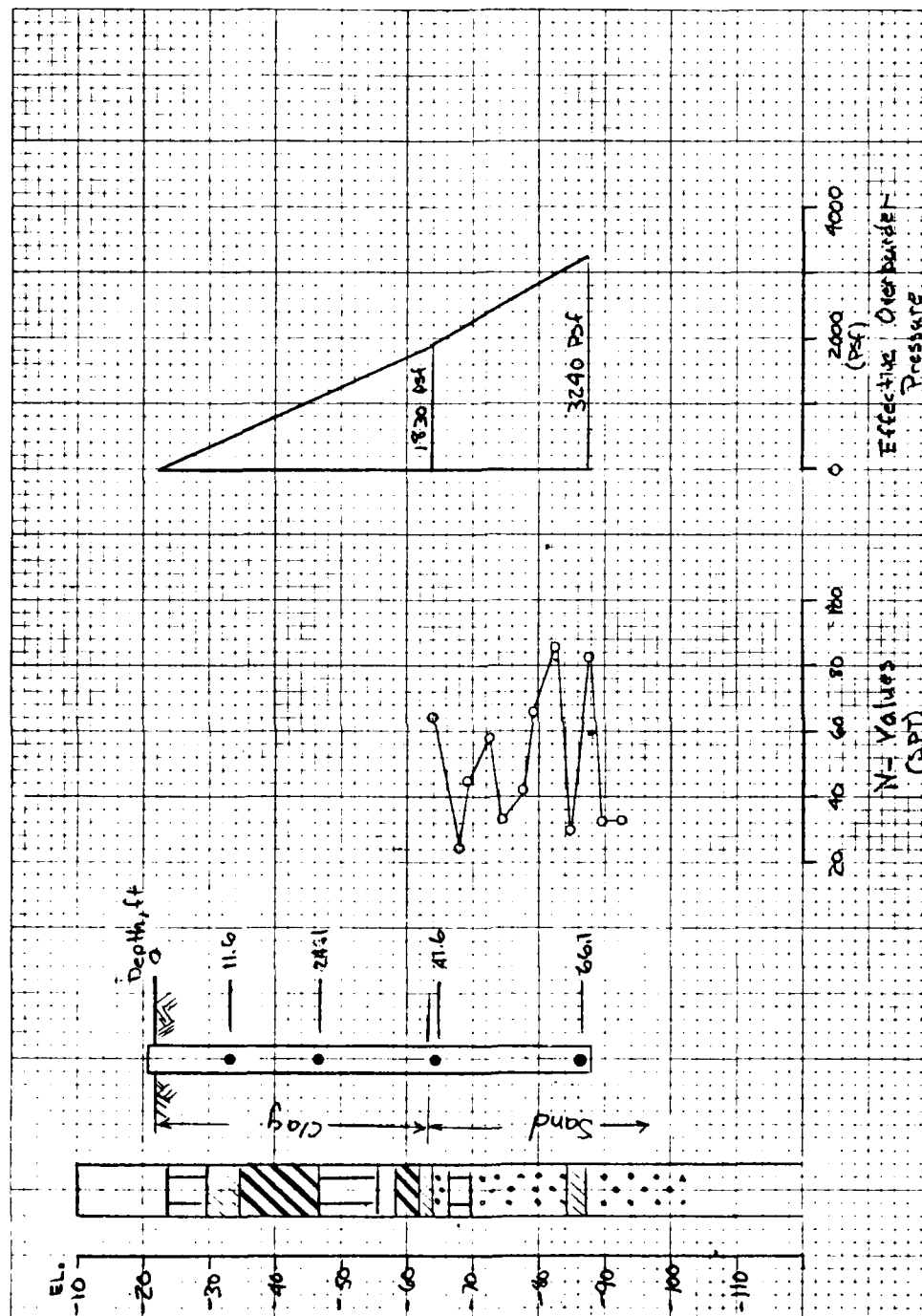


Figure B37. Stratification and SPT Results, Red River, Test Pile No. PT-A-2C

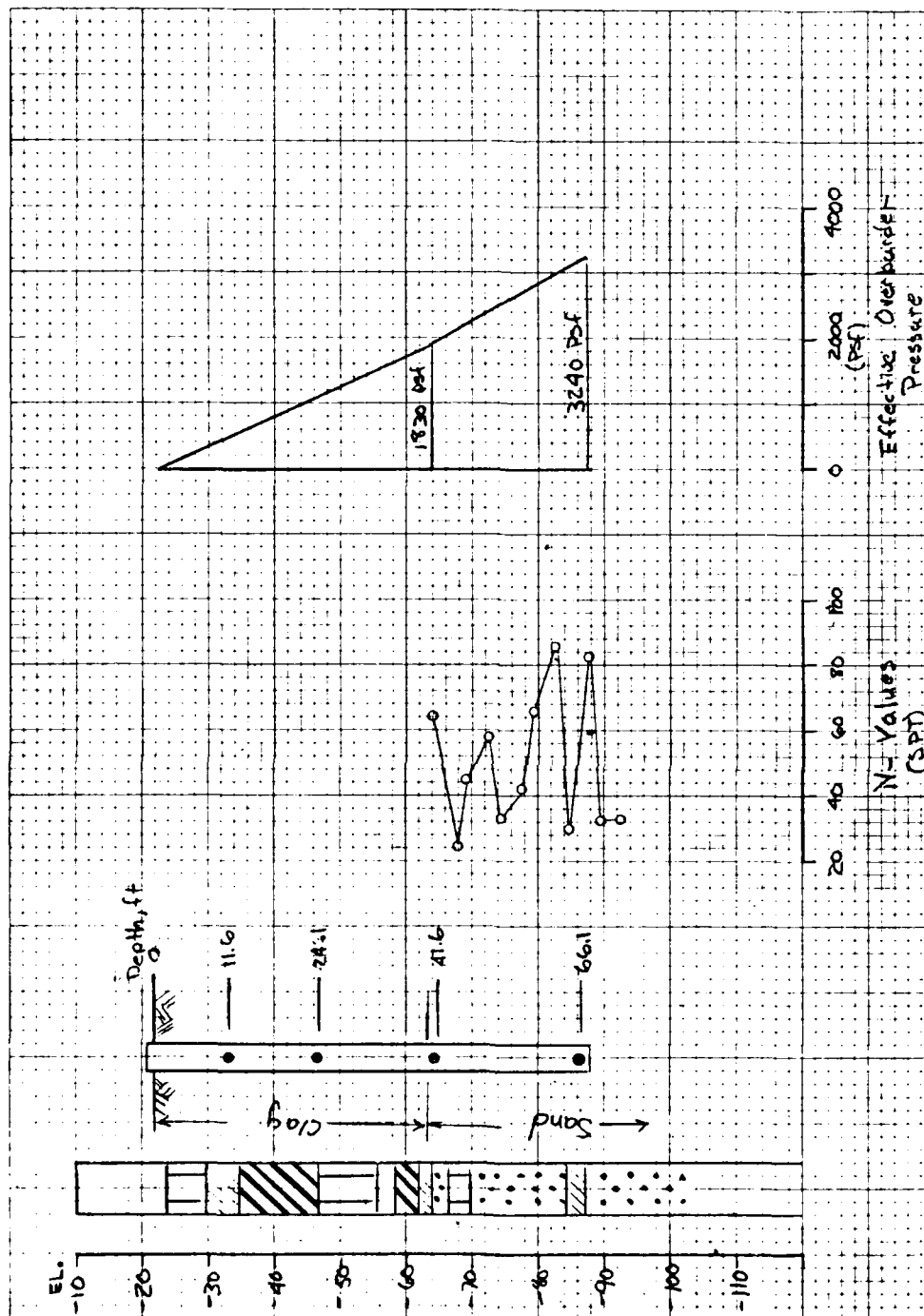


Figure B38. Stratification and SPT Results, Red River, Test Pile No. PT-A-3C

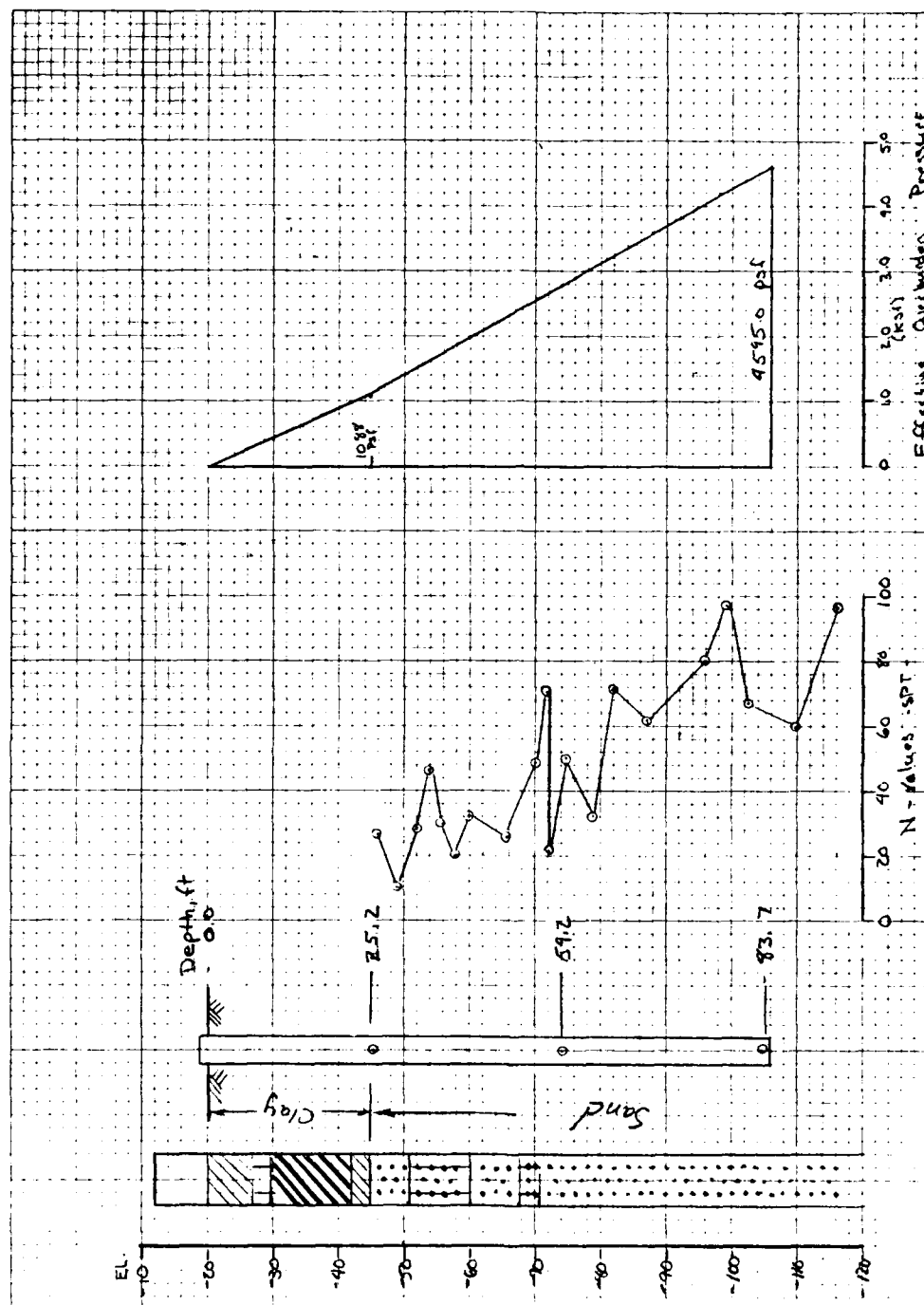


Figure B39. Stratification and SPT Results, Red River, Test Pile No. PT-S-1C

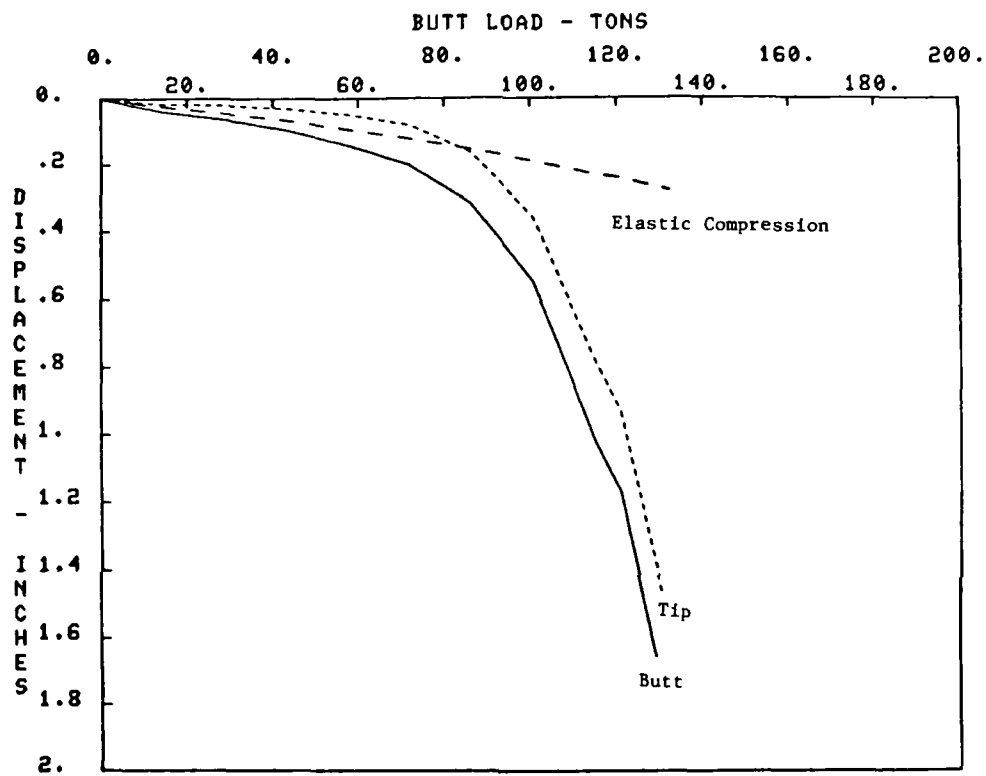


Figure B40. Butt and Tip Performance, Red River, Test Pile No. PT-A-1C

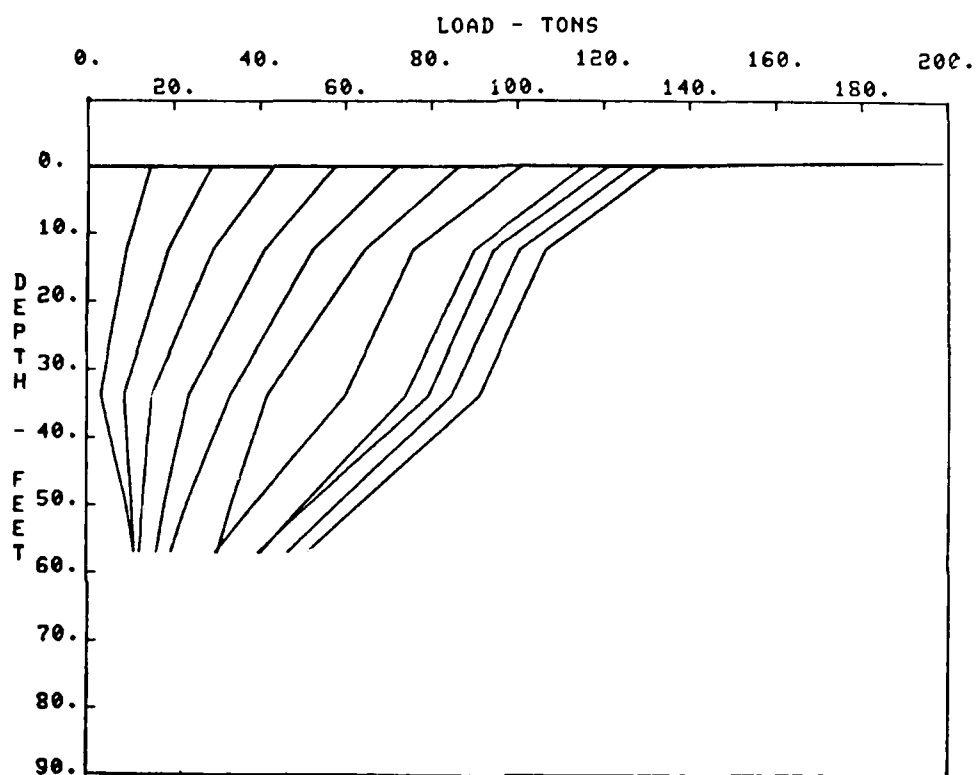


Figure B41. Unadjusted Load Distribution on Pile, Red River, Test Pile No. PT-A-1C

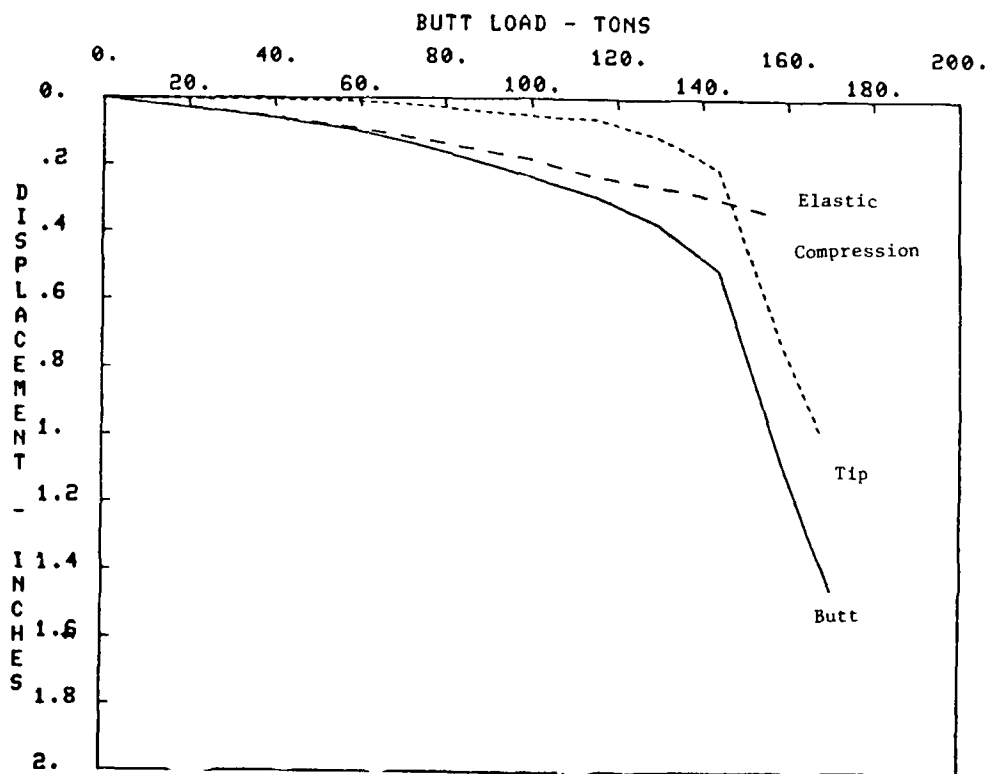


Figure B42. Butt and Tip Performance, Red River, Test Pile No. PT-A-1C Retest

AD-A139 236

LOAD-TRANSFER CRITERIA FOR NUMERICAL ANALYSIS OF
AXIALLY LOADED PILES IN. (U) ARMY ENGINEER WATERWAYS
EXPERIMENT STATION VICKSBURG MS R L MOSHER JAN 84

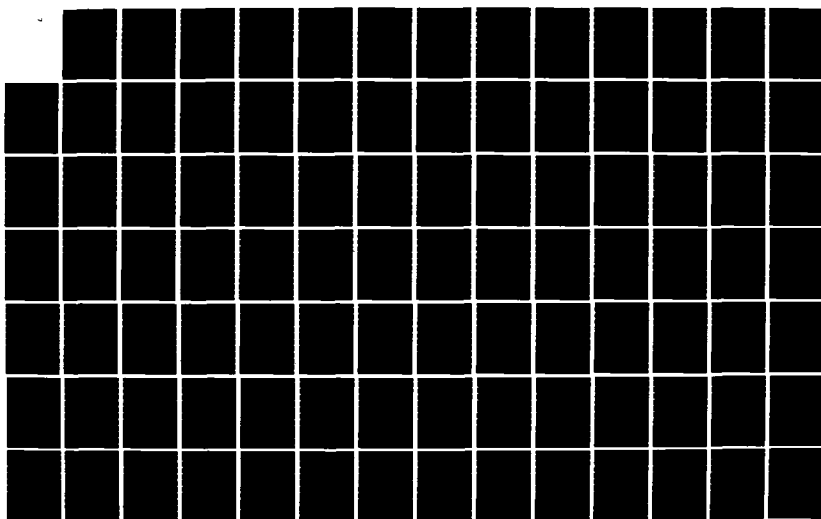
4/5

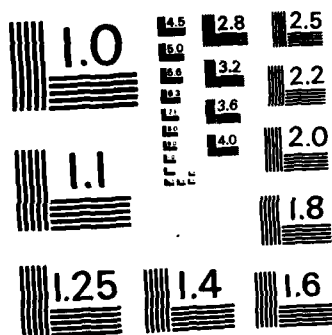
UNCLASSIFIED

WES-TR-K-84-1

F/G 13/13

NL





MICROCOPY RESOLUTION TEST CHART
NATIONAL BUREAU OF STANDARDS-1963-A

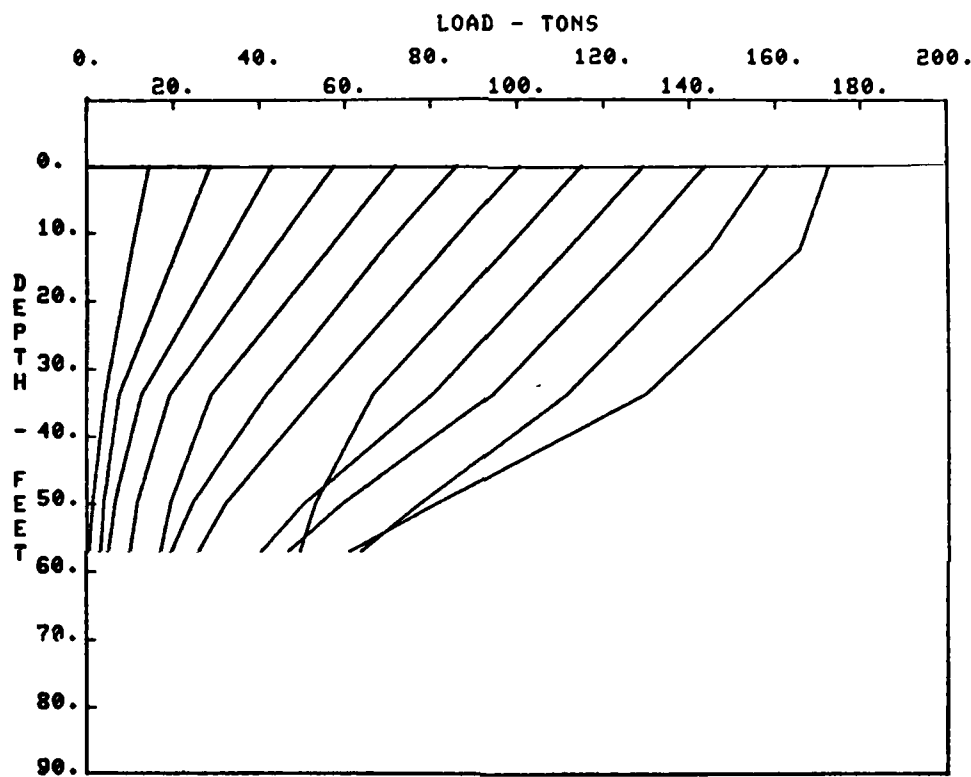


Figure B43. Unadjusted Load Distribution on Pile, Red River, Test Pile No. PT-A-1C Retest

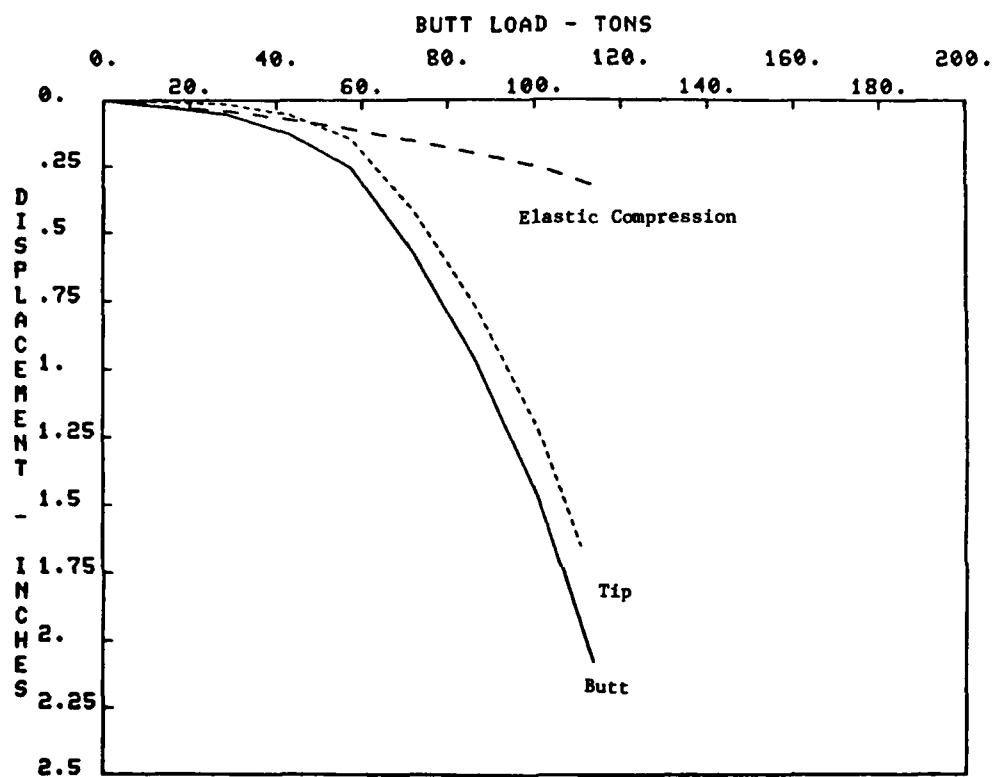


Figure B44. Butt and Tip Performance, Red River, Test Pile No. PT-A-2C

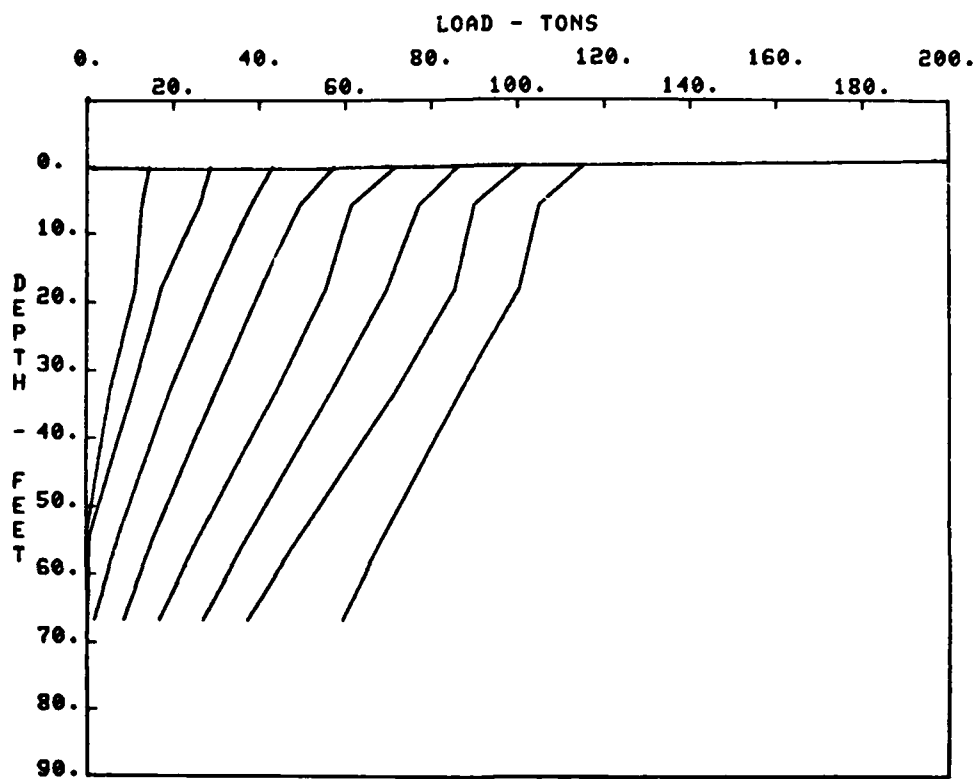


Figure B45. Unadjusted Load Distribution on Pile, Red River, Test Pile No. PT-A-2C

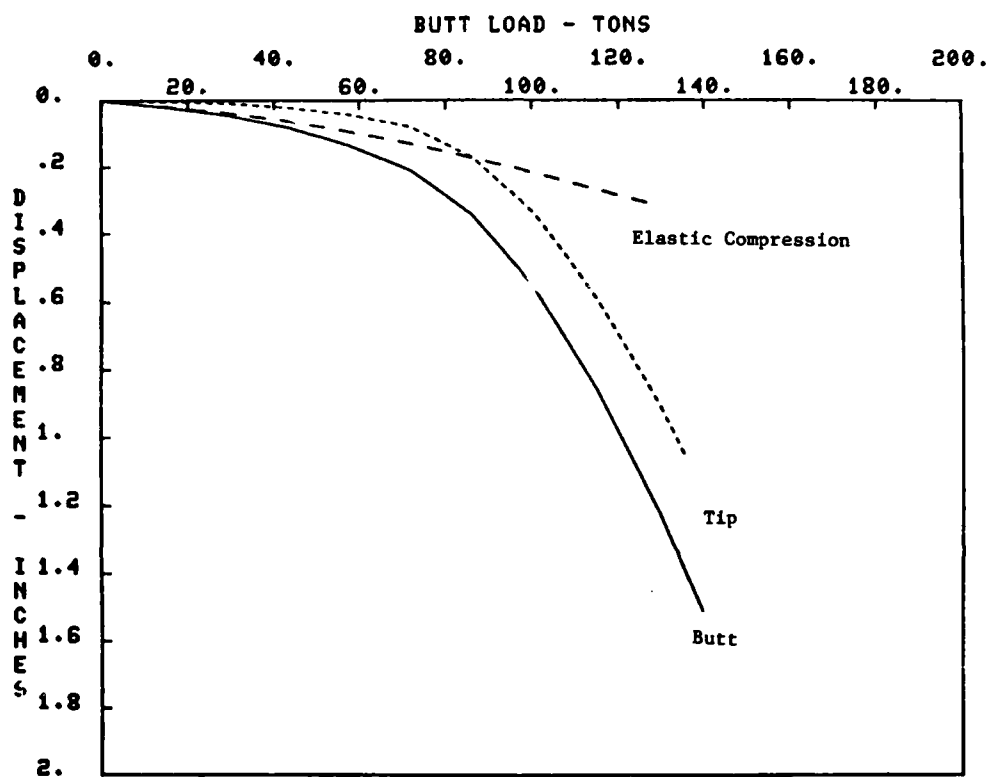


Figure B46. Butt and Tip Performance, Red River, Test Pile No. PT-A-3C

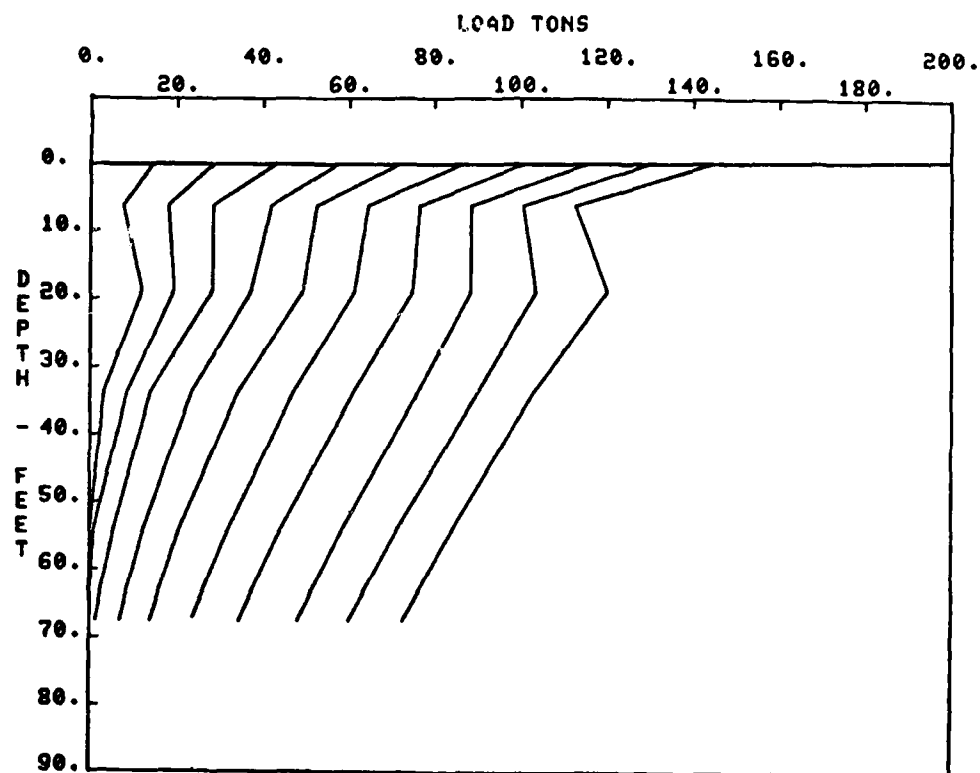


Figure B47. Unadjusted Load Distribution on Pile, Red River, Test Pile No. PT-A-3C

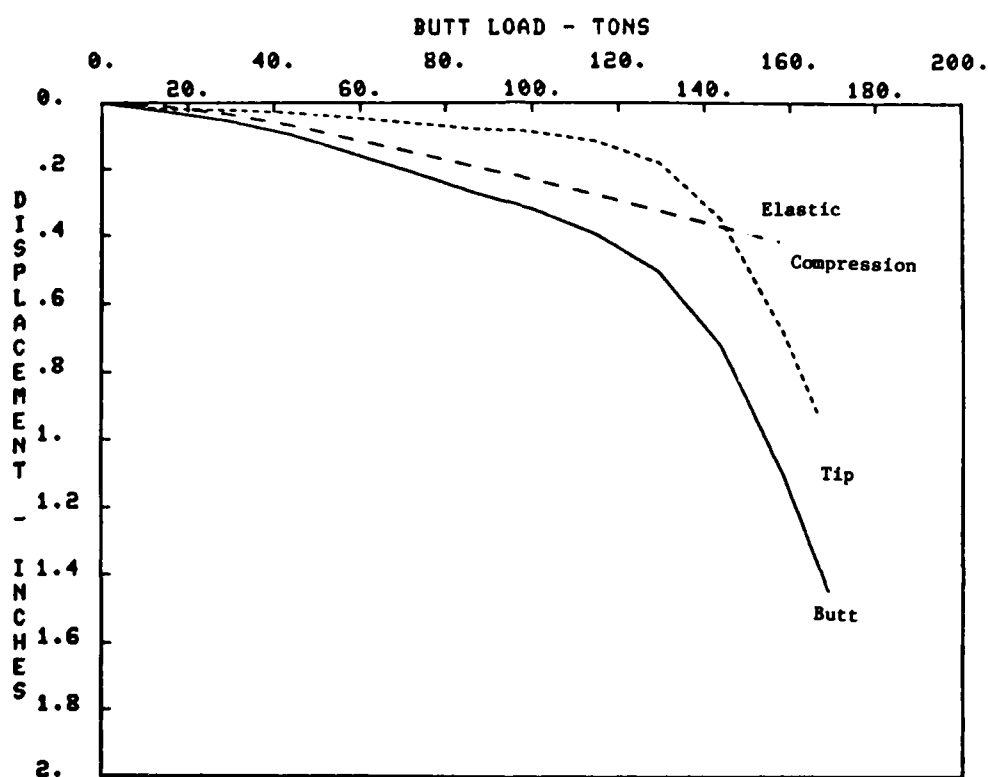


Figure B48. Butt and Tip Performance, Red River, Test Pile No. PT-A-3C Retest

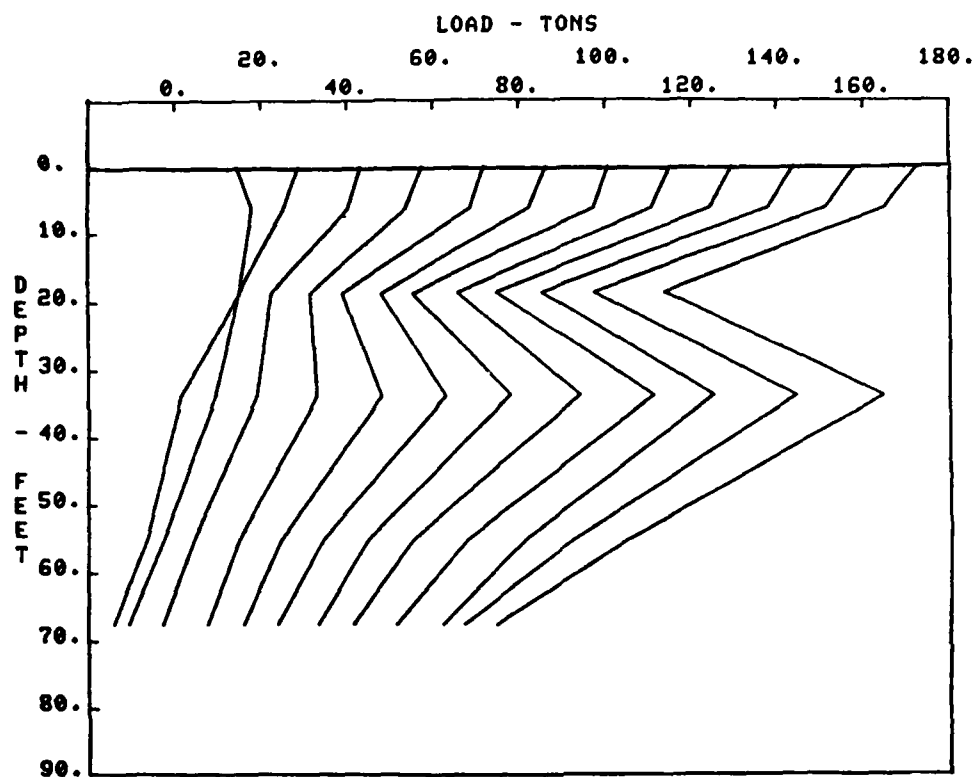


Figure B49. Unadjusted Load Distribution on Pile, Red River, Test Pile No. PT-A-3C Retest

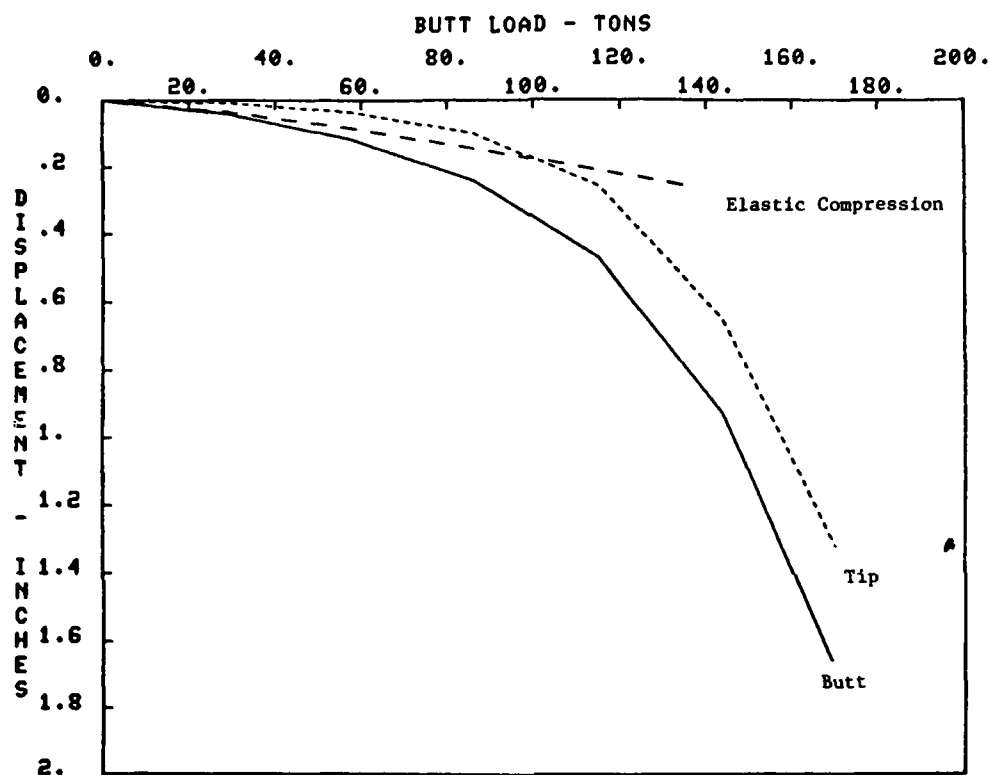


Figure B50. Butt and Tip Performance, Red River, Test Pile No. PT-S-1C

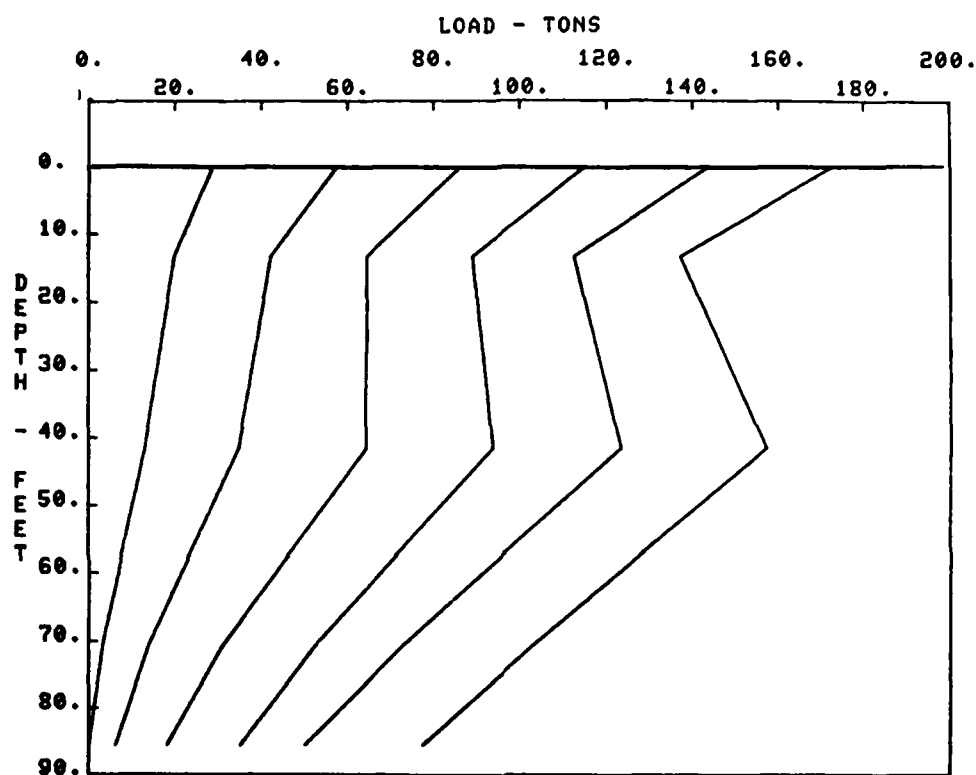


Figure B51. Unadjusted Load Distribution on Pile,
Red River, Test Pile No. PT-S-1C

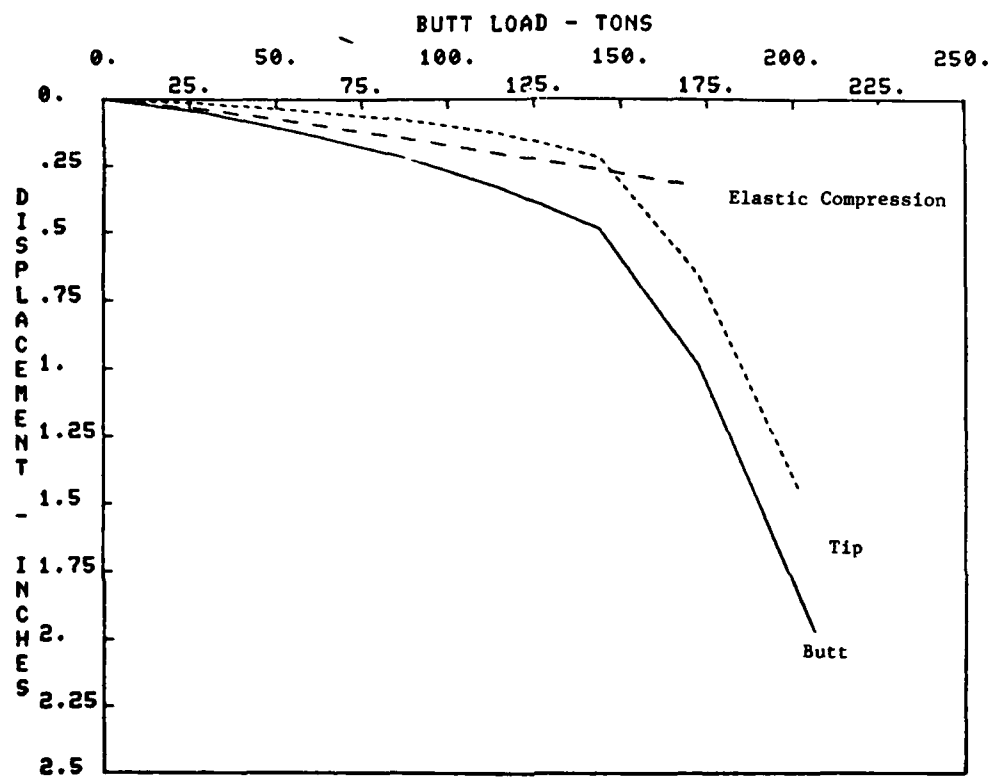


Figure B52. Butt and Tip Performance, Red River, Test Pile No. PT-S-1C Retest

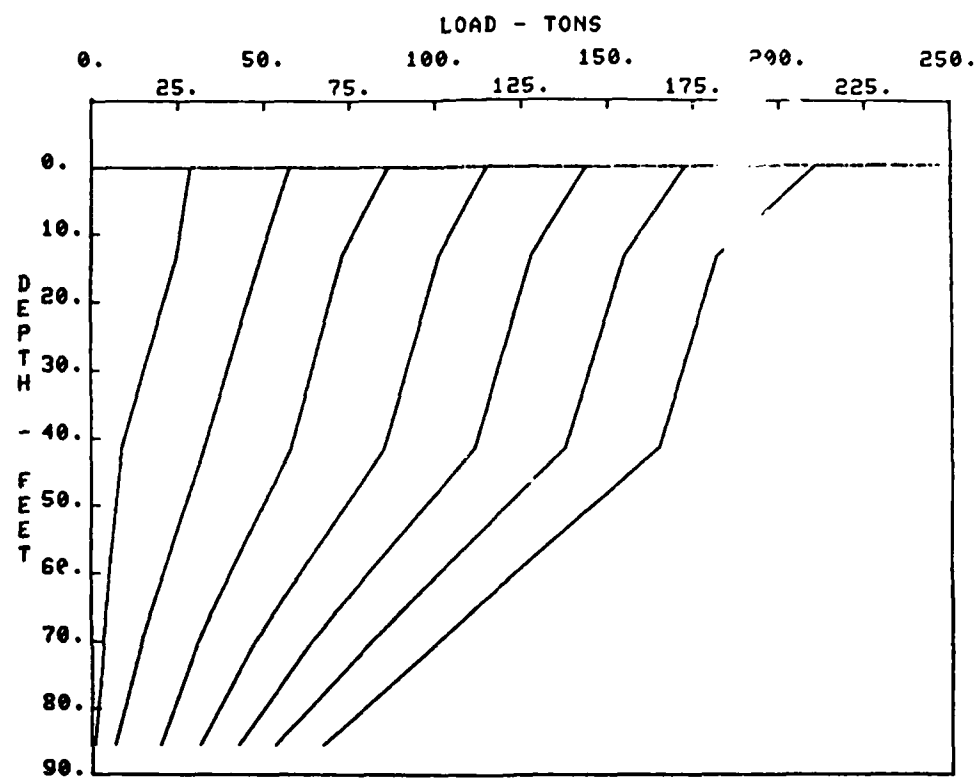


Figure B53. Unadjusted Load Distribution on Pile,
Red River, Test Pile No. PT-S-1C Retest

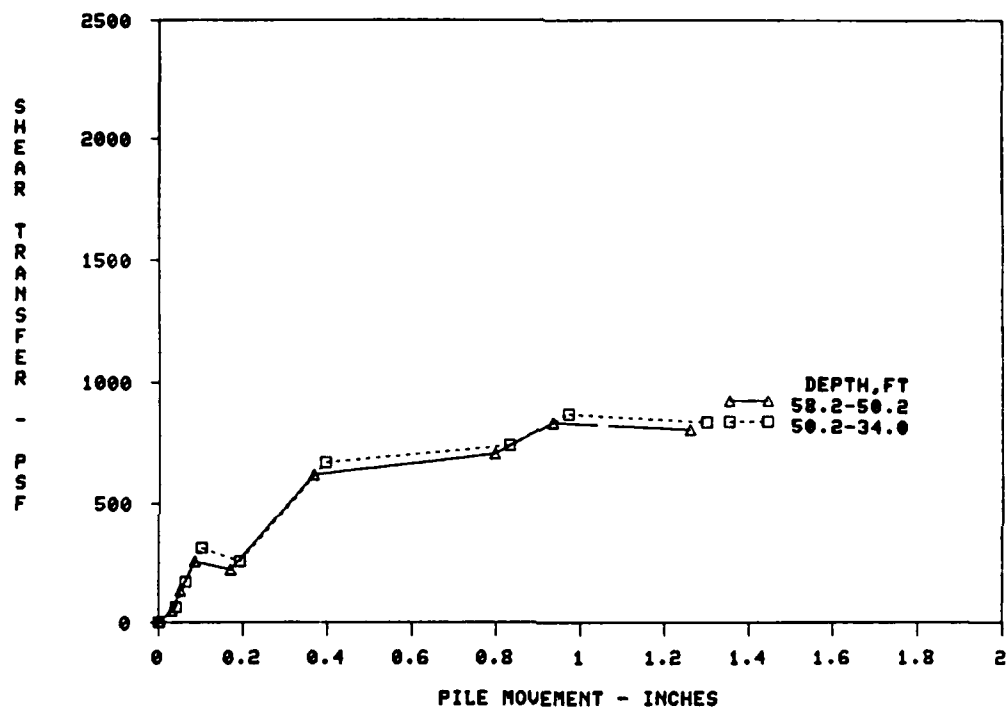


Figure B54. Field f-z Curves, Red River, Test Pile No. PT-A-1C

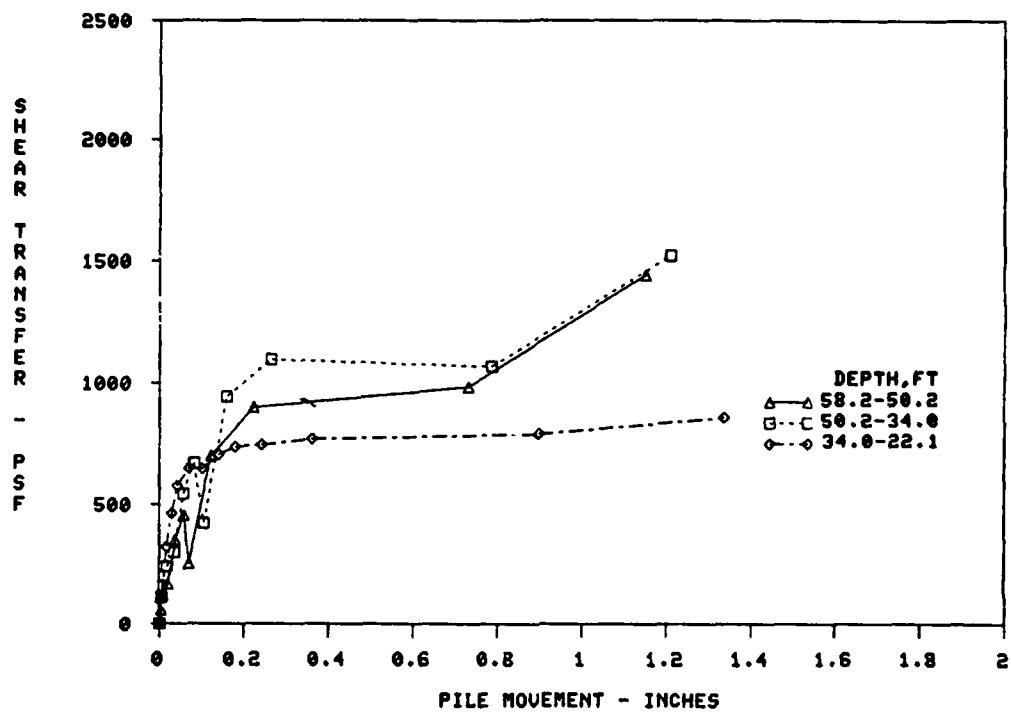


Figure B55. Field f-z Curves, Red River, Test Pile No. PT-A-1C Retest

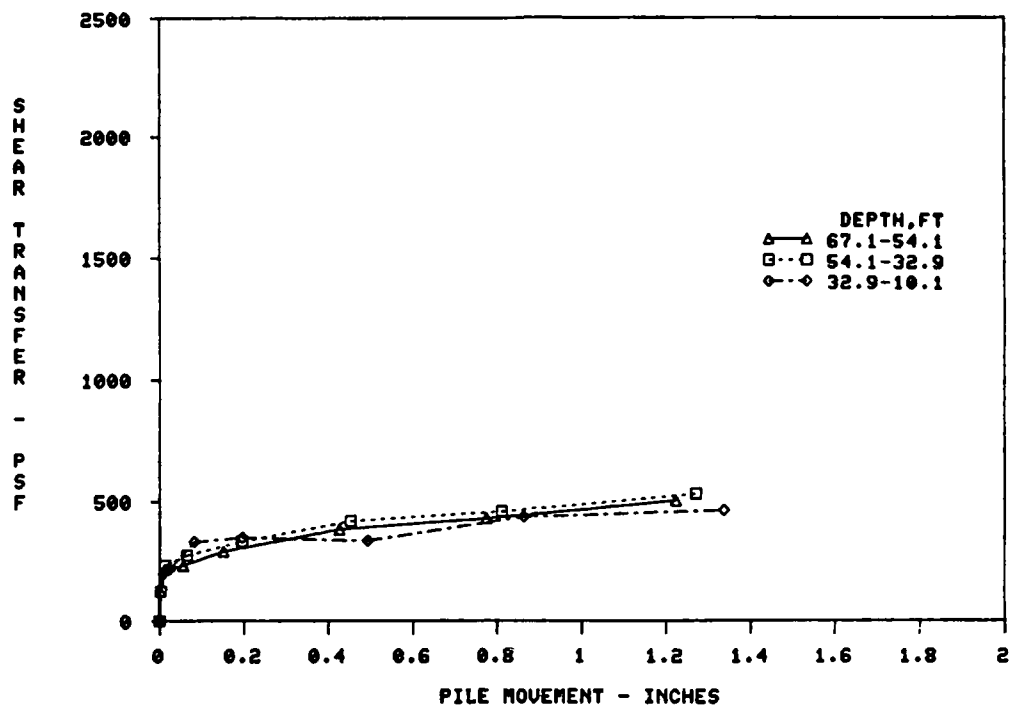


Figure B56. Field f-z Curves, Red River, Test Pile No. PT-A-2C

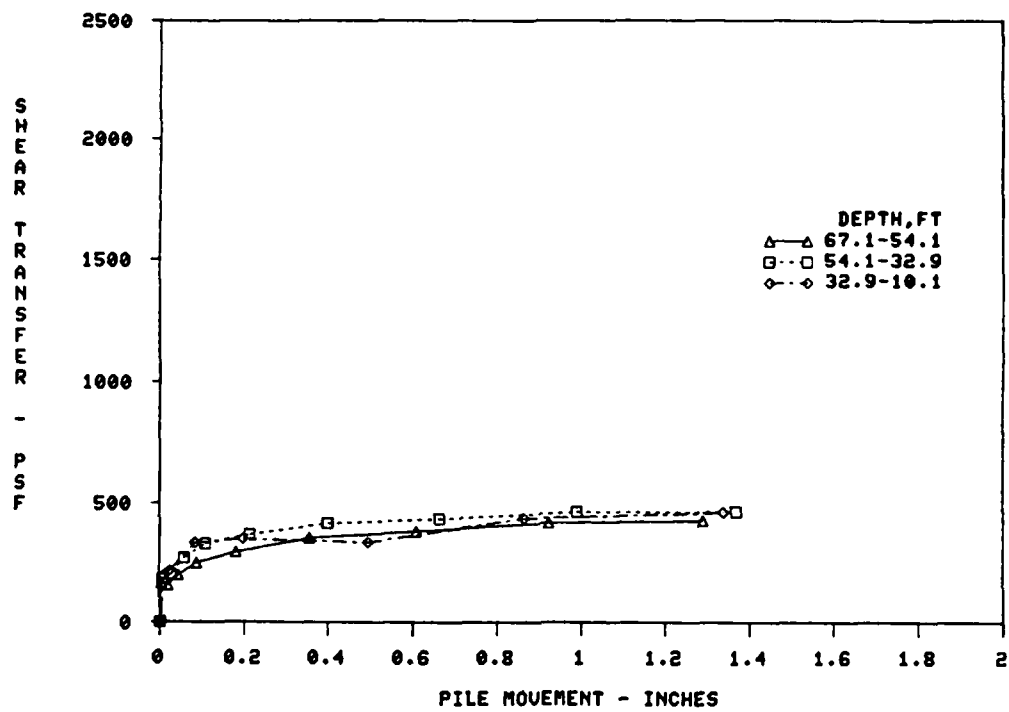


Figure B57. Field f-z Curves, Red River, Test Pile No. PT-A-3C

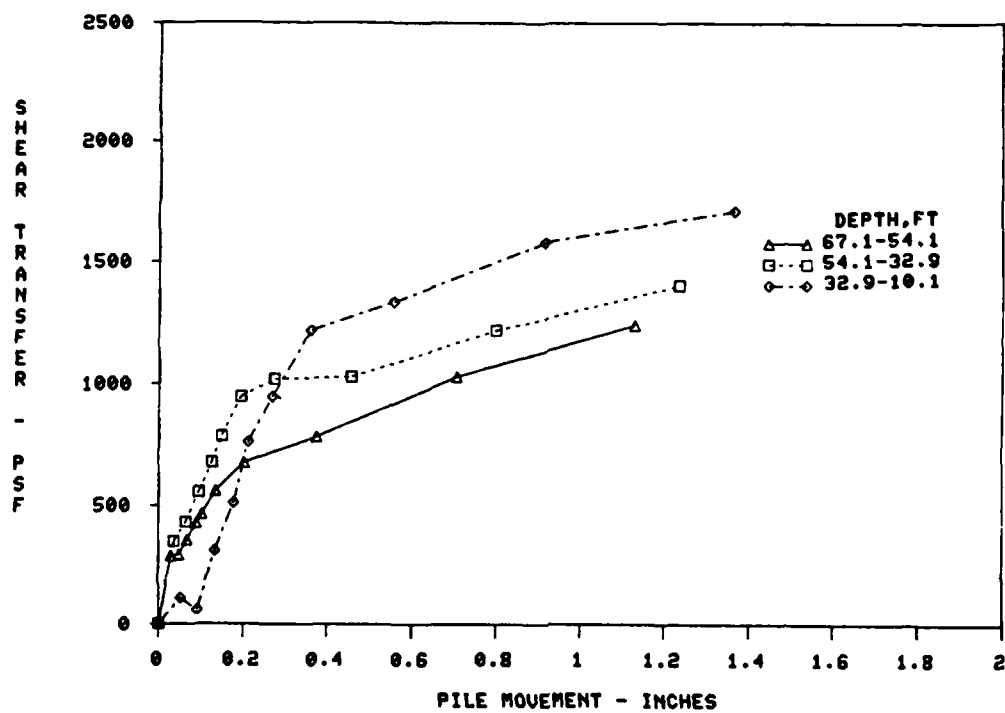


Figure B58. Field f-z Curves, Red River, Test Pile No. PT-A-3C Retest

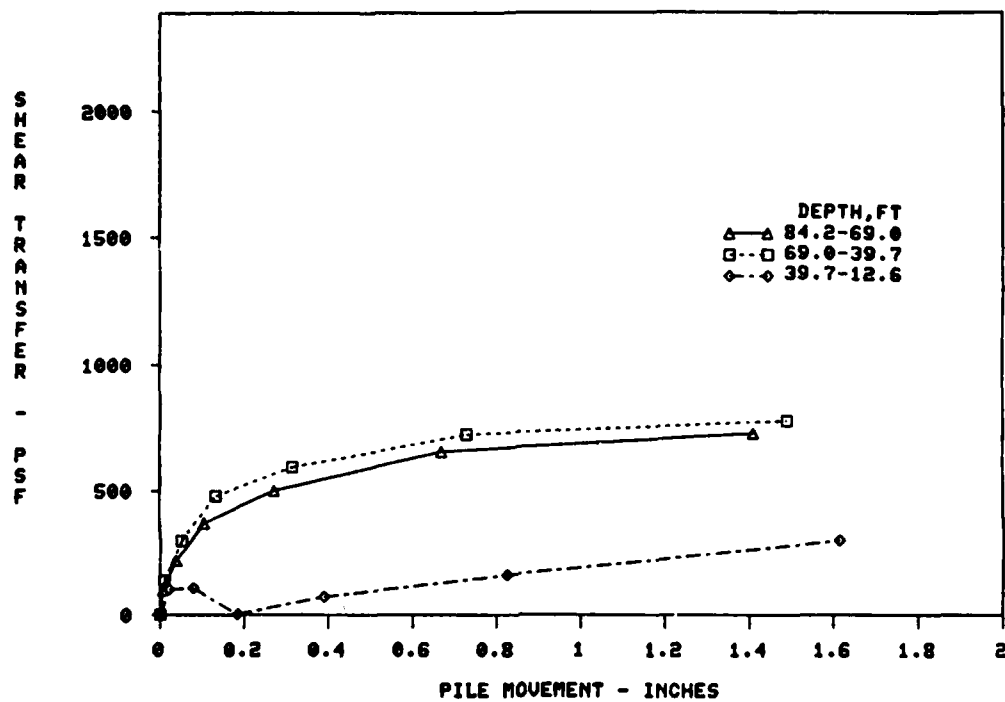


Figure B59. Field f-z Curves, Red River, Test Pile No. PT-S-1C

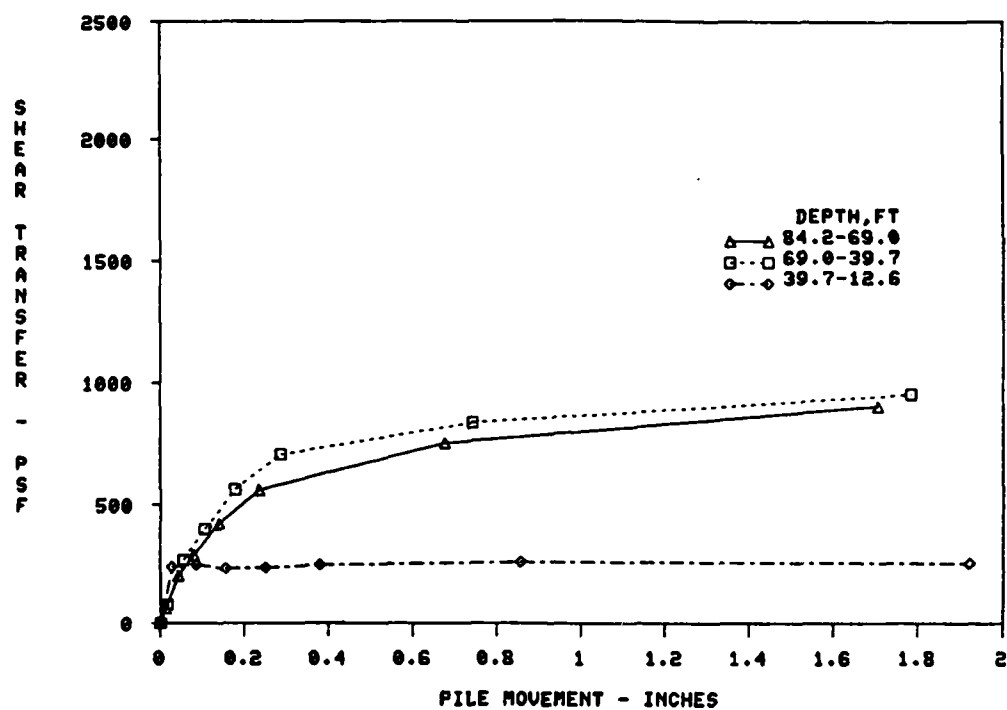


Figure B60. Field f-z Curves, Red River, Test Pile No. PT-S-1C Retest

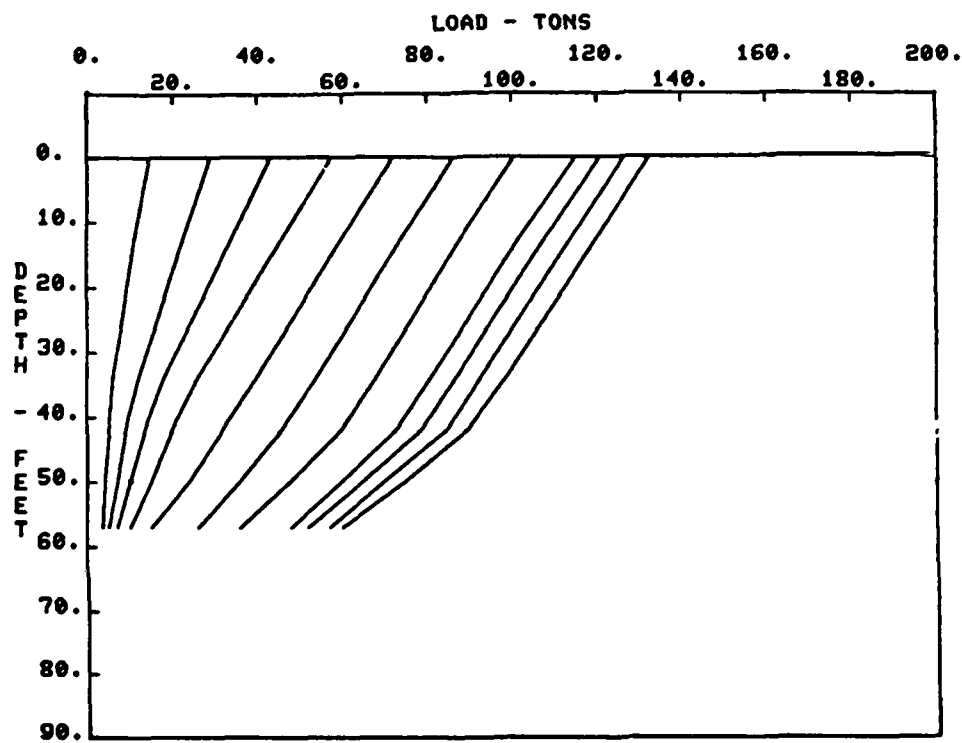


Figure B61. Adjusted Load Distribution in Pile, Red River, Test Pile No. PT-A-1C

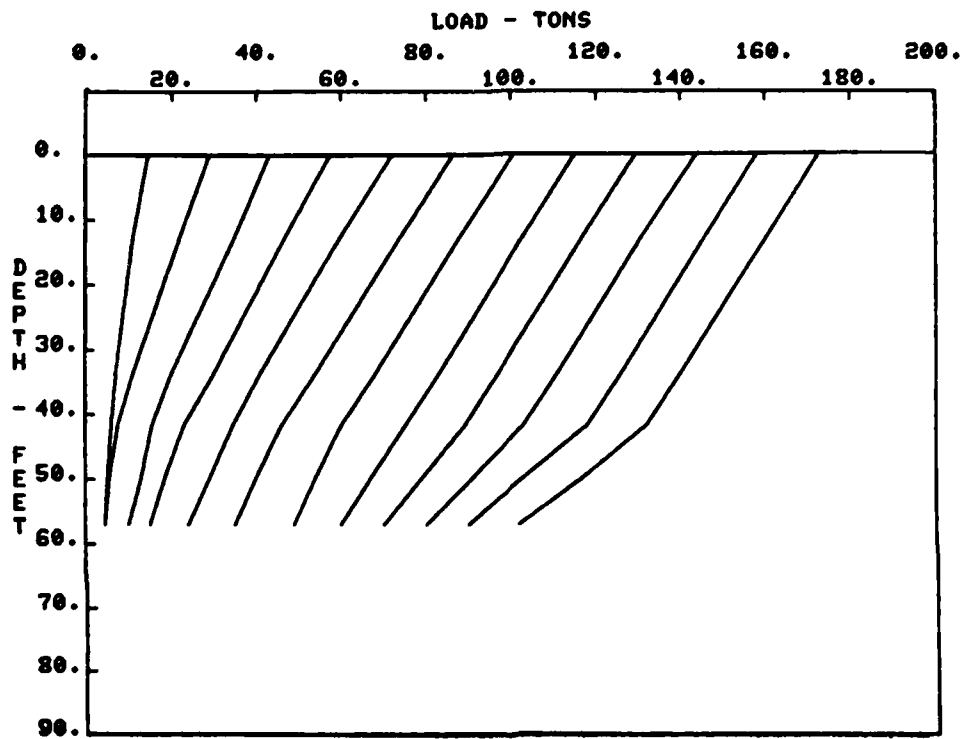


Figure B62. Adjusted Load Distribution in Pile, Red River, Test Pile No. PT-A-1C Retest

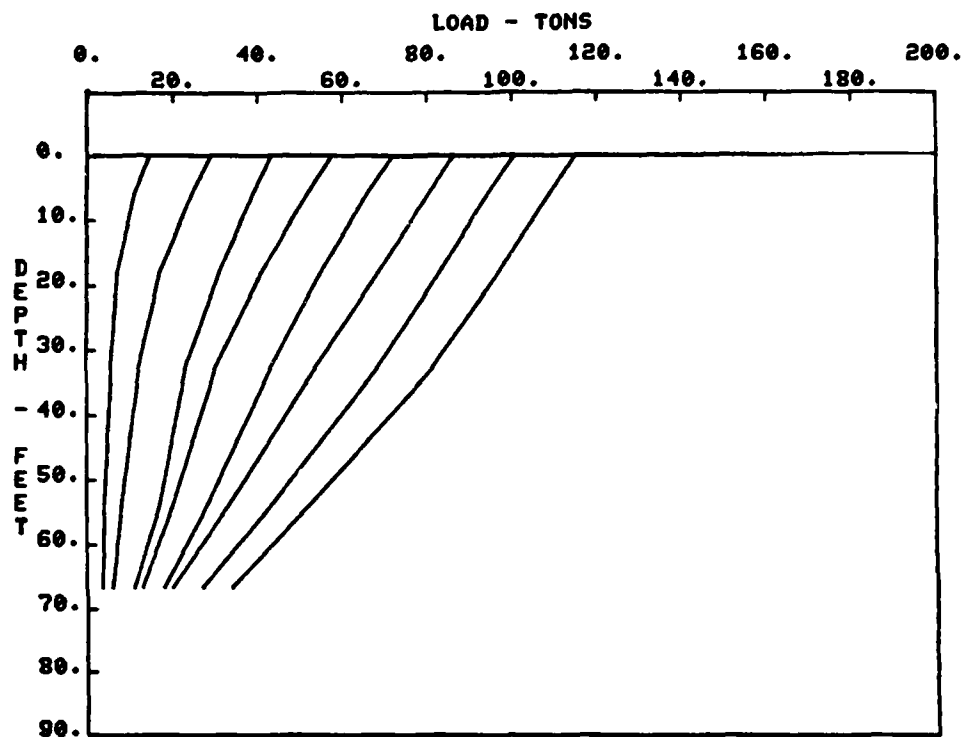


Figure B63. Adjusted Load Distribution in Pile, Red River, Test Pile No. PT-A-2C

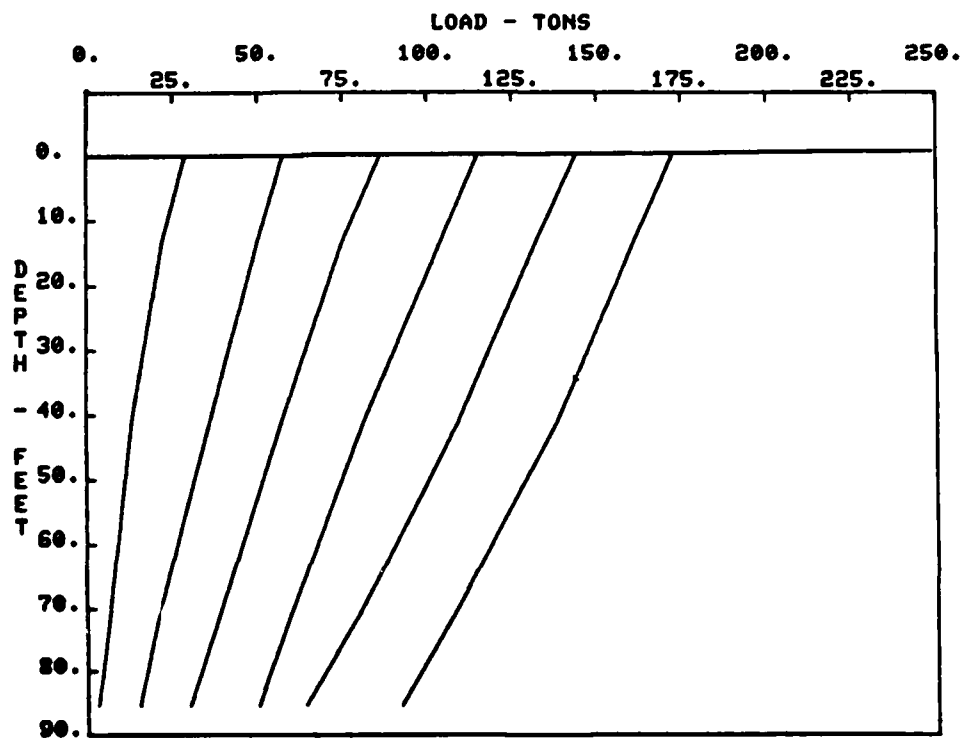


Figure B64. Adjusted Load Distribution in Pile, Red River, Test Pile No. PT-S-1C

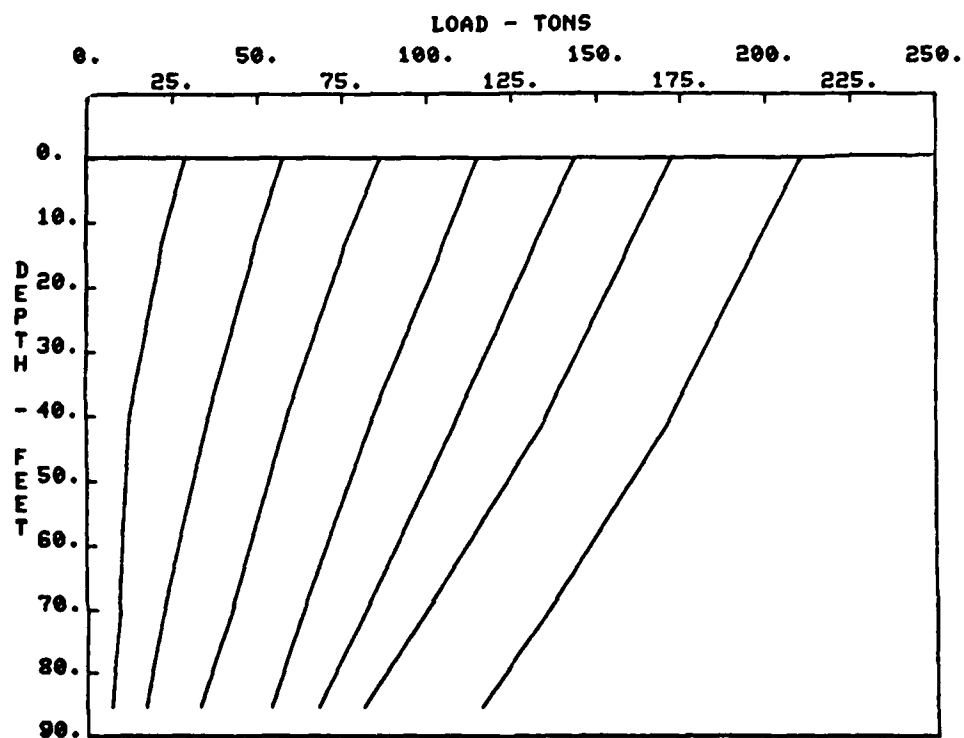


Figure B65. Adjusted Load Distribution in Pile, Red River, Test Pile No. PT-S-1C Retest

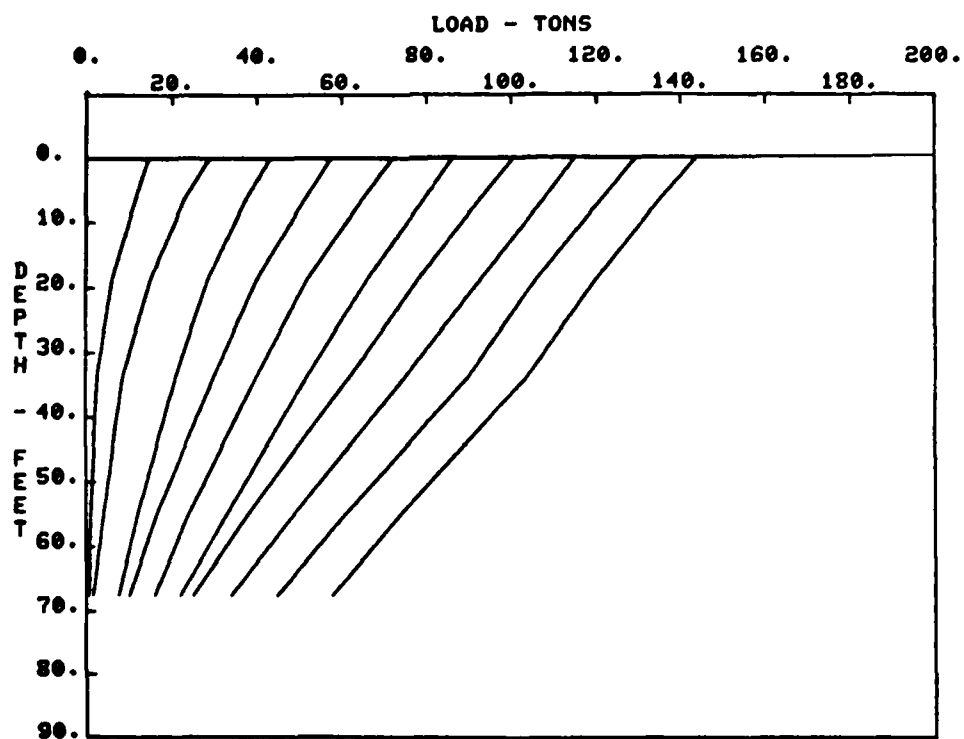


Figure B66. Adjusted Load Distribution in Pile, Red River, Test Pile No. PT-A-3C

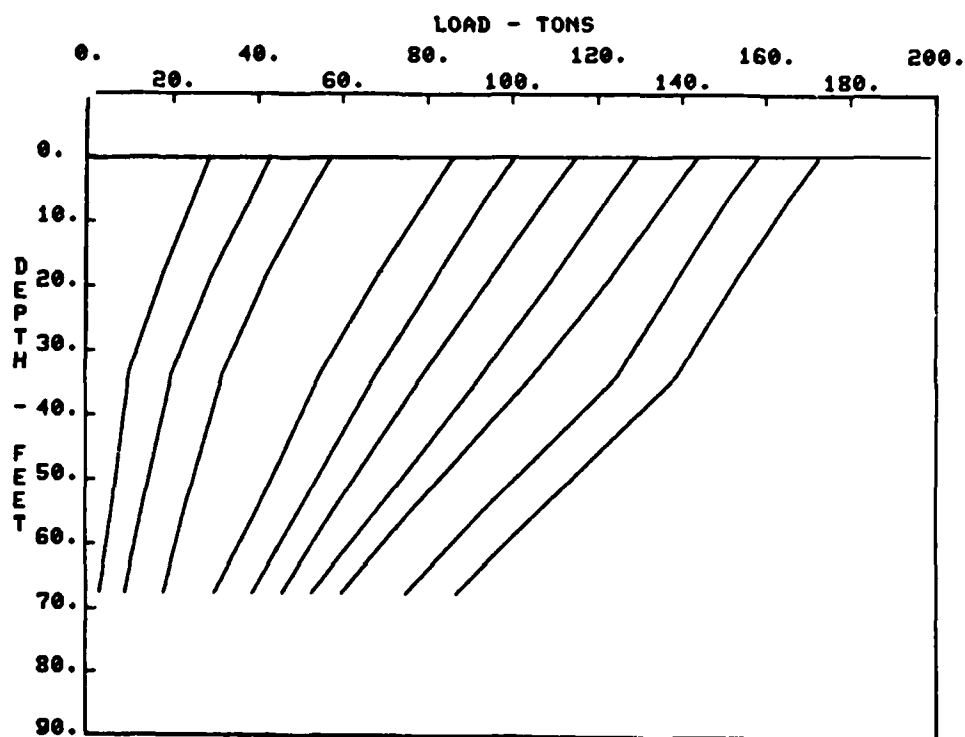


Figure B67. Adjusted Load Distribution in Pile, Red River, Test Pile No. PT-A-1C

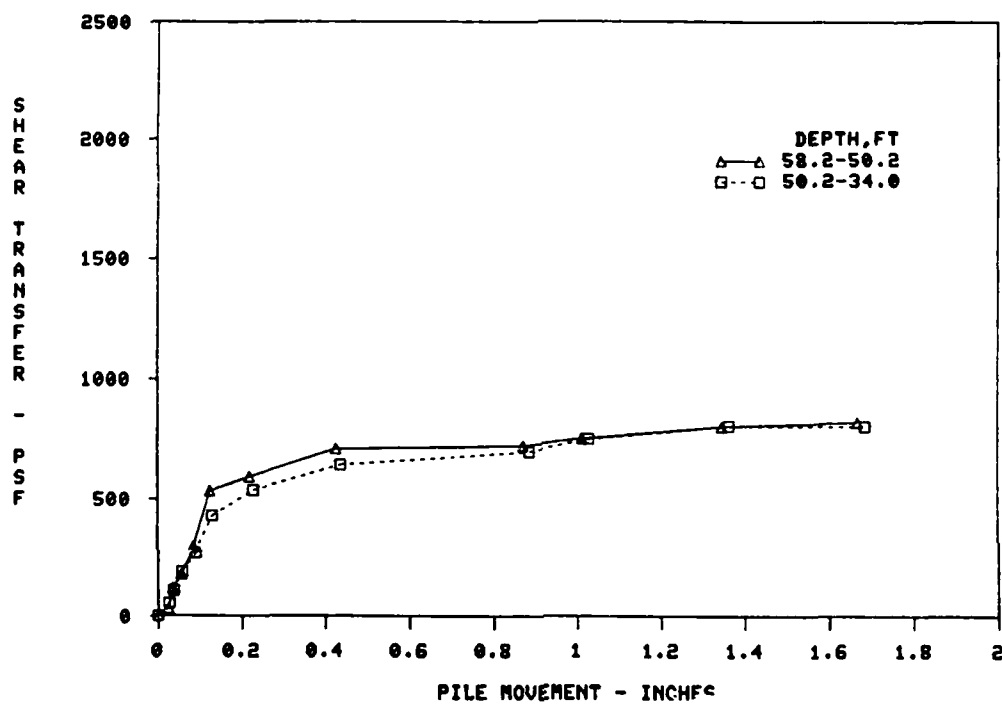


Figure B68. Adjusted f-z Curves, Red River, Test Pile No. PT-A-1C

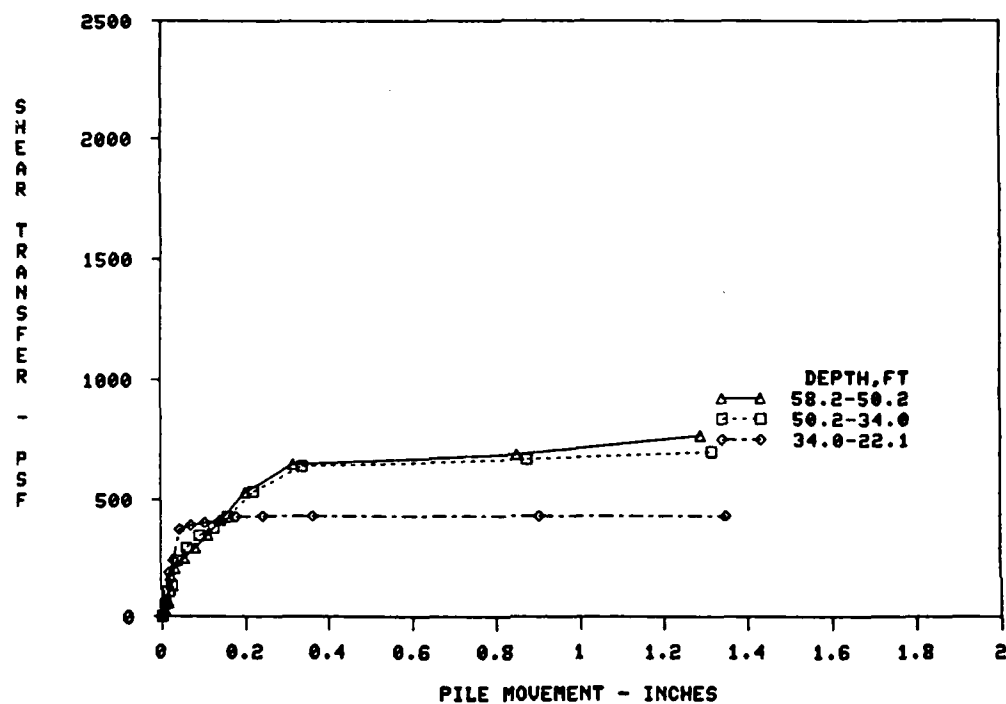


Figure B69. Adjusted f-z Curves, Red River, Test Pile No. PT-A-1C Retest

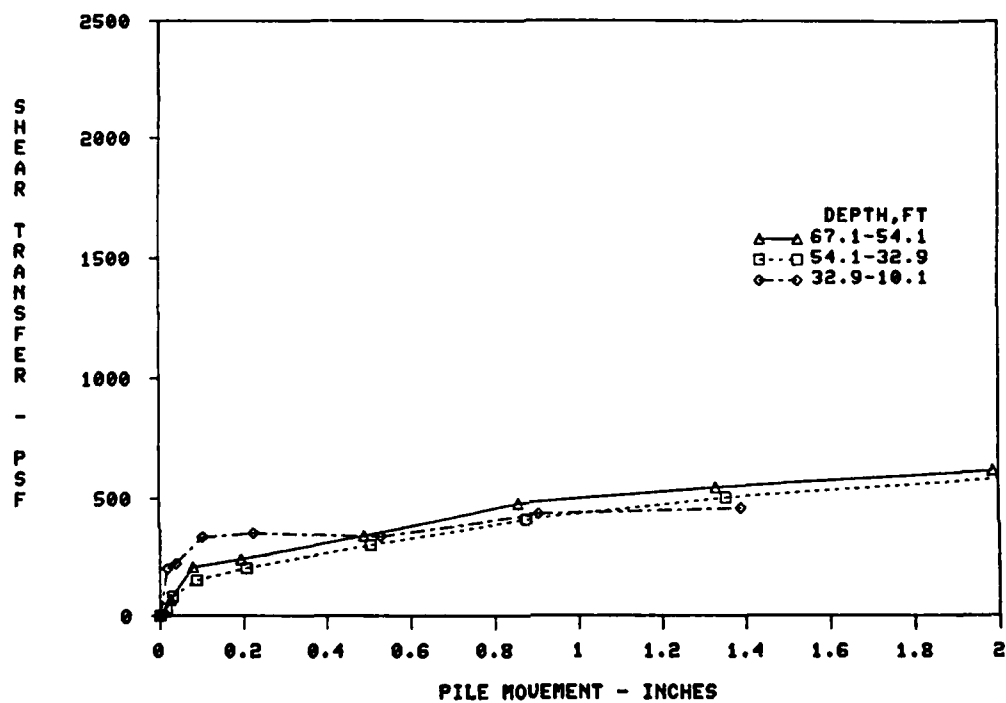


Figure B70. Adjusted f-z Curves, Red River, Test Pile No. PT-A-2C

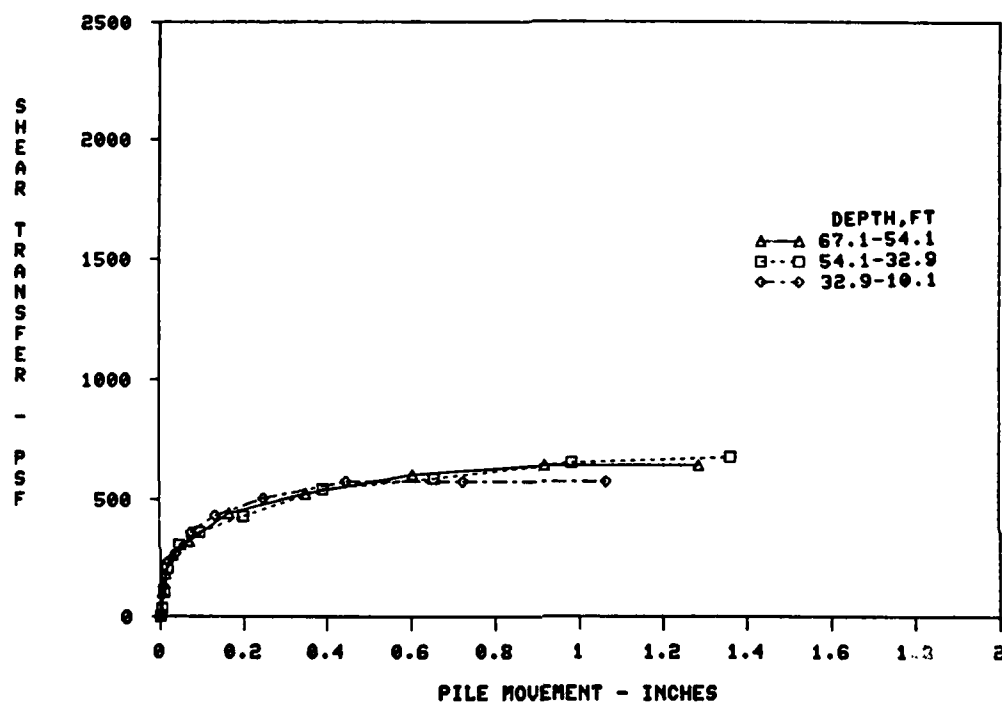


Figure B71. Adjusted $f-z$ Curves, Red River, Test Pile No. PT-A-3C

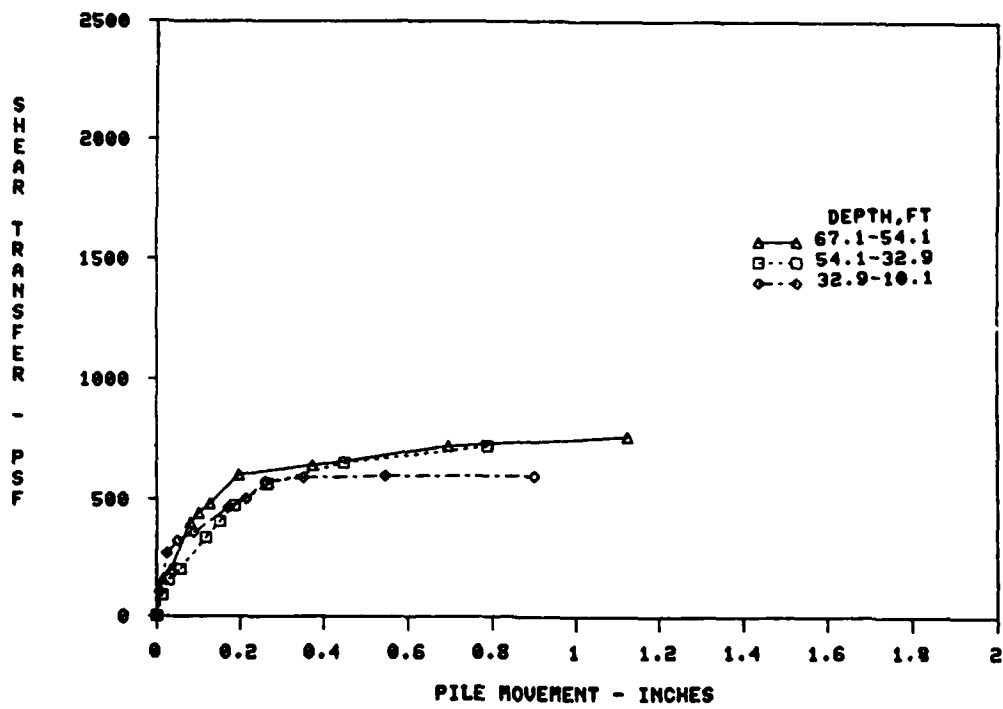


Figure B72. Adjusted $f-z$ Curves, Red River, Test Pile No. PT-A-3C Retest

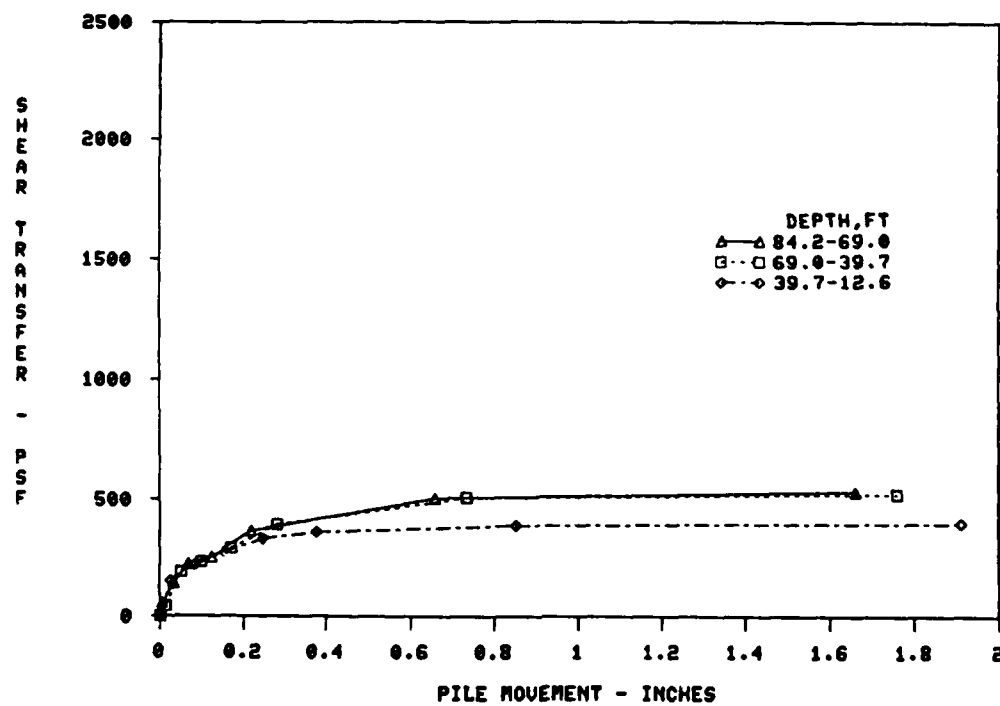


Figure B73. Adjusted f-z Curves, Red River, Test Pile No. PT-S-1C

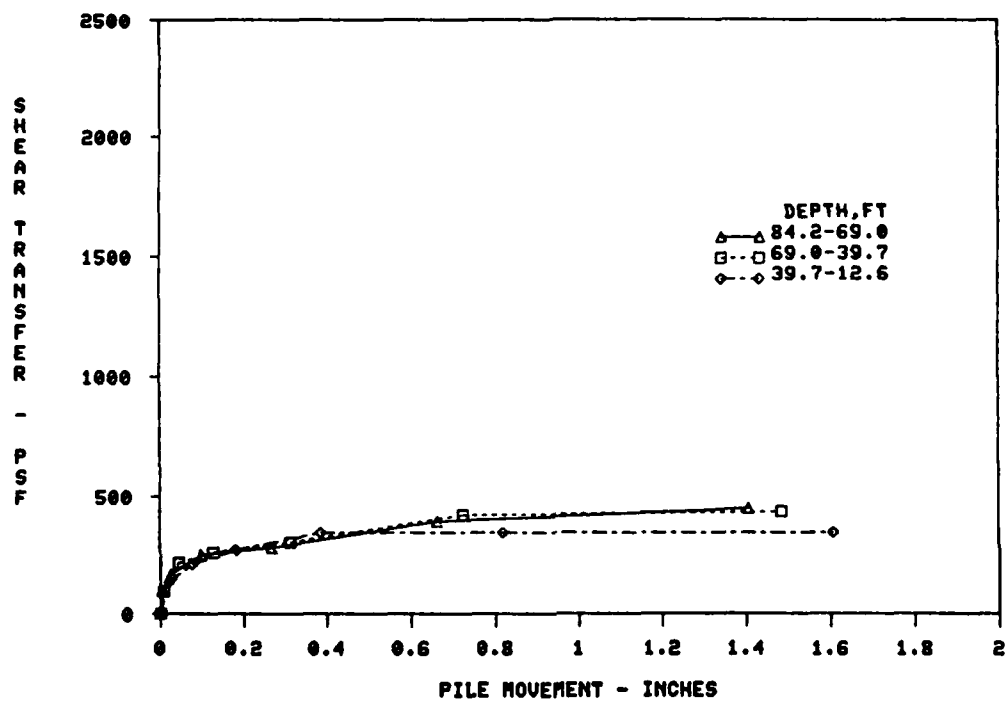


Figure B74. Adjusted f-z Curves, Red River, Test Pile No. PT-S-1C Retest

APPENDIX C

COMPARISON OF AVAILABLE CRITERIA TO FIELD
PILE TEST DATA

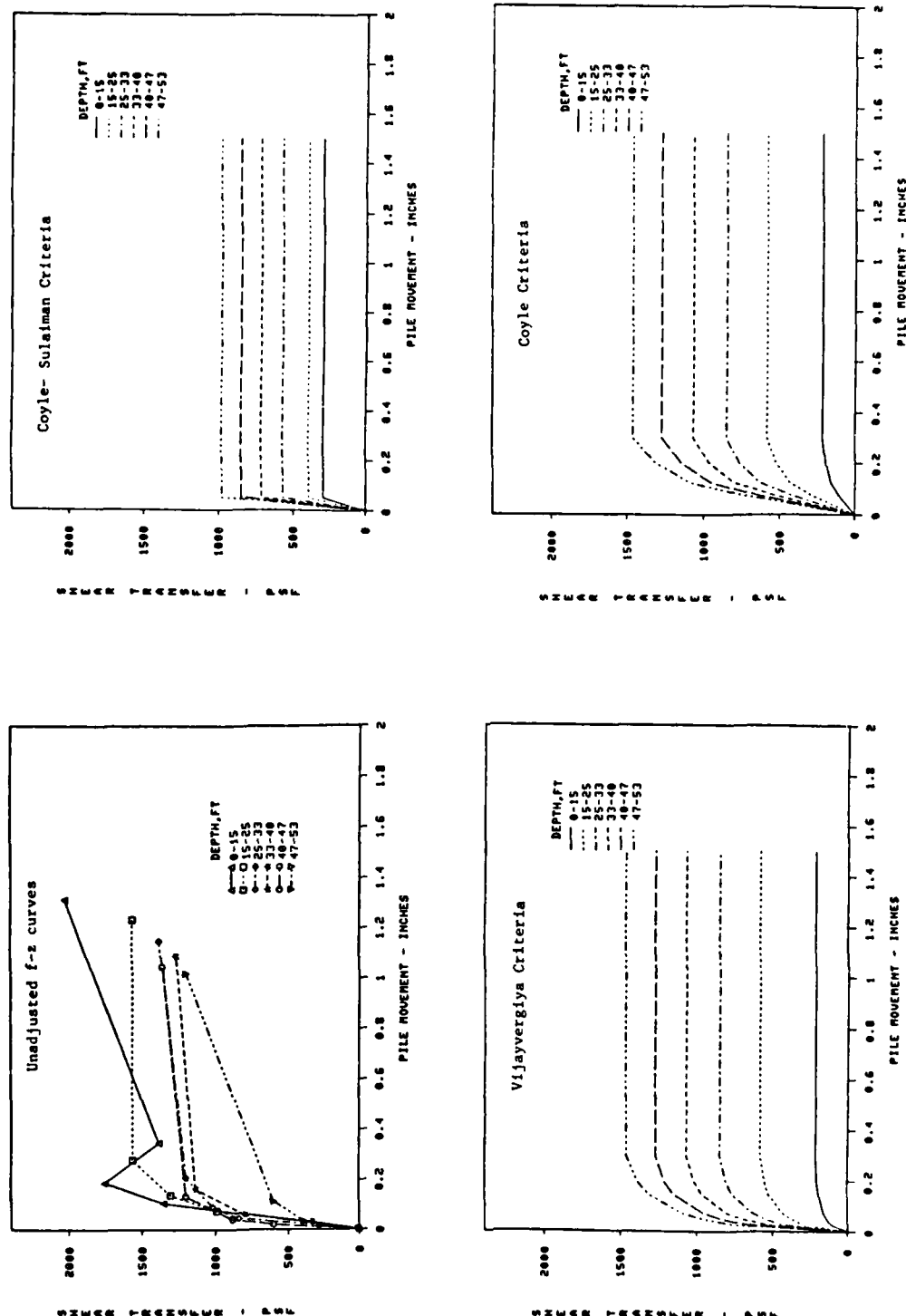


Figure C1. Comparison of f-z Criteria to Unadjusted Field Curves, Arkansas River, Test Pile No. 1

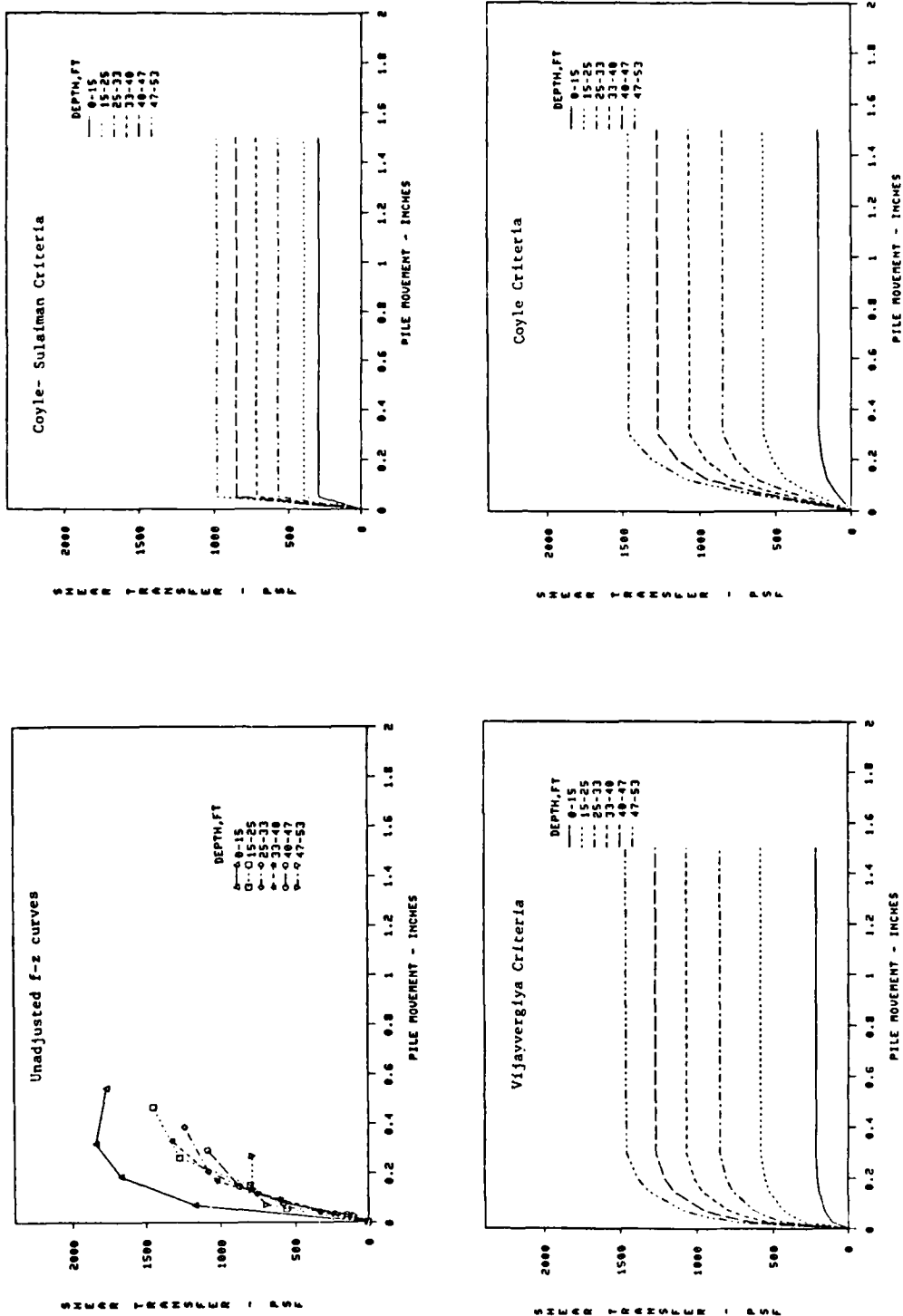


Figure C2. Comparison of f-z Criteria to Unadjusted Field Curves, Arkansas River, Test Pile No. 2

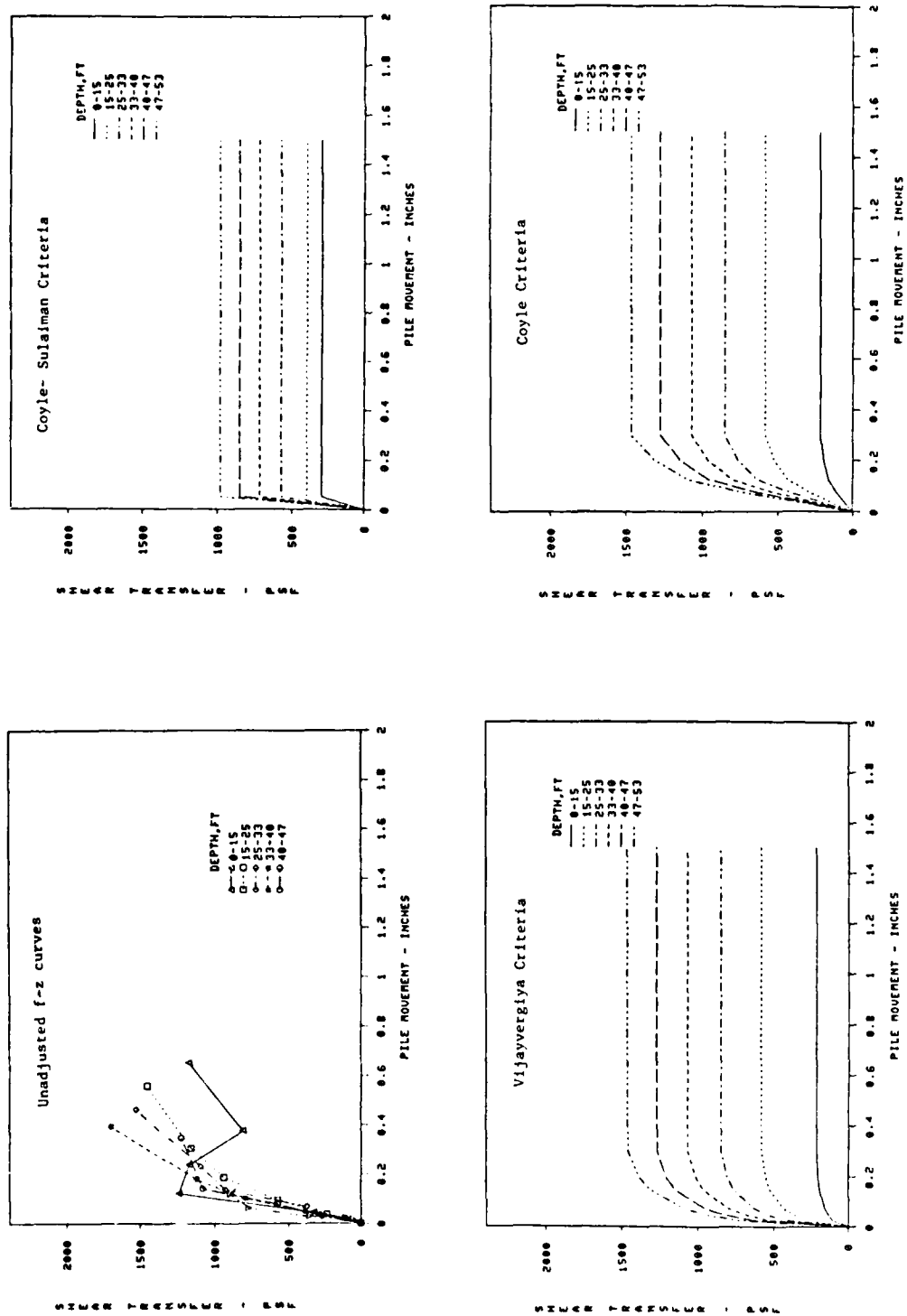


Figure C3. Comparison of f-z Criteria to Unadjusted Field Curves, Arkansas River, Test Pile No.2 Retest

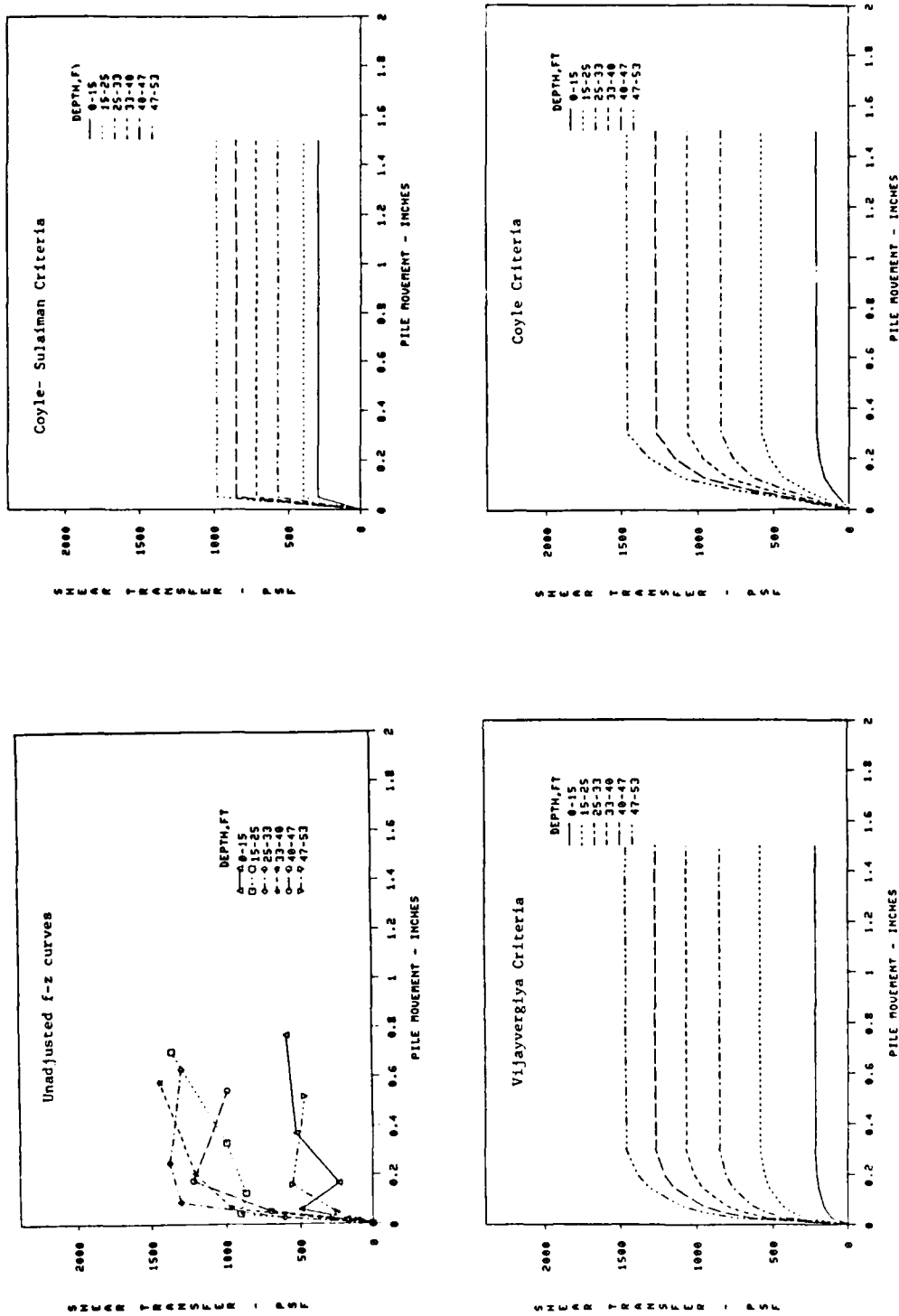


Figure C4. Comparison of f-z Criteria to Unadjusted Field Curves, Arkansas River, Test Pile No. 3

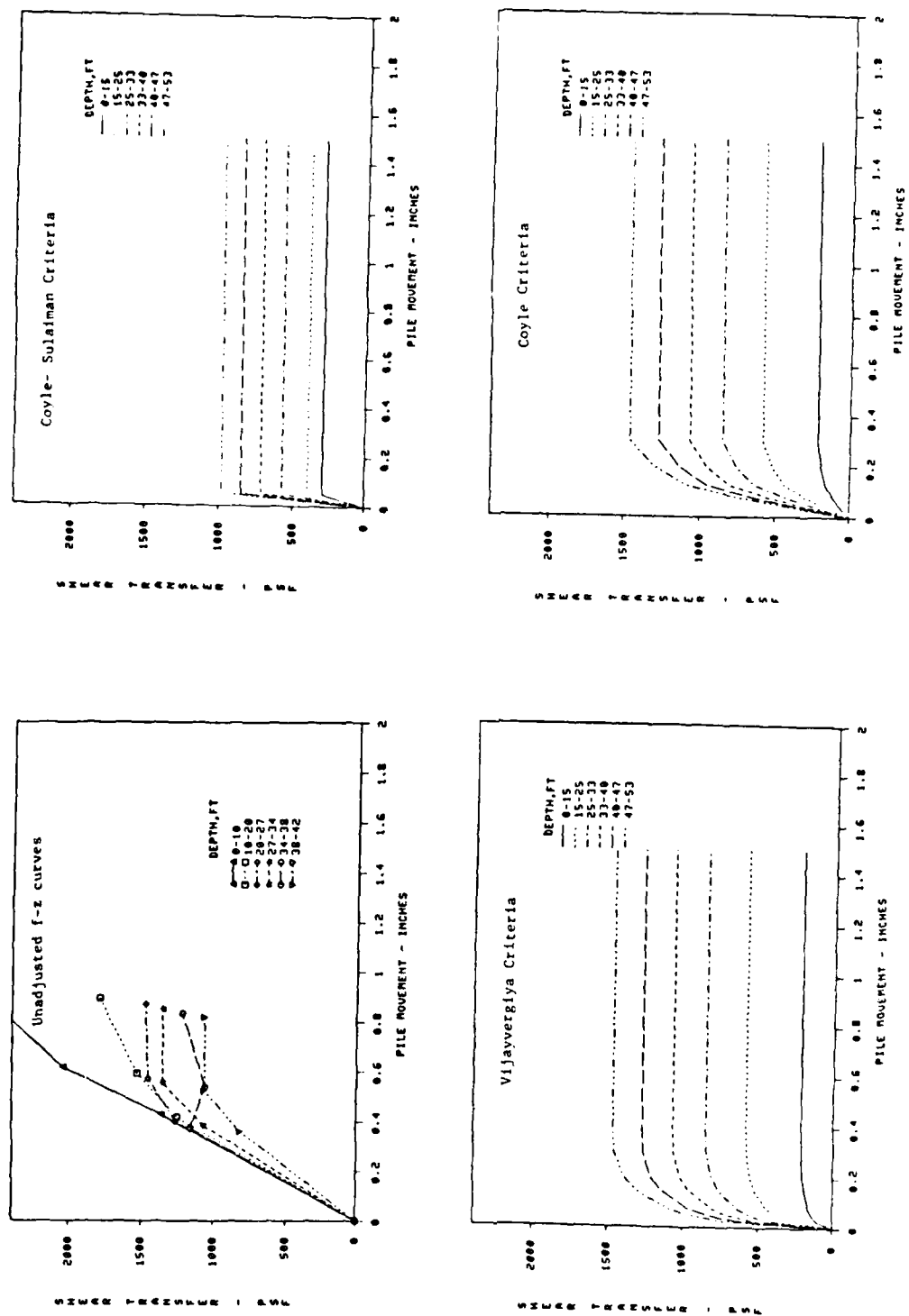


Figure C5. Comparison of f-z Criteria to Unadjusted Field Curves, Arkansas River, Test Pile No. 6

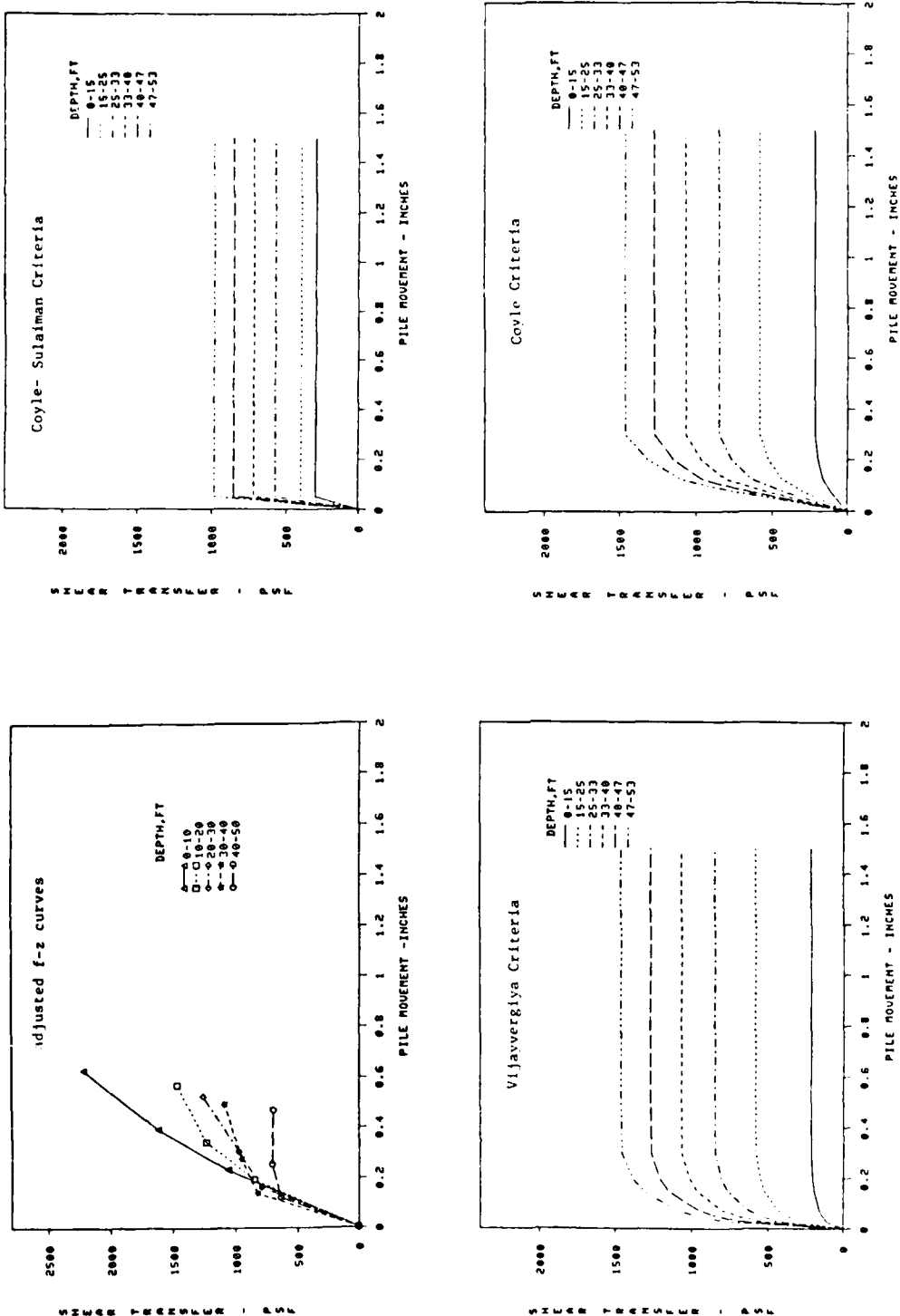


Figure C6. Comparison of f-z Criteria to Unadjusted Field Curves, Arkansas River, Test Pile No. 7, 14HP73

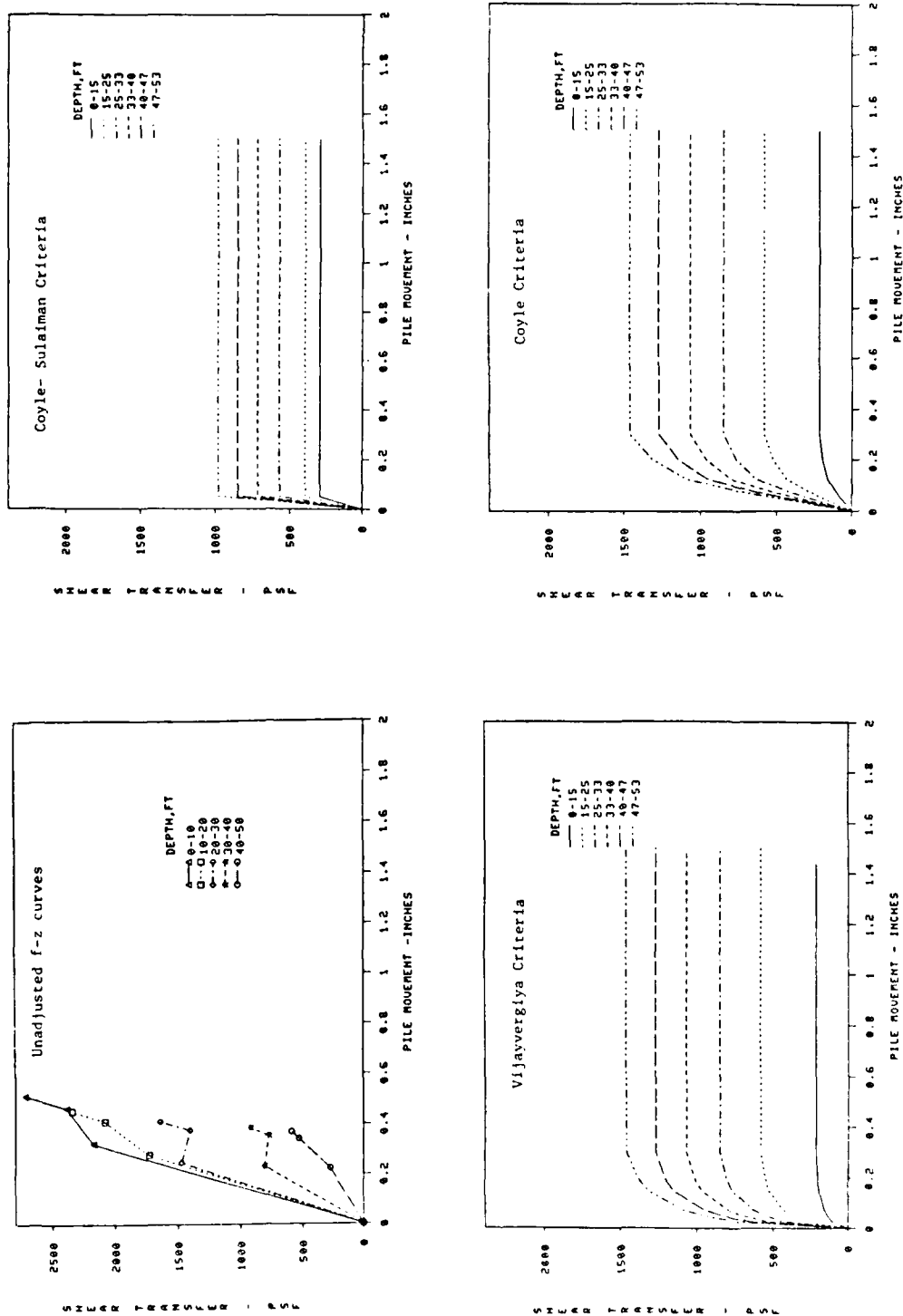


Figure C7. Comparison of f-z Criteria to Unadjusted Field Curves, Arkansas River, Test Pile No. 9, 14HP73

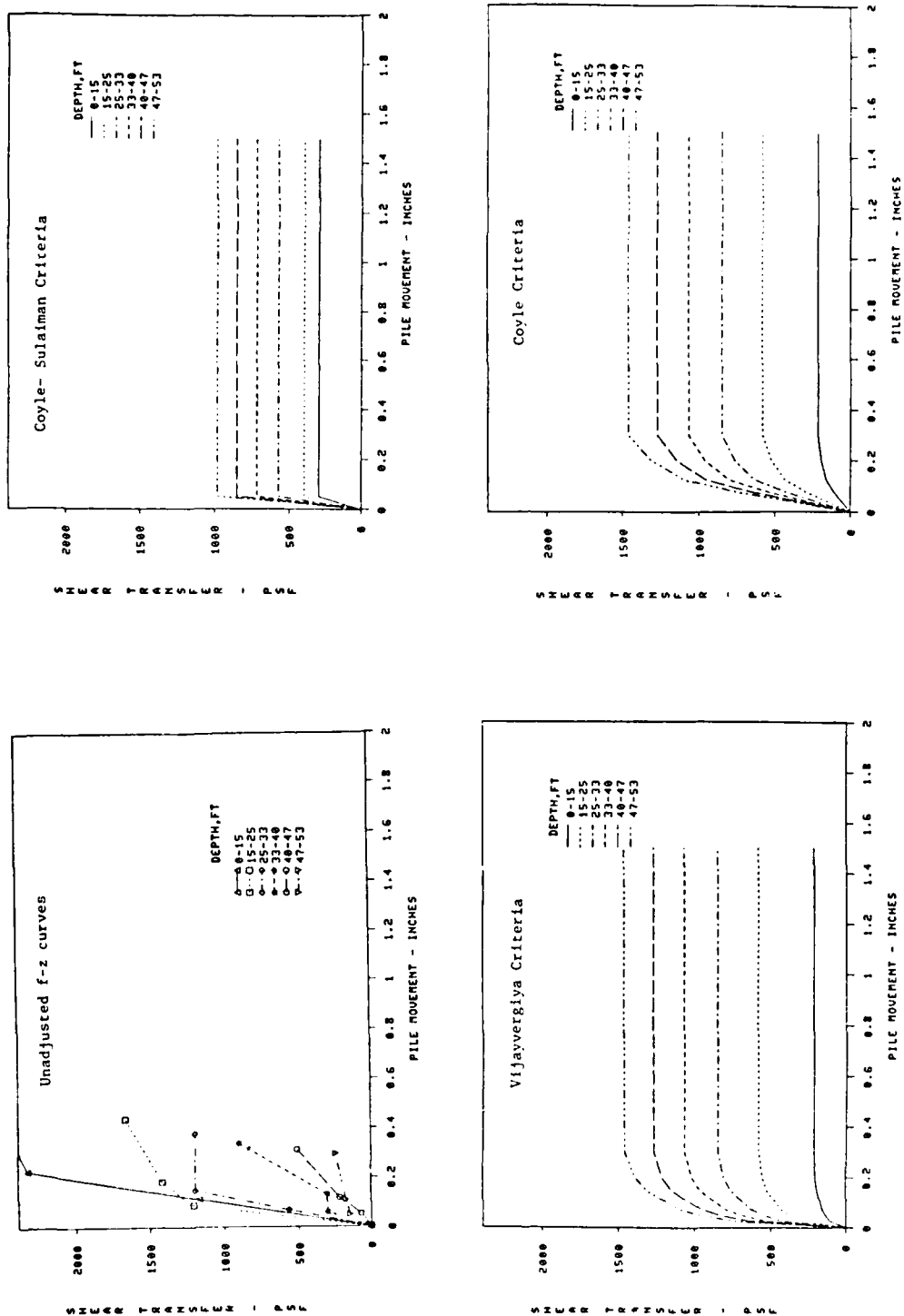


Figure C8. Comparison of f-z Criteria to Unadjusted Field Curves, Arkansas River, Test Pile No. 10

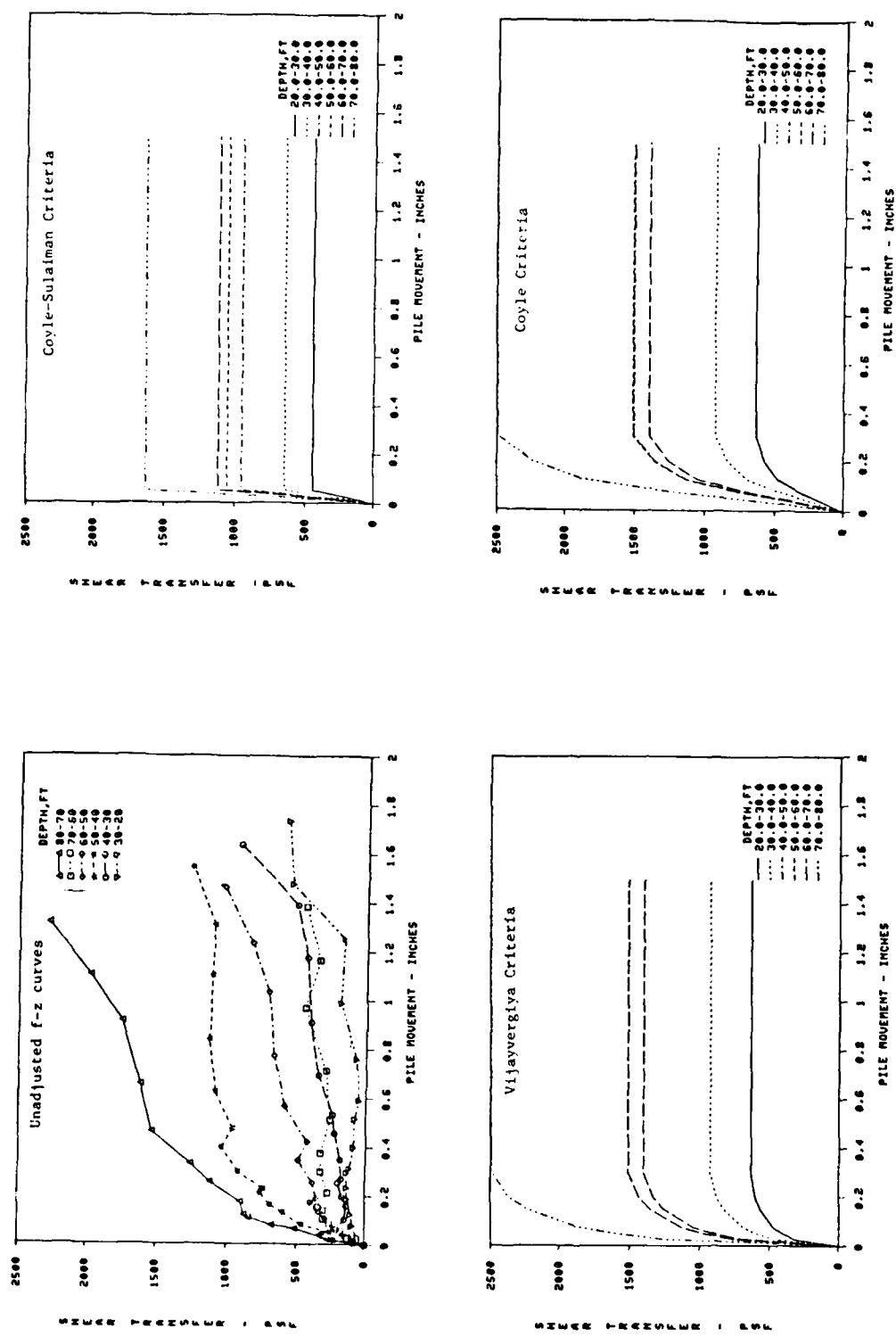


Figure C9. Comparison of f-z Criteria to Unadjusted Field Curves, Ascalmore Creek-Tippo Bayou, Test Pile No. 1

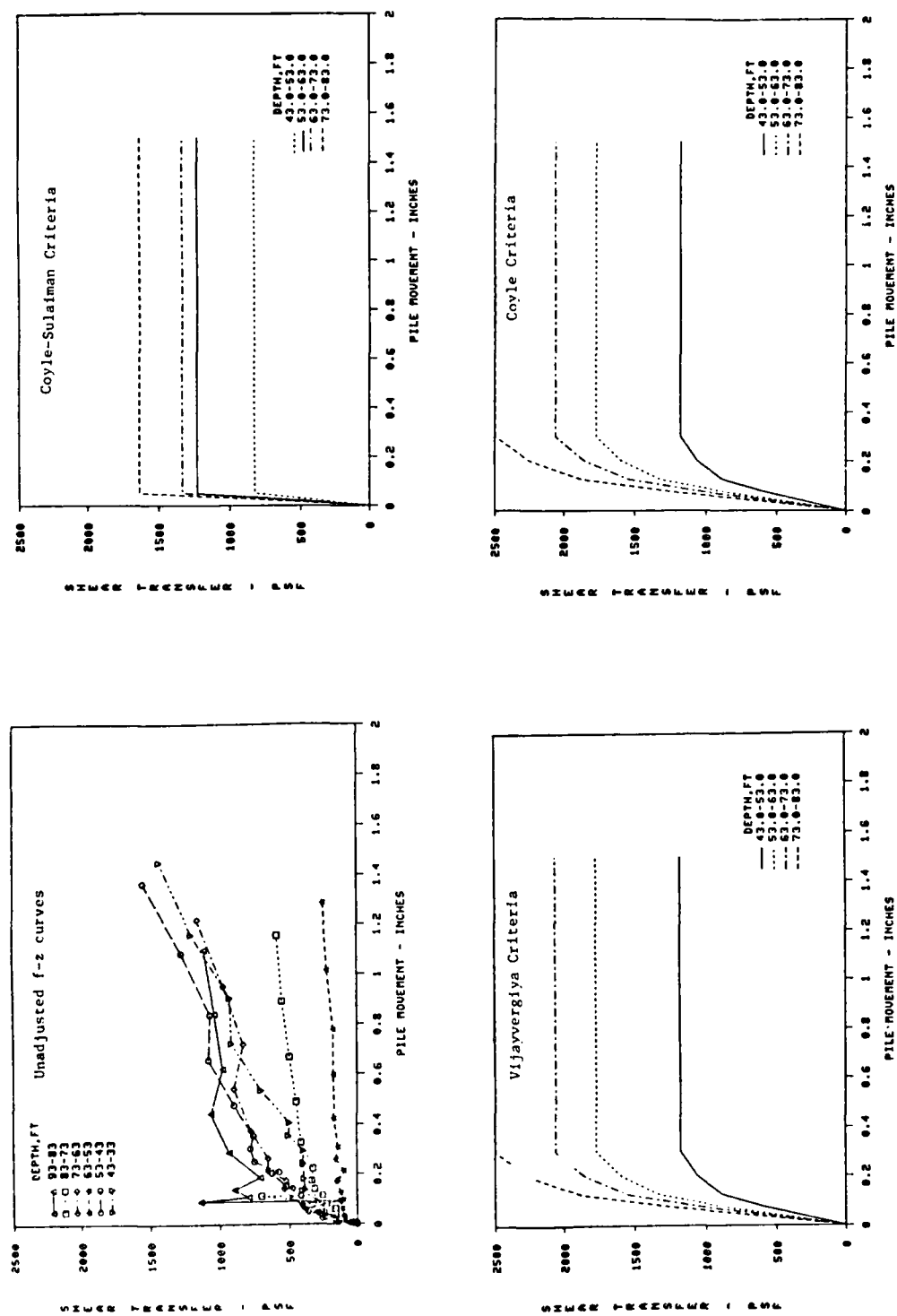


Figure C10. Comparison of f-z Criteria to Unadjusted Field Curves, Ascalmore Creek-Tippo Bayou, Test Pile No. 2

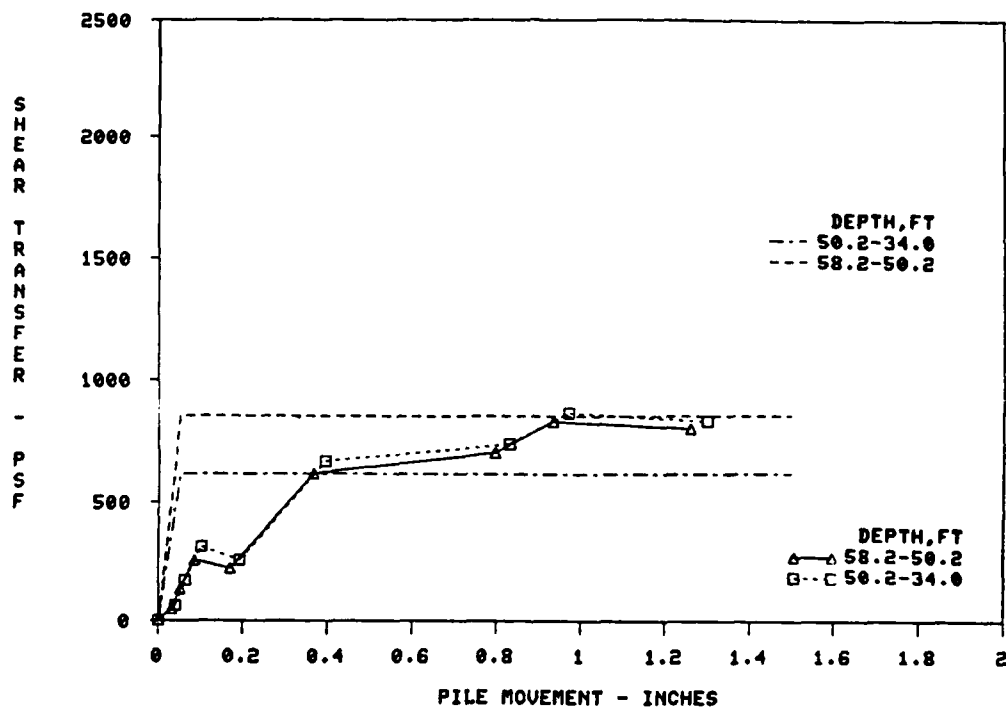


Figure C11. Comparison of f-z Criteria to Unadjusted Field Curves, Red River, Test Pile No. PT-A-1C, Coyle-Sulaiman Criteria

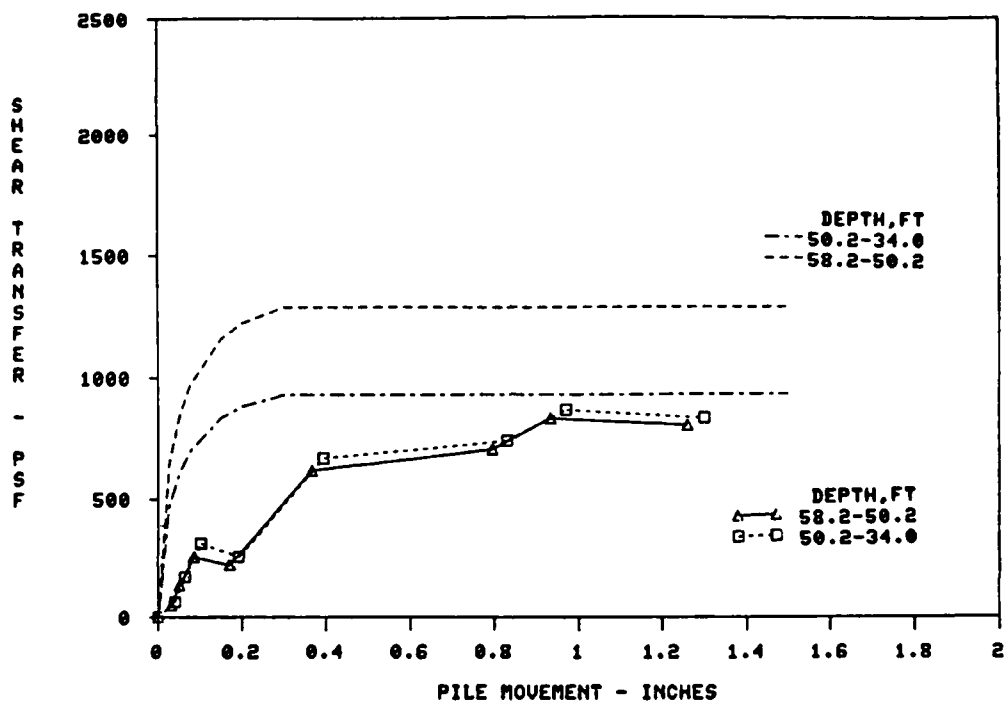


Figure C12. Comparison of f-z Criteria to Unadjusted Field Curves, Red River, Test Pile No. PT-A-1C, Vijayvergiya Criteria

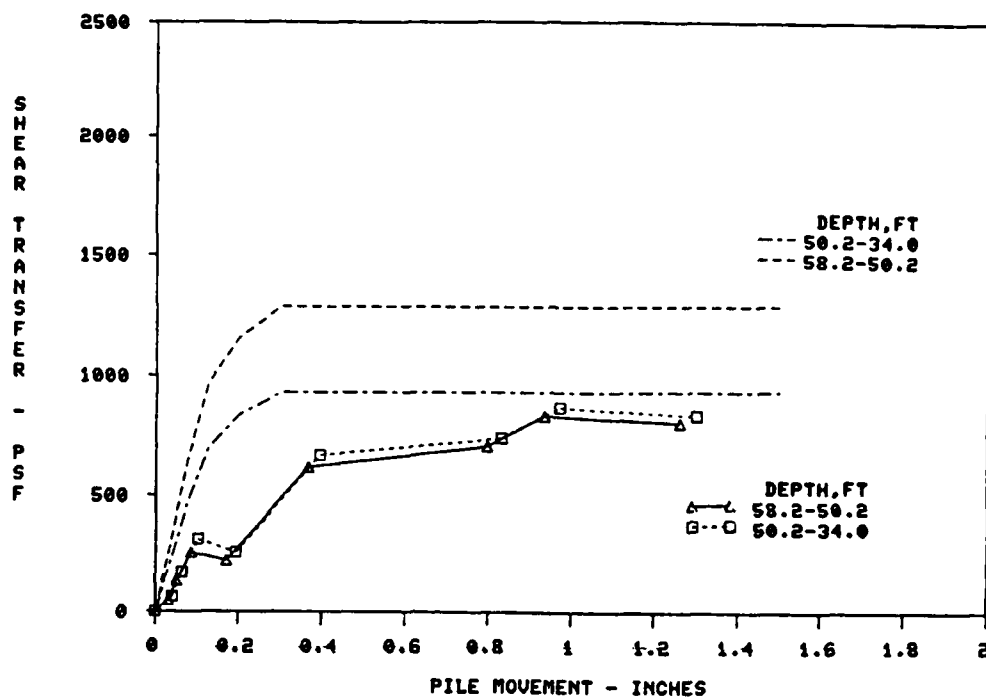


Figure C13. Comparison of f-z Criteria to Unadjusted Field Curves, Red River, Test Pile No. PT-A-1C, Coyle Criteria

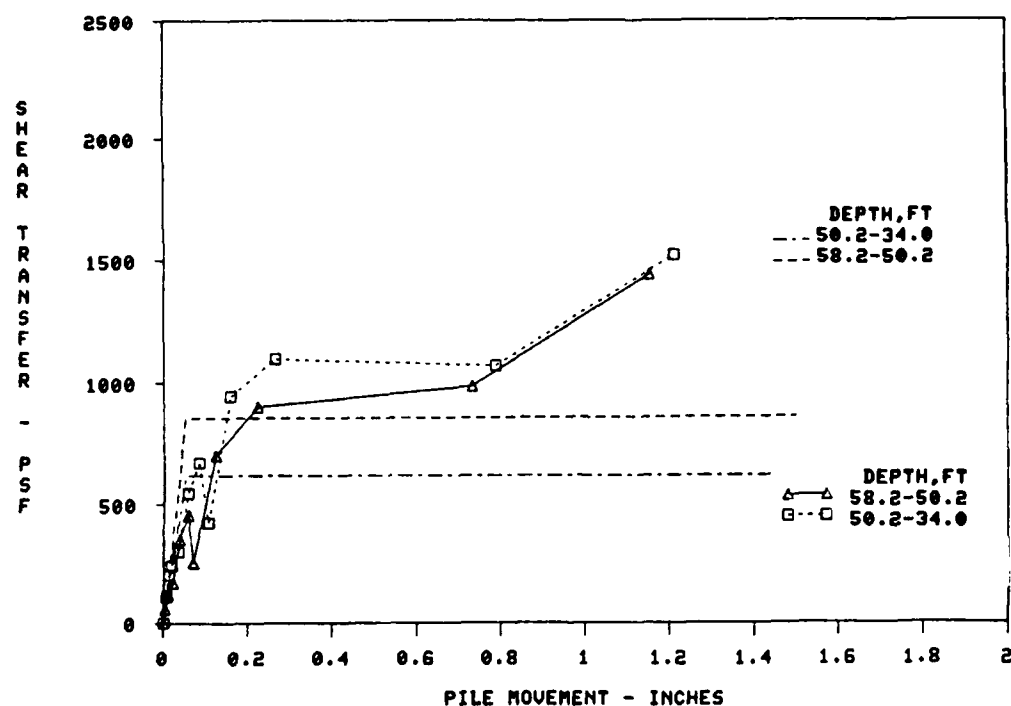


Figure C14. Comparison of f-z Criteria to Unadjusted Field Curves, Red River, Test Pile No. PT-A-1C Retest, Coyle-Sulaiman Criteria

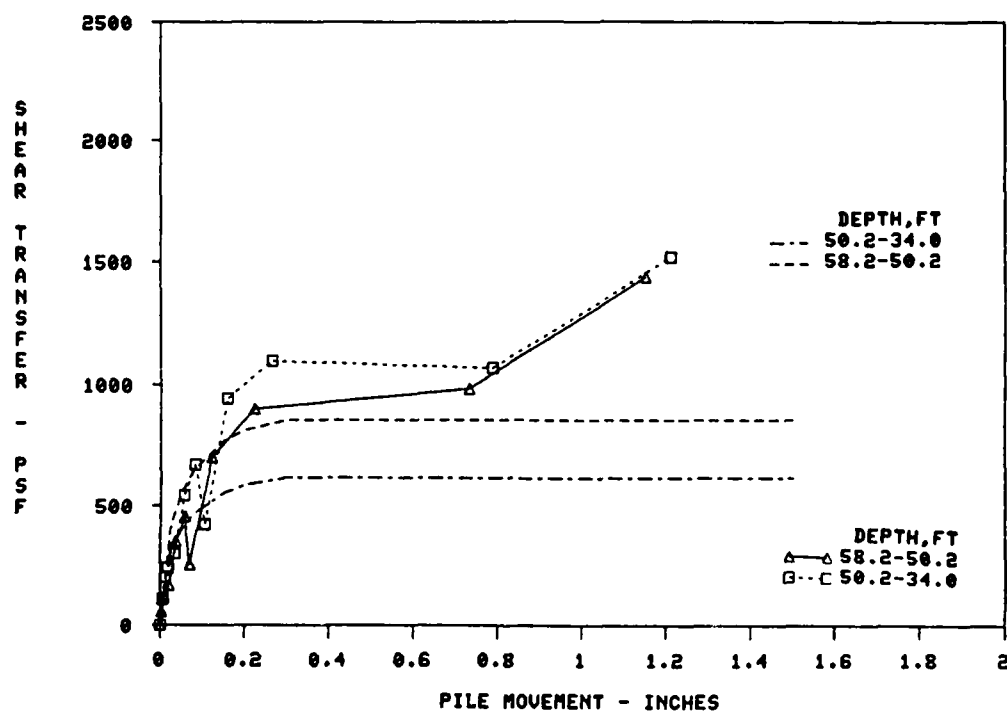


Figure C15. Comparison of f-z Criteria to Unadjusted Field Curves, Red River, Test Pile No. PT-A-1C, Vijayvergiya Criteria

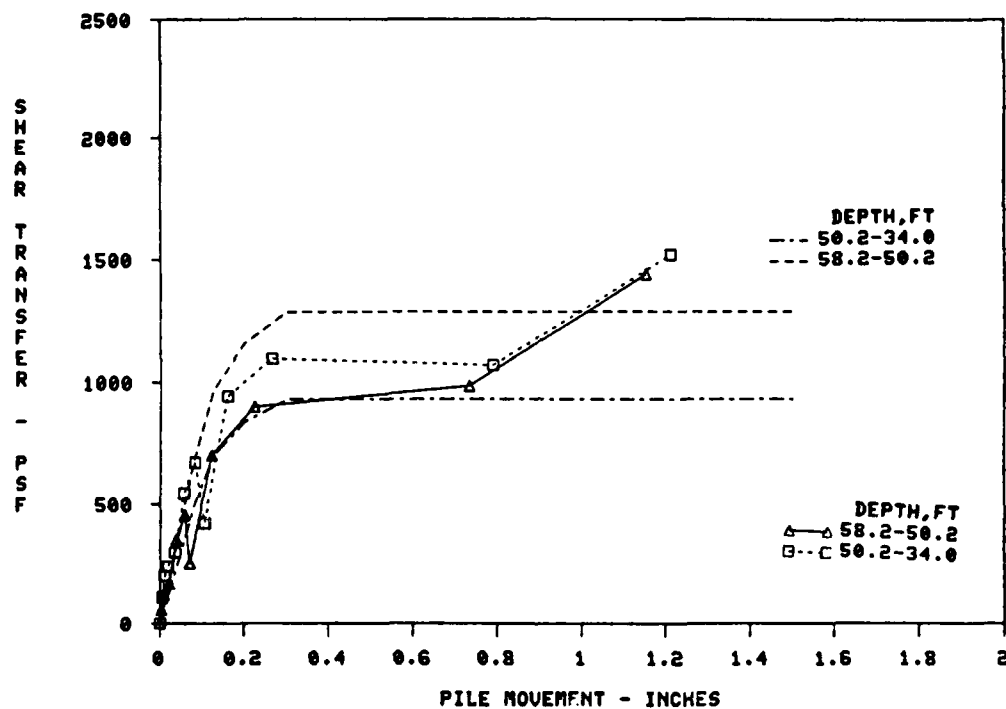


Figure C.16. Comparison of f-z Criteria to Unadjusted Field Curves, Red River, Test Pile No. PT-A-1C Retest, Coyle Criteria

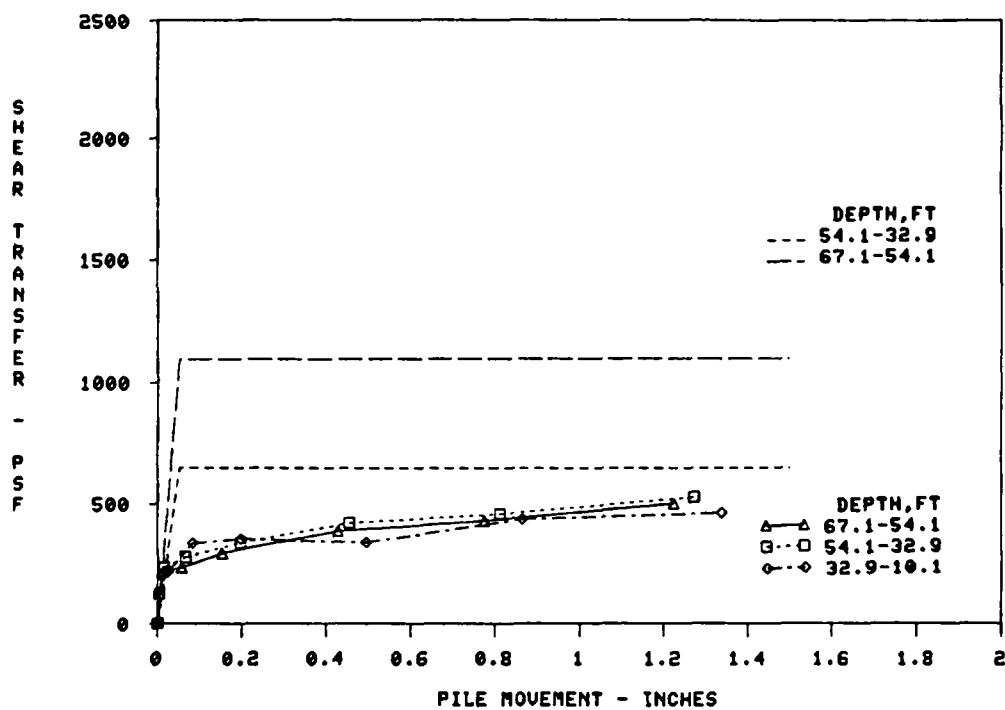


Figure C17. Comparison of f-z Criteria to Unadjusted Field Curves, Red River, Test Pile No. PT-A-2C, Coyle-Sulaiman Criteria

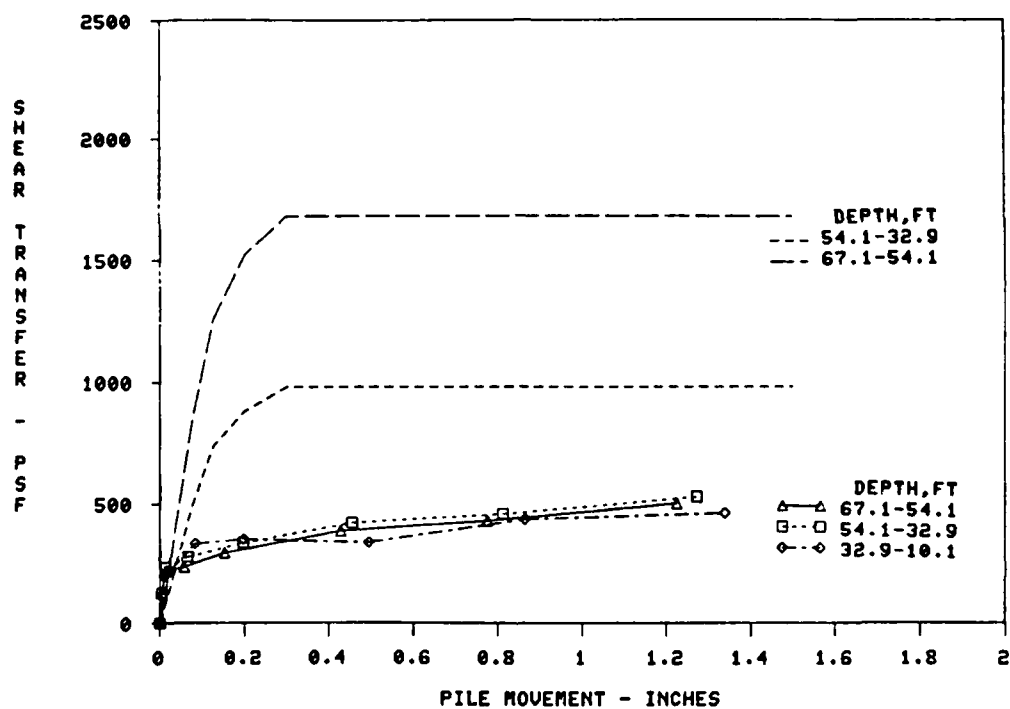


Figure C18. Comparison of f-z Criteria to Unadjusted Field Curves, Red River, Test Pile No. PT-A-2C, Coyle Criteria

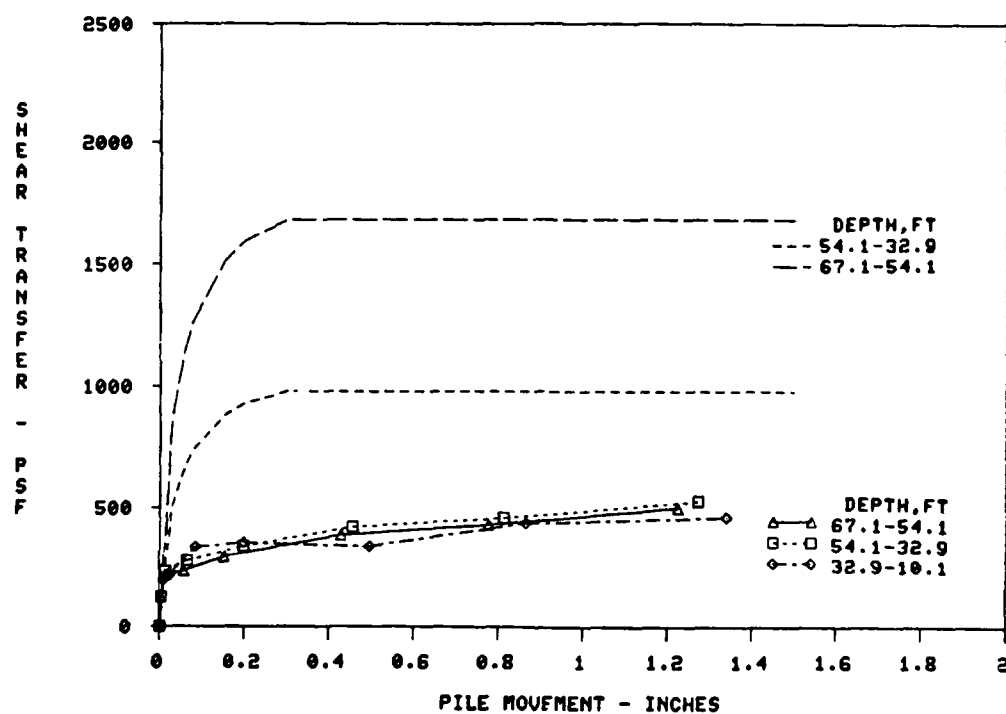


Figure C19. Comparison of f-z Criteria to Unadjusted Field Curves, Red River, Test Pile No. PT-A-2C, Vijayvergiya Criteria

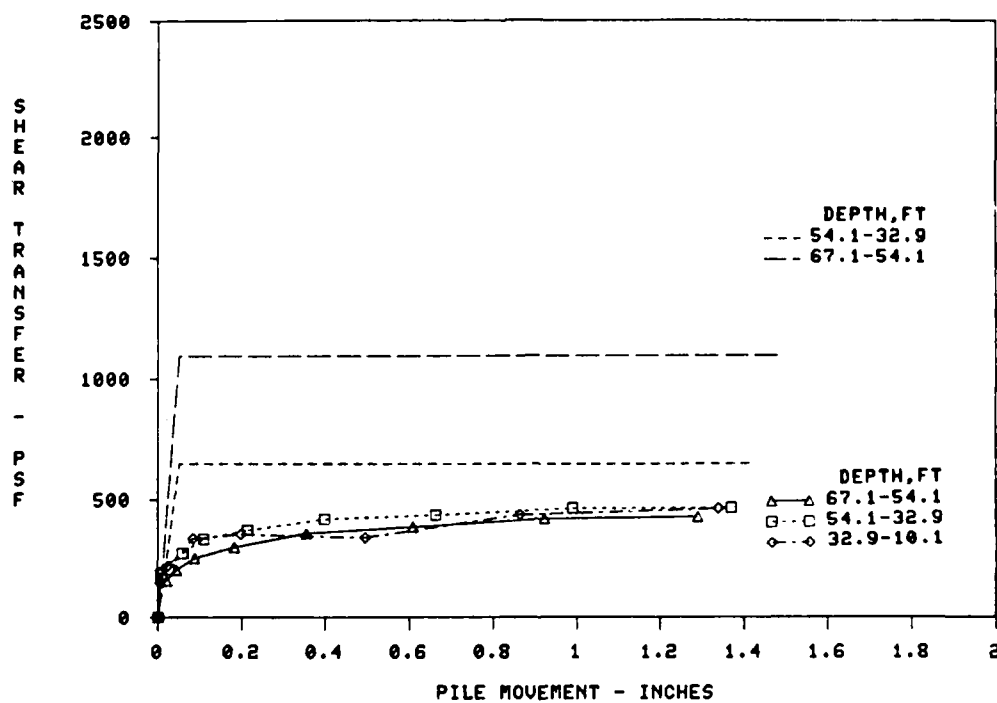


Figure C20. Comparison of f-z Criteria to Unadjusted Field Curves, Red River, Test Pile No. PT-A-3C, Coyle-Sulaiman Criteria

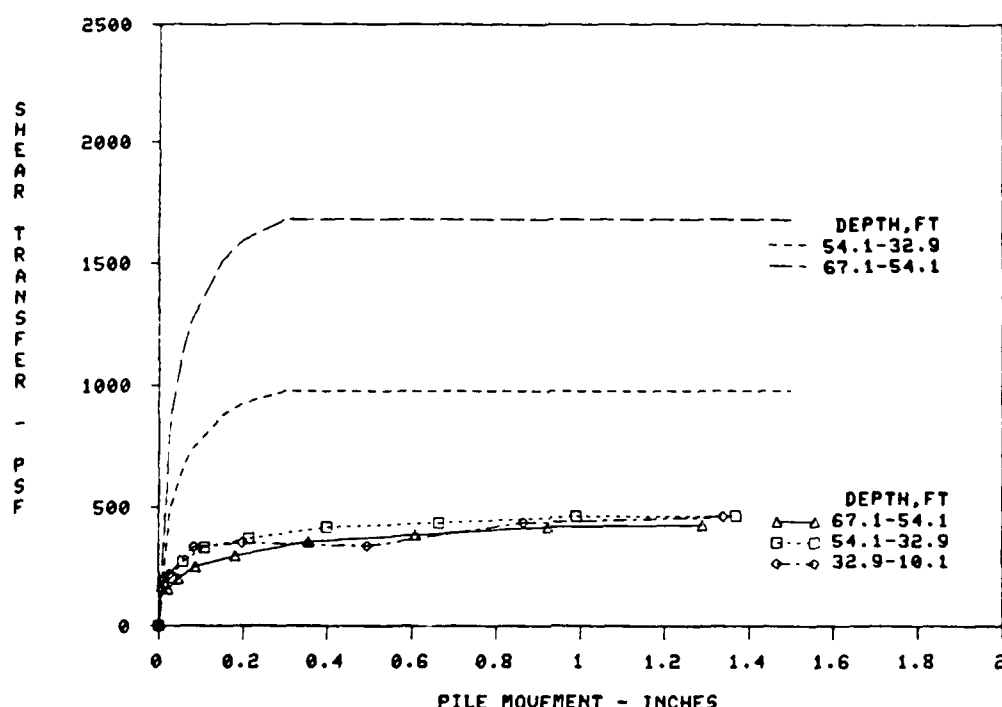


Figure C21. Comparison of f-z Criteria to Unadjusted Field Curves, Red River, Test Pile No. PT-A-3C, Vijayvergiya Criteria

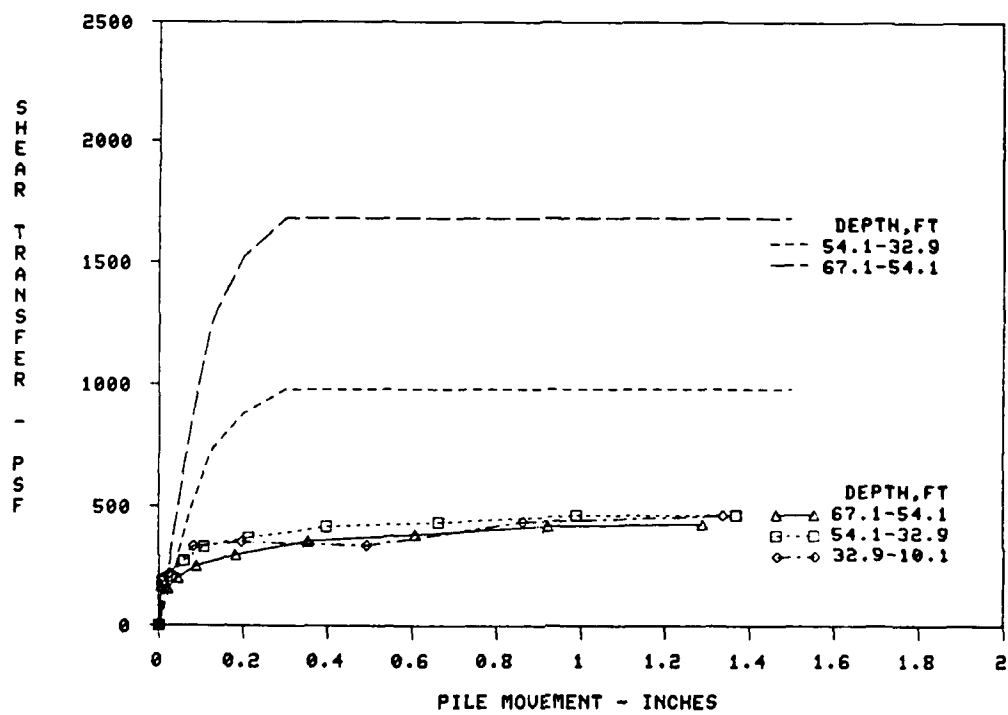


Figure C22. Comparison of f-z Criteria to Unadjusted Field Curves, Red River, Test Pile No. PT-A-3C, Coyle Criteria

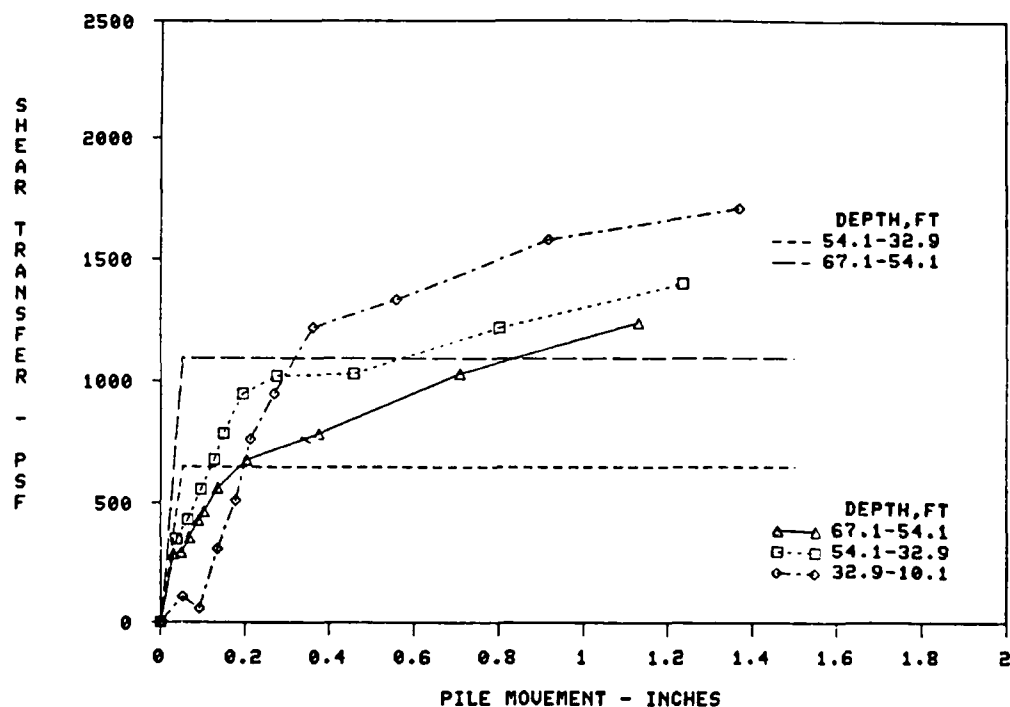


Figure C 23. Comparison of f- z Criteria to Unadjusted Field Curves, Red River, Test Pile No. PT-A-3C Retest, Coyle-Sulaiman Criteria

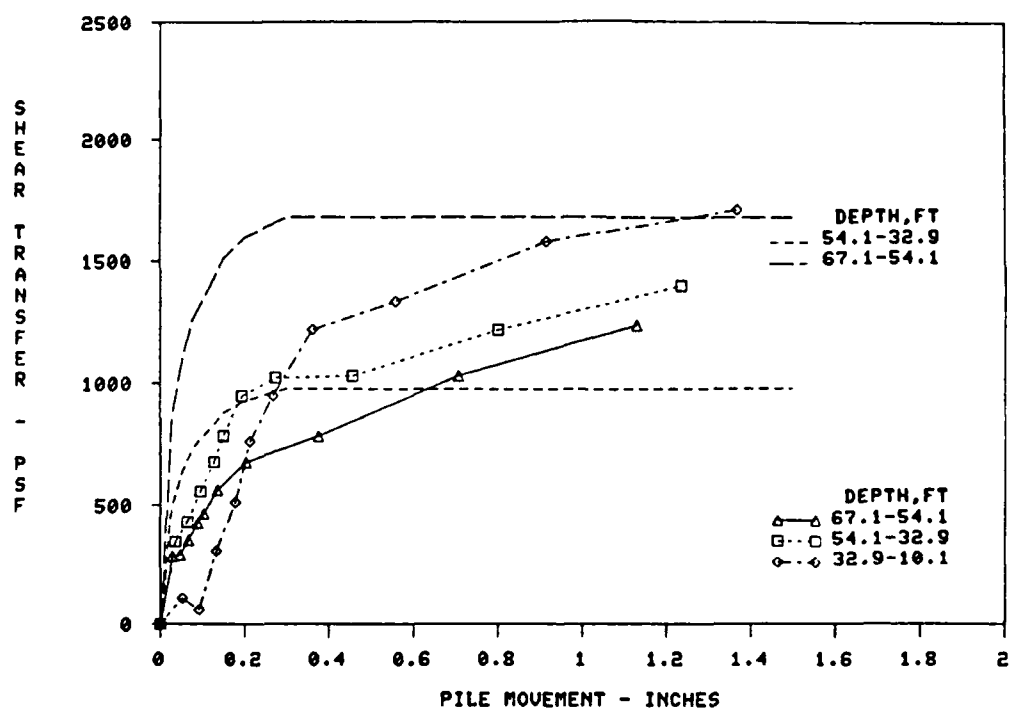


Figure C24. Comparison of f-z Criteria to Unadjusted Field Curves, Red River, Test Pile No. PT-A-3C Retest, Vijayvergiya Criteria

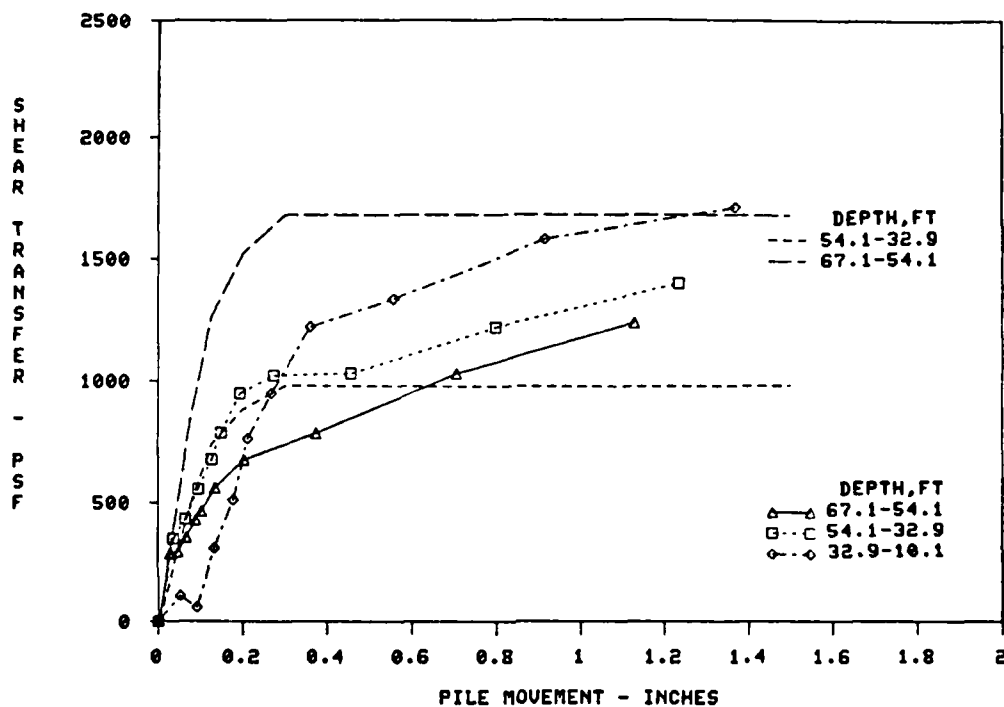


Figure C25. Comparison of f-z Criteria to Unadjusted Field Curves, Red River, Test Pile No. PT-A-3C Retest, Coyle Criteria

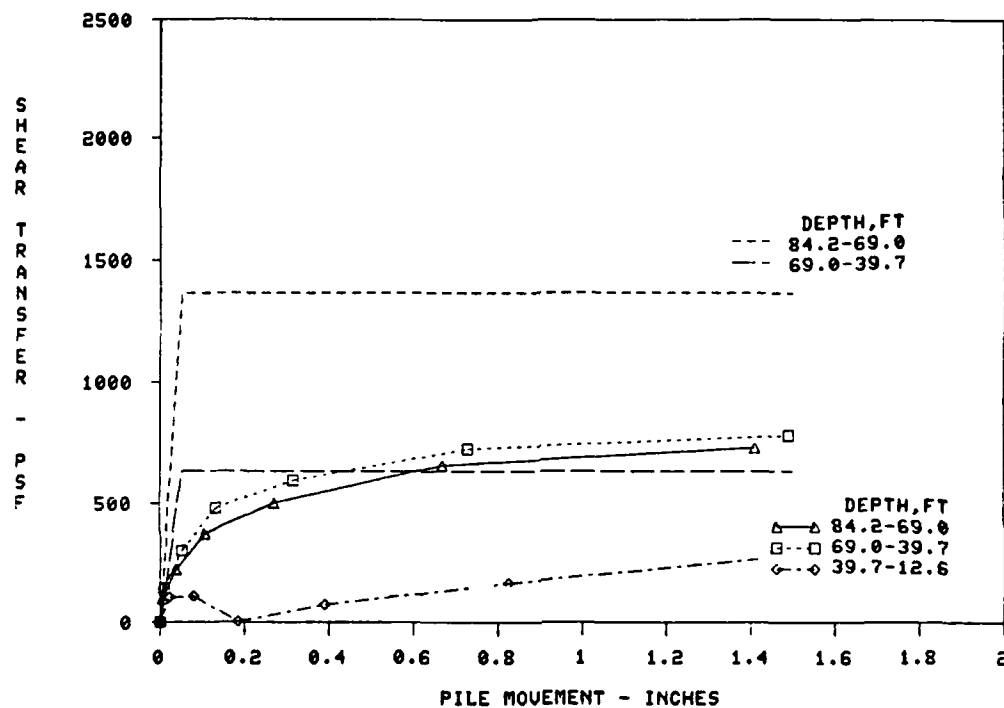


Figure C26. Comparison of f-z Criteria to Unadjusted Field Curves, Red River, Test Pile No. PT-S-1C, Coyle-Sulaiman Criteria

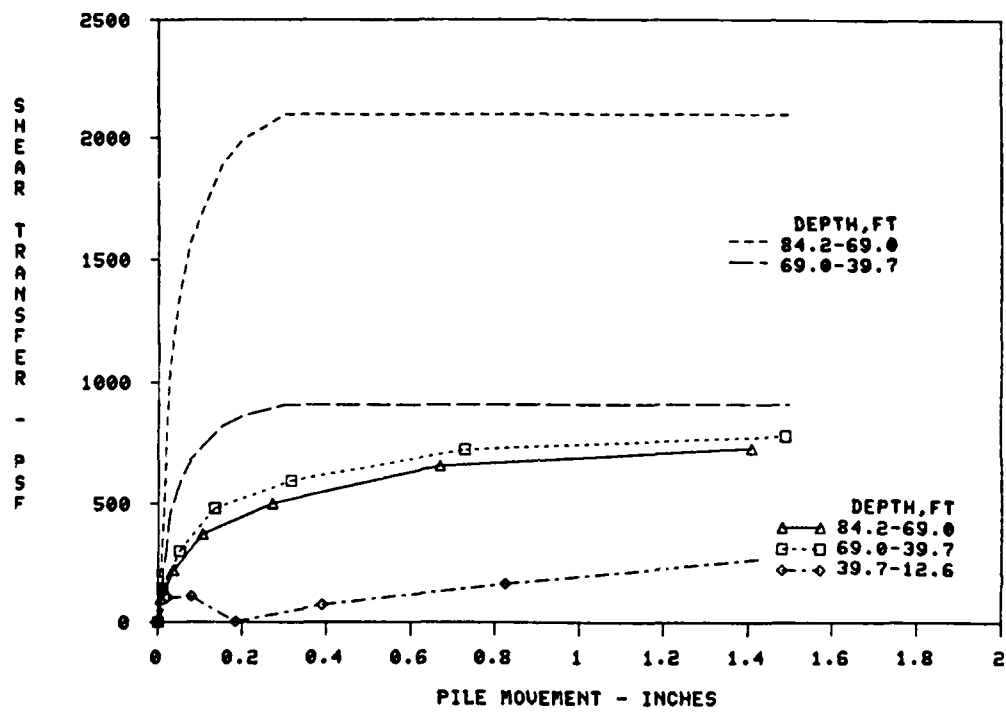


Figure C27. Comparison of f-z Criteria to Unadjusted Field Curves, Red River, Test Pile No. PT-S-1C, Vijayvergiya Criteria

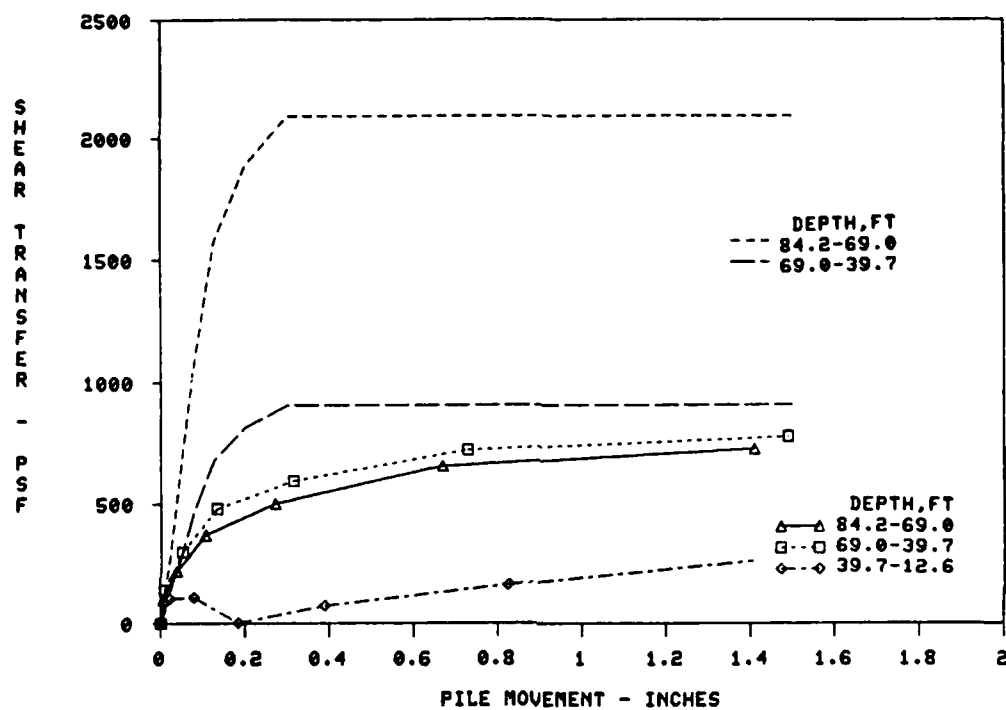


Figure C28. Comparison of f-z Criteria to Unadjusted Field Curves, Red River, Test Pile No. PT-S-1C, Coyle Criteria

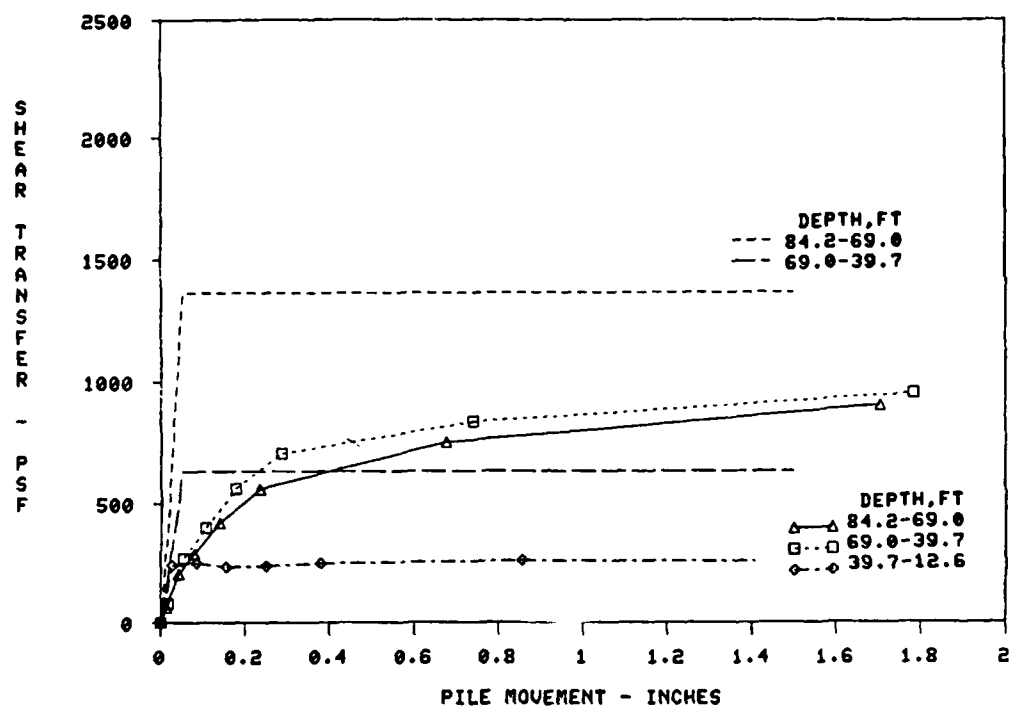


Figure C29, Comparison of f-z Criteria to Unadjusted Field Curves, Red River, Test Pile No. PT-S-1C Retest, Coyle-Sulaiman Criteria

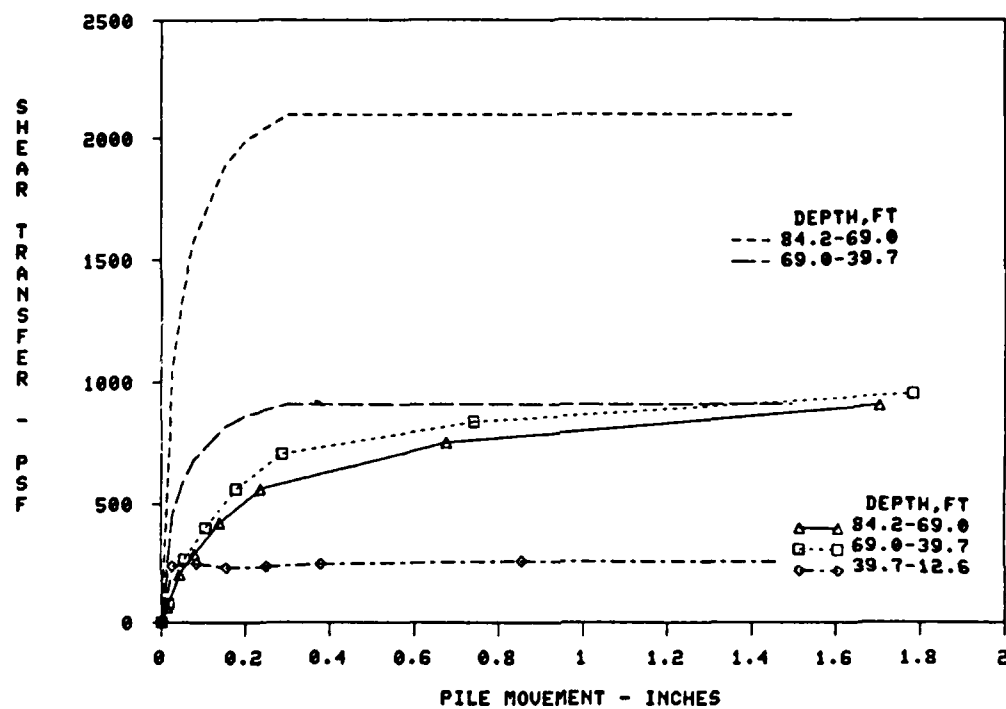


Figure C30. Comparison of f-z Criteria to Unadjusted Field Curves, Red River, Test Pile No. PT-S-1C Retest, Vijayvergiya Criteria

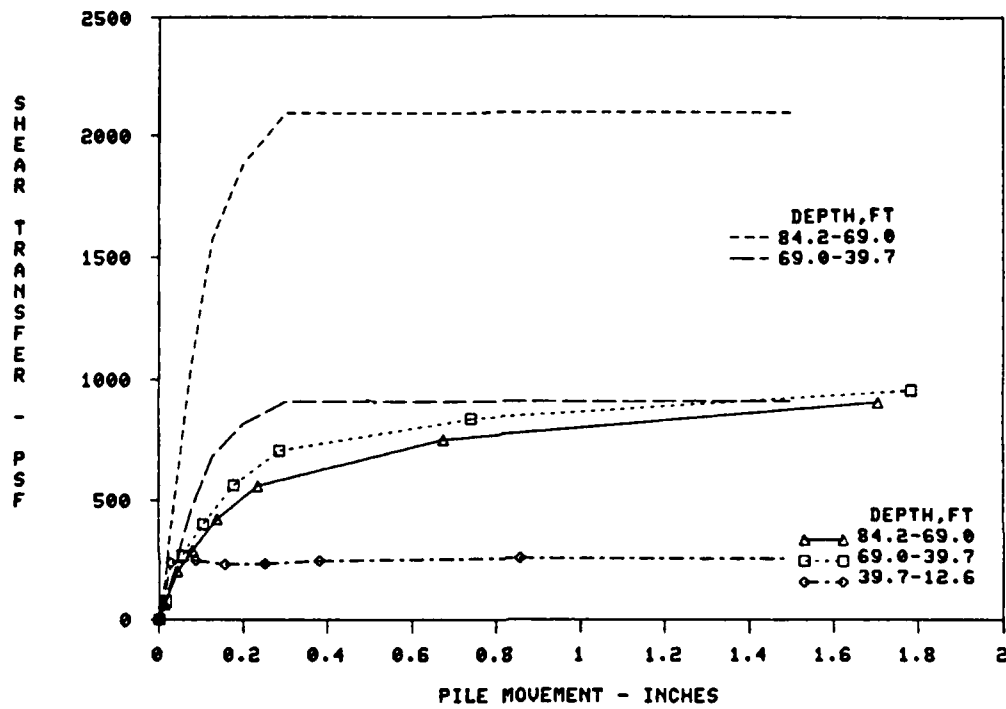


Figure C31. Comparison of $f-z$ Criteria to Unadjusted Field Curves, Red River, Test Pile No. PT-S-1C Retest, Coyle Criteria

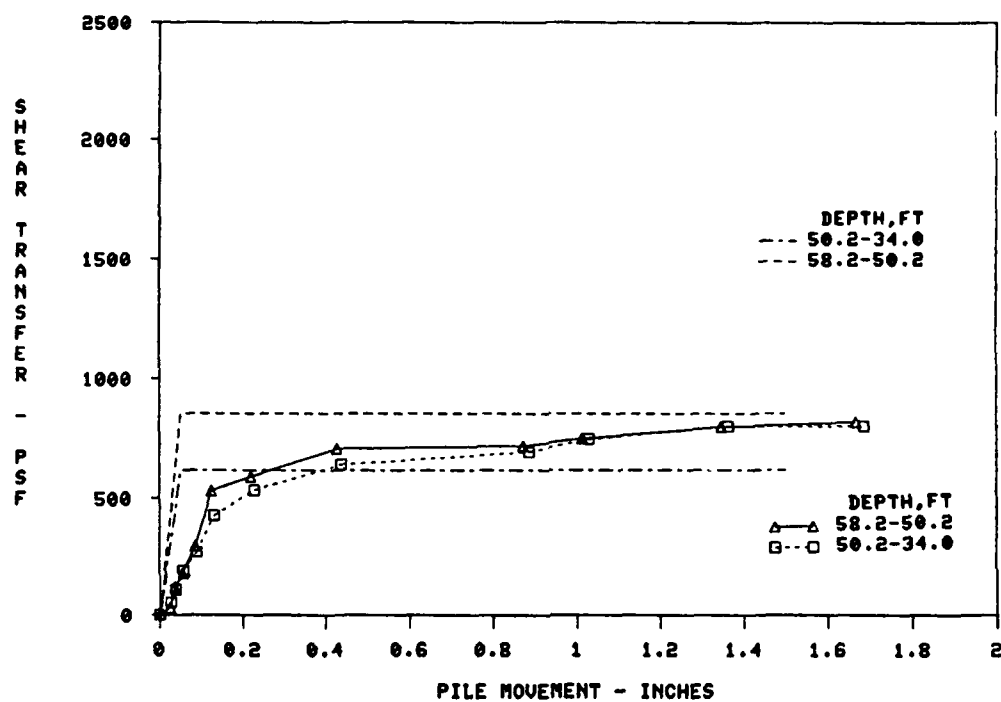


Figure C32. Comparison of f-z Criteria to Adjusted Field Curves, Red River, Test Pile No. PT-A-1C, Coyle-Sulaiman Criteria

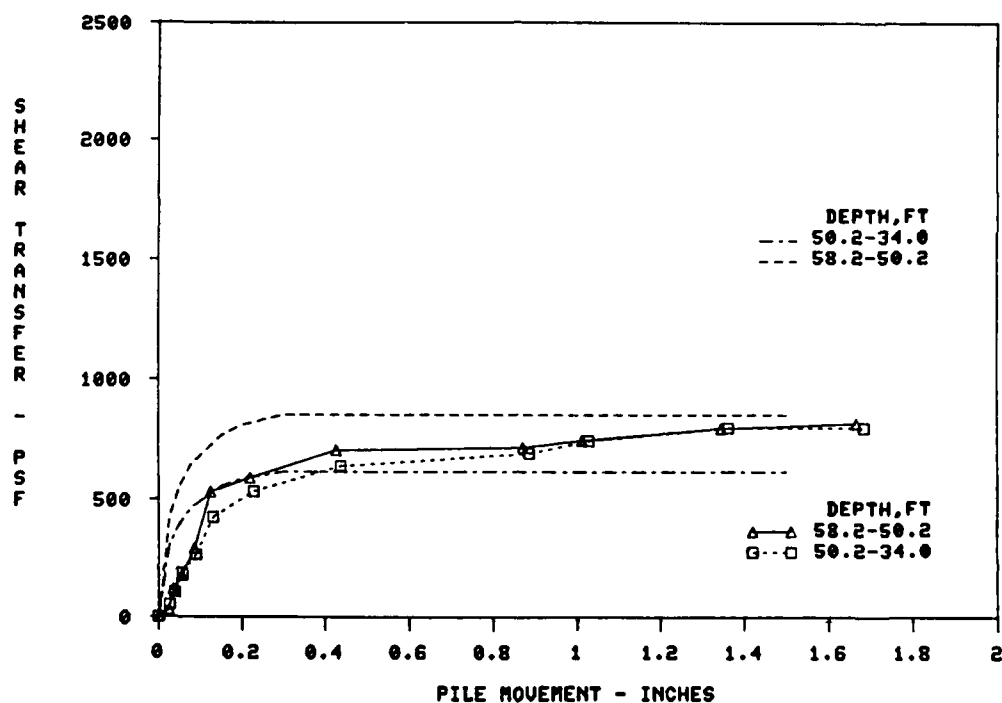


Figure C33. Comparison of f-z Criteria to Adjusted Field Curves, Red River, Test Pile No. PT-A-1C, Vijayvergiya Criteria

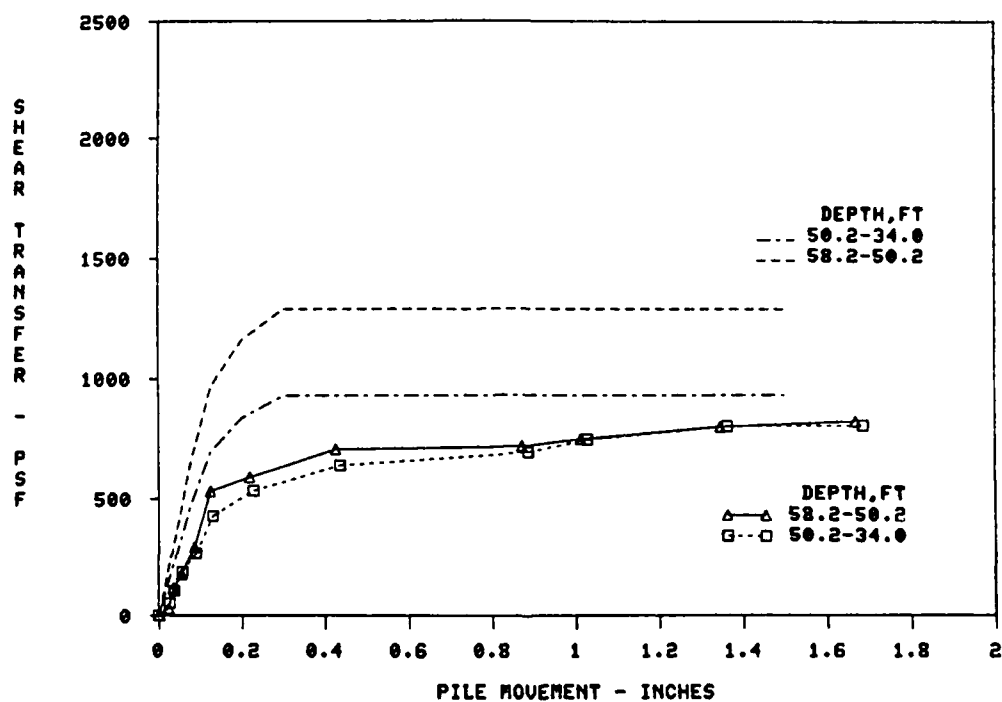


Figure C34. Comparison of f-z Criteria to Adjusted Field Curves, Red River, Test Pile No. PT-A-1C, Coyle Criteria

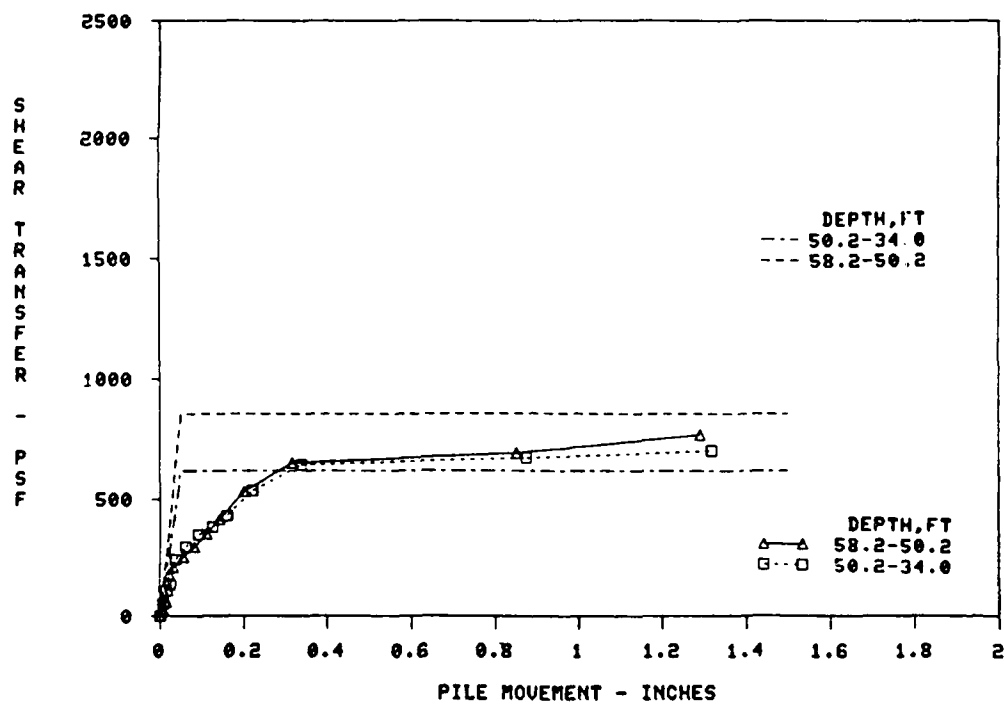


Figure C35. Comparison of f-z Criteria to Adjusted Field Curves, Red River, Test Pile No. PT-A-1C Retest, Coyle-Sulaiman Criteria

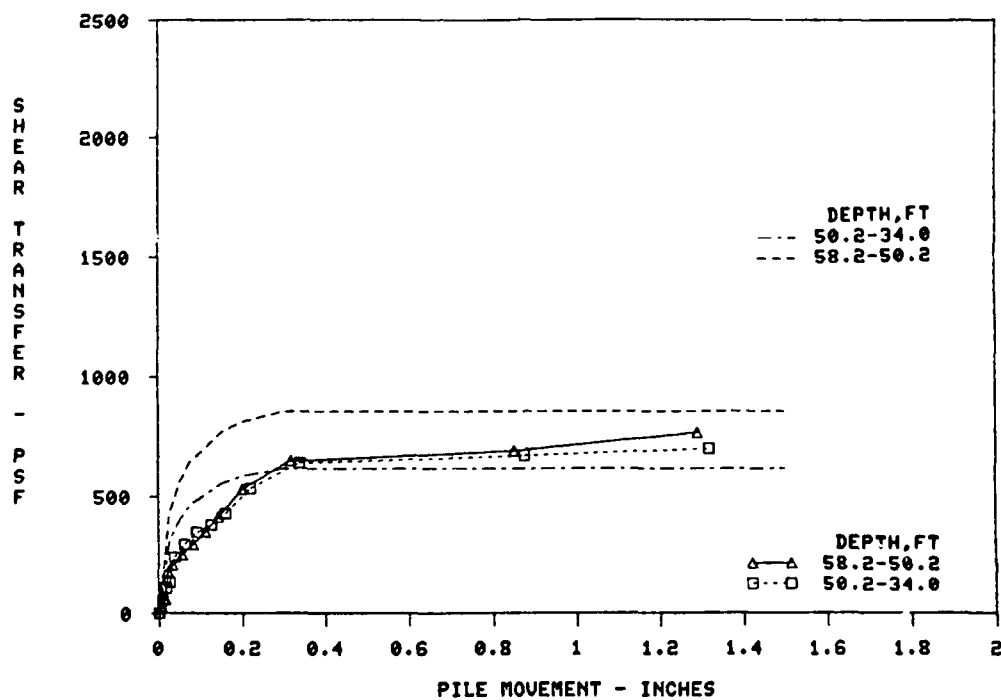


Figure C36. Comparison of f-z Criteria to Adjusted Field Curves, Red River, Test Pile No. PT-A-1C Retest, Vijayvergiya Criteria

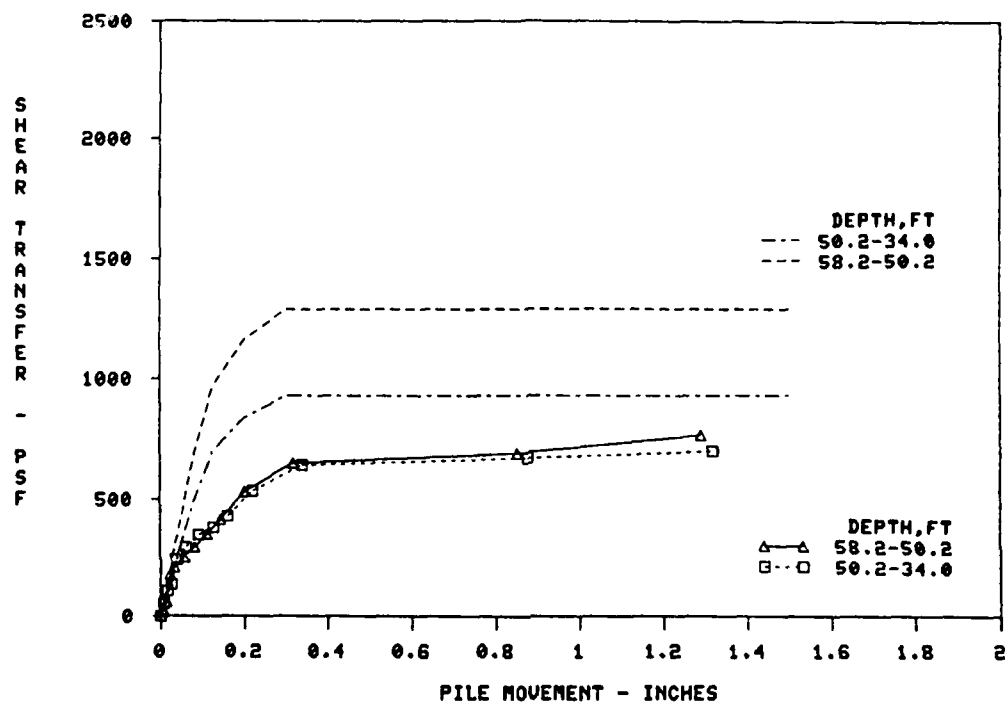


Figure C37. Comparison of f-z Criteria to Adjusted Field Curves, Red River, Test Pile No. FT-A-1C Retest, Coyle Criteria

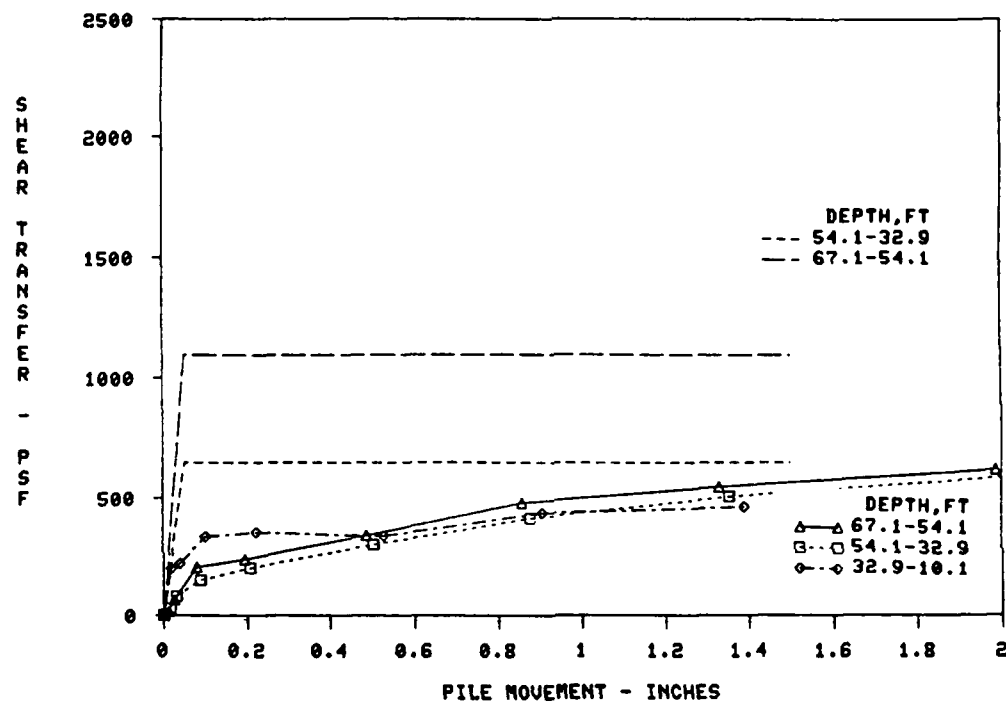


Figure C38. Comparison of f-z Criteria to Adjusted Field Curves, Red River, Test Pile No. PT-A-2C, Coyle-Sulaiman Criteria

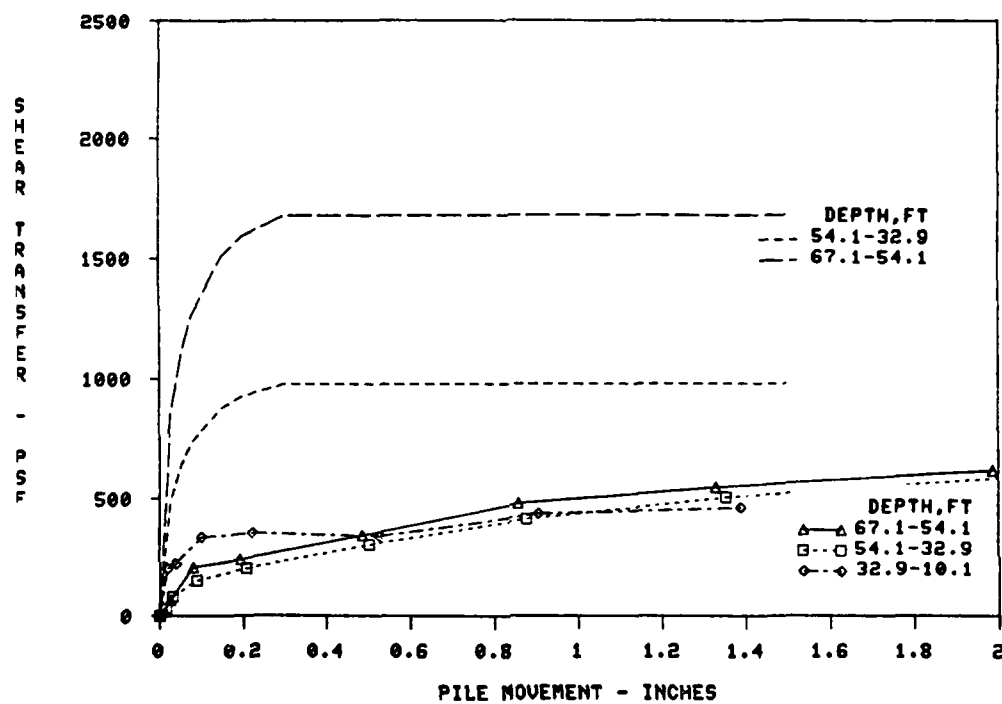
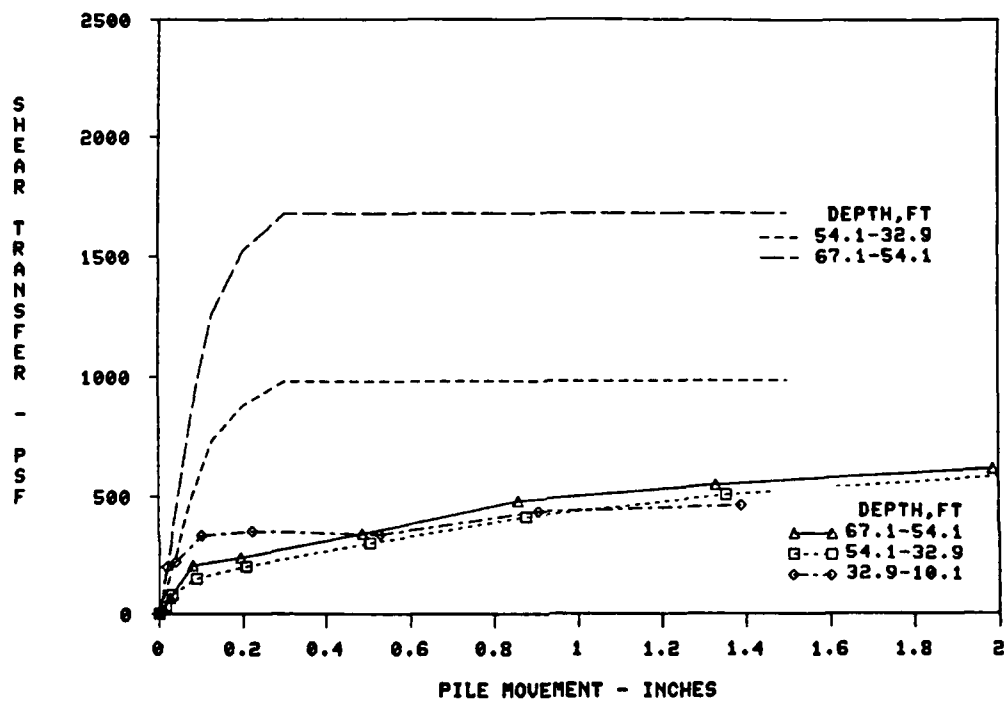


Figure C39. Comparison of f-z Criteria to Adjusted Field Curves, Red River, Test Pile No. PT-A-2C, Vijayvergiya Criteria



Figuer C40. Comparison of f-z Criteria to Adjusted Field Curves, Red River, Test Pile No. PT-A-2C, Coyle Criteria

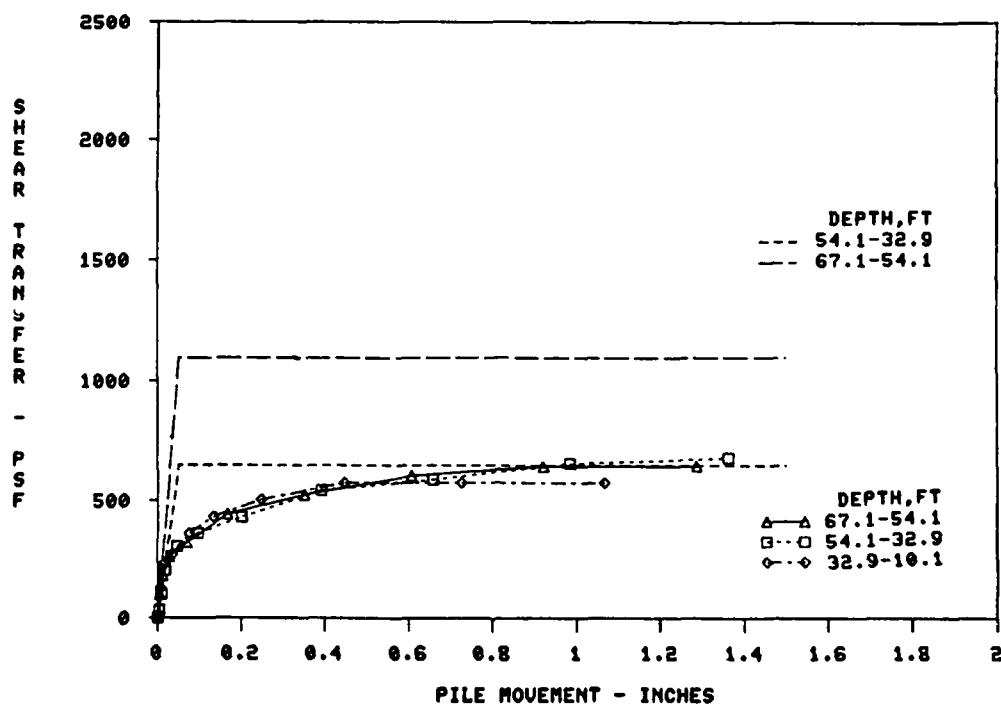


Figure C41. Comparison of f-z Criteria to Adjusted Field Curves, Red River, Test Pile No. PT-A-3C, Coyle-Sulaiman Criteria

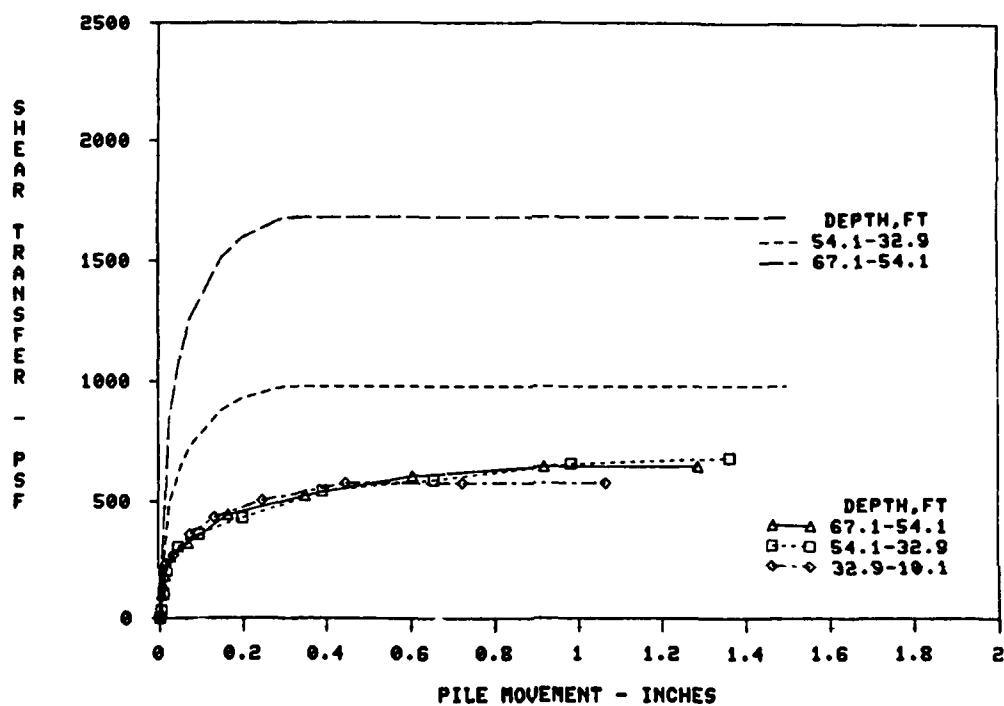


Figure C42. Comparison of f-z Criteria to Adjusted Field Curves, Red River, Test Pile No. PT-A-3C, Vijayvergiya Criteria

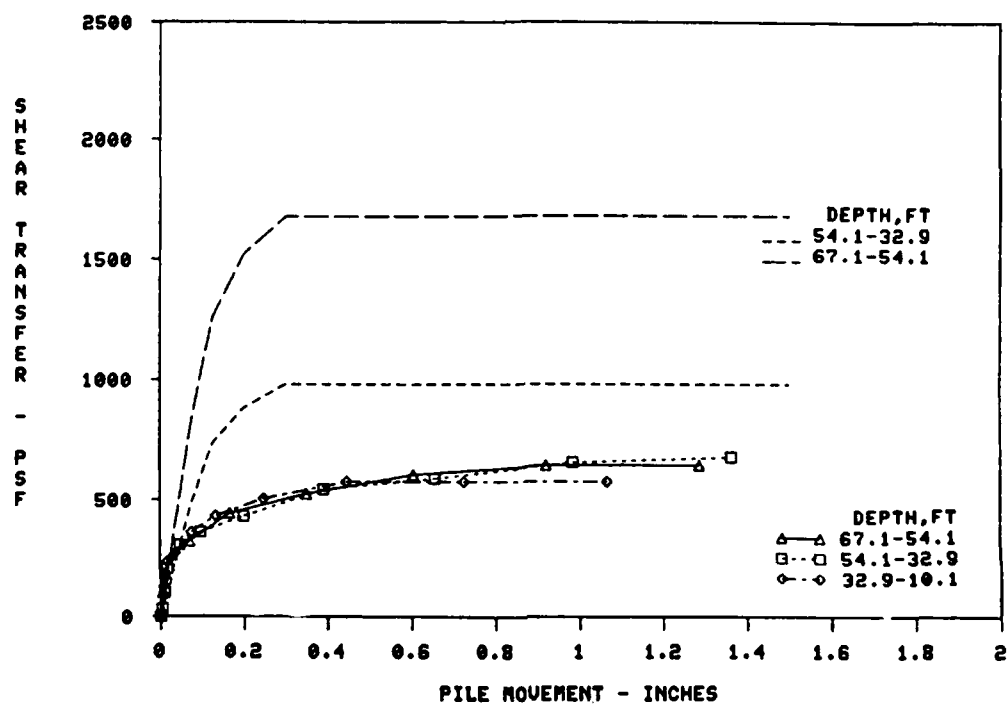


Figure C43. Comparison of f-z Criteria to Adjusted Field Curves, Red River, Test Pile No. PT-A-3C, Coyle Criteria

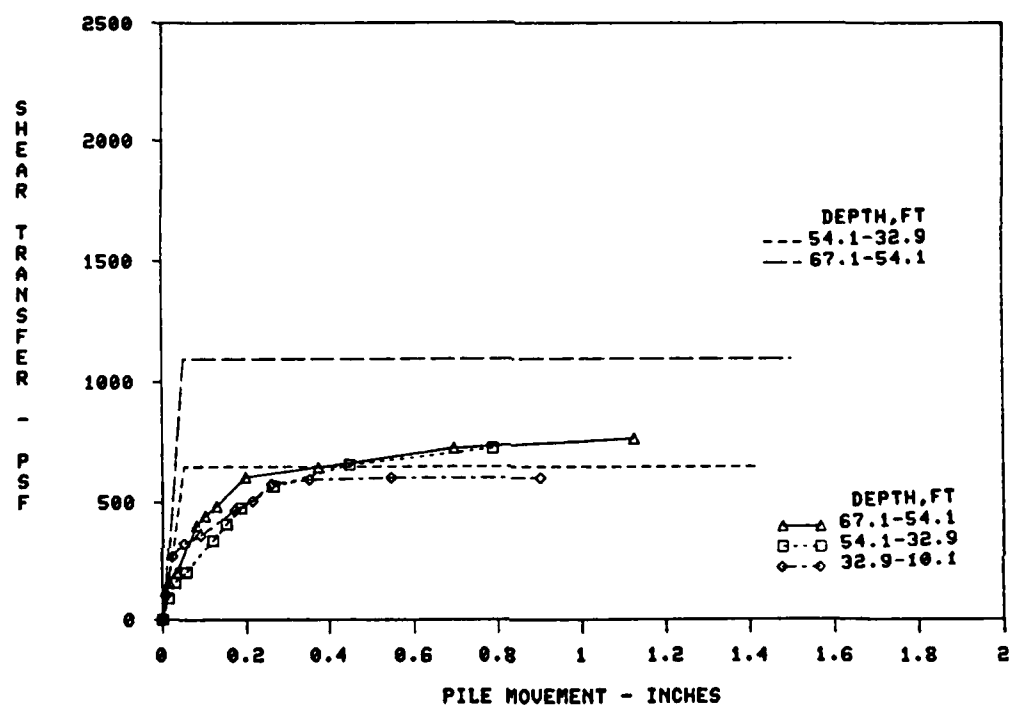


Figure C44. Comparison of f-z Criteria to Adjusted Field Curves, Red River, Test Pile No. PT-A-3C Retest, Coyle-Sulaiman Criteria

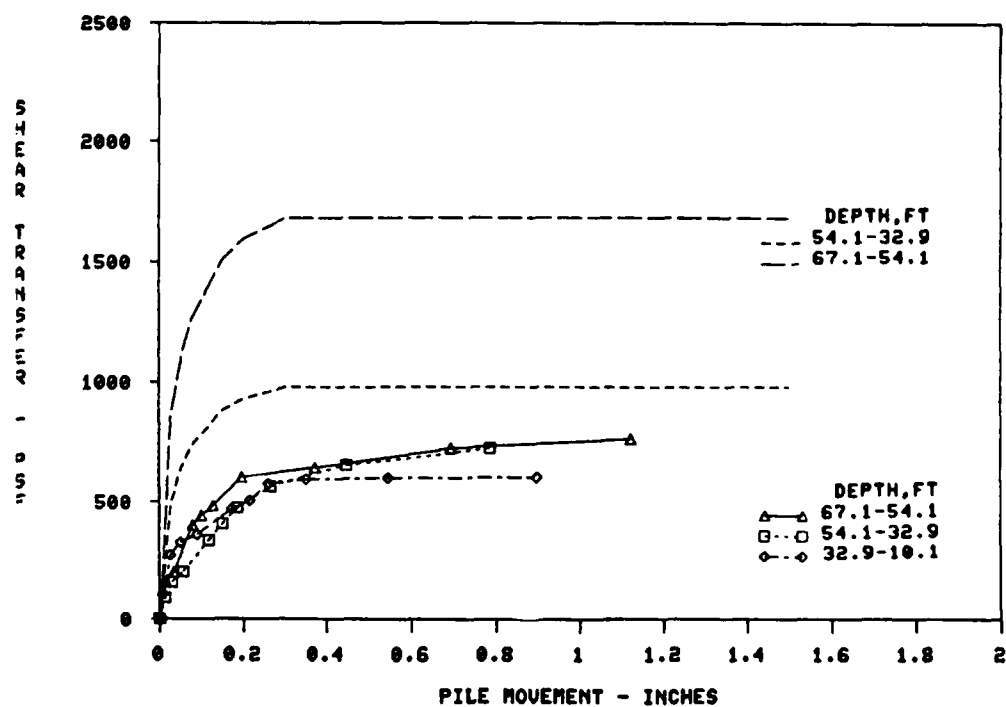


Figure C45. Comparison of f-z Criteria to Adjusted Field Curves, Red River, Test Pile No. PT-A-3C Retest, Vijayvergiya Criteria

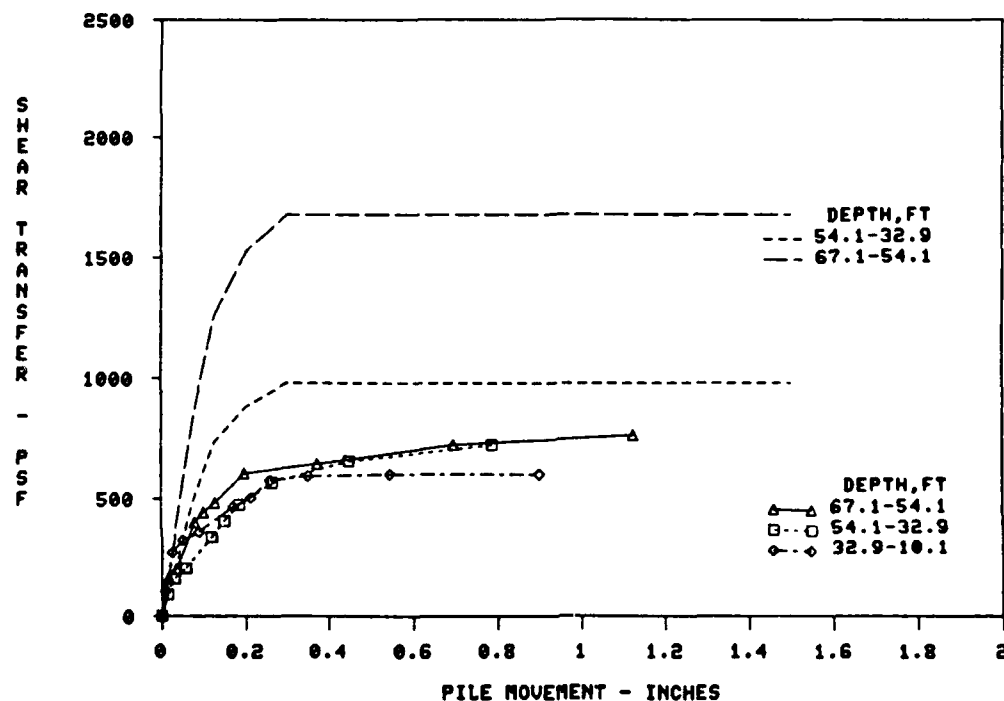


Figure C46. Comparison of f-z Criteria to Adjusted Field Curves, Red River, Test Pile No. PT-A-3C Retest, Coyle Criteria

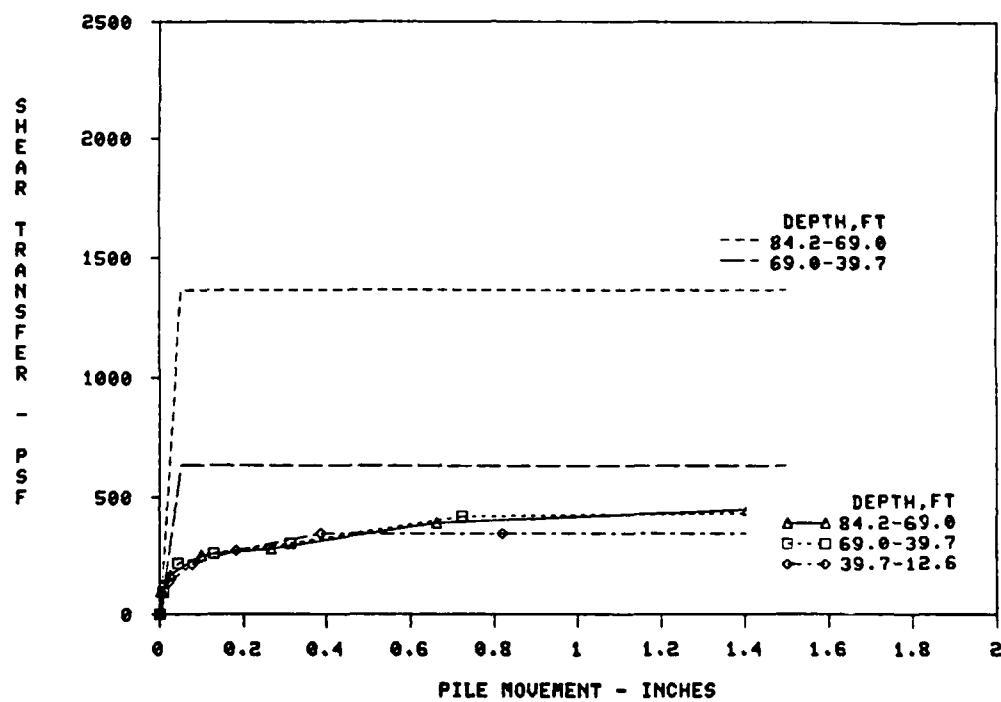


Figure C47. Comparison of f-z Criteria to Adjusted Field Curves, Red River, Test Pile No. PT-S-1C, Coyle-Sulaiman Criteria

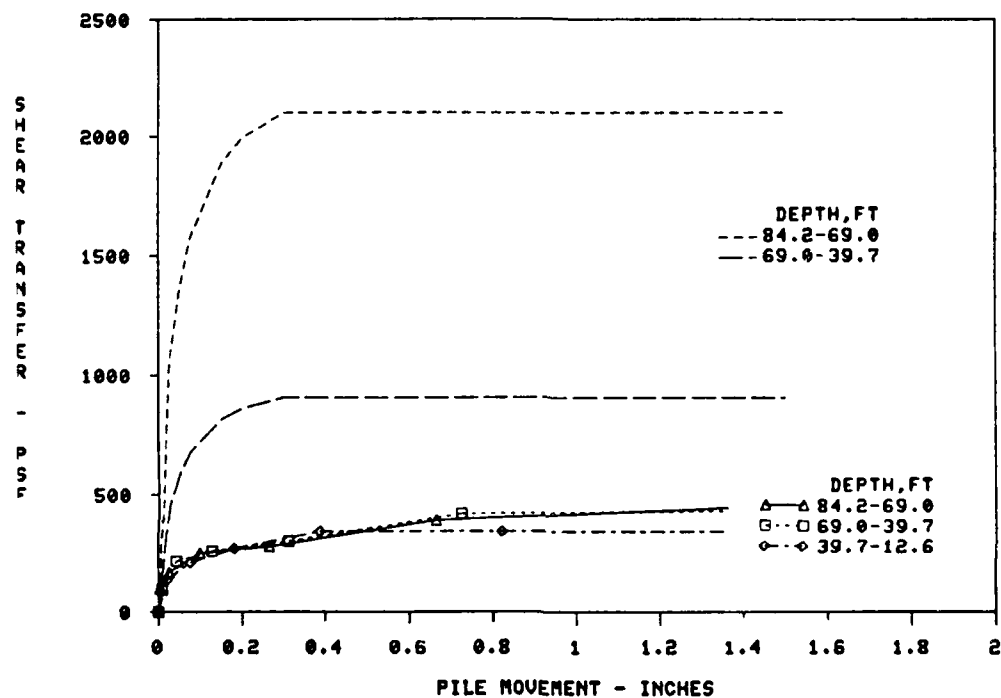


Figure C48. Comparison of f-z Criteria to Adjusted Field Curves, Red River, Test Pile No. PT-S-1C, Vijayvergiya Criteria

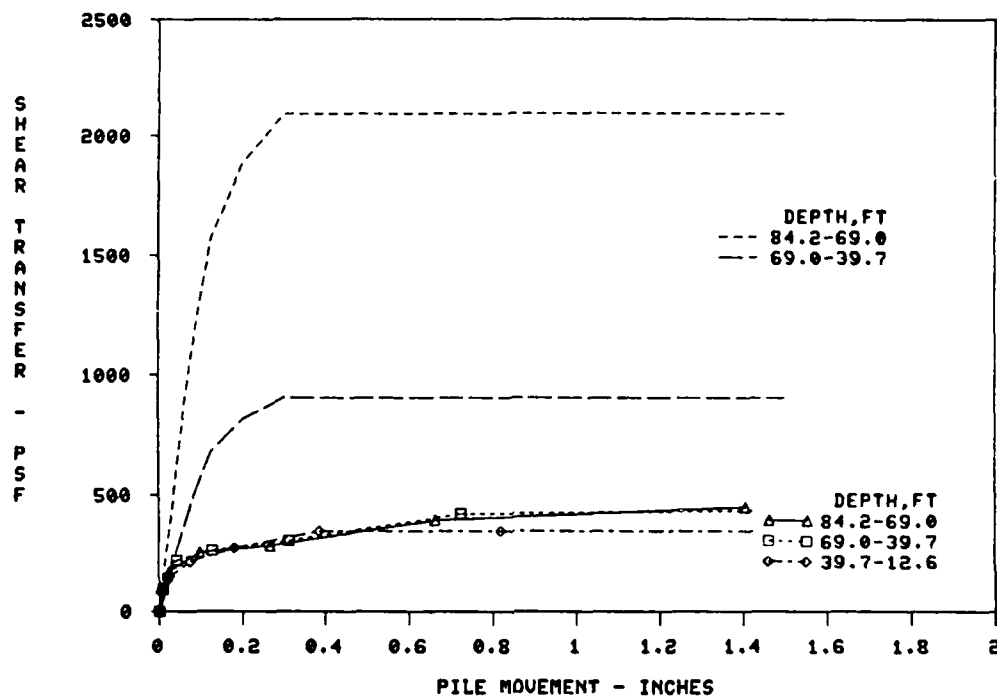


Figure C49. Comparison of f-z Criteria to Adjusted Field Curves, Red River, Test Pile No. PT-S-1C, Coyle Criteria

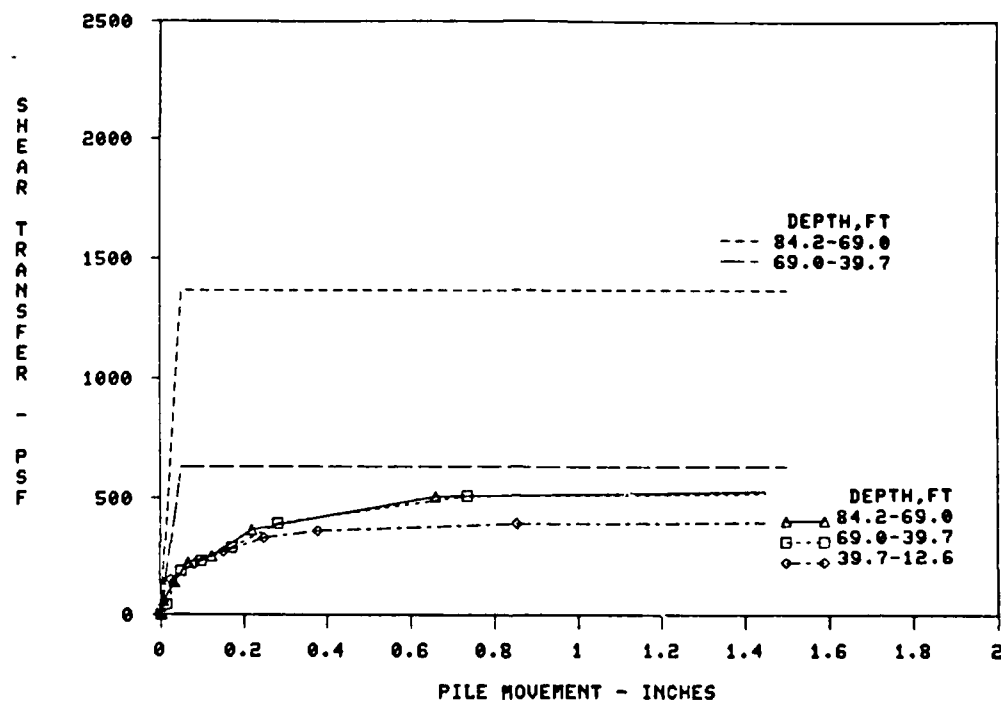


Figure C50. Comparison of f-z Criteria to Adjusted Field Curves, Red River, Test Pile No. PT-S-1C Retest, Coyle-Sulaiman Criteria

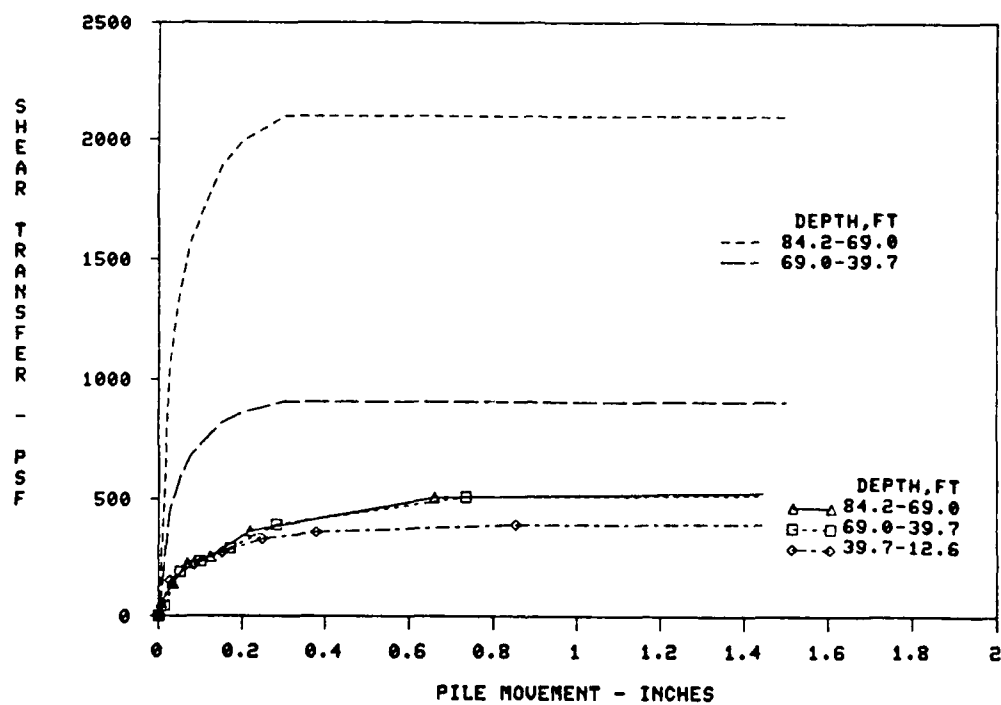


Figure C51. Comparison of f-z Criteria to Adjusted Field Curves, Red River, Test Pile No. PT-S-1C Retest, Vijayvergiya Criteria

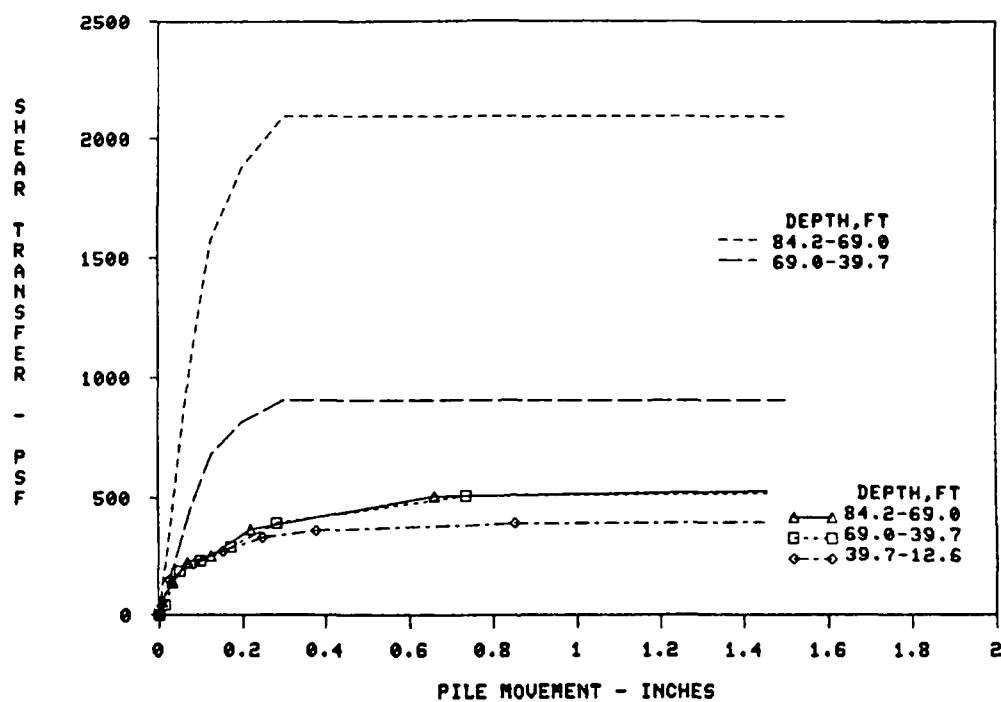


Figure C52. Comparison of f-z Criteria to Adjusted Field Curves, Red River, Test Pile No. PT-S-1C Retest, Coyle Criteria

APPENDIX D

RESULTS OF HYPERBOLIC CURVE
FITTING OF FIELD f - z CURVES

Table D1

Test Site	Test Pile	Depth ft	Initial Modulus E_i , psf/in.	Maximum Side Resistance f_{max} , psf		
				Field	Computed	
Arkansas River L&D No. 4	No. 1 (12" pipe)	0-15	23100	2145	750	800
		15-25	53967	1604	950	1200
		25-33	40587	1418	1200	1540
		33-40	41254	1301	1240	1590
		40-47	60020	1387	1160	1400
		47-53	16325	1284	1160	1400
	No. 2 (16" pipe)	0-15	63492	1896	730	780
		15-25	15115	1438	930	1180
		25-33	7112	2717*	1160	1510
		33-40	8532	2658*	1220	1570
		40-47	10860	1830	1150	1400
		47-53	12009	1961	1150	1400
	No. 2 (Retest)	0-15	16410	1255	730	780
		15-25	8217	2154*	930	1180
		25-33	9217	2374*	1160	1510
		33-40	10044	2985*	1220	1570
		40-47	13144	1599	1150	1400
		47-53	20284	1507	1150	1400
	No. 3 (20" pipe)	0-15	-	1441	700	750
		15-25	19200	1441	910	1150
		25-33	15000	1337	1100	1500
		33-40	18445	1603	1170	1500
		40-47	13478	1071	1050	1290
		47-53	7278	1039	1050	1290
	No. 6 (14HP73)	0-10	-	-	730	780
		10-20	5482	1703	930	1180
		20-27	13477	1712	1160	1510
		27-34	15926	1307	1220	1570
		34-38	6993	1340	1150	1400
		38-42	16920	1305	1150	1400

(Continued)

Table D1 (Continued)

Test Site	Test Pile	Depth ft	Initial Modulus E_f , psf/in.	Maximum Side Resistance f_{max} , psf		
				Field	Computed	
					AD	UAD
Arkansas River L&D No. 4	No. 7 (14HP73)	0-10	-	-	730	780
		10-20	7179	2313	930	1180
		20-30	8286	1730	1160	1510
		30-40	16286	1252	1150	1400
		40-50	49261	726	1150	1400
	No. 9 (14HP73)	0-10	-	-	730	780
		10-20	8450	1801	930	1180
		20-30	15756	1513	1160	1510
		30-40	16462	1356	1150	1400
		40-50	14701	1381	1150	1400
	No. 10 (16" pipe)	0-15	-	-	730	780
		15-25	11139	1956	930	1180
		25-33	12175	1453	1160	1510
		33-40	13150	1561	1220	1570
		40-47	12159	1869	1150	1400
		47-53	10999	1714	1150	1400
Ascalmore Creek-Tippo Bayou Control Structure (unadjusted)	PT-1 (14HP89)	43-53	111086	1211		1200
		53-63	4086	645		1300
		63-73	8019	1253		1350
		73-83	5698	1809		-1350
		83-93	7818	1643		1300
		93-100	8179	2016		1350
	PT-2 (14HP89)	30-40	9225	1315		1000
		40-50	8123	571		1100
		50-60	11086	2178		1950
		60-70	13152	456		670
		70-80	12622	884		1400
		80-90	13716	2517*		1650
	PT-1	40-60	15003	845	990	
		60-80	16233	951	1000	
		80-100	14791	931	1000	

(Continued)

Table D1 (Continued)

Test Site	Test Pile	Depth ft	Initial Modulus E_f , psf/in.	Maximum Side Resistance f_{max} , psf		
				Field	Computed	
					AD	UAD
Red River, L&D No. 1 (unadjusted)	PT-2	30-50	13553	782	990	
		50-70	15791	864	1000	
		70-90	13829	897	1000	
	PT-A-1C (12HP53)	34-50	10952	972	1300	
		50-58	11778	961	1350	
	PT-A-1C (Retest)	34-50	14184	1492	1300	
		50-58	11976	1429	1350	
	PT-A-2C (12HP53)	33-54	9380	500	970	
		54-67	8333	476	1020	
Red River, L&D No. 1 (adjusted)	PT-A-3C (12HP53)	33-54	11148	442	970	
		54-67	8400	576	1020	
	PT-A-3C (Retest)	33-54	11111	1538	970	
		54-67	7143	1408	1020	
	PT-S-1C	40-70	1000	815	1190	
		70-85	8379	765	1250	
	PT-S-1C (Retest)	40-70	6667	1037	1190	
		70-85	5555	992	1250	
	Red River, L&D No. 1 (adjusted)	PT-A-1C	35-50	12561	719	800
50-58			11925	750	820	
PT-A-1C (Retest)		35-50	13071	692	800	
		50-58	12679	735	820	
PT-A-2C		33-54	10146	556	770	
		54-67	9978	671	800	
PT-A-3C		33-54	12513	680	770	
		54-67	11428	741	800	

(Continued)

Table D1 (Continued)

Test Site	Test Pile	Depth ft	Initial Modulus E_f , psf/in.	Maximum Side Resistance f_{max} , psf	
				Field	Computed AD UAD
	PT-A-3C	33-54	12871	775	770
	(Retest)	54-67	14004	807	800
	PT-S-1C	40-70	10731	779	800
		70-85	12113	815	850
	PT-S-1C	40-70	9761	823	800
	(Retest)	70-85	10561	867	850

* = Not used in the Statistic Analysis

AD = Adjusted

UAD = Unadjusted

Appendix E

Procedures for Partially Submerged Piles

Lowering the water table in the vicinity of piles causes an increase in the effective stress in the surrounding soil mass which in turn increases the capacities of the piles. The change in effective stress beginning at the ground surface increases proportional with depth until the water table is reached and then remains constant with increasing depth, Figure E.1. To account for this increase in effective stress in the load-transfer criteria, the relative depth used in determining the maximum side and tip resistances is adjusted to yield an equivalent homogeneous system. An example of this procedure follows:

The soil and pile properties for this example are the same as the step-by-step illustration given in Chapter 5, page 190, but with the water table 20 ft below the ground surface, Figure E.2.

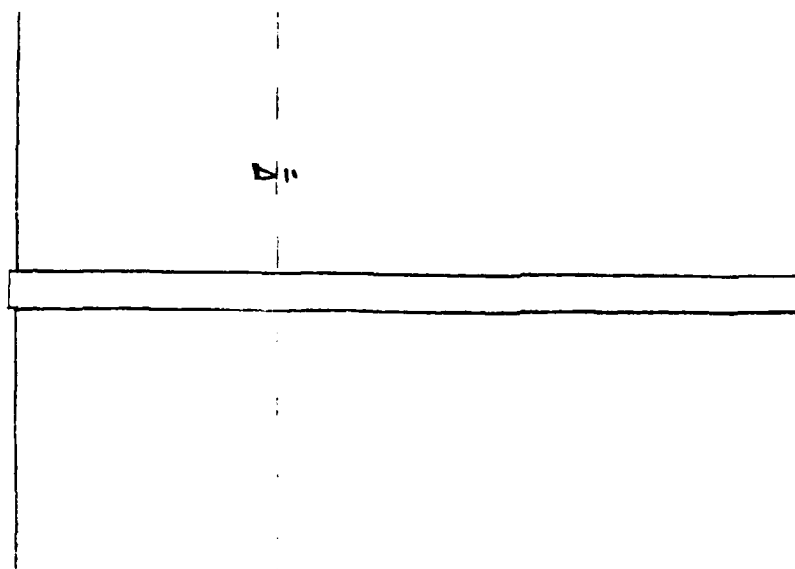
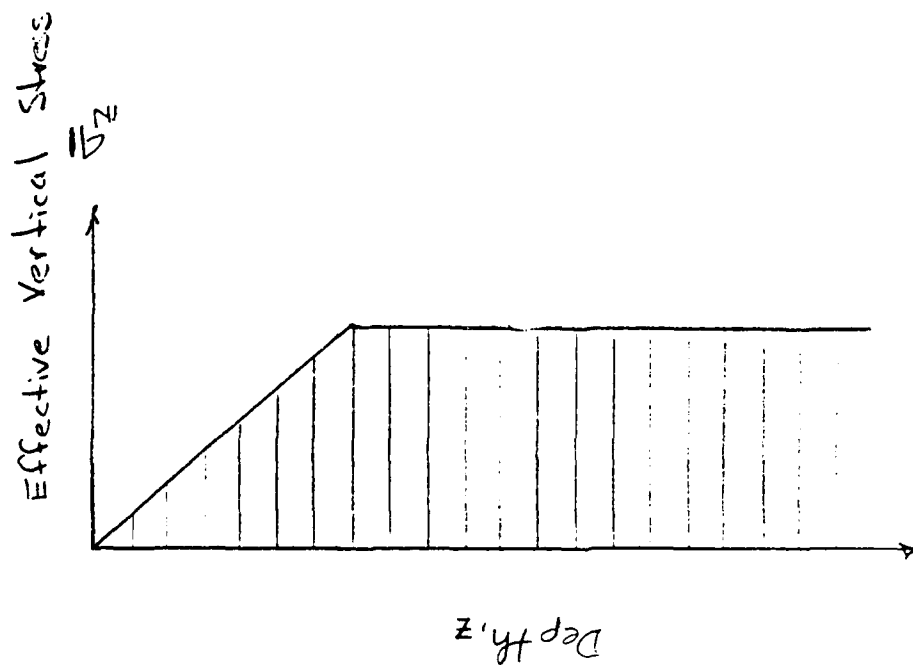


Figure E.1 - Increase in Effective Vertical Stress from Lowering of the Water Table

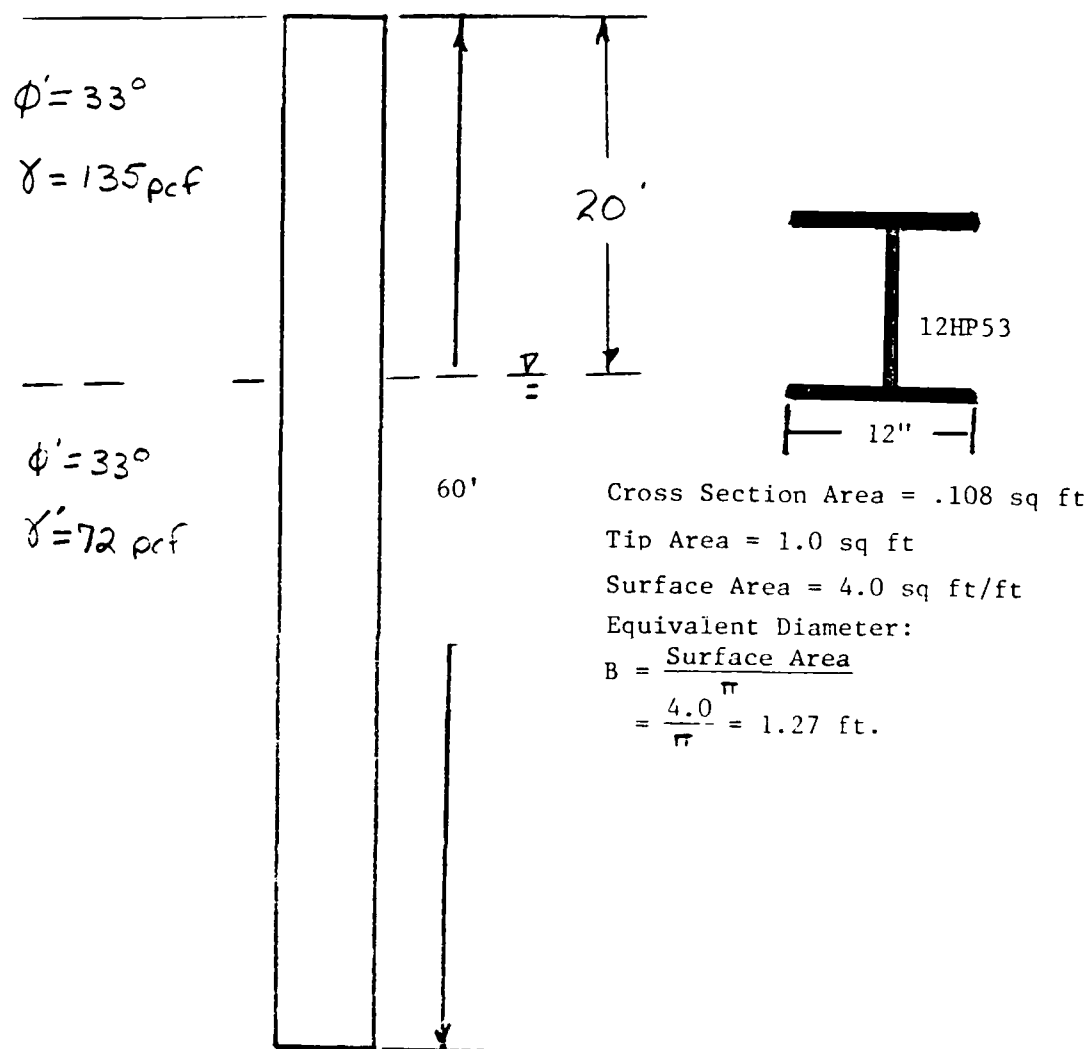


Figure E-2 - Pile and Pile Properties

1. Find the change in effective stress from lowering water level.

Effective Vertical Stress, Psf,
With Water Table at

Depth, ft	Surface	-20 ft.	$\Delta \bar{\sigma}_y$
0	0.0	0.0	0.0
5	360	675	315
10	720	1350	630
20	1440	2700	1260
30	2160	3420	1260
40	2880	4140	1260
50	3600	4860	1260
60	4320	5580	1260

2. Determine the change relative depth, D/B, due to lowering the water table by:

$$\Delta D = \frac{\Delta \sigma_v}{\gamma_{sat}}$$

Depth, ft	$\Delta \sigma_v$	ΔD
0	0	0
5	315	4.4
10	630	8.8
20	1260	17.5
30	1260	17.5
40	1260	17.5
50	1260	17.5
60	1260	17.5

3. Determine the new maximum side and tip resistance.

Depth, f	Surface			*20 ft below surface		
	D/B	f _{max} , psf	ΔD, ft	D, ft	D/B	f _{max} , psf
0	0	0	0.0	0.0	0.0	0.0
5	3.9	360	4.4	9.4	7.4	520
10	7.9	540	8.8	18.8	14.8	750
20	15.7	780	17.5	37.5	29.5	920
30	23.6	860	17.5	47.5	37.4	1000
40	31.5	950	17.5	57.5	45.3	1100
50	39.5	1050	17.5	67.5	53.1	1100
60	47.4	1050	17.5	77.5	61.0	1100
		q _{max} , tsf				q _{max} , tsf
60	47.4	56.0	17.5	77.5	61.0	6.4

4. Develop f-z curves using the expression:

$$f = \frac{Z}{\frac{1}{E_f} + \frac{1}{f_{\max}} (Z)}$$

SHEAR TRANSFER TABLE								
PILE LENGTH	0.	5.	10.	20.	30.	40.	50.	60.
FMAX (PSF)	0.	520.	750.	920.	1000.	1100.	1100.	1100.
PILE MOVEMENT								
Z (IN)	SHEAR TRANSFERRED, F, (PSF)							
0.	0.	0.	0.	0.	0.	0.	0.	0.
0.025	0.	190.	214.	226.	231.	236.	236.	236.
0.050	0.	279.	333.	363.	375.	388.	388.	388.
0.075	0.	330.	409.	455.	474.	495.	495.	495.
0.100	0.	363.	462.	521.	545.	574.	574.	574.
0.150	0.	403.	529.	609.	643.	683.	683.	683.
0.200	0.	427.	571.	665.	706.	754.	754.	754.
0.250	0.	443.	600.	704.	750.	805.	805.	805.
0.300	0.	454.	621.	733.	783.	843.	843.	843.
0.400	0.	469.	649.	772.	828.	895.	895.	895.
0.600	0.	485.	679.	816.	878.	954.	954.	954.
1.000	0.	498.	706.	854.	923.	1008.	1008.	1008.
10.000	0.	518.	745.	913.	992.	1090.	1090.	1090.

AD-A139 236

LOAD-TRANSFER CRITERIA FOR NUMERICAL ANALYSIS OF
AXIALLY LOADED PILES IN (U) ARMY ENGINEER WATERWAYS
EXPERIMENT STATION VICKSBURG MS R L MOSHER JAN 84
WES-TR-K-84-1

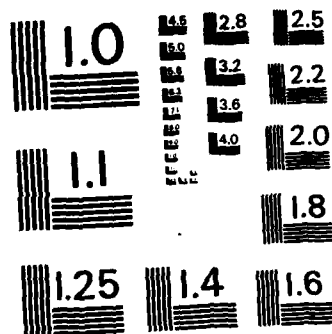
5/5

UNCLASSIFIED

F/G 13/13

NL





MICROCOPY RESOLUTION TEST CHART
NATIONAL BUREAU OF STANDARDS-1963-A

5. Develop P-z curve using expression

$$P = (4Z)^{1/3} P_{\max}$$

where

$$\begin{aligned} P_{\max} &= (q_{\max} A_t) \\ &= (64 \text{ tsf})(2000.0 \frac{\text{lbs}}{\text{tons}})(1.0 \text{ sq ft}) \\ &= 128,000 \text{ lbs} \end{aligned}$$

TIP MOVEMENT(IN)	TIP LOAD(LBS)
0.	0.
0.025	59412.
0.050	74855.
0.075	85687.
0.100	94311.
0.150	107959.
0.200	118825.
0.250	128000.
0.300	136020.
0.400	149710.
0.600	171375.
1.000	203187.
10.000	437754.

Using the above f-z and P-z curves for a water table 20 ft below the ground surface, the pile capacity is 153 tons as compared to 135 with the water table at the surface.

APPENDIX F
LIST OF SYMBOLS

APPENDIX F: LIST OF SYMBOLS

A	= The area or cross-sectional area
a, b	= The constants in the hyperbolic expression
A_s	= The surface area of the pile shaft
A_t	= The area of the tip
B	= The width or diameter of a pile
$2\bar{B}$	= The width of a footing
C_N	= The correction factor to N-values from a standard penetration tests for overburden pressure
c	= the cohesion
c_a	= The adhesion
c_f	= The correction factor for maximum load transferred (Parker and Reese Criteria)
D	= The depth of penetration or depth of overburden
D_c	= The point beyond which the rate of change of the side and tip resistance decreases with depth (critical depth)
D_r	= The relative density of the soil
δ_c, δ_γ	= The shape factors for bearing capacity
δ	= The angle of friction between soil and pile shaft
E	= The modulus of elasticity
E_f	= The initial tangent modulus for shear transfer
E_i	= The initial tangent modulus
E_p	= The modulus of elasticity of the pile
E_s	= The modulus of elasticity of the soil
e_o	= The void ratio
ϵ	= The axial strain
F	= The forces vector

f	= The shear develop along the pile shaft (shear transfer) or load transfer
f_{\max}	= The maximum shear transfer
f_o	= The unit shear stress of the shaft of the pile
f_s	= The maximum side resistance
γ	= The unit weight of soil
h	= The distance between increments
I	= The moment of inertia
I_{ij}	= The influence factor for settlement determined by Mindlin's equations
K, K_s	= The coefficient of lateral earth pressure
K_i	= A modulus in the hyperbolic expression for triaxial data
K_x, K_y	= The spring constants in the Beam-Column analysis
L	= The length of pile
L_i	= The length of i th increment
N_c, N_q, N_γ	= Bearing capacity factors
N_f	= The number of blows per foot from standard penetration test
N_c	= The corrected number of blows per foot from standard penetration test
n	= The exponent determining the rate of variation of E_1 with σ_3
P	= The axial force or tip load
P_a	= The atmospheric pressure
P_i	= Axial force at point i
P_{\max}	= Maximum or ultimate tip load or capacity of a pile
P_u	= The ultimate axial capacity of a pile

P_s	= The ultimate shear resistance or "skin friction" along the shaft
ϕ	= The angle of internal friction.
ϕ'	= The effective angle of internal friction
Q_{max}	= The ultimate bearing capacity of a footing per unit length
q_f	= The in situ normal pressure
q_{max}	= The maximum tip resistance or ultimate bearing capacity per unit area
q_1	= Overburden pressure
q_0	= The unit tip stress
q_x, q_y	= The pressure in the x,y direction, respectively
R_c	= The correction for compression loading (Parker and Reese Criteria)
R_f	= The ratio of compressive strength
σ_1	= The major principal effective stresses
σ_3	= The minor principal effective stresses
σ_n	= The normal stress
σ_v	= The effective overburden stress or pressure
$\Delta\sigma$	= The deviatoric stress ($\sigma_1 - \sigma_3$)
S	= The shear strength of the sand
S_b	= The axial stiffness of a beam
S_s	= The axial stiffness provided by the soil
S_x	= Shear transfer
$\tan\delta$	= The coefficient of friction between the shaft and soil
U	= The displacement vector
U_{ij}	= The displacements vector of the soil

- u = The displacement in the x direction
- U_c = Correlation coefficient for compression loading
 (Parker and Reese Criteria)
- v = The displacement in the y direction
- γ_s = Poisson's ratio for soil
- X = The depth
- X_K = The distance along the pile
- z = The displacement of the pile or pile movement, inches
- z_c = The critical movement of the pile which mobilizes the
 maximum side or tip resistance, inches

END

FILMED

4-84

DTIC